



HAL
open science

Vibration of nonlocal carbon nanotubes and graphene nanoplates

Florian Hache

► **To cite this version:**

Florian Hache. Vibration of nonlocal carbon nanotubes and graphene nanoplates. Mechanics of materials [physics.class-ph]. Université de Bretagne Sud; Florida Atlantic university, 2018. English. NNT : 2018LORIS487 . tel-02130474

HAL Id: tel-02130474

<https://theses.hal.science/tel-02130474>

Submitted on 15 May 2019

HAL is a multi-disciplinary open access archive for the deposit and dissemination of scientific research documents, whether they are published or not. The documents may come from teaching and research institutions in France or abroad, or from public or private research centers.

L'archive ouverte pluridisciplinaire **HAL**, est destinée au dépôt et à la diffusion de documents scientifiques de niveau recherche, publiés ou non, émanant des établissements d'enseignement et de recherche français ou étrangers, des laboratoires publics ou privés.



THESE / UNIVERSITE DE BRETAGNE-SUD
sous le sceau de l'Université Bretagne Loire

pour obtenir le titre de
DOCTEUR DE L'UNIVERSITE DE BRETAGNE-SUD

Mention : Génie Mécanique
Ecole doctorale: SPI

Présentée par
Florian Hache

Préparée à l'unité mixte de recherche DuPuy de Lôme IRDL
FRE CNRS (3744)

Etablissement de rattachement : **FLORIDA ATLANTIC
UNIVERSITY / UNIVERSITE DE BRETAGNE SUD**

Thèse soutenue le 04/05/2018

devant le jury composé de :

M. Noël Challamel
Professeur des universités, Université de Bretagne Sud /
Directeur de thèse

M. Isaac Elishakoff
Professeur des universités, Florida Atlantic University / Directeur
de thèse

M. Francisco Presuel-Moreno
Professeur des universités, Florida Atlantic University

M. Guoqiang Cai
Professeur des universités, Florida Atlantic University

M. Manhar R. Dhanak
Professeur des universités, Florida Atlantic University

Vibration of nonlocal carbon nanotubes and graphene nanoplates

DEDICATION

Cette thèse est dédiée à Marie et Marcel Rault. Chaque mot de cette thèse a été écrit en pensant à vous. Merci pour tout.

ACKNOWLEDGEMENTS

This thesis is the achievement of a very long process. These years at Florida Atlantic University have changed me. I believe I am a better scientist and more generally, a better man than I was three years ago. Of course, it was not always easy. Many times, I thought I could not do it, that I was not good enough. Nevertheless, I remember primarily the good moments. I would like to take the opportunity of here to thank all people who helped me.

I would first like to give my gratitude to my graduate advisors, Professor Challamel and Professor Elishakoff, for their support. They taught me the virtues of patience and perseverance. Besides my advisors, I would like to thank the rest of my thesis committee: Professor Cai, Professor Dhanak and Professor Presuel Moreno. I would like also to thank the Department of Ocean and Mechanical Engineering and Professor Hashemi whose financial support made it possible for me to pursue higher education. Additionally, I would like to give credit to Anastasia Calnick, Marlene Smith and Barbara Steinberg, keystone of the department.

I do not forget Jerome Lagouanère and Osamu Fujita, my sensei for the rest of my life, who are, in my opinion, the examples of good professors. Without them, I would never have thought to be a professor. It was a great honor to work for them.

Throughout my stay, I had the chance to meet many wonderful people. It would be impossible to list the name of all of them. I will always remember the intense discussions with Raul Vidal and Benjamin Herisson, a great person and my two wonderful officemates who became my friends, Vaishak and Giulio. We shared so many good moments. I am looking forward for our next trip. Special thanks to Jenna who trusted me more than I trusted myself.

Thanks also to my friends Maxime and Geoffrey. I have known them for 10 years, 10 years of fun.

I would like to conclude my acknowledgements by thanking the most important people in my life, my sister and my parents. They never doubted me, encouraging me, pushing me to continue, respecting all my decisions. I am so lucky to have them and I am so glad our family became bigger during my PhD. Without them, I would not be the person that I am today. I owe all of it to you. Many thanks.

VIBRATION OF NONLOCAL CARBON NANOTUBES AND GRAPHENE NANOPATES

1. INTRODUCTION	1
1.1. From the importance to deal with beams and plates in vibration	1
1.2. The advent of nanomaterials: brief presentation of carbon nanotubes and graphene nanoplates	2
1.2.1. Carbon nanotubes.....	2
1.2.2. Graphene nanoplates.....	4
1.2.3. Example of issues specific to nanomaterials: the surface effects.....	5
1.3. Different approaches to describe the mechanical behavior of macro and nanostructures in vibration	7
1.3.1. Experimental, analytical and numerical approaches.....	7
1.3.2. Analytical study of macro beams and plates.....	9
1.3.3. Nonlocal theories.....	10
1.3.3.1. Introduction to the nonlocal approaches.....	10

1.3.3.2. Calibration of the small length scale coefficient: from the necessity to develop continualized models.....	11
1.3.4. Asymptotic models.....	12
1.4. Different methods of resolution.....	13

2.TOWARD THE DEVELOPMENT OF THICK BEAM AND PLATE MODELS FOR MACROSTRUCTURES.....15

2.1. Derivation of thick beam models and different applications.....	15
2.1.1. Original Bresse-Timoshenko model.....	15
2.1.2. Truncated version of the Bresse-Timoshenko model through an asymptotic approach.....	18
2.1.3. Bresse-Timoshenko based on slope inertia.....	22
2.1.4. Different solutions.....	24
2.1.4.1. Simply supported beam.....	24
2.1.4.2. Other sets of boundary conditions.....	27
2.1.5. Particular application: cantilever beam with a tip mass.....	31
2.1.5.1. Derivation of the governing differential equation	31
2.1.5.2. Numerical results.....	33
2.1.6. Other applications.....	38

2.2. Thick plate model for macrostructures.....	39
2.2.1. The different models.....	40
2.2.1.1. Original Uflyand-Mindlin.....	40
2.2.1.2. Truncated Uflyand-Mindlin plate theory.....	42
2.2.1.3. Uflyand-Mindlin based on slope inertia.....	46
2.2.2. Natural frequencies for the different Uflyand-Mindlin plate models.....	47
2.2.2.1. Rectangular plate with four edges simply supported.....	48
2.2.2.2. Solutions for two opposite simply supported edges: Levy's approach.....	51

3. NONLOCAL PHENOMENOLOGICAL MODELS: ASYMPTOTIC AND ENGINEERING APPROACHES.....70

3.1. Different beam models.....	71
3.1.1. Asymptotic derivation of nonlocal beam models.....	71
3.1.1.1. Asymptotic model with a partial nonlocality along the horizontal direction.....	71
3.1.1.2. Asymptotic model with a partial nonlocality along the vertical direction.....	74
3.1.1.3. Asymptotic model with a full nonlocality.....	78

3.1.2. Nonlocal engineering beams approaches.....	80
3.1.2.1. Bernoulli-Euler model: the fourth order phenomenological approach.....	80
3.1.2.2. Sixth order phenomenological thin beam model.....	82
3.1.2.3. Nonlocal original Bresse-Timoshenko model.....	83
3.1.2.4. Truncated Bresse-Timoshenko model.....	85
3.1.2.5. Bresse-Timoshenko based on slope inertia.....	86
3.1.3. Solution and parametric analysis.....	87
3.2. Different plates models.....	95
3.2.1. Asymptotic derivation of nonlocal beam models.....	95
3.2.1.1. Asymptotic model with a partial nonlocality along the two directions of the plan.....	95
3.2.1.2. Asymptotic model with a partial nonlocality along the thickness of the plate.....	98
3.2.1.3. Asymptotic model with a full nonlocality.....	101
3.2.2. Nonlocal engineering plate approaches.....	103
3.2.2.1. The nonlocal fourth order phenomenological Kirchhoff-Love model.....	103
3.2.2.2. 6 th order phenomenological thin plate model.....	105
3.2.2.3. Nonlocal original Uflyand-Mindlin model.....	106
3.2.2.4. Truncated Uflyand-Mindlin model.....	109
3.2.2.5. Uflyand-Mindlin based on slope inertia.....	109

3.2.3. Solution.....110

4. MICROSTRUCTURED AND NONLOCAL CONTINUALIZED MODELS: THE RESOLUTION OF THE SMALL LENGTH SCALE COEFFICIENT'S PARADOX.....122

4.1. Different nonlocal thin beam models.....122

4.1.1. Microstructured model.....122

4.1.2. Phenomenological models: the small length scale paradox.....124

4.1.2.1. Fourth order Eringen phenomenological model.....124

4.1.2.2. Sixth order phenomenological model.....126

4.1.3. Resolution of the paradox: the continualized models.....127

4.1.3.1. Fourth order continualized model.....127

4.1.3.2. Sixth order continualized model.....129

4.2. Different nonlocal thin plate models.....131

4.2.1. Microstructured model.....131

4.2.2. Phenomenological thin plate models.....135

4.2.2.1. Fourth order phenomenological model.....135

4.2.2.2. Sixth order phenomenological model.....138

4.2.3. Continualized models.....	142
4.1.3.1. Fourth order continualized model.....	142
4.1.3.2. Sixth order continualized model.....	145
4.3. Nonlocal thick plate models.....	147
4.3.1. Microstructured beam-grid model.....	147
4.3.2. Nonlocal Uflyand-Mindlin plate model.....	151
4.3.2.1. Solution in statics.....	152
4.3.2.2. Solution for free vibration.....	158
4.3.3. Fourth order continualized model.....	163
4.3.4. Sixth order continualized model.....	166
4.4. Discussion: superiority of the continualized models over the traditional phenomenological models.....	170
 5. CONCLUSION AND RECOMMENDATIONS.....	171
 REFERENCES.....	177

1. INTRODUCTION

1.1. From the importance to deal with beams and plates in vibration

As explains Sathyamoorthy [1] in the preface of his monography: “Various types of thin-walled structural components are commonly found in spacecrafts, missiles, aircrafts, land-based vehicles, underwater vessels and structures, chemical processing equipment and modern housing. These structures are usually built up of beams, plates, ad shell-type structural elements. Since these structural components are important in so many of these modern structures, engineers and designers must have a good knowledge of their structural behavior when they are subjected to static, dynamic, and environmental loads”. Numerous researches have been dedicated to describe the behavior in vibration of beams and plates (the reader may refer to the book of Timoshenko that describes with accuracy the history of strength of materials [2]. Hereinafter, different particular engineering applications will be studied and briefly described in the present section.

First of all, many industrial systems can be viewed as a problem of free vibration of uniform cantilever beams with a concentrated tip mass [3]: flexible robot arms in microelectronic industry [4-6], mast antenna structures [7], wind tunnel stings carrying an airplane [8,9] or stock-bridge dampers used for damping out aeolian vibrations on high-voltage transmission lines [10]. For those different applications, particularly sensitive to vibrations, it is extremely important to predict their behavior in order to control it.

One of the most frequent problems in engineering industry is the presence of structural defects such as cracks that can be a serious threat for the safety of the system, reduce the lifetime and lead to failure of the component. Consequently, it is crucial to be able to locate the crack to prevent the structure from potential damages. Different techniques exist in this purpose. One of them is to detect changes of natural frequencies due to crack presence. This methodology is effective, inexpensive, fast and non-destructive. The principle of this method has been widely detailed in the literature [11-13]. It requires to develop very realistic models that provide the natural frequencies, knowing different crack parameters such as, for instance, the location and the depth of the crack. During this PhD, the different

models to describe the mechanical behavior of beams in free vibration have been extended to deal with the particular case of cracked structures and the main results will be briefly given in this thesis.

Other issues frequently encountered in mechanical engineering will be investigated such as the one of dynamic instability of structures subjected to an external axial load varying in time periodically, responsible of many failures of engineering structures [14] or random vibrations of beams, extensively studied in the past decades [15]. By definition, random vibration analysis describe the mechanical behavior of systems subjected to loads varying randomly with time [16]. Many structures used in the daily life are subjected to random vibration [17,18]: bridge and offshores structures in the wind, a building excited by earthquakes and wind, aerospace systems excited by atmospheric and boundary layer turbulence and jet noise or electronic components due to support motions. Random vibrations are also frequently encountered in military industry with rockets and jet engines due to turbulences [18,19].

It is worth noticing that, although it can be a source of important damages within a mechanism, vibrations can also be used for useful tasks, “such as the use of a vibrator to massage the body, to compact loose soil, to increase the workability of wet concrete and to shake sugar, pepper and salt from their containers” [20].

1.2. The advent of nanomaterials: brief presentation of carbon nanotubes and graphene nanoplates

1.2.1. Carbon nanotubes

A wide part of the literature is devoted to carbon nanotubes (CNTs), also called buckytubes, and their applications (the reader may refer for instance to the papers of Thostenson et al. [21], Sinnott and Andrews [22], Baughman et al. [23], Popov [24], Dai [25] and Liew Zhang Zhang [26]) and although his discovery in 1991 by Iijima [27] after decades of experiments [28-30] is very recent, the check on Google Scholar of the term “Carbon nanotubes” yields, at the end of the year 2017, 1 400 000 hits showing a huge interest of the scientific community for this material. Thus, the number of publications with a title containing the words “carbon nanotubes” globally increased over the last decades (see Fig. 1). In 2008, Carbon nanotubes is in the top ten of the most significant advances in materials sciences established by the journal Mater Today [31].

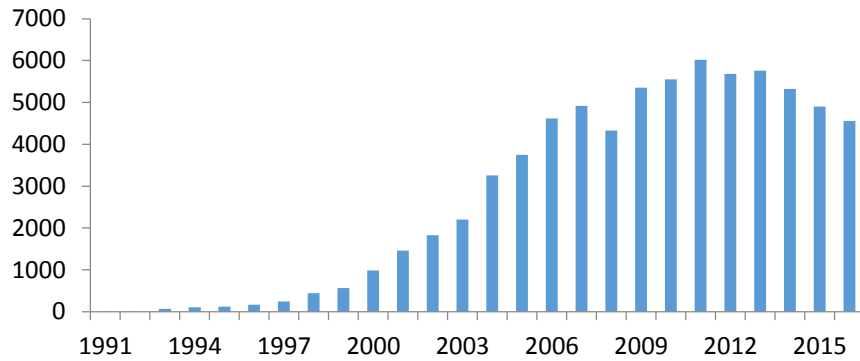


Fig. 1. Number of new publications containing the expression “carbon nanotubes” on Google Scholar

CNT is an extremely versatile material. By its amazing properties, it has a huge number of potential commercial applications [32]. Hundred times stronger than any common carbon steel, with a Young modulus five times higher than steel [33,34] and a large breaking strain [35], his mechanical behavior is much better than any other material. Thus, it is considered to use them as the main component of a new generation of composites [21,22], more efficient than the traditional ones.

CNT is also seen as a possible revolution in biomedical sciences: carrier for drug and vaccine delivery [36-38], cancer therapy [39-42], biosensors [37,43-45], scaffold material [46,47]. In addition to all these possible applications, carbon nanotubes are also characterized by amazing thermal and electric properties. Thermally stable up to 2800°C in vacuum, the thermal conductivity can reach up to 3500 W/mK at room temperature [48], almost 10 times more important than copper wires [21,49]. Thus, it is a perfect candidate for a new generation of electronic devices [23].

1.2.2. Graphene nanoplates

As for carbon nanotubes, graphene present a huge interest for the scientific community, as testifies the number of publications with a title containing the word “graphene” on Google Scholar (see Fig. 2)

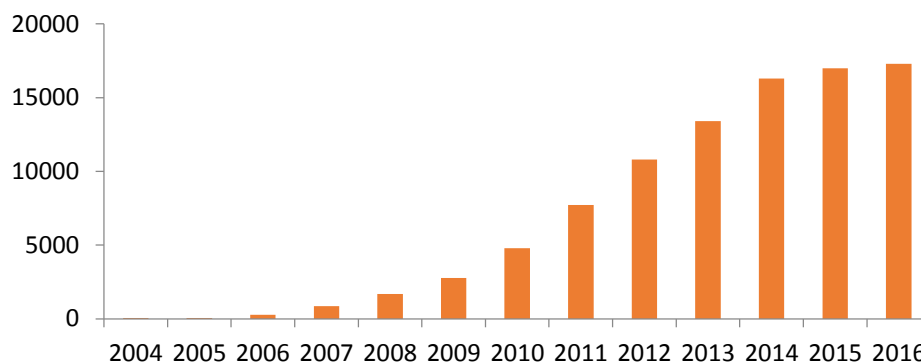


Fig. 2. Number of new publications containing the word “graphene” on Google Scholar

Graphene is a two-dimensional carbon allotrope, first isolated in 2004 by Novoselov et al. [50]. Geim and Novoselov received the Nobel Prize in Physics in 2010 [51-53] for their work about this new material that shows the remarkable properties of this new material [54]. Specifically, graphene is a single layer of carbon in which the atoms are arranged in hexagons which form a honeycomb lattice as shown in Fig. 3.

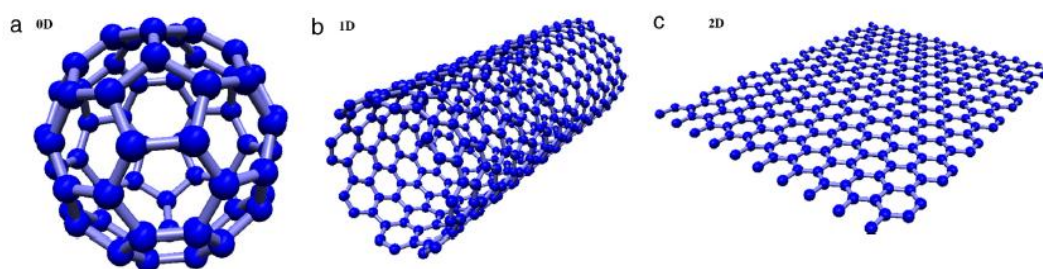


Fig. 3. Nanoscopic (a) C60 fullerene, (b) carbon nanotube and (c) graphene sheet [55]

It can be turn into fullerene, carbon nanotubes or graphite. Thus, graphite, material used for pencil leads, can be represented by a superposition of at least ten layers of graphene. Graphene is a new material with many superior properties: high electron mobility, big young modulus, huge thermal conductivity, excellent optical absorption, impermeability to any gases, ... [56]. Thus, there is a wide range of possible applications.

The electronic behavior of graphene has been investigated by many researchers these past years [54-58]. It is a zero-gap semiconductor and consequently, as explained Reich [59], “electrons in graphene move so fast that they seem to have no mass, and are, in effect, moving at the speed of light”. Thus, by using graphene, electrons move 70 times faster than by using silicon [60] and the carrier mobility reaches up to $200\,000\text{ cm}^2\text{V}^{-1}\text{s}^{-1}$ [26,61]. Because of this very high conductivity, scientists have the idea of ultrafast electronics, and specifically of a new generation of transistors.

In neurosciences, graphene may be used to build electrodes, implemented in the brain of a patient in order to have an image of his brain, smaller and more efficient than the traditional twisted wire electrodes [62,63].

In photonics, graphene has remarkable properties [56,64] (for example, graphene photonics devices can, in theory, be used for a wide spectral range from ultraviolet to infrared), hence a wide range of applications: photodetectors, optical modulators, isolator, solar cells, biosensors ... For all these applications, working prototypes are expected by the next decade, but the manufacturing cost needs to decrease before it will appear on the market.

1.2.3. Example of issues specific to nanomaterials: the surface effects

Carbon nanotubes can be seen as tubes of carbon atoms arranged in a hexagonal array or as a graphene sheet rolled into a cylindrical tube [65] and the coiling has a real influence on the properties of nanotubes [21]. This last is defined through a vector, called “chiral vector” \vec{C}_h expressed following two integers m and n and two subsidiary vectors \vec{a}_1 and \vec{a}_2 as shown in Fig. 4 with $\vec{C}_h = n\vec{a}_1 + m\vec{a}_2$. Carbon nanotubes are classified in three categories: zigzag when $m = 0$, armchair when $m = n$ and chiral for any other couple (m, n) . Figure 5 shows a carbon nanotubes arranged in ziz-zag and armchair. The couple (m, n) determines some mechanical properties of the carbon nanotubes such as the Young and shear modulus, the Poisson’s ratio, the thickness of the tube [66]. Naturally, it also changes the natural frequencies of the tube. However, it does not explicitly affect the different equations in the analytical models [67,68]. Consequently, the chiral effect will not be taken into account in the present thesis.

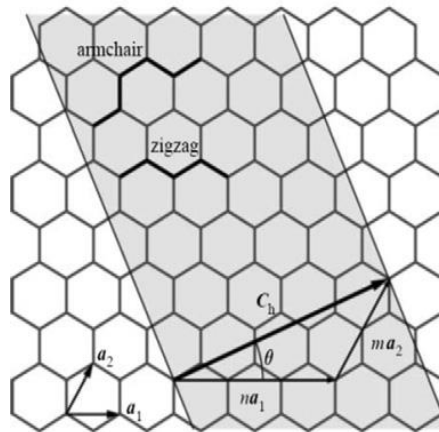


Fig. 4. Unrolled graphene sheet with definitions of basis unit vectors and chiral vector [65]

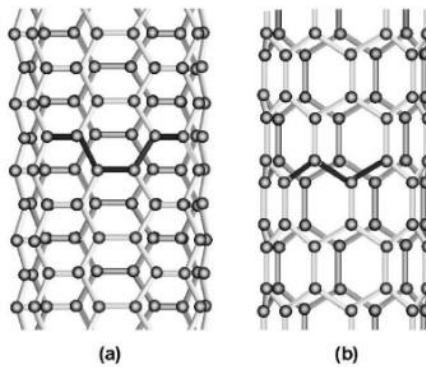


Fig. 5. Two different possible atomistic arrangements for a carbon nanotube: (a) in zigzag and (b) armchair [21]

Other effects possibly influence the behavior of the nanotube. Among them, the surface effects are present in any material at a nanoscale. The surface effect phenomena is explained by Shah and Ahmad [69] as follows: “Nanomaterials possess a large fraction of surface atoms per unit volume. Due to the vast surface area, all nanomaterials possess a huge surface energy and thus are thermodynamically unstable or metastable...Atoms or molecules possess fewer nearest neighbors or coordination numbers and thus have dangling or unsatisfied bonds exposed to the surface. Because of the dangling bonds on the surface, surface atoms or molecules and the sub surface atoms or molecules are smaller than that between interior atoms or molecules. When solid particles are very small, such a decrease in bond length between the surface atoms and interior atoms becomes significant and the lattice constants of the entire solid particles show an appreciable reduction. The extra energy possessed by the surface atoms is described as surface energy, surface free energy or surface

tension". Numerous publications have been devoted these last years to the introduction of surface effect [70-74]. In a sake of simplicity, these effects will not be taken into account hereinafter.

1.3. Different approaches to describe the mechanical behavior of macro and nanostructures in vibration

1.3.1. Experimental, analytical and numerical approaches

Three different approaches are used to observe and predict the mechanical behavior of macrostructures and carbon nanostructures (carbon nanotubes and graphene nanoplates): experimental, analytical and numerical [26]. Moreover, within both approaches, numerical tools can be used.

It is difficult to manipulate carbon nanotubes and graphene plates and so, to perform experiments on them. The main techniques to characterize carbon nanotubes are listed and detailed by Belin and Epron [75], Cooper et al. [76] and Shah and Ahmad [68]: photoluminescence spectroscopy, X-ray Photoelectron Spectroscopy (XPS), Scanning Tunneling Microscopy (STM), neutron or/and X-ray diffraction, Transmission Electronic Microscopic (TEM) (see for instance Fig. 6), infrared spectroscopy and Raman spectroscopy. Graphene is mainly studied by Atomic Force Microscopy. As explained by Liew et al. [26], *"AFM is a type of scanning probe microscopy that can visualize, measure, and manipulate matter at the nanoscale level. AFM is an effective technique used to investigate sample surfaces down to the nanometer scale. AFM can not only characterize sample surfaces but can also alter the sample surface through manipulation."*

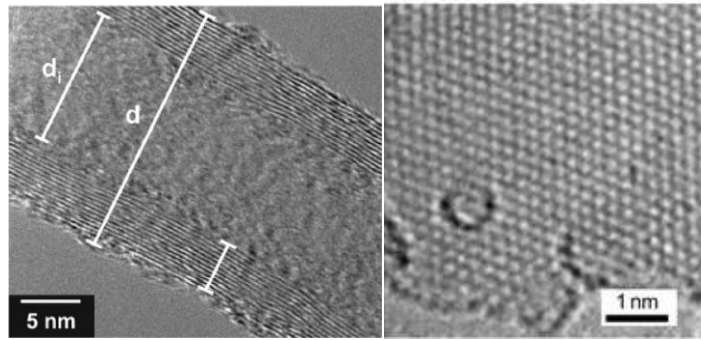


Fig. 6. TEM micrograph of a multi-walled carbon nanotubes (left) [77] and a fullerene molecule on a graphene monolayer (right) [78]

Theoretically, the approaches are separated in two categories [79,80]: atomistic modelling and continuum mechanics.

Atomistic modelling must be coupled with numerical tools and includes techniques such as Molecular Dynamics Simulations (MD), Tight-Bending Molecular Dynamics (TBMD) [81,82] and quantum mechanics calculations (QM). These methods have been and are still widely used in the literature to predict the behavior of carbon nanotubes and graphene plate [26,83,84]. For example, the chiral effect, previously described, is investigated through atomistic modelling. In the MD or Molecular Dynamic simulations (MD), an attempt is performed to minimize the variation of system energy associated with changes in atomic positions [83]. In principle, atoms are considered as particles interacting each other through several types of potential fields. Consequently, the mechanical behavior of a nanoscale material may be studied by numerically finding the minimum potential energy surface. Indeed, planar structures such as graphene sheets may deform to attain the lowest energy configuration. In this method, the differential equations of motions of particles are coupled. The TBMD and QM methods slightly differ in the definition of potentials. Therefore, even if this method provides accurate results [84], it is also highly time consuming and needs much computational efforts. Thus, a compromise must be done between the time to compute the results and the accuracy of those results.

Continuum mechanics represents the structure as continuous. The objective is to describe analytically the mechanical behavior of the structure (for instance in vibration or buckling) through equations. The obtained solution is exact. Thus, this approach, compared to atomistic models, is much simpler and less computationally expensive [80,84] and consequently, It is the one chosen for this PhD.

This PhD thesis attempts to answer to the following question: how to analytically describe the mechanical behavior in vibration of macrostructures and carbon nanostructure? Specifically, the objective of the overall dissertation is, for different kinds of structures (beams and plates), at different scales (macro and nano) and for different particular loads (free vibration, under random vibrations, ...), to develop the best model to describe the answer of the system.

1.3.2. Analytical study of macro beams and plates

The oldest known model describing the transverse vibration of beams has been proposed by Bernoulli [85] and the first solution of the problem by Euler [86]. This theory, commonly referred as the Bernoulli-Euler (BE) model is valid for thin beams. For thick beams, it overestimates the natural frequencies because it does not take into account the rotary inertia and the shear effects. Following to the works of Bresse [87] and Rayleigh [88], Timoshenko [89] introduced his governing differential equations that take into account shear deformation and rotary inertia. This model is the Original Bresse-Timoshenko (OBT) model. An extensive review of this approach was provided recently by Elishakoff, Kaplunov and Nolde [90]. This thesis proposes two alternative Bresse-Timoshenko models: the truncated Bresse-Timoshenko model (TBT) [91-95] and the Bresse-Timoshenko model based on slope inertia (SBT) [91-95]. Other approaches have been considered in the literature (one may refer to the reviews of Ghugal and Shimpi [96] and Hajianmaleki and Qatu [97]).

Analogically, the vibration of plates has been widely investigated the last centuries. The first theory has been initiated by Sophie Germain [98] and Lagrange [99]. This Germain-Lagrange theory established the governing partial differential equations describing the mechanical behavior of thin plates in vibrations. A few years later, Kirchhoff [100] brought many additional results about theory of thin plates. Although this theory, referred as the Kirchhoff-Love (KL) theory or Classical Plate Theory, analogically to the Bernoulli-Euler model for thin beam, is very accurate for thin plates, it neglects the effects of shear deformation and rotatory inertia resulting in the over-estimation of vibration frequencies. Thus, the classical plate theory produces accurate solutions until the thickness-to-length ratio reaches a value of about 1/20 [20,101], ratio above which a plate is considered as thick. In the last century, lot of efforts have been made to describe the behavior of thick plates. The First order Shear Deformation Theory, also called Uflyand-Mindlin plate theory following to the works of Uflyand [102] and Mindlin [103,104] includes the effects of shear deformation and rotary

inertia. This theory constitutes an extension of the Bresse-Timoshenko beam theory for plates and as for beams, it will be proposed hereinafter a truncated version of this theory, presented in the literature a few decades ago [105-109], and another one based on slope inertia [108,109]. Since the last decades, the Uflyand-Mindlin plate model has been widely studied in the literature [110-114].

These different theories are sufficient to describe the mechanical behavior of macro beams and plates. However, they do not capture the small scale effects such as the inter-atomic interactions that cannot be neglected at a nanoscale and consequently, they do not provide satisfying results: new sets of theories have to be developed.

1.3.3. Nonlocal theories

1.3.3.1. Introduction to the nonlocal approaches

As explained before, there is a real interest to analytically describe, through the derivation of governing differential equations, the mechanical behavior of small scale structures. Most of nanomaterials cannot be considered as homogeneous at small scales. At an extremely fine scale, some effects such as the interactions between two successive atoms cannot be ignored. Thus, there is a need to adapt classical mechanics to take into account these specific interactions at the material scale. Thus, nonlocal continuum theories, initiated in the 60's [115-122], in contrast to the traditional and previously described local ones, can be used to capture the discreteness of the material at the subscale. In the nonlocal theories, the stress at a certain point is "a functional of the strain field at every point in the body" [119,120,123].

The phenomenological nonlocal stress gradient elasticity model, proposed by Eringen [123], postulates a stress gradient nonlocal law, using a differential operator, as follows:

$$[1 - \eta^2 \nabla^2] \boldsymbol{\sigma} = \mathbf{D} : \boldsymbol{\varepsilon} \quad (1.1)$$

where \mathbf{D} is the elasticity tensor, $\boldsymbol{\sigma}$ and $\boldsymbol{\varepsilon}$ are the macroscopic stress and strain tensors and ∇^2 is the Laplacian operator. η is a nonlocal parameter equal to $e_0 a$, with a the internal characteristic length and e_0 the small length scale coefficient. This coefficient is supposed constant, independent of the load, or the geometry of the structure, depending only on the

considered material. Even if it is commonly admitted that it is smaller than unity, Wang and Varadan [124] suggested that it goes from 0 to 7.

One of the aims of this thesis is to investigate the nonlocal extension of the different Bresse-Timoshenko, Uflyand-Mindlin and asymptotic models

1.3.3.2. Calibration of the small length scale coefficient: from the necessity to develop continualized models

One of the main issues of these last decades has been to calibrate this coefficient. Thus, in his original paper, Eringen [123] proposed $e_0 \approx 0.39$. A possible approach is to calibrate this coefficient by considering the analytical equivalence between lattice and nonlocal models [125], as it has been done recently in the literature (see for instance [126-129]). Then, a calibration of the small length scale coefficient is made possible by equating the buckling load in statics or the natural frequencies in dynamics in the two models. Thus, the small length-scale coefficient e_0 lies between $1/\sqrt{24}$ and $1/\sqrt{6}$ with the buckling and vibration mode, the geometry and the load. Thus, the constant coefficient is not constant, leading to a paradoxical result.

Furthermore, in parallel to the nonlocal continuum theories, a basic approach to model nanostructures and the interatomic interactions within them is to represent by an assembly of finite number of beams connected by springs [130], representing the bonds between the atoms, cells of the lattice. The asymptotic equivalence between discrete and continuous systems is not new and has already been established a few centuries ago by Lagrange [99]. It appears that this representation is particularly accurate to describe the mechanical behavior of nanostructures in which the atoms are the cells and the bonds between the atoms may be represented by the springs. For instance, Hencky [131] investigated the mechanical behavior of Bernoulli-Euler beams by considering a chain of rigid segmented beams connected by elastic rotational springs. This work has been, since the last decades, extended to thin plates [126,132-138] models. Recently, Duan et al. [127], Zhang et al. [128] and Kocsis et al. [139] derived discrete equations to describe the behavior in vibration [127] and buckling [128] of thick microstructured beams including shear effects by introducing in the model additional shear springs. The derivation of lattice models for thick plates in free vibration has not been investigated and yet, it presents an interest for the scientific community.

As explained before, for the nonlocal phenomenological Eringen's approach, a paradox appears because the constant small length scale coefficient is structural dependent. To solve this paradox, alternative nonlocal models have emerged in order to keep a constant small length scale coefficient based on micromechanics arguments. In recent years, this new subset of continualized theories raised the attention of the scientific community and the number of publications devoted to this topic has increased exponentially [134,135,140,141]. The continualization process is based on the derivation of continuous equations from the reference discrete lattice model [142]. Starting from the lattice model, the difference operators are approximated by equivalent continuous differential ones and expanded by using the Taylor series [141] or an expansion based on the use of Padé approximants [143-146]. In the continualized approaches, the small length scale coefficient is constant by definition [142] and is associated with the internal characteristic length of the lattice spacing. The objective is to develop continuous equations that contain the characteristic properties of a discrete structure [142]. The continualized process is applied for thin beams [126,133,135,147] and plates [126,134,135]. Recently, Duan et al. [127] and Zhang et al. [148] proposed a continualized model for thick beams in buckling [148] and vibration [127]. This topic will be addressed hereinafter.

1.3.4. Asymptotic models

The Bresse-Timoshenko and Uflyand-Mindlin models are phenomenological models. They are based on postulated constitutive laws or energy functional, leading potentially to some approximation in the governing differential equations, whence the different Bresse-Timoshenko and Uflyand-Mindlin models (original, truncated and based on slope inertia). In addition to the phenomenological models, another family of beam and plate models attracted much attention these last decades. Indeed, the asymptotic models have been used for beams [95,149,150] and plates [109,151-153].

For plates, this method starts from the 3-dimensional equations and, by expanding some variables (displacements, stresses, strains) in power series in term of small parameters (for instance the thickness ratio [95,154] or the nonlocal parameter [152]), it yields approximate equations [47], the accuracy and the complexity of the equations increasing with the order of the expansion [155]. Likewise, considering a two-dimensional problem, the governing differential equations in displacement for beams are obtained [156].

Thus, as it will be shown hereinafter, the asymptotic methods validates, at the lowest order, the Bernoulli-Euler [149] and Kirchhoff-Love [157] models and at the second order, the truncated Bresse-Timoshenko [95,150] and Uflyand-Mindlin [109].

The extension of the asymptotic derivation to include the nonlocal effect is very recent. Thus, Chebakov, Kaplunov and Rogerson [152] proposed an asymptotic derivation of the thin plate equations by using the integral formulation of the nonlocal stress-strain constitutive law [119]. To our best knowledge, in the literature, the asymptotic derivation based on the series expansions of the deflection of the nonlocal beam and plates equations starting from the gradient form of the stress-strain relation Eq. (1.1) has not been performed. One of the objectives of this thesis is to present such derivations.

Thus, there are many different theories to describe the mechanical behavior of beams and plates at different scales. The choice of the model depends on the need. For all of them, once the equations are derived, the natural frequencies of the structures have to be determined. In this purpose, different methods exist.

1.4. Different methods of resolution of governing differential equations

In the different analytical models described hereinafter, the behavior of beams and plates is described by a governing differential equation in displacement from which the natural frequencies can be extracted.

For a beam simply supported at both ends and an all edge simply supported plate, a closed-form solution is derived for all the models through the Navier approach. Thus, it allows us to perform a simple and efficient comparison of the different models. For beams, considering any other set of boundary conditions, the problem is reduced to the determination of the roots of a characteristic equation, leading to an exact solution. For plates having two opposite edges simply supported, the Lévy approach is used in order to have a characteristic equation, and so, an exact solution. Thus, considering the Kirchhoff-Love plate model and by using this method, the characteristic equations have been derived in a first time derived for thin rectangular plates [158-161]. A few decades later, scientists proposed to extend these results to the case of thick plates (see for instance [108,162]).

For other boundary conditions, there is no method leading to an exact solution and numerical tools are needed. Among them, the Rayleigh-Ritz method, initiated by Rayleigh [88] and developed by Ritz [163] is widely used in the literature [20,164,165]. The displacements are set as series of functions (trigonometric, polynomial, ...) that satisfy the geometric plate boundary conditions [166-169]. The coefficients associated to these functions must minimize the energy functional, yielding to the approximated natural frequencies. An increase of the number of admissible functions leads to a better accuracy of the model but also increases the computational time [20].

Other numerical approaches such as the Gorman's superposition method [170-173] or the well-known finite element analysis [174,175] could be used. This thesis being devoted to the study analytical models with exact and closed-form solutions, the different numerical methods will not be considered.

2. TOWARDS THE DEVELOPMENT OF THICK BEAM AND PLATE MODELS FOR MACROSTRUCTURES

This chapter starts by presenting the different derivations of the local thin Bernoulli-Euler and thick Bresse-Timoshenko models (original, truncated and based on slope inertia), introduced in the previous chapter. Thus, different approaches are considered: based on the use of equilibrium equations, via the variational principle and through the asymptotical reduction method. For each of these models, the first natural frequencies are calculated for different boundary conditions (simply supported at both end, clamped at both end, clamped-simply supported and cantilever) and the models are compared. The governing differential equation and the solutions of a beam with a tip mass is further investigated. A brief survey of the results obtained during this PhD thesis about stability of beams, cracked beams and beams subjected to random vibrations will also be included. Then, these results are extended to derive three versions of the Uflyand-Mindlin plate model. The natural frequencies are obtained for plates with at least two simply supported opposite edges.

2.1. Derivation of thick beam models and different applications

2.1.1. Original Bresse-Timoshenko model

Consider a beam of length L , shear modulus G , cross-section A , Young modulus E , Poisson's ratio ν , density ρ , moment of inertia I . v is the transverse deflection of the beam, ψ "the slope of the deflection curve when the shearing force is neglected" (the one given in the Bernoulli-Euler thin beam model) [176] and β the shear angle (see Fig. 7), v is related to ψ and β via [89]:

$$\beta = \frac{\partial v}{\partial x} - \psi \quad (2.1)$$

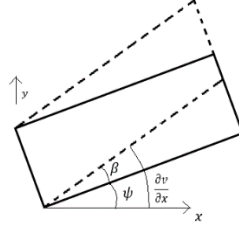


Fig. 7: Bending and shear deformation : Angle ψ (continuous lines) and angle β (dashed lines)

The constitutive laws in bending moment and shearing force are:

$$M = EI \frac{\partial \psi}{\partial x} \quad (2.2)$$

$$V_y = -\kappa AG \left(\frac{\partial v}{\partial x} - \psi \right) \quad (2.3)$$

where κ is the shear coefficient, V_y is the shearing force, M is the bending moment.

The equilibrium equation is:

$$-V_y + \frac{\partial M}{\partial x} - \rho I \frac{\partial^2 \psi}{\partial t^2} = 0 \quad (2.4)$$

Substituting the expressions of Eqs. (2.2) and (2.3) into Eq. (2.4), one obtains the first equation of motion

$$EI \frac{\partial^2 \psi}{\partial x^2} + \kappa AG \left(\frac{\partial v}{\partial x} - \psi \right) - \rho I \frac{\partial^2 \psi}{\partial t^2} = 0 \quad (2.5)$$

The shear force is related to the transverse displacement through the following equation:

$$\frac{\partial V_y}{\partial x} = -\rho A \frac{\partial^2 v}{\partial t^2} \quad (2.6)$$

Combining Eqs. (2.3) and (2.6) yields to the second equation of motion

$$\kappa AG \left(\frac{\partial^2 v}{\partial x^2} - \frac{\partial \psi}{\partial x} \right) - \rho A \frac{\partial^2 v}{\partial t^2} = 0 \quad (2.7)$$

Manipulating the equations of motions Eqs. (2.5) and (2.7) leads to the governing differential equation,

$$EI \frac{\partial^4 v}{\partial x^4} + \rho A \frac{\partial^2 v}{\partial t^2} - \rho I \left(1 + \frac{E}{\kappa G} \right) \frac{\partial^4 v}{\partial t^2 \partial x^2} + \frac{\rho^2 I}{\kappa G} \frac{\partial^4 v}{\partial t^4} = 0 \quad (2.8)$$

This equation contains a fourth order time derivative term. There is an important debate about this term. Checking the different contributions of the terms in Eq (2.8) Weaver, Timoshenko and Young [176] showed that the fourth order time derivative term is extremely small and can be neglected compared to the other terms. A detailed study of this term and its influence on the natural frequencies of the beam is provided hereinafter.

Furthermore, a variational derivation of Bresse-Timoshenko beam equations has been proposed in the literature (see for instance [177-179]). Thus, the kinetic energy and the strain energies due to the bending moment V_b and the shear effect V_s are expressed as

$$T = \frac{1}{2} \int_0^L \rho A \left(\frac{\partial v}{\partial t} \right)^2 dx + \frac{1}{2} \int_0^L \rho I \left(\frac{\partial \psi}{\partial t} \right)^2 dx \quad (2.9)$$

$$V_b = \frac{1}{2} \int_0^L EI \left(\frac{\partial \psi}{\partial x} \right)^2 dx \quad (2.10)$$

$$V_s = \frac{1}{2} \int_0^L \kappa GA \left(\frac{\partial v}{\partial x} - \psi \right)^2 dx \quad (2.11)$$

It is worth noticing that the bending strain energy, through the use of ψ , and the energy V_s include in their expression the influence of the shear effect. The kinetic should only describe the effect of rotary inertia. However, by using ψ in the second term of the energy, Timoshenko made a correction of the rotary inertia via the shear effect. Thus, this effect may be possibly overcorrected. This issue will be further investigated in the section devoted to the Bresse-Timoshenko model based on slope inertia.

The application of the Hamilton's principle leads to the differential equations of motions Eqs. (2.5) and (2.7), leading to the governing differential equation Thus, Eq. (2.8) is obtained. Furthermore, the associated boundary conditions are:

$$\left(EI \frac{\partial \psi}{\partial x} \right) \delta \psi \Big|_0^L = 0 \quad (2.12)$$

$$\left[\kappa GA \left(\frac{\partial v}{\partial x} - \psi \right) \right] \delta v \Big|_0^L = 0 \quad (2.13)$$

2.1.2. Truncated version of the Bresse-Timoshenko model through an asymptotic approach

In the literature [90,180-184], it has been suggested to delete the fourth order time derivative in the governing differential equation, leading to a *simpler* equation. Thus, the truncated Bresse-Timoshenko model [184] is derived by correcting Eq. (2.5) by

$$EI \frac{\partial^2 \psi}{\partial x^2} + \kappa AG \left(\frac{\partial v}{\partial x} - \psi \right) - \rho I \frac{\partial^3 v}{\partial x \partial t^2} = 0 \quad (2.14)$$

Elimination of ψ from Eqs. (2.7) and (2.14) results in the truncated Bresse-Timoshenko equation

$$EI \frac{\partial^4 v}{\partial x^4} + \rho A \frac{\partial^2 v}{\partial t^2} - \rho I \left(1 + \frac{E}{\kappa G} \right) \frac{\partial^4 v}{\partial t^2 \partial x^2} = 0 \quad (2.15)$$

In the truncated Bresse-Timoshenko model, the fourth order time derivative is not present. As it will be shown hereinafter, a direct consequence is that, in contrast to the original Bresse-Timoshenko model, it predicts only one branch of natural frequencies. Stephen [185] argued that the second branch in the original model was “unphysical” and so, it should be disregarded, although this statement has been, by the next, contradicted by some other authors.

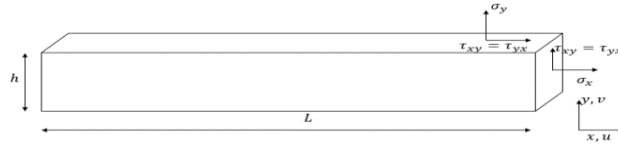


Fig. 8: Beam of length L , height h , displacements u and v in the x and y direction, respectively

An asymptotic derivation of this truncated Bresse-Timoshenko is now proposed hereinafter, u denotes the displacement in the x direction. First of all, the stress-displacement relationship (plane stress assumptions) are expressed as [179]:

$$\sigma_x = \frac{E}{(1-\nu^2)} \left(\frac{\partial u}{\partial x} + \nu \frac{\partial v}{\partial y} \right); \sigma_y = \frac{E}{(1-\nu^2)} \left(\frac{\partial v}{\partial y} + \nu \frac{\partial u}{\partial x} \right); \tau_{xy} = \frac{E}{2(1+\nu)} \left(\frac{\partial u}{\partial y} + \frac{\partial v}{\partial x} \right) \quad (2.16)$$

where σ_x and σ_y are the normal stresses following the x and y direction and $\tau_{xy} = \tau_{yx}$ is the shear stress, respectively (see Fig. 8).

The equilibrium equations are [186]

$$\frac{\partial \sigma_x}{\partial x} + \frac{\partial \tau_{xy}}{\partial y} - \rho \frac{\partial^2 u}{\partial t^2} = 0; \quad \frac{\partial \tau_{yx}}{\partial x} + \frac{\partial \sigma_y}{\partial y} - \rho \frac{\partial^2 v}{\partial t^2} = 0 \quad (2.17)$$

Substituting Eq. (2.16) into Eq. (2.17), one obtains a system of two equations with the displacements u and v as unknowns:

$$\frac{E}{2(1+\nu)} \frac{\partial^2 u}{\partial y^2} + \frac{E}{2(1-\nu)} \frac{\partial^2 v}{\partial x \partial y} + \frac{E}{(1-\nu^2)} \frac{\partial^2 u}{\partial x^2} - \rho \frac{\partial^2 u}{\partial t^2} = 0 \quad (2.18)$$

$$\frac{E}{(1-\nu^2)} \frac{\partial^2 v}{\partial y^2} + \frac{E}{2(1-\nu)} \frac{\partial^2 u}{\partial x \partial y} + \frac{E}{2(1+\nu)} \frac{\partial^2 v}{\partial x^2} - \rho \frac{\partial^2 v}{\partial t^2} = 0 \quad (2.19)$$

The boundary conditions require that the shear stress vanish on the free surfaces of the beam [187]:

$$\sigma_y(x, h/2) = \sigma_y(x, -h/2) = 0; \quad \tau_{yx}(x, h/2) = \tau_{yx}(x, -h/2) = 0 \quad (2.20)$$

The asymptotic method is based on the power series expansion of the displacements. Thus, u and v are expressed as follows:

$$u = \sum_{k=0}^{\infty} u_k(x, t) \frac{y^k}{k!}; \quad v = \sum_{k=0}^{\infty} v_k(x, t) \frac{y^k}{k!} \quad (2.21)$$

Define, arbitrarily, an angle of rotation θ_0 , different from ψ or β , such as:

$$\theta_0 = \frac{\partial u}{\partial y}(x, 0, t) = u_1(x, t) \quad (2.22)$$

Naturally, the transverse displacement v is symmetric in the axial coordinate y with respect to the neutral layer. From Eqs. (2.18) and (2.19), it is deduced that the displacement u is antisymmetric. Thus, only the even terms for u and the odd terms for v are retained, leading to:

$$u = \sum_{k=1}^{\infty} u_{2k-1}(x, t) \frac{y^{2k-1}}{(2k-1)!}; \quad v = \sum_{k=0}^{\infty} v_{2k}(x, t) \frac{y^{2k}}{(2k)!} \quad (2.23)$$

Setting $c^2 = G/\rho$, substituting Eqs. (2.23) into Eqs. (2.18) and (2.19), it yields to, for any integer k a differential relationship between $v_{2(k+1)}$, u_{2k+1} and v_{2k} and another between u_{2k+1} , u_{2k-1} and v_{2k}

$$v_{2(k+1)} = -\frac{1+\nu}{2} \frac{\partial u_{2k+1}}{\partial x} - \frac{1-\nu}{2} \frac{\partial^2 v_{2k}}{\partial x^2} + \frac{1-\nu}{2c^2} \frac{\partial^2 v_{2k}}{\partial t^2} \quad (2.24)$$

$$u_{2k+1} = -\frac{1+\nu}{1-\nu} \frac{\partial v_{2k}}{\partial x} - \frac{2}{1-\nu} \frac{\partial^2 u_{2k-1}}{\partial x^2} + \frac{1}{c^2} \frac{\partial^2 u_{2k-1}}{\partial t^2} \quad (2.25)$$

Substituting Eq. (2.16) into Eq. (2.20), the boundary conditions are given in term of displacement:

$$\frac{\partial v(x, h/2, t)}{\partial y} + \nu \frac{\partial u(x, h/2, t)}{\partial x} = 0; \quad \frac{\partial u(x, h/2, t)}{\partial y} + \nu \frac{\partial v(x, h/2, t)}{\partial x} = 0 \quad (2.26)$$

Substituting Eq. (2.23) into Eq. (2.26), it yields to:

$$\sum_{k=1}^{\infty} \left(v_{2k} + \nu \frac{\partial u_{2k-1}}{\partial x} \right) \frac{\left(\frac{h}{2}\right)^{2k-1}}{(2k-1)!} = 0 \quad (2.27)$$

$$\sum_{k=0}^{\infty} \left(u_{2k+1} + \frac{\partial v_{2k}}{\partial x} \right) \frac{\left(\frac{h}{2}\right)^{2k}}{(2k)!} = 0 \quad (2.28)$$

Dimensionless variables are defined as follows:

$$\bar{u}_i = L^{i-1} u_i; \quad \bar{v}_i = L^{i-1} v_i; \quad \xi = \frac{x}{L}; \quad \bar{h} = \frac{h}{2L}; \quad \bar{t} = \frac{htc}{2L^2} \quad (2.29)$$

Eq. (2.27) and Eq. (2.28) are re-expressed as, at the fourth order:

$$\left(\bar{v}_2 + \nu \frac{\partial \bar{u}_1}{\partial \xi} \right) + \frac{\bar{h}^2}{6} \left(\bar{v}_4 + \nu \frac{\partial \bar{u}_3}{\partial \xi} \right) + \frac{\bar{h}^4}{120} \left(\bar{v}_6 + \nu \frac{\partial \bar{u}_5}{\partial \xi} \right) + o(\bar{h}^4) = 0 \quad (2.30)$$

$$\left(\bar{u}_1 + \frac{\partial \bar{v}_0}{\partial \xi} \right) + \frac{\bar{h}^2}{2} \left(\bar{u}_3 + \frac{\partial \bar{v}_2}{\partial \xi} \right) + \frac{\bar{h}^4}{24} \left(\bar{u}_5 + \frac{\partial \bar{v}_4}{\partial \xi} \right) + o(\bar{h}^4) = 0 \quad (2.31)$$

and Eqs. (2.24) and (2.25), under the non-dimensional form are

$$\bar{u}_{2k+1} = \mathcal{A}_L^b \bar{u}_{2k-1} + \mathcal{B}_L^b \bar{v}_{2k} \quad (2.32)$$

$$\bar{v}_{2(k+1)} = \mathcal{C}_L^b \bar{v}_{2k} + \mathcal{F}_L^b \bar{u}_{2k+1} \quad (2.33)$$

where the operators \mathcal{A}_L^b , \mathcal{B}_L^b , \mathcal{C}_L^b and \mathcal{F}_L^b are defined as follows:

$$\mathcal{A}_L^b = \bar{h}^2 \frac{\partial^2}{\partial \bar{t}^2} - \frac{2}{(1-\nu)} \frac{\partial^2}{\partial \xi^2}; \quad \mathcal{B}_L^b = -\frac{1+\nu}{1-\nu} \frac{\partial}{\partial \xi}; \quad (2.34)$$

$$\mathcal{C}_L^b = \frac{1-\nu}{2} \left(\bar{h}^2 \frac{\partial^2}{\partial \bar{t}^2} - \frac{\partial^2}{\partial \xi^2} \right); \quad \mathcal{F}_L^b = -\frac{1+\nu}{2} \frac{\partial}{\partial \xi}$$

Substituting Eqs. (2.32) and (2.33) into Eqs. (2.30) and (2.31), it yields a system of equations in θ and \bar{v}_0 , expressed in a matrix form:

$$\begin{pmatrix} M_{11} & M_{12} \\ M_{21} & M_{22} \end{pmatrix} \begin{pmatrix} \bar{v}_0 \\ \theta_0 \end{pmatrix} = \begin{pmatrix} 0 \\ 0 \end{pmatrix}$$

with:

$$\begin{aligned} M_{11} &= -\frac{\partial^2}{\partial \bar{x}^2} - \left[\frac{\partial^2}{\partial \bar{t}^2} + \frac{1}{6}(1-\nu) \frac{\partial^4}{\partial \xi^4} \right] \nu \bar{h}^2 \\ &\quad + \frac{1}{12} \left[(1-\nu)(3\nu-1) \frac{\partial^4}{\partial \xi^2 \partial \bar{t}^2} - \frac{1-\nu+2\nu^2}{10} \frac{\partial^6}{\partial \xi^6} \right] \bar{h}^4 + O(\bar{h}^4) \\ M_{12} &= (\nu-1) \left\{ -\frac{\partial}{\partial \xi} - \frac{(\nu+2)}{6} \bar{h}^2 \frac{\partial^3}{\partial \xi^3} \right. \\ &\quad \left. + \frac{1}{12} \left[\frac{(2\nu+3)}{10} \frac{\partial^5}{\partial \xi^5} + (\nu+3) \frac{\partial^5}{\partial \xi \partial \bar{t}^2} \right] \bar{h}^4 \right\} + O(\bar{h}^4) \\ M_{21} &= \frac{\partial}{\partial \bar{x}} + \frac{\nu}{2} \bar{h}^2 \frac{\partial^3}{\partial \xi^3} - \left(\frac{1}{2} \nu \frac{\partial^3}{\partial \xi \partial \bar{t}^2} + \frac{1+2\nu}{24} \frac{\partial^5}{\partial \xi^5} \right) \bar{h}^4 + O(\bar{h}^4) \\ M_{22} &= 1 - \frac{2+\nu}{2} \bar{h}^2 \frac{\partial^5}{\partial \xi^5} + \left(\frac{1}{2} \frac{\partial^2}{\partial \bar{t}^2} + \frac{3+2\nu}{24} \frac{\partial^4}{\partial \xi^4} \right) \bar{h}^4 + O(\bar{h}^4) \end{aligned} \quad (2.35)$$

The determinant of the differential matrix system has to vanish. It leads to the governing differential equation in displacement \bar{v}_0 at different orders:

- Zeroth order

$$\left[\frac{2}{3}(\nu+1) \frac{\partial^4 \bar{v}_0}{\partial \xi^4} + \frac{\partial^2 \bar{v}_0}{\partial \bar{t}^2} \right] = 0 \quad (2.36)$$

- Second order

$$\left[\frac{2}{3}(\nu+1) \frac{\partial^4 \bar{v}_0}{\partial \xi^4} + \frac{\partial^2 \bar{v}_0}{\partial \bar{t}^2} \right] - \frac{2}{3} \left[\frac{(\nu+1)}{5} \frac{\partial^6 \bar{v}_0}{\partial \xi^6} + (\nu+2) \frac{\partial^4 \bar{v}_0}{\partial \xi^2 \partial \bar{t}^2} \right] \bar{h}^2 = 0 \quad (2.37)$$

These two equations are written under the dimensional form as follows:

- Zeroth order

$$EI \frac{\partial^4 v}{\partial x^4} + \rho A \frac{\partial^2 v}{\partial t^2} = 0 \quad (2.38)$$

- Second order

$$EI \frac{\partial^4 v}{\partial x^4} + \rho A \frac{\partial^2 v}{\partial t^2} - \frac{EI^2}{A\kappa_0} \frac{\partial^6 v}{\partial x^6} - \rho I \left(1 + \frac{E}{\kappa G} \right) \frac{\partial^4 v}{\partial x^2 \partial t^2} = 0 \quad (2.39)$$

with:

$$\kappa_0 = \frac{5}{3}; \tilde{\kappa} = \frac{2(1 + \nu)}{3 + 2\nu}$$

At the zeroth order, the asymptotic model coincides with the Bernoulli-Euler model for thin beams. Thus, the Bernoulli-Euler model is asymptotically consistent. One recognizes in the asymptotic model at the second order an equation, close to the one of the truncated Bresse-Timoshenko model with an additional sixth order spatial derivative. It is worth noticing that Eq. (2.37) can be rewritten as

$$\frac{2}{3}(\nu + 1) \left[1 - \frac{\bar{h}^2}{5} \frac{\partial^2}{\partial \xi^2} \right] \frac{\partial^4 \bar{v}_0}{\partial \xi^4} + \frac{\partial^2 \bar{v}_0}{\partial \bar{t}^2} - \frac{2}{3}(\nu + 2) \frac{\partial^4 \bar{v}_0}{\partial \xi^2 \partial \bar{t}^2} \bar{h}^2 = 0 \quad (2.40)$$

Multiplying by $[1 + (\bar{h}^2/5)(\partial^2/\partial \xi^2)]$ Eq. (2.40) and neglecting the terms in \bar{h}^4 results in an equation without a sixth order space derivative term:

$$\begin{aligned} \frac{2}{3}(\nu + 1) \frac{\partial^4 \bar{v}_0}{\partial \xi^4} + \frac{\partial^2 \bar{v}_0}{\partial \bar{t}^2} + \left[\frac{1}{5} - \frac{2}{3}(\nu + 2) \right] \frac{\partial^4 \bar{v}_0}{\partial \xi^2 \partial \bar{t}^2} \bar{h}^2 - \frac{2}{15}(\nu \\ + 2) \frac{\partial^6 \bar{v}_0}{\partial \xi^4 \partial \bar{t}^2} \bar{h}^4 = 0 \end{aligned} \quad (2.41)$$

Under the dimensional form, it yields to the governing differential equation of the truncated Bresse-Timoshenko as obtained by Elishakoff, Kaplunov and Nolde [90] with a shear correction factor $\kappa = 5(\nu + 1)/(6 + 5\nu)$.

This value of κ has been used implicitly by Timoshenko himself [188] and explicitly in numerous papers [90,189,190].

The relevant question now is to investigate the variational derivation of this truncated version.

2.1.3. Bresse-Timoshenko based on slope inertia

Based on the truncated Bresse-Timoshenko model, it is suggested to replace the kinetic energy in Eq. (2.9) by:

$$T = \frac{1}{2} \int_0^L \rho A \left(\frac{\partial v}{\partial t} \right)^2 dx + \frac{1}{2} \int_0^L \rho I \left(\frac{\partial^2 v}{\partial t \partial x} \right)^2 dx \quad (2.42)$$

The difference between Eqs. (2.9) and (2.42) is the second term of the kinetic energy. The original Bresse-Timoshenko includes in the expression of the kinetic energy a correction of the shear effect, already present in the shear strain energy. Thus, it overcorrected the shear effect. So, it is suggested to replace $\partial\psi/\partial t$ by $\partial^2 v/\partial t\partial x$, following the spirit of the truncated Bresse-Timoshenko derivation. This model is a new version of the Bresse-Timoshenko model based on the modification of the angle including the shear effect by the slope in order to take into account only the rotary inertia. It will be referred hereinafter as a Bresse-Timoshenko model based on slope inertia.

By applying the Hamilton principle, it results in the following partial differential equations of motion:

$$\rho A \frac{\partial^2 v}{\partial t^2} - \kappa GA \left(\frac{\partial^2 v}{\partial x^2} - \frac{\partial \psi}{\partial x} \right) - \rho I \frac{\partial^4 v}{\partial x^2 \partial t^2} = 0 \quad (2.43)$$

$$EI \frac{\partial^2 \psi}{\partial x^2} + \kappa GA \left(\frac{\partial v}{\partial x} - \psi \right) = 0 \quad (2.44)$$

with the boundary condition Eq. (2.12) unchanged and Eq. (2.13) replaced by:

$$\left[\kappa GA \left(\frac{\partial v}{\partial x} - \psi \right) + \rho I \left(\frac{\partial^3 v}{\partial t^2 \partial x} \right) \right] \delta v \Big|_0^L = 0 \quad (2.45)$$

Compared to Eq. (2.8), this equation contains an additional term containing the time derivative. After some manipulations, Eqs. (2.43) and (2.44) lead to the following governing differential equation:

$$EI \frac{\partial^4 v}{\partial x^4} + \rho A \frac{\partial^2 v}{\partial t^2} - \rho I \left(1 + \frac{E}{\kappa G} \right) \frac{\partial^4 v}{\partial x^2 \partial t^2} + \frac{\rho EI^2}{\kappa GA} \frac{\partial^6 v}{\partial x^4 \partial t^2} = 0 \quad (2.46)$$

Compared to the governing differential equation of the original Bresse-Timoshenko model, it is seen that Eq. (2.46) contains an additional term, underlined in the last equation. Thus, the three versions of the Bresse-Timoshenko model differ in the expression of a dynamic term. Let us now compare the different Bresse-Timoshenko models in free vibration considering different boundary conditions.

2.1.4. Different solutions

2.1.4.1. Simply supported beam

The governing differential equations in displacement of the different models can be written in a generic form as follows:

$$EI \frac{\partial^4 v(x, t)}{\partial x^4} + \rho A \frac{\partial^2 v(x, t)}{\partial t^2} - \rho I \left(1 + \frac{E}{\kappa G} \right) \frac{\partial^4 v(x, t)}{\partial t^2 \partial x^2} + \gamma_1 \frac{\rho^2 I \partial^4 v(x, t)}{\kappa G \partial t^4} + \gamma_2 \frac{\rho E I^2}{\kappa G A} \frac{\partial^6 v}{\partial x^4 \partial t^2} = 0 \quad (2.47)$$

where γ_1 and γ_2 are control parameters such as (γ_1, γ_2) is equal to (1,0), (0,0) and (0,1) for the original Bresse-Timoshenko model, the truncated Bresse-Timoshenko theory and the Bresse-Timoshenko model based on slope inertia, respectively. The variable ψ is governed by the same equation.

For a beam that is simply supported at both ends, the displacement is expressed following the Navier expression:

$$v = \left(\sin \frac{m\pi x}{L} \right) A_m \exp(j\omega t) \quad (2.48)$$

where $j = \sqrt{-1}$, m is the frequency mode number and ω is the natural frequency.

The different dimensionless parameters are defined as follows

$$r = \frac{I}{AL^2}; s = \frac{EI}{\kappa AGL^2} = \vartheta r; \vartheta = \frac{E}{\kappa G}, \Omega = \sqrt{\frac{\rho A}{EI}} L^2 \omega \quad (2.49)$$

r is the slenderness ratio. For a rectangular cross section, r is proportional to the ratio between the thickness and the length of the beam. s is a parameter related to the slenderness ratio and consequently, it also characterizes the shear effect.

Substituting Eqs. (2.48) and (2.49) into the governing differential equation, it leads to:

$$(m\pi)^4 - \Omega^2 [1 + (m\pi)^2 (r + s) + (m\pi)^4 \gamma_2 sr] + \gamma_1 \Omega^4 sr = 0 \quad (2.50)$$

The non-dimensional natural frequency is determined for each of the three versions of the Bresse-Timoshenko:

• Original Bresse-Timoshenko :

$$\Omega^2 = \begin{cases} \frac{1 + (m\pi)^2(r + s) - \sqrt{[1 + (m\pi)^2(r + s)]^2 - 4sr(m\pi)^4}}{2sr} \\ \frac{1 + (m\pi)^2(r + s) + \sqrt{[1 + (m\pi)^2(r + s)]^2 - 4sr(m\pi)^4}}{2sr} \end{cases} \quad (2.51)$$

Thus, there are two different solutions: the original Bresse-Timoshenko model has two branches of natural frequencies.

• Truncated Bresse-Timoshenko and Bresse-Timoshenko based on slope inertia:

$$\Omega^2 = \frac{(m\pi)^4}{[1 + (m\pi)^2(r + s) + \gamma_2 rs(m\pi)^4]} \quad (2.52)$$

First of all, the natural frequencies Ω are calculated in Table 1 for the Bernoulli-Euler model and the three versions of the Bresse-Timoshenko model (original, truncated and based on slope inertia). The couple (s, r) is taken equal to $(\sqrt{0.04}; \sqrt{0.02})$ as chosen by Iyengar [9] and Bruch and Mitchell [4]. In this case, the shear coefficient is $2/3$. This value is the one taken by Timoshenko himself [88].

Mode	BE	OBT	TBT	SBT
1	9.87	9.77	9.77	9.77
2	39.48	38.02	38.01	37.99
3	88.83	82.00	81.85	81.68
4	157.91	138.31	137.66	136.84
5	246.74	203.72	201.90	199.32
6	355.31	275.60	271.66	265.46
7	483.61	351.96	344.80	332.39
8	631.65	431.37	419.86	398.01
9	799.44	512.78	495.89	460.95
10	986.96	595.49	572.31	520.37
11	1194.22	678.99	648.76	575.83
12	1421.22	762.96	725.03	627.17
13	1667.96	847.15	801.02	674.43
14	1934.44	931.39	876.68	717.75
15	2220.66	1015.58	951.98	757.35
16	2526.62	1099.64	1026.94	793.49
17	2852.33	1183.53	1101.57	826.45
18*	3197.75	1262.24		

Table 1. Variation of the dimensionless frequency Ω with ($s = \sqrt{0.04}; r = \sqrt{0.02}$) for a simply supported beam (* Note: 18th frequency belongs to the second branch)

As explained before, the original Bresse-Timoshenko model admits two branches of natural frequencies. For this particular couple (s,r), the second branch is reached for the 18th natural frequency. This second branch of frequencies is not present in the two other Bresse-Timoshenko models (truncated and based on slope inertia). The difference between the Bresse-Timoshenko models is very small for low orders of frequencies and increases with the order.

Moreover, an additional comparison of the results with those in the literature is performed in Table 2 by listing the five first natural frequencies for a couple of parameter (\sqrt{r}, κ) equal to $(0.1/\sqrt{12}, 5/6)$ given by Moallemi-Oreh and Karkon [191], Ferreira [192] and Lee and Schultz [193] by using finite element analysis. As is seen, even for the reported highest frequency, the difference between the models is small.

Mode	BE	OBT	TBT	SBT	FEM	Lee Schultz [193]	Ferreira [192]
1	9.87	9.71	9.71	9.71	9.71	9.71	9.71
2	39.48	37.09	37.05	36.99	37.09	37.09	37.09
3	88.83	78.15	77.76	77.25	78.19	78.15	78.19
4	157.91	128.67	127.16	124.99	128.80	128.67	129.92
5	246.74	185.32	181.55	175.39	185.73	185.32	187.93

Table 2. Dimensionless frequency Ω for a simply supported beam with $\sqrt{r} = 0.1/\sqrt{12}$

This section has been dedicated to the case of a simply supported beam. Now the solution is proposed for other sets of boundary conditions. In this case, a close-form solution is not obtained and more computational efforts are necessary to determine the natural frequency through a characteristic equation.

2.1.4.2. Other sets of boundary conditions

Three other sets of boundary conditions are considered: clamped-simply supported, cantilever and clamped at both ends. In this case, the solution of the governing differential equation is found by separation of variables in the form [4]

$$v(\xi, t) = LU(\xi) \exp(j\omega t) \quad (2.53)$$

$$\psi(\xi, t) = \Psi(\xi) \exp(j\omega t) \quad (2.54)$$

where $\xi = x/L$

The functions $U(x)$ and $\Psi(x)$ constitute normal modes. Substitution of Eqs. (2.49) and (2.53) into Eq. (2.47) leads to the non-dimensional governing differential equation, also satisfied by Ψ :

$$\frac{d^4 U}{d\xi^4} + 2a \frac{d^2 U}{d\xi^2} + bU(\xi) = 0 \quad (2.55)$$

where a and b are two non-dimensional parameters defined as follows :

$$a = \frac{\Omega^2(r+s)}{2(1-\gamma_2 sr \Omega^2)}, b = \frac{\Omega^2(\gamma_1 \Omega^2 rs - 1)}{(1-\gamma_2 sr \Omega^2)} \quad (2.56)$$

For both equations, the roots are given by:

$$r_{\pm}^2 = \pm \sqrt{a^2 - b} - a \quad (2.57)$$

For the truncated Bresse-Timoshenko theory and the Bresse-Timoshenko theory based on slope inertia, whatever value of the natural frequency, r_+ is a real whereas r_- is a complex number. For the original Bresse-Timoshenko theory, one can show that there is a transition frequency Ω^t above which r_+ and r_- are both complex numbers [194]. Consequently, in the original Bresse-Timoshenko theory, there are two branches of natural frequencies, as already investigated in the particular case of a beam that is simply supported at both ends. For more details about this second branch of frequencies, one may refer to different papers in the literature [167,195-200]. Hereinafter, only the study the first branch of natural frequencies, for which the frequency is below the transition one, is conducted.

The general solution of the differential equation is found

$$U(\xi) = A \cosh \beta_1 \xi + B \sinh \beta_1 \xi + C \cos \beta_2 \xi + D \sin \beta_2 \xi \quad (2.58)$$

$$\Psi(\xi) = E \cosh \beta_1 \xi + F \sinh \beta_1 \xi + G \cos \beta_2 \xi + H \sin \beta_2 \xi \quad (2.59)$$

where A, B, C, D, E, F, G and H are parameters and β_1 and β_2 are expressed as follows:

$$\beta_1 = \left(\sqrt{a^2 - b} - a \right)^{\frac{1}{2}}; \beta_2 = \left(\sqrt{a^2 - b} + a \right)^{\frac{1}{2}} \quad (2.60)$$

For $\Omega \geq \Omega^t$, the solutions of these equations are expressed with purely trigonometric mode shapes.

Substituting Eqs. (2.58) and (2.59) into the non-dimensional equations of motion leads to:

$$\Psi(\xi) = Am_1 \sinh \beta_1 \xi + Bm_1 \cosh \beta_1 \xi + Cm_2 \sin \beta_2 \xi - Dm_2 \cos \beta_2 \xi \quad (2.61)$$

where

$$m_1 = \frac{\Omega^2 s + \beta_1^2 (1 - \gamma_2 \Omega^2 sr)}{\beta_1}; m_2 = \frac{\Omega^2 s - \beta_2^2 (1 + \gamma_2 \Omega^2 sr)}{\beta_2} \quad (2.62)$$

Table 3 lists the different boundary conditions investigated in the present thesis by using the non-dimensional displacements. For a beam simply supported at both ends, the closed form solution has been determined before.

Simply supported - clamped	Clamped - clamped	Cantilever
$U(0) = 0$	$U(0) = 0$	$U(0) = 0$
$\Psi'(0) = 0$	$\Psi(0) = 0$	$\Psi(0) = 0$
$U(1) = 0$	$U(1) = 0$	$\Psi'(1) = 0$
$\Psi(1) = 0$	$\Psi(1) = 0$	$(1 - \gamma_2 r^2 \alpha \vartheta)U'(1) - \Psi(1) = 0$

Table 3: Boundary conditions

Substituting the expressions of U and Ψ into the equations related to the boundary conditions leads to a system of four equations. In order to have a non-trivial solution, the determinant of this system vanishes. Thus, it yields a characteristic equation for the different boundary conditions:

Simply supported-clamped beam

$$m_2(m_2\beta_2 - m_1\beta_1)\sinh(\beta_1)\cos(\beta_2) - m_1(\beta_1m_1 - m_2\beta_2)\cosh(\beta_1)\sin(\beta_2) = 0 \quad (2.63)$$

Clamped-clamped beam

$$-2m_1m_2[1 - \cosh(\beta_1)\cos(\beta_2)] + (m_1^2 - m_2^2)\sin(\beta_2)\sinh(\beta_1) = 0 \quad (2.64)$$

Cantilever beam

$$m_1m_2\{\beta_2^2 + \beta_2m_2 - \alpha\gamma_2r^2\vartheta\beta_2^2\} + m_1m_2\{\alpha\gamma_2r^2\vartheta\beta_1^2 - \beta_1^2 + \beta_1m_1\} - \{\beta_1\beta_2(m_1^2 - m_2^2)(1 - \alpha\gamma_2r^2\vartheta) + \beta_1m_1^2m_2 + \beta_2m_1m_2^2\}\cos(\beta_2)\cosh(\beta_1) + \{2\beta_1\beta_2m_1m_2(1 - \alpha\gamma_2r^2\vartheta) + \beta_1m_1m_2^2 - \beta_2m_1^2m_2\}\sin(\beta_2)\sinh(\beta_1) = 0 \quad (2.65)$$

In order to compare the different models, a beam with a ratio L/h , a Poisson's ratio ν and a shear coefficient κ equal to 5, 0.3 and 0.833333, respectively, is taken. These values are the same as those adopted in the paper of Khaji et al [201]. The value of the shear coefficient is also the one used by Weaver, Timoshenko and Young [176]. The results for first four natural frequencies are given in Table 4.

For the first frequencies (for instance the fundamental one), the three versions of the Bresse-Timoshenko model provide very similar results. Indeed, the influence of the fourth order time derivative in the governing differential equation of the original Bresse-Timoshenko model is negligible compared to the other terms. The difference between the different models increases naturally with the order of frequency, as it has been established for a beam that is simply

supported at both ends. Moreover, table 4 trends to show that the frequencies gotten from the truncated model are smaller than with the original model.

		Frequency			
		1 st	2 nd	3 rd	4 th
Simply supported	BE	9.87	39.48	88.82	157.91
	OBT	9.24	32.05	61.14	92.64
	TBT	9.23	31.66	59.30	88.12
	SBT	9.23	31.64	57.78	84.56
Simple-clamped	BE	15.40	49.96	104.24	178.26
	OBT	13.39	39.69	64.78	100.16
	TBT	13.36	36.23	62.96	90.87
	SBT	13.34	36.02	62.77	86.04
Clamped-clamped	BE	22.36	61.66	120.90	199.86
	OBT	17.01	43.43	75.12	107.01
	TBT	17.81	42.64	72.00	104.00
	SBT	18.03	41.88	70.65	104.46
Cantilever	BE	3.51	22.03	61.69	120.96
	OBT	3.33	20.27	49.23	81.80
	TBT	3.24	20.19	47.96	77.78
	SBT	3.23	19.88	47.01	70.80

Table 4. Four first natural frequencies Ω of a beam for different boundary conditions $L/h = 5$

Moreover, in order to compare the results with those of the literature obtained for different methods, Table 5 compares the first five natural frequencies evaluated via the suggested model with those evaluated by Labuschagne et al. [202] who utilized 2D elastodynamic simulation to establish the governing differential equation for the particular case of a cantilever beam and solved the problem by using the Galerkin approximation with Hermite piecewise bicubic functions.

Mode	2D elastodynamic model [202]	BE	OBT	TBT	SBT
1	3.49	3.51	3.49	3.49	3.49
2	20.94	22.01	20.91	20.90	20.88
3	54.49	-	-	-	-
	55.19	61.71	54.99	54.85	54.61
4	100.38	120.89	99.74	99.02	97.77
5	152.92	200.00	151.84	149.69	145.65

Table 5. Dimensionless frequency Ω for a cantilever beam with $\sqrt{r} = 0.1/\sqrt{12}$

One may notice in this table that the 2D elastodynamic model admits two third natural frequencies, one being an intruding value. The table confirms the previous results, namely that the three versions of the Bresse-Timoshenko model lead to similar results and the Bernoulli-Euler model overestimates the natural frequencies.

2.1.5. Particular application: cantilever beam with a tip mass

2.1.5.1. Derivation of the governing differential equation

Consider now the cantilever beam with a concentrated tip mass at $x = L$. In 1974, Iyengar [9] established the equations to describe the mechanical behavior of Bresse-Timoshenko beams under transverse vibrations and showed that the effect of the mass was more important for higher modes. Bruch and Mitchell [4] confirmed these equations and studied the influence of different parameters, like the radius of gyration of the tip mass or the dimensionless tip mass. Specifically, they explained that the natural frequency decreases by increasing the slenderness ratio or the tip mass.

The tip mass is not a mass point and consequently, an additional kinetic energy related to the mass has to be taken into account [203]:

$$T_t = \frac{1}{2}M \left(\frac{\partial v}{\partial t}(L) \right)^2 + \frac{1}{2}B \left(\frac{\partial \psi}{\partial t}(L) \right)^2 \quad (2.66)$$

where M is the tip mass, B is the mass moment of inertia of the tip mass. This energy does not change the governing differential equation. It has been shown [95] that if the additional terms is changed in the model based on slope inertia, then the change of the kinetic energy of the tip mass would overcorrect the correction done in the model. Consequently, the kinetic energy induced by the tip mass is assumed to be the same in the original Bresse-Timoshenko model and in the model based on slope inertia.

However, the tip mass affects the boundary conditions. Thus, the general boundary conditions for the three versions of the Bresse-Timoshenko model are replaced by:

$$\left(EI \frac{\partial \psi}{\partial x} \right) \delta \psi \Big|_0^L - [\omega^2 B \psi(L)] \delta \psi = 0 \quad (2.67)$$

$$\left[\kappa GA \left(\frac{\partial v}{\partial x} - \psi \right) + \gamma_2 \rho I \frac{\partial^3 v}{\partial t^2 \partial x} \right] \delta v \Big|_0^L - [\omega^2 M v(L)] \delta v = 0 \quad (2.68)$$

For a clamped-free beam with a concentrated tip mass, it results in the following dimensionless equations [9,204]:

$$\begin{aligned} U(0) &= 0 \\ \Psi(0) &= 0 \\ (1 - \gamma_2 \Omega^2 r s) \frac{dU}{d\xi}(1) - \Psi(1) &= \frac{\Omega^2 s M}{m} U(1) \\ \frac{d\Psi}{d\xi}(1) &= \theta \Omega^2 \Psi(1) \end{aligned} \quad (2.69)$$

with $\theta = B/\rho AL^3$ [4], $m = \rho AL$ is the total mass of the beam and $\delta = M/m$ is the concentrated mass over beam mass ratio.

Substituting the expressions of the displacements given by Eqs. (2.58) and (2.61) into Eq. (2.69) leads to a system of equations, written in the matrix form:

$$\begin{pmatrix} 1 & 0 & 1 & 0 \\ 0 & m_1 & 0 & -m_2 \\ R_1 & R_2 & R_3 & R_4 \\ R'_1 & R'_2 & R'_3 & R'_4 \end{pmatrix} \begin{pmatrix} A \\ B \\ C \\ D \end{pmatrix} = \begin{pmatrix} 0 \\ 0 \\ 0 \\ 0 \end{pmatrix} \quad (2.70)$$

where:

$$\begin{aligned}
R_1 &= (m_1 - \beta_1(1 - \gamma_2\Omega^2rs)) \sinh \beta_1 + \Omega^2rs\delta \cosh \beta_1 \\
R_2 &= (m_1 - \beta_1(1 - \gamma_2\Omega^2rs)) \cosh \beta_1 + \Omega^2rs\delta \sinh \beta_1 \\
R_3 &= (\beta_2(1 - \gamma_2\Omega^2rs) + m_2) \sin \beta_2 + \Omega^2rs\delta \cos \beta_2 \\
R_4 &= -(\beta_2(1 - \gamma_2\Omega^2rs) + m_2) \cos \beta_2 + \Omega^2rs\delta \sin \beta_2 \\
R'_1 &= \left(\beta_1 \cosh \beta_1 - \frac{\theta}{\Omega^2} \sinh \beta_1\right) m_1; R'_2 = \left(\beta_1 \sinh \beta_1 - \frac{\theta}{\Omega^2} \cosh \beta_1\right) m_1 \\
R'_3 &= \left(\beta_2 \cos \beta_2 - \frac{\theta}{\Omega^2} \sin \beta_2\right) m_2; R'_4 = \left(\beta_2 \sin \beta_2 + \frac{\theta}{\Omega^2} \cos \beta_2\right) m_2
\end{aligned}$$

The determinant of the squared matrix is taken equal to zero in order to have an infinite number of solution (vibration). It leads to the following equation:

$$\begin{aligned}
m_1(R_3R'_4 - R_4R'_3 + R_4R'_1 - R_1R'_4) - m_2(R_2R'_3 - R_3R'_2 + R_1R'_2 - R_2R'_1) \\
= 0
\end{aligned} \tag{2.71}$$

The solution of this equation are the natural frequencies.

For the Bernoulli-Euler model, the equation has been derived by Erturk and Inman [204]:

$$\begin{aligned}
1 + \cos \sqrt{\Omega} \cosh \sqrt{\Omega} + \sqrt{\Omega}\delta(\cos \sqrt{\Omega} \sinh \sqrt{\Omega} - \sin \sqrt{\Omega} \cosh \sqrt{\Omega}) \\
- \Omega^{\frac{3}{2}}\theta(\cosh \sqrt{\Omega} \sin \sqrt{\Omega} + \sinh \sqrt{\Omega} \cos \sqrt{\Omega}) \\
+ \Omega^2\delta\theta(1 - \cos \sqrt{\Omega} \cosh \sqrt{\Omega}) = 0
\end{aligned} \tag{2.72}$$

Eq. (2.72) is obtained from Eq. (2.71) when r and s are taken as converging towards zero.

2.1.5.2. Numerical results

In order to be able to compare the different Bresse-Timoshenko models, the values of the parameters are taken as equal to those used in the literature for a rectangular cross section, namely the ratio E/G and the shear parameter κ equal to $8/3$ and $2/3$, respectively [4,9]. In this case $s = 4r$. Table 6 lists the three first non-dimensional natural frequencies Ω evaluated by the Bernoulli-Euler model and the three versions of the Bresse-Timoshenko model.

δ	First frequency				Second frequency				Third frequency			
	BE	OBT	TBT	SBT	BE	OBT	TBT	SBT	BE	OBT	TBT	SBT
$\theta = 0.004; \sqrt{r} = 0.02$												
0.5	2.00	1.99	1.99	1.99	15.36	15.06	15.06	15.08	39.58	38.24	38.23	38.27
1	1.55	1.55	1.55	1.55	14.95	14.66	14.66	14.67	39.58	38.24	38.23	38.27
2	1.16	1.15	1.15	1.15	10.70	14.42	14.41	14.45	39.58	38.24	38.23	38.27
3	0.96	0.96	0.96	0.95	14.61	14.33	14.33	14.33	39.58	38.24	38.23	38.27
5	0.76	0.75	0.75	0.75	14.53	14.25	14.25	14.26	39.58	38.24	38.23	38.26
$\theta = 0.04; \sqrt{r} = 0.02$												
0.5	1.90	1.90	1.90	1.90	8.88	8.81	8.81	8.81	26.87	25.87	25.87	25.86
1	1.50	1.50	1.50	1.50	8.87	8.79	8.79	8.79	26.02	25.06	25.05	25.05
2	1.14	1.13	1.13	1.13	8.86	8.79	8.79	8.79	25.47	24.52	24.51	24.52
3	0.95	0.95	0.95	0.95	8.86	8.79	8.79	8.79	25.26	24.31	24.31	24.31
5	0.75	0.75	0.75	0.75	8.86	8.78	8.78	8.78	25.07	24.13	24.13	24.14

Table 6. Variation of the dimensionless natural frequency Ω with non-dimensional mass ratio

$$\delta (\theta = 0.004; \sqrt{r} = 0.02) \text{ and } (\theta = 0.04; \sqrt{r} = 0.02)$$

In Table 6, it is seen that the difference between the three versions of the Bresse-Timoshenko model, whatever the considered order of frequency, decreases when the dimensionless inertia property θ increases. Thus, for the third mode shape and a couple (\sqrt{r}, δ) equal to $(0.02, 5)$, the relative error between the truncated Bresse-Timoshenko model and the Bresse-Timoshenko model based on slope inertia is 0.07% when $\theta = 0.004$ versus 0.07% when $\theta = 0.04$.

In order to study the effect of the slenderness ratio on the natural frequency with a tip mass, Fig. 9 depicts, for $\theta = 0.04$ and a mass ratio δ equal to unity, the non-dimensional fundamental natural frequency is plotted versus the slenderness ratio when the tip and the beam have the same mass. Although the three versions of the Bresse-Timoshenko model provide similar result, a difference between the model based on slope inertia and the two others occurs and increase with r . However, this difference is smaller than 1.2%, even for large values of the slenderness ratio.

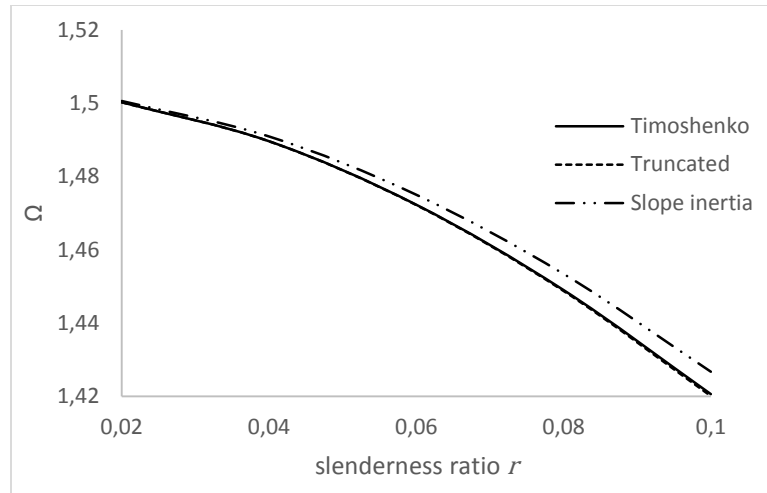


Fig. 9. Variation of fundamental frequency with the slenderness ratio ($\theta = 0.04$)

Table 7 lists the non-dimensional natural frequencies calculated for different values of the couple (r, δ) investigated in the literature (see for example [205]). The case of $\sqrt{r} = 0.000316$ coincides with the one of a very thin beam, described by the Bernoulli-Euler model and for $\delta = 0$ there is no tip mass. In this case, the study is reduced to the one conducted before. It shows again that the different Bresse-Timoshenko models provide very similar for low orders of frequencies.

	First frequency			Second frequency			Third frequency		
	OBT	TBT	SBT	OBT	TBT	SBT	OBT	TBT	SBT
δ	$\sqrt{r} = 0.000316$								
0	3.52	3.52	3.52	22.03	22.03	22.03	61.69	61.69	61.69
0.2	2.61	2.61	2.61	18.21	18.21	18.21	53.56	53.56	53.56
0.4	2.17	2.17	2.17	17.18	17.18	17.18	52.06	52.06	52.06
0.6	1.89	1.89	1.89	16.69	16.69	16.69	51.44	51.44	51.44
0.8	1.70	1.70	1.70	16.43	16.43	16.43	51.10	51.10	51.10
1.0	1.56	1.56	1.56	16.25	16.25	16.23	50.89	50.89	50.89
δ	$\sqrt{r} = 0.02$								
0.0	3.50	3.50	3.50	21.47	21.48	21.46	58.15	58.11	58.04
0.2	2.61	2.60	2.61	17.83	17.83	17.82	50.87	50.84	50.80
0.4	2.16	2.16	2.16	16.83	16.83	16.83	49.49	49.46	49.43
0.6	1.89	1.89	1.89	16.37	16.37	16.37	48.91	48.89	48.86
0.8	1.69	1.69	1.69	16.11	16.11	16.11	48.60	48.57	48.55
1.0	1.55	1.55	1.55	15.94	15.94	15.94	48.40	48.38	48.35
δ	$\sqrt{r} = 0.04$								
0.0	3.46	3.46	3.46	20.02	19.99	19.94	50.56	50.22	49.58
0.2	2.58	2.58	2.58	16.82	16.81	16.78	44.89	44.64	44.25
0.4	2.15	2.15	2.15	15.92	15.92	15.89	43.74	43.51	43.17ju
0.6	1.88	1.88	1.88	15.50	15.50	15.47	43.26	43.03	42.71
0.8	1.69	1.69	1.68	15.26	15.26	15.23	42.99	42.77	42.46
1.0	1.54	1.54	1.54	15.10	15.10	15.08	42.82	42.60	42.30

Table 7a. Variation of the dimensionless frequency Ω with r and δ ($\nu = 0.3; \kappa = 5/6$).

	First frequency			Second frequency			Third frequency		
	OBT	TBT	SBT	OBT	TBT	SBT	OBT	TBT	SBT
δ	$\sqrt{r} = 0.06$								
0	3.40	3.40	3.40	18.14	18.06	18.34	42.89	42.14	41.51
0.2	2.55	2.55	2.55	15.48	15.43	15.50	38.60	38.01	37.28
0.4	2.12	2.12	2.12	14.70	14.65	14.68	37.66	37.10	36.34
0.6	1.85	1.85	1.85	14.33	14.29	14.29	37.25	36.71	35.94
0.8	1.67	1.67	1.67	14.12	14.08	14.07	37.03	36.49	35.72
1.0	1.53	1.53	1.53	13.98	13.94	13.92	36.88	36.36	35.58
δ	$\sqrt{r} = 0.08$								
0.0	3.32	3.32	3.32	16.23	16.09	16.29	36.53	35.47	33.55
0.2	2.50	2.49	2.52	14.06	13.96	13.98	33.22	32.33	30.76
0.4	2.08	2.08	2.09	13.39	13.30	13.28	32.43	31.59	30.08
0.6	1.82	1.82	1.83	13.07	12.99	12.94	32.08	31.27	29.78
0.8	1.64	1.64	1.65	12.89	12.80	12.75	31.89	31.09	29.61
1.0	1.50	1.50	1.54	12.76	12.68	12.62	31.76	30.98	29.50
δ	$\sqrt{r} = 0.1$								
0.0	3.23	3.22	3.23	14.47	14.28	14.31	31.50	30.27	27.08
0.2	2.45	2.44	2.47	12.70	12.55	12.48	28.89	27.81	25.35
0.4	2.04	2.04	2.06	12.14	12.00	11.89	28.20	27.19	24.89
0.6	1.79	1.79	1.80	11.86	11.74	11.61	27.90	26.92	24.67
0.8	1.61	1.61	1.63	11.70	11.58	11.44	27.73	26.77	24.55
1.0	1.48	1.48	1.49	11.59	11.47	11.33	27.62	26.67	24.48

Table 7b. Variation of the dimensionless frequency Ω with r and δ ($\nu = 0.3; \kappa = 5/6$).

2.1.6. Other applications

Structural defects such as cracks may be present in mechanical structures. One of the most important aspects of the modern structural dynamics is to develop analytical models and tools to anticipate the mechanical behavior of a structure with a crack and to predict eventual damage due to this crack. Cracks reduce the natural frequencies of a structure because the latter becomes more flexible [11,207-209]. Therefore, one of the crack identification methods is to detect changes of natural frequencies due to crack presence. This methodology is effective, inexpensive, fast and non-destructive. Hereinafter, the beam is divided into two beam segments and the crack section is simulated by an equivalent rotational spring with a rigidity k_s . Thus, it induces a change in strain energy of the beam due to the presence of the crack is equal to the stiffness of the spring. Using the three versions of the Bresse-Timoshenko model, the natural frequencies will be determined following the geometric characteristics of the crack and by the inverse method, knowing some parameters such as the critical depth of the crack, the crack will be located. It is shown that the crack reduces the natural frequency and this reduction is more important when the crack is deeper. The location of the crack is also an important parameter.

Different investigations have been carried out about the instability parametric instability of beams considering the three versions of the Bresse-Timoshenko model [95]. Indeed, numerous investigators showed a real interest for this issue in past decades [14,210-214]. The reader may also refer to the paper by Hagedorn and Koval [215] who showed that the rotary inertia and shear effects create new instability regions, widen the pre-existent regions of instability, and cause a shift of the instability regions to the left in the stability chart. More specifically, Elishakoff et al. [92,93] demonstrated that the three versions of the Bresse-Timoshenko model lead, for small slenderness ratios, to regions of dynamic instabilities that are extremely close to each other. When the ratio increases, the models do not predict the same instability regions and the difference increases with the ratio.

The study of the response of a beam under random excitations in presence of different damping (Voigt, transverse and rotary viscous) has been widely investigated in the literature [181,216-220] considering the Bernoulli-Euler model [221] and more recently [181], the truncated version of the Bresse-Timoshenko model. Although the Bernoulli-Euler model and the Bresse-Timoshenko models provide both finite mean-square displacement, the Bresse-Timoshenko equation produces a finite mean-square stress, contrary to the classical Euler-Bernoulli theory.

One can determine the displacement for the three versions of the Bresse-Timoshenko model [91] and the previously mentioned kinds of damping. Thus, for a thin beam, the mean-square displacement is the same for the Bernoulli-Euler model and the Bresse-Timoshenko models. When the slenderness ratio increases, a difference between these approaches occurs.

2.2. Thick plate models for macrostructures

As explained in a previous chapter, the mechanical behavior of plate can be described by the Kirchhoff-Love theory for thin plates and different versions of the Uflyand-Mindlin plate theory for thick plates. In this section, we derive the different versions of the Uflyand-Mindlin plate theory: the Original Uflyand-Mindlin model (OUM), the Truncated Uflyand-Mindlin theory (TUM) and the Uflyand-Mindlin plate model based on slope inertia (SUM). Three kinds of derivations are considered: variational one for the OUM and SUM model, through the use of equilibrium equations for the TUM and OUM model and asymptotically for the TUM model.

The closed form solution is provided for a plate with all edges simply supported and for a plate with two opposite edges that are simply supported, an exact solution is proposed, obtained by using the Lévy's method. A special notation will be adopted for the boundary conditions, commonly used in the literature [158,159,162,222]. Hereinafter, plates with two opposite edges simply supported at $x = 0$ and $x = a$ will be considered and six cases will be studied: SSSS (all edges simply supported), SFSF (the edges $y=0$ and $y=b$ are free), SFSF (the edges $y=0$ and $y=b$ are free), SSSF ($y=0$ is simply supported, $y=b$ is free), SSSC ($y=0$ is simply supported, $y=b$ is clamped), SCSF ($y=0$ is clamped, $y=b$ is free).

2.2.1. The different models

2.2.1.1. Original Uflyand-Mindlin

Considering a x, y, z -system of Cartesian coordinates and a rectangular plate of length a , width b and uniform thickness h , bending rigidity $D = Eh^3/12(1 - \nu^2)$, as shown in Fig. 10.

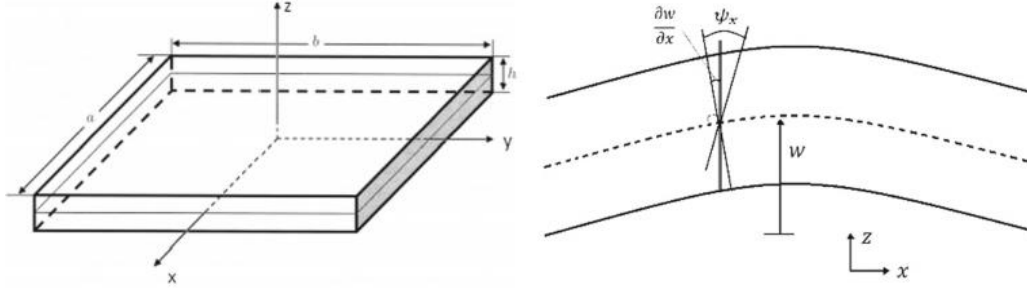


Fig. 10. Plate of dimensions $a \times b \times h$ and rotations of a transverse normal about the y axis

[108]

ψ_x and ψ_y are the bending rotations of a transverse normal about the x and y axes, respectively, as shown in Fig. 10.

First of all, the derivation of the original Uflyand-Mindlin through the use of equilibrium equations is proposed.

The three-dimensional equilibrium equations are:

$$\begin{aligned} \frac{\partial \sigma_x}{\partial x} + \frac{\partial \tau_{yx}}{\partial y} + \frac{\partial \tau_{zx}}{\partial z} &= \rho \frac{\partial^2 u}{\partial t^2} \\ \frac{\partial \tau_{yx}}{\partial x} + \frac{\partial \sigma_y}{\partial y} + \frac{\partial \tau_{zy}}{\partial z} &= \rho \frac{\partial^2 v}{\partial t^2} \\ \frac{\partial \tau_{zx}}{\partial x} + \frac{\partial \tau_{yz}}{\partial y} + \frac{\partial \sigma_z}{\partial z} &= \rho \frac{\partial^2 w}{\partial t^2} \end{aligned} \quad (2.73)$$

The bending and twisting moments and the transverse shearing forces are related to the normal and shear stresses as follows:

$$\begin{pmatrix} M_x \\ M_y \\ M_{yx} \end{pmatrix} = \int_{-h/2}^{h/2} \begin{pmatrix} \sigma_x \\ \sigma_y \\ \tau_{yx} \end{pmatrix} z dz; \quad \begin{pmatrix} Q_x \\ Q_y \end{pmatrix} = \int_{-h/2}^{h/2} \begin{pmatrix} \tau_{xz} \\ \tau_{yz} \end{pmatrix} dz \quad (2.74)$$

Multiplying Eq. (2.73) by z , integrating over the plate thickness and substituting Eq. (2.74) yields:

$$\begin{aligned}\frac{\partial M_x}{\partial x} + \frac{\partial M_{yx}}{\partial y} - Q_x &= \frac{\rho h^3}{12} \frac{\partial^2 \psi_x}{\partial t^2} \\ \frac{\partial M_{yx}}{\partial x} + \frac{\partial M_y}{\partial y} - Q_y &= \frac{\rho h^3}{12} \frac{\partial^2 \psi_y}{\partial t^2} \\ \frac{\partial Q_x}{\partial x} + \frac{\partial Q_y}{\partial y} &= \rho h \frac{\partial^2 w}{\partial t^2}\end{aligned}\quad (2.75)$$

In the Mindlin's [103] plate theory, the bending and twisting moments and the shear forces Q_x and Q_y are given by, for an isotropic material,

$$\begin{aligned}M_x &= D \left(\frac{\partial \psi_x}{\partial x} + \nu \frac{\partial \psi_y}{\partial y} \right); M_y = D \left(\frac{\partial \psi_y}{\partial y} + \nu \frac{\partial \psi_x}{\partial x} \right) \\ M_{yx} &= \frac{D}{2} (1 - \nu) \left(\frac{\partial \psi_y}{\partial x} + \frac{\partial \psi_x}{\partial y} \right) \\ Q_x &= \kappa G h \left(\psi_x + \frac{\partial w}{\partial x} \right); Q_y = \kappa G h \left(\psi_y + \frac{\partial w}{\partial y} \right)\end{aligned}\quad (2.76)$$

Substituting Eq. (2.76) into Eq. (2.75) yields to the equations of motion:

$$\begin{aligned}\frac{D}{2} \left[(1 - \nu) \nabla^2 \psi_x + (1 + \nu) \left(\frac{\partial^2 \psi_x}{\partial x^2} + \frac{\partial \psi_y}{\partial x \partial y} \right) \right] - \kappa G h \left(\psi_x + \frac{\partial w}{\partial x} \right) &= \frac{\rho h^3}{12} \frac{\partial^2 \psi_x}{\partial t^2} \\ \frac{D}{2} \left[(1 - \nu) \nabla^2 \psi_y + (1 + \nu) \left(\frac{\partial \psi_x}{\partial x \partial y} + \frac{\partial^2 \psi_y}{\partial y^2} \right) \right] - \kappa G h \left(\psi_y + \frac{\partial w}{\partial y} \right) &= \frac{\rho h^3}{12} \frac{\partial^2 \psi_y}{\partial t^2} \\ \kappa G h \left(\nabla^2 w + \frac{\partial \psi_x}{\partial x} + \frac{\partial \psi_y}{\partial y} \right) &= \rho h \frac{\partial^2 w}{\partial t^2}\end{aligned}\quad (2.77)$$

where ∇^2 is the Laplace operator. After different manipulations of the equations of motion, it leads to the governing differential equation of the original Uflyand-Mindlin plate model

$$D \nabla^4 w + \rho h \frac{\partial^2 w}{\partial t^2} - \rho \frac{h^3}{12} \left(1 + \frac{12 D}{h^3 \kappa G} \right) \frac{\partial^2}{\partial t^2} \nabla^2 w + \frac{\rho^2 h^3}{12 \kappa G} \frac{\partial^4 w}{\partial t^4} = 0 \quad (2.78)$$

Furthermore, as for beams and the original Bresse-Timoshenko model, the OUM model is also derived variationnally, as widely investigated in the literature [20,102,103,112-114,223,224].

The potential and kinetic energies of the plate are given by, respectively

$$\begin{aligned}V &= \iint_{\mathfrak{D}} \frac{1}{2} \left(D \left\{ \left(\frac{\partial \psi_x}{\partial x} + \frac{\partial \psi_y}{\partial y} \right)^2 - 2(1 - \nu) \left[\frac{\partial \psi_x}{\partial x} \frac{\partial \psi_y}{\partial y} - \frac{1}{4} \left(\frac{\partial \psi_x}{\partial y} + \frac{\partial \psi_y}{\partial x} \right)^2 \right] \right\} \right. \\ &\quad \left. + \kappa G h \left[\left(\frac{\partial w}{\partial x} + \psi_x \right)^2 + \left(\frac{\partial w}{\partial y} + \psi_y \right)^2 \right] \right) dx dy\end{aligned}\quad (2.79)$$

$$T = \frac{1}{2} \iint_{\mathfrak{D}} \rho h \left(\frac{\partial w}{\partial t} \right)^2 + \frac{\rho h^3}{12} \left[\left(\frac{\partial \psi_x}{\partial t} \right)^2 + \left(\frac{\partial \psi_y}{\partial t} \right)^2 \right] dx dy \quad (2.80)$$

where \mathfrak{D} is the area of the mid-surface of the plate.

According to the Hamilton's principle, one obtains the governing differential equation and the boundary conditions. For example, at the boundaries of the plate, for edges parallel to the x axis,

$$\begin{aligned} D \left(\frac{\partial \psi_x}{\partial x} + \nu \frac{\partial \psi_y}{\partial y} \right) &= 0 \text{ or } \psi_x \\ \frac{\partial \psi_x}{\partial y} + \frac{\partial \psi_y}{\partial x} &= 0 \text{ or } \psi_y \quad \text{are specified} \\ \kappa G h \left(\psi_y + \frac{\partial w}{\partial y} \right) &= 0 \text{ or } w \end{aligned} \quad (2.81)$$

Analogously for beams, a truncated version of the Uflyand-Mindlin plate model is proposed.

2.2.1.2. Truncated Uflyand-Mindlin plate theory

Extending the truncated Bresse-Timoshenko derivation to the case of thick plates, it is suggested to replace $\partial^2 \psi_x / \partial t^2$ and $\partial^2 \psi_y / \partial t^2$ in Eq. (2.77) by $\partial^3 w / \partial x \partial t^2$ and $\partial^3 w / \partial y \partial t^2$, respectively. Thus, it leads to the governing differential equation in displacement of the truncated Uflyand-Mindlin plate model:

$$D \nabla^4 w + \rho h \frac{\partial^2 w}{\partial t^2} - \rho \frac{D}{\kappa G} \frac{\partial^2}{\partial t^2} \nabla^2 w = 0 \quad (2.82)$$

As for beams, the asymptotic derivation of this truncated model is now proposed.

Start by the three-dimensional equilibrium equations for a plate:

$$(\lambda_L + G) \begin{pmatrix} \frac{\partial}{\partial x} \\ \frac{\partial}{\partial y} \\ \frac{\partial}{\partial z} \end{pmatrix} \left(\theta + \frac{\partial w}{\partial z} \right) + G \left(\nabla^2 + \frac{\partial^2}{\partial z^2} \right) \begin{pmatrix} u \\ v \\ w \end{pmatrix} = \rho \frac{\partial^2}{\partial t^2} \begin{pmatrix} u \\ v \\ w \end{pmatrix} \quad (2.83)$$

where λ_L is the Lamé coefficient and θ is defined as

$$\theta = \frac{\partial u}{\partial x} + \frac{\partial v}{\partial y} \quad (2.84)$$

On the free surfaces, the normal and shear stresses vanish, resulting in

$$\sigma_z \left(x, \frac{h}{2} \right) = \sigma_z \left(x, -\frac{h}{2} \right); \sigma_{yz} \left(x, \frac{h}{2} \right) + \sigma_{yz} \left(x, -\frac{h}{2} \right) = 0 \quad (2.85)$$

In the reduction method, the displacements are expanded in power series as follows:

$$\theta = \sum_{k=0}^{\infty} \theta_k(x, y, t) z^k; w = \sum_{k=0}^{\infty} w_k(x, y, t) z^k \quad (2.86)$$

Substituting Eq. (2.86) into Eq. (2.85), it yields:

$$\begin{aligned} & \sum_{n=1}^{\infty} 2(\lambda_L + 2G)n \left(\frac{h}{2} \right)^{2n-1} w_{2n} + \lambda_L \left(\frac{h}{2} \right)^{2n-1} \theta_{2n-1} = 0 \\ & \nabla^2 w_0 + \sum_{n=1}^{\infty} \left\{ \left(\frac{h}{2} \right)^{2n} \nabla^2 w_{2n} + (2n-1) \left(\frac{h}{2} \right)^{2n-2} \theta_{2n-1} \right\} = 0 \\ & \left(G \nabla^2 - \rho \frac{\partial^2}{\partial t^2} \right) w_{2n} + (\lambda_L + 2G)(2n+1)(2n+2)w_{2n+2} + (\lambda_L + G)(2n \\ & \quad + 1)\theta_{2n+1} = 0 \\ & (\lambda_L + G)2n \nabla^2 w_{2n} + \left((\lambda_L + 2G) \nabla^2 - \rho \frac{\partial^2}{\partial t^2} \right) \theta_{2n-1} + G2n(2n+1)\theta_{2n+1} \\ & \quad = 0 \end{aligned} \quad (2.87)$$

where $c^2 = G/\rho$.

The variables are rewritten under the dimensionless form as follows:

$$\bar{\theta}_n = L^n \theta_n; \bar{w}_n = L^{n-1} w_n; \bar{\nabla}^2 = L^2 \nabla^2; \bar{h} = \frac{h}{2L}; \bar{t} = \frac{htc}{2L^2} = \frac{\bar{h}tc}{2L} \quad (2.88)$$

The two summations re-written as:

$$\begin{aligned} & \sum_{n=0}^{\infty} [2(\lambda_L + 2G)(n+1)\bar{w}_{2n+2} + \lambda_L \bar{\theta}_{2n+1}] \bar{h}^{2n} = 0 \\ & \bar{\nabla}^2 \bar{w}_0 + \sum_{n=0}^{\infty} \{ \bar{h}^2 \bar{\nabla}^2 \bar{w}_{2n+2} + (2n+1) \bar{\theta}_{2n+1} \} \bar{h}^{2n} = 0 \end{aligned} \quad (2.89)$$

At the fourth order

$$\begin{aligned} & 2(\lambda_L + 2G)(\bar{w}_2 + 2\bar{w}_4 \bar{h}^2 + 3\bar{w}_6 \bar{h}^4) + \lambda_L (\bar{\theta}_1 + \bar{\theta}_3 \bar{h}^2 + \bar{\theta}_5 \bar{h}^4) = 0 \\ & \bar{\nabla}^2 (\bar{w}_0 + \bar{h}^2 \bar{w}_2 + \bar{h}^4 \bar{w}_4) + \bar{\theta}_1 + \bar{h}^2 3\bar{\theta}_3 + \bar{h}^4 5\bar{\theta}_5 = 0 \end{aligned} \quad (2.90)$$

Moreover, for any integer n, the relationships between \bar{w}_{2n+2} , \bar{w}_{2n} and $\bar{\theta}_{2n+1}$ and between $\bar{\theta}_{2n+3}$, \bar{w}_{2n+2} and $\bar{\theta}_{2n+1}$ are, respectively :

$$\bar{\theta}_{N+3} = \frac{1}{(N+3)(N+2)} \mathcal{A}_L^p \bar{\theta}_{N+1} + \frac{1}{N+3} \mathcal{B}_L^p \bar{w}_{N+2}; \quad N = 0, 2, 4, \dots \quad (2.91)$$

$$\bar{w}_{N+2} = \frac{1}{(N+1)(N+2)} \mathcal{C}_L^p \bar{w}_N + \frac{1}{(N+2)} \mathcal{F}_L^p \bar{\theta}_{N+1}; \quad N = 0, 2, 4, \dots$$

Where the operators \mathcal{A}_L^p , \mathcal{B}_L^p , \mathcal{C}_L^p and \mathcal{F}_L^p are defined as follows ::

$$\begin{aligned} \mathcal{A}_L^p &= - \left[\frac{(\lambda + 2G)}{G} \bar{\nabla}^2 - \bar{h}^2 \frac{\partial^2}{\partial \bar{t}^2} \right]; \mathcal{B}_L^p = - \frac{(\lambda_L + G)}{G} \bar{\nabla}^2 \\ \mathcal{C}_L^p &= - \frac{G}{(\lambda + 2G)} \left[\bar{\nabla}^2 - \bar{h}^2 \frac{\partial^2}{\partial \bar{t}^2} \right]; \mathcal{F}_L^p = - \frac{(\lambda_L + G)}{(\lambda_L + 2G)} \end{aligned} \quad (2.92)$$

Substituting Eq. (2.91) Into Eq. (2.90), it leads in two equations in θ_1 and \bar{w}_0 , expressed in a matrix form:

$$\begin{pmatrix} M_{11} & M_{12} \\ M_{21} & M_{22} \end{pmatrix} \begin{pmatrix} \bar{w}_0 \\ \theta_1 \end{pmatrix} = \begin{pmatrix} 0 \\ 0 \end{pmatrix} \quad (2.93)$$

where the coefficients M_{11} , M_{12} , M_{21} and M_{22} are:

$$\begin{aligned} M_{11} &= -20(G - \lambda_L) \frac{\partial^2}{\partial \bar{t}^2} \bar{\nabla}^2 \bar{h}^4 + (2G + 3\lambda_L) \bar{\nabla}^6 \bar{h}^4 \\ &\quad + 120(2G + \lambda_L) \left(\frac{\partial^2}{\partial \bar{t}^2} \bar{h}^2 - \bar{\nabla}^2 \right) - 20\lambda \bar{\nabla}^4 \bar{h}^2 \\ M_{12} &= 20(4G + 3\lambda_L) \bar{\nabla}^2 \bar{h}^2 - 120(2G + \lambda_L) - 20(3G + 2\lambda_L) \frac{\partial^2}{\partial \bar{t}^2} \bar{h}^4 \\ &\quad - (6G + 5) \bar{\nabla}^4 \bar{h}^4 \\ M_{21} &= (2G + 3\lambda_L) \bar{\nabla}^6 \bar{h}^4 + 12\lambda_L \left(\frac{\partial^2}{\partial \bar{t}^2} \bar{h}^4 - \bar{\nabla}^2 \bar{h}^2 \right) \bar{\nabla}^2 - 24(2G + \lambda_L) \bar{\nabla}^2 \\ M_{22} &= 12(4G + 3\lambda_L) \bar{\nabla}^2 \bar{h}^2 - 12(2G + \lambda_L) \frac{\partial^2}{\partial \bar{t}^2} \bar{h}^4 - (6G + 5\lambda_L) \bar{\nabla}^4 \bar{h}^4 \\ &\quad - 24(2G + \lambda_L) \end{aligned} \quad (2.94)$$

In order to have a nontrivial solution, the determinant of the matrix has to vanish. It results in governing differential equations at different orders:

0th order

$$(\lambda_L + G) \bar{\nabla}^4 \bar{w}_0 + \frac{3}{4} (\lambda_L + 2G) \frac{\partial^2 \bar{w}_0}{\partial \bar{t}^2} = 0 \quad (2.95)$$

2nd order

$$\begin{aligned}
 -10(3\lambda_L + 4G) \frac{\partial^2}{\partial \bar{t}^2} \bar{\nabla}^2 \bar{h}^2 \bar{w}_0 - 4(\lambda_L + G) \bar{\nabla}^6 \bar{w}_0 \bar{h}^2 + 20(\lambda_L + G) \bar{\nabla}^4 \bar{w}_0 \\
 + 15(\lambda_L + 2G) \frac{\partial^2 \bar{w}_0}{\partial \bar{t}^2} = 0
 \end{aligned} \tag{2.96}$$

Or, in the dimensional form:

0th order

$$D\nabla^4 + \rho h \frac{\partial^2}{\partial t^2} = 0 \tag{2.97}$$

2nd order

$$D\nabla^4 + \rho h \frac{\partial^2}{\partial t^2} - \frac{2(2-\nu)\rho h^3}{(1-\nu)} \frac{\partial^2}{\partial t^2} \nabla^2 - D \frac{1}{20} \nabla^6 h^2 = 0 \tag{2.98}$$

The equation at the zeroth order coincides with the traditional Kirchhoff-Love plate model valid for thin plates. Thus, this model is asymptotically consistent at the lowest order [225]. In an analogous reasoning to the one of the asymptotic beam derivation at the second order, as suggested in the literature [109], Eq. (2.96) is multiplied by $[1 + (\bar{h}^2/5)\bar{\nabla}^2]$ and neglecting the terms in h^4 leads to:

$$\begin{aligned}
 20(\lambda_L + G) \bar{\nabla}^4 \bar{w}_0 + [3(\lambda_L + 2G) - 10(3\lambda_L + 4G)] \bar{h}^2 \frac{\partial^2}{\partial \bar{t}^2} \bar{\nabla}^2 \bar{w}_0 \\
 + 15(\lambda_L + 2G) \frac{\partial^2 \bar{w}_0}{\partial \bar{t}^2} = 0
 \end{aligned} \tag{2.99}$$

Thus, using the dimensional variables, the equation is reduced to:

$$D\nabla^4 + \rho h \frac{\partial^2}{\partial t^2} - \frac{\rho h^3}{12} \left[1 + \frac{12D}{h^3 G} \frac{6-\nu}{5} \right] \frac{\partial^2}{\partial t^2} \nabla^2 = 0 \tag{2.100}$$

One recognize the governing differential equation of the truncated Uflyand-Mindlin plate model with a shear coefficient equal to $\kappa = 5/(6-\nu)$. Thus, the truncated Uflyand-Mindlin plate theory is asymptotically consistent.

As for beams and the Bresse-Timoshenko model, it is suggested to derive variationnally the Uflyand-Mindlin plate model through the same correction based on slope inertia done for the truncated approach.

2.2.1.3. Uflyand-Mindlin based on slope inertia

In the literature, it has been suggested to replace the kinetic energy given in Eq. (2.80) that overcorrects the shear effect by:

$$T = \frac{1}{2} \iint_{\mathfrak{D}} \frac{\rho h^3}{12} \left[\left(\frac{\partial^2 w}{\partial t \partial x} \right)^2 + \left(\frac{\partial^2 w}{\partial t \partial y} \right)^2 \right] + \rho h \left(\frac{\partial w}{\partial t} \right)^2 dx dy \quad (2.101)$$

Using Hamilton's principle and integrating by parts, it yields to the equations of motion,

$$\frac{D}{2} \left[(1 - \nu) \nabla^2 \psi_x + (1 + \nu) \frac{\partial \Phi}{\partial x} \right] - \kappa G h \left(\psi_x + \frac{\partial w}{\partial x} \right) = 0 \quad (2.102)$$

$$\frac{D}{2} \left[(1 - \nu) \nabla^2 \psi_y + (1 + \nu) \frac{\partial \Phi}{\partial y} \right] - \kappa G h \left(\psi_y + \frac{\partial w}{\partial y} \right) = 0 \quad (2.103)$$

$$\kappa G h (\nabla^2 w + \Phi) = \rho h \left(1 - \frac{h^2}{12} \nabla^2 \right) \frac{\partial^2 w}{\partial t^2} \quad (2.104)$$

From Eqs. (2.102)-(2.104), one obtains the governing differential equation

$$D \nabla^4 w + \rho h \frac{\partial^2 w}{\partial t^2} - \frac{\rho h^3}{12} \left(1 + \frac{12 D}{h^3 \kappa G} \right) \frac{\partial^2}{\partial t^2} \nabla^2 w + \underline{\frac{\rho h^2 D}{12 \kappa G} \frac{\partial^2}{\partial t^2} \nabla^4 w} = 0 \quad (2.105)$$

The fourth-order time derivative term in the original Uflyand-Mindlin equation is not present, replaced by a term, underlined in the equation.

For boundary conditions, for edges parallel to the x axis:

$$\begin{aligned} D \left(\frac{\partial \psi_x}{\partial x} + \nu \frac{\partial \psi_y}{\partial y} \right) = 0 \text{ or } \psi_x \\ \frac{\partial \psi_x}{\partial y} + \frac{\partial \psi_y}{\partial x} = 0 \text{ or } \psi_y \quad \text{are specified} \\ \kappa G h \left(\psi_y + \frac{\partial w}{\partial y} \right) - \frac{\rho h^3}{12} \frac{\partial^2 w}{\partial t^2 \partial y} = 0 \text{ or } w \end{aligned} \quad (2.106)$$

It is worth noticing that the two first boundary conditions match with those of the original Uflyand-Mindlin plate model. For the last equation, used for instance for a free edge, the boundary conditions do not match. Thus the models differ in both the governing differential equation and the boundary conditions.

2.2.2. Natural frequencies for the different Uflyand-Mindlin plate models

Three control parameters γ_1, γ_2 and γ_3 are introduced with $(\gamma_1, \gamma_2, \gamma_3)$ equals to $(1,0,0)$, $(0,0,1)$ and $(0,1,0)$ for the original Uflyand-Mindlin plate theory, the truncated Uflyand-Mindlin theory and the Uflyand-Mindlin model based on slope inertia, also denoted OUM, TUM and SUM, respectively. Thus, the equations of motion are rewritten in a general way as, setting $C = D(1 - \nu)/2$:

$$D\zeta_{,x} + C\varphi_{,y} - \kappa^2 Gh(\psi_x + w_{,x}) = \gamma_1 \frac{\rho h^3}{12} \ddot{\psi}_x + \gamma_3 \frac{\rho h^3}{12} \frac{\partial^3 w}{\partial x \partial t^2} \quad (2.107)$$

$$D\zeta_{,y} - C\varphi_{,x} - \kappa^2 Gh(\psi_y + w_{,y}) = \gamma_1 \frac{\rho h^3}{12} \ddot{\psi}_y + \gamma_3 \frac{\rho h^3}{12} \frac{\partial^3 w}{\partial y \partial t^2} \quad (2.108)$$

$$\kappa Gh(\psi_{x,x} + \psi_{y,y} + w_{,xx} + w_{,yy}) = \left(\rho h - \gamma_2 \frac{\rho h^3}{12} \nabla^2 \right) \ddot{w} \quad (2.109)$$

where the function φ is introduced such as [226]:

$$\varphi = \psi_{x,y} - \psi_{y,x} \quad (2.110)$$

Differentiating Eqs. (2.107) and (2.108) with respect to y and x , respectively and subtracting Eq. (2.108) to Eq. (2.107), one obtains:

$$C\nabla^2 \varphi - \kappa Gh\varphi = \gamma_1 \frac{\rho h^3}{12} \frac{\partial^2}{\partial t^2} \varphi \quad (2.111)$$

Moreover, the different governing differential equations of the three versions of the Uflyand-Mindlin plate model are written in the general form as follows [108,109]:

$$D \left(1 + \gamma_2 \frac{\rho h^2}{12\kappa G} \frac{\partial^2}{\partial t^2} \right) \nabla^4 w + \rho h \frac{\partial^2 w}{\partial t^2} - \rho \frac{h^3}{12} \left(1 + \frac{12 D}{h^3 \kappa G} \right) \frac{\partial^2}{\partial t^2} \nabla^2 w + \gamma_1 \frac{\rho^2 h^3}{12\kappa G} \frac{\partial^4 w}{\partial t^4} = 0 \quad (2.112)$$

Thus, the system is described by two uncoupled equations Eqs. (2.111) and (2.112).

It is assumed that

$$(w; \psi_x; \psi_y; \varphi)(x, y, t) = (\bar{w}; \bar{\psi}_x; \bar{\psi}_y; \bar{\varphi})(x, y) e^{i\omega t} \quad (2.113)$$

Substituting Eq. (2.113) into Eqs. (2.111) and (2.112) leads to:

$$C\nabla^2 \bar{\varphi} - \left(\kappa^2 Gh - \gamma_1 \frac{\rho h^3}{12} \omega^2 \right) \bar{\varphi} = 0 \quad (2.114)$$

$$\begin{aligned}
D \left(1 - \frac{\rho h^2}{12 \kappa^2 G} \omega^2 \gamma_2 \right) \nabla^4 \bar{w} + \rho \frac{h^3}{12} \left(1 + \frac{12 D}{h^3 \kappa^2 G} \right) \omega^2 \nabla^2 \bar{w} \\
+ \left(\gamma_1 \frac{\rho^2 h^3}{12 \kappa^2 G} \omega^2 - \rho h \right) \omega^2 \bar{w} = 0
\end{aligned} \tag{2.115}$$

The rotation angles ψ_x and ψ_y are found from the transverse deflection w and the parameter $\bar{\varphi}$ by the following relationships:

$$\begin{aligned}
\left(\kappa G h - \gamma_1 \frac{\rho h^3}{12} \omega^2 \right) \bar{\psi}_x \\
= \frac{\partial}{\partial x} \left[-\rho \omega^2 \frac{D \left(1 - \gamma_2 \frac{h^2}{12} \nabla^2 \right)}{\kappa G} - D \nabla^2 - \kappa G h + \gamma_3 \frac{\rho h^3}{12} \omega^2 \right] \bar{w} \\
+ C \frac{\partial \bar{\varphi}}{\partial y}
\end{aligned} \tag{2.116}$$

$$\begin{aligned}
\left(\kappa^2 G h - \gamma_1 \frac{\rho h^3}{12} \omega^2 \right) \bar{\psi}_y \\
= \frac{\partial}{\partial y} \left[-\rho \omega^2 \frac{D \left(1 - \gamma_2 \frac{h^2}{12} \nabla^2 \right)}{\kappa^2 G} - D \nabla^2 - \kappa^2 G h + \gamma_3 \frac{\rho h^3}{12} \omega^2 \right] \bar{w} \\
- C \frac{\partial \bar{\varphi}}{\partial x}
\end{aligned} \tag{2.117}$$

2.2.2.1. Rectangular plates with four edges simply supported

A derivation of the solution for an all-round simply supported plate is proposed. In this case, analogously to beams, the solution is given by Navier [227]

$$\bar{w}(x, y) = a \sin\left(\frac{n\pi y}{b}\right) \sin\left(\frac{m\pi x}{a}\right) \tag{2.118}$$

where m and n are the number of half-waves in the x and y -direction, respectively.

Consider the following nondimensional quantities:

$$\Omega = \omega b^2 \sqrt{\frac{\rho h}{D}}; \beta = \frac{E}{G(1-\nu^2)}; \eta = \frac{h}{b}; \bar{h} = \frac{h}{a}; \xi = \frac{x}{a}; \chi = \frac{a}{b}; \bar{\nabla}_{mn} = \pi^2 [(\chi n)^2 + m^2] \tag{2.119}$$

Substituting Eq. (2.118) and (2.119) into Eq. (2.115),

$$\bar{\nabla}_{mn}^2 - \chi^4 \Omega^2 \left[1 + \bar{\nabla}_{mn} \frac{\bar{h}^2}{12} \left(1 + \frac{\beta}{\kappa^2} \right) + \bar{\nabla}_{mn}^2 \frac{\beta \bar{h}^4}{144 \kappa^2} \gamma_2 \right] + \frac{\beta \chi^8 \bar{h}^4}{144 \kappa^2} \gamma_1 \Omega^4 = 0 \quad (2.120)$$

The solution of the original Uflyand-Mindlin plate problem is given by [110,228,229]:

$$\Omega = \frac{12}{\chi^2 \bar{h}^2} \sqrt{\frac{\kappa^2}{2\beta}} \left(1 + \bar{\nabla}_{mn} \frac{\bar{h}^2}{12} \left(1 + \frac{\beta}{\kappa^2} \right) \right. \\ \left. \pm \sqrt{\left[1 + \bar{\nabla}_{mn} \frac{\bar{h}^2}{12} \left(1 + \frac{\beta}{\kappa^2} \right) \right]^2 - \frac{\beta \bar{h}^4}{36 \kappa^2} \bar{\nabla}_{mn}^2} \right)^{\frac{1}{2}} \quad (2.121)$$

There are two different solutions, and so two different branches of frequencies.

For the two other versions of the Uflyand-Mindlin (truncated and based on slope, the natural frequencies are given by:

$$\Omega = \frac{\bar{\nabla}_{mn}}{\chi^2 \sqrt{1 + \frac{\bar{h}^2}{12} \left(1 + \frac{\beta}{\kappa^2} \right) \bar{\nabla}_{mn} + \bar{\nabla}_{mn}^2 \frac{\beta \bar{h}^4}{144 \kappa^2} \gamma_2}} \quad (2.122)$$

Because the expression of the natural frequency has a positive additional term in the denominator, the Uflyand-Mindlin model based on slope inertia provides smaller values for natural frequencies than does the truncated Uflyand-Mindlin model. In contrast to the original model, the truncated theories lead to a single branch of natural frequencies. This result is also valid, as it will be shown hereinafter, for plates with simply supported two opposite edges.

For the Kirchhoff-Love plate model:

$$\Omega_{KL} = \frac{\bar{\nabla}_{mn}}{\chi^2} \quad (2.123)$$

The Uflyand-Mindlin plate theories lead to smaller natural frequencies compared to the Kirchhoff-Love plate model. Indeed, when the rotary inertia and the shear effects are taken into account, the difference with the classical theory increases with the vibration mode number. For low orders of frequencies, the three versions of the Uflyand-Mindlin plate model provide the same natural frequencies. Although the original and truncated models lead to very similar results, the frequencies calculated from the model based on slope inertia are smaller than for the two other Uflyand-Mindlin plate models. The difference increases with the frequency.

A plate simply supported at all edges has already been investigated in the literature. Consequently, the results can be compared to the existing ones. Different models and method of resolution are considered: the Higher Order Shear Deformation Theory (HSDT) given by Shufrin [230], the two dimensional Rayleigh-Ritz method (2D Ritz) [231], the three dimensional Rayleigh-Ritz method [231], the Differential Quadrature Method (DQM) [232] and the analytical solution from the three dimensional elasticity equations [233], the three dimensional DQM and Rayleigh-Ritz methods providing the same results. The five first natural frequencies are listed in Table 8, as it has been done in the literature [109]. The aim of the numerical method is to confirm the results obtained via Eq. (2.121).

It is seen from Table 8 that the original Uflyand-Mindlin plate model provide results, close to those obtained by using the three dimensional methods. The numerical models (Rayleigh-Ritz method) lead to slightly bigger natural frequencies. Indeed, these models give an upper bound of the results. For high order of frequencies, the original Uflyand-Mindlin plate model has natural frequencies that are close to those of the higher-shear deformation theory, supposed to be naturally more accurate than the Uflyand-Mindlin plate models. However, compared to the exact three dimensional solution, the model based on slope inertia is better than the two other versions of the Uflyand-Mindlin plate model.

In any case, for the first natural frequencies, the three different versions of the Uflyand-Mindlin lead to similar results. It is worth noticing that, as it will be detailed before, the original model, because it contains a fourth order time derivative in the governing differential equations, has two branches of frequencies. The two other models (truncated and based on slope inertia) lead to only one branch.

$(\chi\bar{h})$	3D anal	KL	OUM	TUM	SUM	HSDT	2D [231]	3D DQM
0.001	19.74	19.74	19.74	19.74	19.74	-	19.74	-
	49.35	49.35	49.35	49.35	49.35	-	49.35	-
	78.95	78.96	78.96	78.96	78.96	-	78.96	-
	98.69	98.69	98.69	98.69	98.69	-	98.69	-
	128.30	128.30	128.30	128.30	128.30	-	128.30	-
0.1	18.89	19.74	19.08	19.23	19.07	19.07	-	19.09
	45.61	49.35	45.58	46.31	45.39	45.49	-	45.62
	70.10	78.96	70.02	71.57	69.33	69.81	-	70.10
	85.49	98.69	85.37	87.54	84.15	85.06	-	85.49
	107.37	128.30	107.18	110.33	104.86	106.74	-	107.37
0.2	17.51	19.74	17.50	17.89	17.33	17.45	-	17.53
	38.47	49.35	38.38	39.74	36.82	38.19	-	38.48
	49.14	78.96	55.59	57.77	51.41	55.30	-	55.79
	55.78	98.69	65.72	68.36	59.30	65.31	-	66.00
	66.00	128.30	79.48	85.65	69.17	78.99	-	-

Table 8. Comparison study of frequency parameters Ω for an all edges simply supported squared plate [109]

2.2.2.2. Solutions for two opposite simply supported edges: Lévy's approach

Consider a plate with simple supports along edges $\xi = 0$ and $\xi = 1$. In the Lévy approach (see for instance Chen and Liu [234], Szilard [235] and Jomehzadeh and Saidi [226]):

$$\bar{w}(\xi, \eta) = \sum_{m=1}^{\infty} a W_m(\eta) \sin(m\pi\xi) \quad (2.124)$$

$$\bar{\psi}_x(\xi, \eta) = \sum_{m=1}^{\infty} \phi_x(\eta) \cos(m\pi\xi); \bar{\psi}_y(\xi, \eta) = \sum_{m=1}^{\infty} \phi_y(\eta) \sin(m\pi\xi)$$

Substituting Eq. (2.124) into Eq. (2.110),

$$\bar{\varphi}(\xi, \eta) = \frac{1}{a} \sum_{m=1}^{\infty} \varphi_m(\eta) \cos(m\pi\xi) \quad (2.125)$$

Using the non-dimensional parameters, substituting Eqs. (2.124) and (2.125) into Eqs. (2.114) and (2.115), it yields:

$$\Lambda_1 \frac{d^4 W_m}{d\eta^4} + \Lambda_2 \frac{d^2 W_m}{d\eta^2} + \Lambda_3 W_m = 0 \quad (2.126)$$

$$\Lambda_4 \frac{d^2 \varphi_m}{d\eta^2} + \Lambda_5 \varphi_m = 0 \quad (2.127)$$

where the different coefficients Λ_i ($i = 1, \dots, 5$) of the differential equation are given by

$$\begin{aligned} \Lambda_1 &= \chi^4 \left(1 - \gamma_2 \frac{\beta \chi^4 \bar{h}^4}{144\kappa} \Omega^2 \right); \\ \Lambda_2 &= \left[\chi^6 \Omega^2 \frac{\bar{h}^2}{12} \left(1 + \frac{\beta}{\kappa} \right) - 2(\chi m\pi)^2 \left(1 - \frac{\beta \chi^4 \bar{h}^4}{144\kappa} \Omega^2 \gamma_2 \right) \right] \\ \Lambda_3 &= \left[(m\pi)^4 - \chi^4 \Omega^2 \left[(m\pi)^4 \frac{\beta \bar{h}^4}{144\kappa} \gamma_2 + \frac{(m\pi \bar{h})^2}{12} \left(1 + \frac{\beta}{\kappa} \right) + 1 \right] + \frac{\beta \chi^8 \bar{h}^4}{144\kappa} \gamma_1 \Omega^4 \right] \\ \Lambda_4 &= \beta \chi^2 \frac{\bar{h}^2}{24} (1 - \nu); \Lambda_5 = - \left[(m\pi)^2 \beta \frac{\bar{h}^2}{24} (1 - \nu) + \kappa - \gamma_1 \frac{\beta \chi^4 \bar{h}^4}{144} \Omega^2 \right] \end{aligned} \quad (2.128)$$

The non-dimensional rotations $\bar{\psi}_x$ and $\bar{\psi}_y$ are expressed, following Eqs. (2.116) and (2.117), respectively:

$$\begin{aligned} & \left(\kappa^2 - \gamma_1 \Omega^2 \beta \frac{\chi^4 \bar{h}^4}{144} \right) \bar{\psi}_x \\ &= -m\pi \left[\left[\frac{\beta^2 \chi^4 \bar{h}^4}{144} \Omega^2 \frac{1}{\kappa} \left(1 + (m\pi)^2 \gamma_2 \frac{\bar{h}^2}{12} \right) - (m\pi)^2 \frac{\beta \bar{h}^2}{12} + \kappa \right. \right. \\ & \quad \left. \left. - \gamma_3 \Omega^2 \beta \frac{\chi^4 \bar{h}^4}{144} \right] W_m + \left[\chi^2 \frac{\beta \bar{h}^2}{12} - \frac{\beta^2 \chi^6 \bar{h}^6}{1728} \Omega^2 \frac{1}{\kappa} \gamma_2 \right] \frac{d^2 W_m}{d\eta^2} \right] \\ & \quad + \chi \beta \frac{\bar{h}^2}{24} (1 - \nu) \frac{\partial \varphi_m}{\partial \eta} \end{aligned} \quad (2.129)$$

$$\begin{aligned}
& \left(\kappa - \gamma_1 \Omega^2 \beta \frac{\chi^4 \bar{h}^4}{144} \right) \bar{\psi}_y \\
& = -\chi \frac{\partial}{\partial \eta} \left[\left[\frac{\beta^2 \chi^4 \bar{h}^4}{144} \Omega^2 \frac{1}{\kappa} \left(1 + (m\pi)^2 \gamma_2 \frac{\bar{h}^2}{12} \right) - (m\pi)^2 \frac{\beta \bar{h}^2}{12} + \kappa \right. \right. \\
& \quad \left. \left. - \gamma_3 \Omega^2 \beta \frac{\chi^4 \bar{h}^4}{144} \right] W_m + \left[\chi^2 \frac{\beta \bar{h}^2}{12} - \frac{\beta^2 \chi^6 \bar{h}^6}{1728} \Omega^2 \frac{1}{\kappa} \gamma_2 \right] \frac{d^2 W_m}{d\eta^2} \right] \\
& \quad + m\pi \beta \frac{\bar{h}^2}{24} (1 - \nu) \varphi_m
\end{aligned} \tag{2.130}$$

First of all, the solutions of the governing differential equations are found by determining the roots of the characteristic polynomial of Eq. (2.126), given by:

$$r_{\pm}^2 = \frac{-\Lambda_2 \pm \sqrt{\Lambda_2^2 - 4\Lambda_1\Lambda_3}}{2\Lambda_1} \tag{2.131}$$

In the literature, two transition frequencies Ω_-^t and Ω_+^t have been introduced. r_- and r_+ being both positive, equal to $(m\pi/\alpha)$, for Ω equal to 0, the transition frequencies are defined such as, for Ω greater than Ω_-^t and Ω_+^t , r_- and r_+ are imaginary number, respectively. Ω_-^t and Ω_+^t depend on the model, the boundary conditions, the geometric parameters such as the thickness ratio and for each model, these transition can occur only once. It has been shown in the literature [108] that whatever the frequency, for the truncated Uflyand-Mindlin plate model, r_+ is always real. The case of Ω greater than Ω_-^t and Ω_+^t is often ignored in the literature. Hashemi and Arsanjani [162] for instance calculated only the first frequencies, for which the transition frequencies are not reached.

Thus, different cases have to be considered following the value of the frequency Ω .

If $\Omega \leq \Omega_-^* < \Omega_+^t$ then r_- and r_+ are both real. The solution of the differential equation is given by

$$W_m(\eta) = C_1 \cosh r_+ \eta + C_2 \sinh r_+ \eta + C_3 \cosh r_- \eta + C_4 \sinh r_- \eta \tag{2.132}$$

If $\Omega_-^* < \Omega \leq \Omega_+^*$ then r_- is not real anymore and $\cosh r_- \eta$ and $\sinh r_- \eta$ are replaced by $\cos \tilde{r}_- \eta$ and $\sin \tilde{r}_- \eta$, respectively.

where \tilde{r}_- and \tilde{r}_+ are defined as follows

$$\tilde{r}_-^2 = \frac{\Lambda_2 + \sqrt{\Lambda_2^2 - 4\Lambda_1\Lambda_3}}{2\Lambda_1}; \tilde{r}_+^2 = \frac{\Lambda_2 - \sqrt{\Lambda_2^2 - 4\Lambda_1\Lambda_3}}{2\Lambda_1} \quad (2.133)$$

If $\Omega_-^* < \Omega$; $\Omega_+^* < \Omega$ then, r_- and r_+ are both complex numbers. Thus, $\cosh r_- \eta$, $\sinh r_- \eta$, $\cosh r_+ \eta$ and $\sinh r_+ \eta$ are replaced by $\cos \tilde{r}_- \eta$, $\sin \tilde{r}_- \eta$, $\cos \tilde{r}_+ \eta$ and $\sin \tilde{r}_+ \eta$, respectively.

Thus, before calculating the natural frequencies of a plate, it is important to consider all the possible expression of the displacements. These expressions depend on the natural frequencies, function of χ , the thickness ratio \bar{h} , the mode shape number m , the shear coefficient κ and the Poisson's ratio ν .

The roots of the characteristic equation Eq. (2.127) are:

$$u_{\pm} = \pm \sqrt{\frac{\Lambda_5}{\Lambda_4}} \quad (2.134)$$

Thus, φ_m is expressed as follows [108,226]:

$$\varphi_m(\eta) = C_5 \sinh u_+ \eta + C_6 \cosh u_+ \eta \quad (2.135)$$

Each edge of the plate can be clamped, simply supported or free. The boundary conditions are given, for each of these cases, by

Clamped:

$$w = 0; \psi_x = 0; \psi_y = 0 \quad (2.136)$$

Simply supported:

$$w = 0; \frac{\partial \psi_y}{\partial y} + \nu \frac{\partial \psi_x}{\partial x} = 0; \psi_x = 0 \quad (2.137)$$

Free:

$$\kappa Gh \left(\psi_y + \frac{\partial w}{\partial y} \right) - \gamma_2 \frac{\rho h^3}{12} \omega^2 \frac{\partial w}{\partial y} = 0; \frac{\partial \psi_y}{\partial y} + \nu \frac{\partial \psi_x}{\partial x} = 0; \frac{1}{2} (1 - \nu) D \left(\frac{\partial \psi_x}{\partial y} + \frac{\partial \psi_y}{\partial x} \right) = 0 \quad (2.138)$$

2.2.2.2.1. Two opposite edges simply supported and two other edges both clamped or free

In these problems, the plate has two plans of symmetry with respect to the central axis. Thus, in this case, the ξ axis is arbitrarily located at the center of the plate. This observation will help to considerably reduce the complexity and the calculation time in the determination of the natural frequencies.

First of all, the natural frequencies are obtained for a thin plate as the solutions of the following characteristic equations [108,158,229], for $m\pi < \Omega$:

- SCSC plate

$$2\Omega_1\tilde{\Omega}_2 \left[1 - \cosh \frac{\Omega_1}{\chi} \cos \frac{\tilde{\Omega}_2}{\chi} \right] + (\Omega_1^2 - \tilde{\Omega}_2^2) \sinh \frac{\Omega_1}{\chi} \sin \frac{\tilde{\Omega}_2}{\chi} = 0 \quad (2.139)$$

- SFSF plate

$$\begin{aligned} & \{ \Omega_1^2 [k - (1 - \nu)(m\pi)^2]^4 - \tilde{\Omega}_2^2 [k + (1 - \nu)(m\pi)^2]^4 \} \sinh \frac{\Omega_1}{\chi} \sin \frac{\tilde{\Omega}_2}{\chi} \\ & + 2\Omega_1\tilde{\Omega}_2 \left[(\Omega_1\tilde{\Omega}_2)^2 - \nu(1 - \nu)(m\pi)^4 \right] \left(1 - \cosh \frac{\Omega_1}{\chi} \cos \frac{\tilde{\Omega}_2}{\chi} \right) \\ & = 0 \end{aligned} \quad (2.140)$$

where

$$\Omega_1 = \frac{1}{b} \sqrt{(m\pi)^2 + \Omega^2}; \Omega_2 = \frac{1}{b} \sqrt{(m\pi)^2 - \Omega^2}; \tilde{\Omega}_2 = \frac{1}{b} \sqrt{\Omega^2 - (m\pi)^2} \quad (2.141)$$

If $\Omega \leq m\pi$ then $\tilde{\Omega}_2$, $\cos(\tilde{\Omega}_2/\chi)$ and $\sin(\tilde{\Omega}_2/\chi)$ are replaced by Ω_2 , $\cosh(\Omega_2/\chi)$ and $\sinh(\Omega_2/\chi)$, respectively.

For a thick plate, as explained before, there are two plans of symmetry. Thus, it is assumed that the displacement functions are either symmetric or antisymmetric with respect to the central axis. Thus, the two cases have to distinguished.

Symmetric modes

Restricting to this family of modes, the antisymmetric terms (in sine and hyperbolic sine) are deleted in the expression of the displacements. In other words, C_2 , C_4 and C_5 are taken equal to zero. The edges $\xi = -1/2$ and $\xi = 1/2$ are simply supported. The two other edges, at $\eta = -1/2$ and $\eta = 1/2$ are clamped or free. Because the deflection W_m being symmetric, $d^2W/d\eta^2$ is antisymmetric and it is deduced that the rotation ψ_y is also antisymmetric and so, from Eq. (2.130), φ_m is antisymmetric too. Thus, the displacement are expressed as follows:

- For $\Omega \leq \Omega_-^t < \Omega_+^t$

$$\begin{aligned} W_m(\eta) &= C_1 \cosh r_+ \eta + C_3 \cosh r_- \eta \\ \varphi_m(y) &= C_5 \sinh u_+ \eta \end{aligned} \quad (2.142)$$

If $\Omega_-^t < \Omega$ then $\cosh r_- \eta$ is replaced by $\cos \tilde{r}_- \eta$. If Ω is greater than both Ω_-^t and Ω_+^t , then $\cosh r_- \eta$ and $\cosh r_+ \eta$ are replaced by $\cos \tilde{r}_- \eta$ and $\cos \tilde{r}_+ \eta$, respectively.

Substituting the expressions of the displacements into the boundary equations, it leads to a system of three equations with three unknowns, written under the matrix form:

$$Z_S(C_i)_{i=1,3,5} = 0 \quad (2.143)$$

Where Z_S is a matrix 3×3 . In order to have a non trivial solution, the determinant of Z_S must vanish and it provides the natural frequencies of the plate.

It is found that the antisymmetric modes are obtained for odd values of n .

Antisymmetric modes

Analogically to the symmetric modes, in this case, C_1 , C_3 and C_6 vanish. The displacement is expressed as:

- $\Omega \leq \Omega_-^* < \Omega_+^*$ then $r_-^2 \geq 0; r_+^2 > 0$.

$$\begin{aligned} W_m(\eta) &= C_2 \sinh r_+ \eta + C_4 \sinh r_- \eta \\ \varphi_m(y) &= C_6 \cosh u_+ \eta \end{aligned} \quad (2.144)$$

If $\Omega_-^t < \Omega$ then $\sinh r_- \eta$ is replaced by $\sin \tilde{r}_- \eta$. If Ω is greater than both Ω_-^t and Ω_+^t , then $\sinh r_- \eta$ and $\sinh r_+ \eta$ are replaced by $\sin \tilde{r}_- \eta$ and $\sin \tilde{r}_+ \eta$, respectively. Applying the boundary conditions, one obtains a system of three equations with three unknown, put under the matrix form:

$$Z_{AS}(C_i)_{i=2,4,6} = 0 \quad (2.145)$$

Where Z_{AS} is a matrix 3×3 . In order to have a non trivial solution, the determinant of Z_{AS} must vanishes leading to the natural frequencies of the plate.

It is found that the antisymmetric modes are obtained for even values of n .

Thus, the natural frequencies of the plate problem are the value of Ω for which for which two matrices 3×3 (namely 18 coefficients) vanish. For other sets of boundary conditions, as it will be seen hereinafter, the natural frequencies are calculating by vanishing the determinant of a matrix 6×6 (namely 36 coefficients). Thus, the distinction of the symmetric and antisymmetric modes, as [159] and Gorman [160,172] did reduces the calculation time and is a very efficient way to simplify the problem.

For a SCSC plate:

$$Z_S = \begin{pmatrix} C_{r_+} & C_{r_-} & 0 \\ H_{1+}C_{r_+} & H_{1-}C_{r_-} & -\frac{\chi\bar{\beta}}{m\pi}u_+C_{u_+} \\ H_{1+r_+}S_{r_+} & H_{1-r_-}S_{r_-} & -\frac{\bar{\beta}m\pi}{\chi}S_{u_+} \end{pmatrix}$$

$$Z_{AS} = \begin{pmatrix} S_{r_+} & S_{r_-} & 0 \\ H_{1+}S_{r_+} & H_{1-}S_{r_-} & -\frac{\bar{\beta}\chi}{m\pi}u_+S_{u_+} \\ H_{1+r_+}C_{r_+} & H_{1-r_-}C_{r_-} & -\frac{\bar{\beta}m\pi}{\chi}C_{u_+} \end{pmatrix} \quad (2.146)$$

where,

$$H_1(x) = \frac{\beta^2\chi^4\bar{h}^4}{144} \frac{\Omega^2}{\kappa} - [\chi^2x + (m\pi)^2] \frac{\beta\bar{h}^2}{12} \left(1 - \gamma_2\Omega^2\bar{h}^4\chi^4 \frac{\beta}{144\kappa}\right) + \kappa^2$$

$$- \gamma_3\Omega^2\beta \frac{\chi^4\bar{h}^4}{144}$$

$$H_2(x) = \chi \left(\kappa - [\gamma_1 + \gamma_2] \frac{\beta\bar{h}^4\chi^4}{144} \Omega^2 - H_1(x) \right) \quad (2.147)$$

$$H_3(x) = [\chi^2x + \nu(m\pi)^2]$$

$$H_{i+} = H_i(-r_+^2); H_{i\bar{+}} = H_i(\bar{r}_+^2); H_{i-} = H_i(-r_-^2); H_{i\bar{-}} = H_i(\bar{r}_-^2) \quad (i = 1,2,3)$$

$$C_x = \cosh x; S_x = \sinh x; \tilde{C}_x = \cos \tilde{x}; \tilde{S}_x = \sin \tilde{x}; \bar{\beta} = (1 - \nu) \frac{\beta\bar{h}^2}{24}$$

For a SFSF plate:

$$Z_S = \begin{pmatrix} H_{3+}H_{1+}C_{r_{\pm}}/2 & H_{3-}H_{1-}C_{r_{\pm}}/2 & \bar{\beta}(1-\nu)\chi m\pi u_+ C_{u_{\pm}}/2 \\ H_{2+}r_+ S_{r_{\pm}}/2 & H_{2-}r_- S_{r_{\pm}}/2 & m\pi\bar{\beta}S_{u_{\pm}}/2 \\ m\pi\chi H_{1+}r_+ S_{r_{\pm}}/2 & m\pi\chi H_{1-}r_- S_{r_{\pm}}/2 & -\frac{\bar{\beta}}{2}[\chi^2 u_+^2 + (m\pi)^2]S_{u_{\pm}}/2 \end{pmatrix} \quad (2.148)$$

$$Z_{AS} = \begin{pmatrix} H_{3+}H_{1+}S_{r_{\pm}}/2 & H_{3-}H_{1-}S_{r_{\pm}}/2 & \bar{\beta}(1-\nu)\chi m\pi u_+ S_{u_{\pm}}/2 \\ H_{2+}r_+ C_{r_{\pm}}/2 & H_{2-}r_- C_{r_{\pm}}/2 & m\pi\bar{\beta}C_{u_{\pm}}/2 \\ m\pi\chi H_{1+}r_+ C_{r_{\pm}}/2 & m\pi\chi H_{1-}r_- C_{r_{\pm}}/2 & -\frac{\bar{\beta}}{2}(1-\nu)[\chi^2 u_+^2 + (m\pi)^2]C_{u_{\pm}}/2 \end{pmatrix}$$

In both cases, if $\Omega_-^t < \Omega$ then $-r_-^2$, $C_{r_{\pm}}/2$; $r_- S_{r_{\pm}}/2$; $S_{r_{\pm}}/2$ and $r_- C_{r_{\pm}}/2$ are replaced by \tilde{r}_-^2 , $\tilde{C}_{r_{\pm}}/2$, $-\tilde{r}_- \tilde{S}_{r_{\pm}}/2$, $\tilde{S}_{r_{\pm}}/2$ and $\tilde{r}_- \tilde{C}_{r_{\pm}}/2$, respectively. If Ω is greater than both Ω_-^t and Ω_+^t then $r_-^2 < 0$; $r_+^2 < 0$, $-r_+^2$, $C_{r_{\pm}}/2$; $r_- S_{r_{\pm}}/2$; $S_{r_{\pm}}/2$ and $r_+ C_{r_{\pm}}/2$ are replaced by \tilde{r}_-^2 , $\tilde{C}_{r_{\pm}}/2$, $-\tilde{r}_+ \tilde{S}_{r_{\pm}}/2$, $\tilde{S}_{r_{\pm}}/2$ and $\tilde{r}_+ \tilde{C}_{r_{\pm}}/2$, respectively

2.2.2.2. Two other opposite edges with differing boundary conditions

For a plate having two opposite edges that are simply supported and the two other that are different (SSSF, SSSC and SCSF), the origin of the coordinate system is taken at a corner of the plate. Thus, the edges $\xi = 0$ and $\xi = 1$ are simply supported. The boundary conditions, three at each edge, are applied at $\eta = 0$ and $\eta = 1$. Thus, it results in a system of six equations, written under the matrix form as follows:

$$Z(C_i)_{i=1,2,3,4,5,6} = 0 \quad (2.149)$$

with Z is a matrix 6×6 . In order to have a non trivial solution, the determinant of Z must vanishes, leading to an exact equation. The roots of this equation are the natural frequencies.

The coefficients of the matrix Z have been given in the literature for different sets of boundary conditions for thin plates [158] and thick plates [108].

For a thin plate [158], for $m\pi < \Omega$, the characteristic equations for the three different sets of boundary conditions are

- SSSF

$$\begin{aligned} & \tilde{\Omega}_2[\Omega + (1 - \nu)(m\pi)^2]^2 \sinh \frac{\Omega_1}{\chi} \cos \frac{\tilde{\Omega}_2}{\chi} \\ & - \Omega_1[k - (1 - \nu)(m\pi)^2]^2 \cosh \frac{\Omega_1}{\chi} \sin \frac{\tilde{\Omega}_2}{\chi} = 0 \end{aligned} \quad (2.150)$$

- SSSC

$$\Omega_1 \cosh \frac{\Omega_1}{\chi} \sin \frac{\tilde{\Omega}_2}{\chi} - \tilde{\Omega}_2 \sinh \frac{\Omega_1}{\chi} \cos \frac{\tilde{\Omega}_2}{\chi} = 0 \quad (2.151)$$

- SCSF

$$\begin{aligned} & \Omega_1 \tilde{\Omega}_2 [\Omega^2 - (1 - \nu)^2 (m\pi)^4] + (m\pi)^2 [(1 - 2\nu)\Omega^2 - (1 - \nu)^2 (m\pi)^4] \sinh \frac{\Omega_1}{\chi} \sin \frac{\tilde{\Omega}_2}{\chi} \\ & + \Omega_1 \tilde{\Omega}_2 [\Omega^2 + (1 - \nu)^2 (m\pi)^4] \cosh \frac{\Omega_1}{\chi} \cos \frac{\tilde{\Omega}_2}{\chi} = 0 \end{aligned} \quad (2.152)$$

For each of these models, for $\Omega \leq m\pi$, $\tilde{\lambda}_2$, $\sin(\tilde{\Omega}_2/\chi)$ and $\cos(\tilde{\Omega}_2/\chi)$ are replaced by Ω_2 , $\sin(\Omega_2/\chi)$ and $\cos(\Omega_2/\chi)$, respectively Leissa [159].

For a SSSF plate,

- For Ω smaller than both Ω_-^t and Ω_+^t .

$$\begin{aligned} & Z_{12} = H_{3+}H_{1+}; Z_{14} = H_{3-}H_{1-}; Z_{16} = \chi\bar{\beta}(1 - \nu)m\pi u_+; Z_{21} = H_{2+}r_+; Z_{23} \\ & = H_{2-}r_-; Z_{25} = \bar{\beta}m\pi; \\ & Z_{31} = -2\chi m\pi r_+ H_{1+}; Z_{33} = -2\chi m\pi r_- H_{1-}; Z_{35} = \bar{\beta}[\chi^2 u_+^2 + (m\pi)^2]; Z_{41} = S_{r_+}; Z_{42} \\ & = C_{r_+}; \\ & Z_{43} = S_{r_-}; Z_{44} = C_{r_-}; Z_{51} = H_{3+}H_{1+}S_{r_+}; Z_{52} = H_{3+}H_{1+}C_{r_+}; Z_{53} = H_{3-}H_{1-}S_{r_-}; Z_{54} \\ & = H_{3-}H_{1-}C_{r_-} \\ & Z_{55} = \bar{\beta}(1 - \nu)\chi m\pi u_+ S_{u_+}; Z_{56} = \bar{\beta}(1 - \nu)\chi m\pi u_+ C_{u_+}; Z_{61} = H_{1+}S_{r_+}; Z_{62} \\ & = H_{1+}C_{r_+}; \\ & Z_{63} = H_{1-}S_{r_-}; Z_{64} = H_{1-}C_{r_-}; Z_{65} = -\frac{\bar{\beta}\chi}{m\pi}S_{u_+}; Z_{66} = \frac{\bar{\beta}\chi}{m\pi}C_{u_+}; \\ & Z_{11} = Z_{13} = Z_{15} = Z_{22} = Z_{24} = Z_{26} = Z_{32} = Z_{34} = Z_{36} = Z_{45} = Z_{46} = 0 \end{aligned} \quad (2.153)$$

- $\Omega_-^t < \Omega$ then the coefficients $Z_{14}, Z_{23}, Z_{33}, Z_{43}, Z_{44}, Z_{53}, Z_{54}, Z_{63}$ and Z_{64} are replaced by

$$\begin{aligned}\tilde{Z}_{14} &= \tilde{H}_{3-}\tilde{H}_{1-}; \tilde{Z}_{23} = \tilde{H}_{2-}\tilde{r}_-; \tilde{Z}_{33} = -2m\pi\chi\tilde{H}_{1-}\tilde{r}_-; \tilde{Z}_{43} = \tilde{S}_{r-}; \tilde{Z}_{44} = \tilde{C}_{r-} \\ \tilde{Z}_{53} &= \tilde{H}_{3-}\tilde{H}_{1-}\tilde{S}_{r-}; \tilde{Z}_{54} = \tilde{H}_{3-}\tilde{H}_{1-}\tilde{C}_{r-}; \tilde{Z}_{63} = \tilde{H}_{1-}\tilde{S}_{r-}; \tilde{Z}_{64} = \tilde{H}_{1-}\tilde{C}_{r-}\end{aligned}\quad (2.154)$$

- For Ω greater than both Ω_-^t and Ω_+^t , the matrix Z is given by the coefficients \tilde{Z}_{ij} with $\tilde{Z}_{14}, \tilde{Z}_{23}, \tilde{Z}_{33}, \tilde{Z}_{43}, \tilde{Z}_{44}, \tilde{Z}_{53}, \tilde{Z}_{54}, \tilde{Z}_{63}$ and \tilde{Z}_{64} given in the previous equations and the other coefficient given by

$$\begin{aligned}\tilde{Z}_{16} &= Z_{16}; \tilde{Z}_{25} = Z_{25}; \tilde{Z}_{35} = Z_{35}; \tilde{Z}_{55} = Z_{55}; Z_{56} = \tilde{Z}_{56}; \tilde{Z}_{65} = Z_{65}; \tilde{Z}_{66} = Z_{66} \\ Z_{12} &= \tilde{H}_{3+}\tilde{H}_{1+}; Z_{21} = \tilde{H}_{2+}\tilde{r}_+; Z_{31} = -2m\pi\chi\tilde{H}_{1+}\tilde{r}_+; Z_{41} = \tilde{S}_{r+} \\ Z_{42} &= \tilde{C}_{r+}; Z_{51} = \tilde{H}_{3+}\tilde{H}_{1+}\tilde{S}_{r+}; Z_{52} = \tilde{H}_{3+}\tilde{H}_{1+}\tilde{C}_{r+}; Z_{61} = \tilde{r}_+\tilde{H}_{1+}\tilde{S}_{r+}; Z_{62} \\ &= \tilde{r}_+\tilde{H}_{1+}\tilde{C}_{r+}; \\ Z_{11} &= Z_{13} = Z_{15} = Z_{22} = Z_{24} = Z_{26} = Z_{32} = Z_{34} = Z_{36} = Z_{45} = Z_{46} = 0\end{aligned}\quad (2.155)$$

For a SSSC plate

- For Ω smaller than both Ω_-^t and Ω_+^t

$$\begin{aligned}Z_{12} &= Z_{14} = 1; Z_{16} = Z_{11} = Z_{13} = Z_{15} = Z_{21} = Z_{23} = Z_{25} = Z_{32} = Z_{34} = Z_{36} \\ &= Z_{45} = Z_{46} = 0 \\ Z_{22} &= H_{3+}H_{1+}; Z_{24} = H_{3-}H_{1-}; Z_{26} = \bar{\beta}(1-\nu)\chi m\pi u_+; Z_{32} = H_{1+}; Z_{34} = H_{1-}; Z_{36} \\ &= -\bar{\beta}\frac{m\pi}{\chi} \\ Z_{41} &= S_{r+}; Z_{42} = C_{r+}; Z_{43} = S_{r-}; Z_{44} = C_{r-}; Z_{51} = H_{1+}S_{r+}; Z_{52} = H_{1+}C_{r+}; Z_{53} \\ &= H_{1-}S_{r-} \\ Z_{54} &= H_{1-}C_{r-}; Z_{55} = -\frac{\bar{\beta}\chi}{m\pi}u_+S_{u+}; Z_{56} = -\frac{\bar{\beta}\chi}{m\pi}u_+C_{u+}; Z_{61} = H_{1+}r_+C_{r+}; Z_{62} \\ &= H_{1+}r_+S_{r+}; \\ Z_{63} &= H_{1-}r_-C_{r-}; Z_{64} = H_{1-}r_-S_{r-}; Z_{65} = -\bar{\beta}\frac{m\pi}{\chi}C_{u+}; Z_{66} = -\bar{\beta}\frac{m\pi}{\chi}S_{u+}\end{aligned}\quad (2.156)$$

- $\Omega_-^t < \Omega \leq \Omega_+^*$ then the coefficients $\tilde{Z}_{24}, \tilde{Z}_{34}, \tilde{Z}_{43}, \tilde{Z}_{44}, \tilde{Z}_{53}, \tilde{Z}_{54}, \tilde{Z}_{63}$ and \tilde{Z}_{64} are replaced by

$$\begin{aligned} Z_{24} &= \tilde{H}_{3-}\tilde{H}_{1-}; Z_{34} = \tilde{H}_{1-}; Z_{43} = \tilde{S}_{r-}; Z_{44} = \tilde{C}_{r-}; \\ Z_{53} &= \tilde{H}_{1-}\tilde{S}_{r-}; Z_{54} = \tilde{H}_{1-}\tilde{C}_{r-}; Z_{63} = \tilde{H}_{1-}\tilde{r}_-\tilde{C}_{r-}; Z_{64} = -\tilde{H}_{1-}\tilde{r}_-\tilde{S}_{r-} \end{aligned} \quad (2.157)$$

- For Ω greater than both Ω_-^t and Ω_+^t , the matrix Z is given by the coefficients \tilde{Z}_{ij} with $\tilde{Z}_{24}, \tilde{Z}_{34}, \tilde{Z}_{43}, \tilde{Z}_{44}, \tilde{Z}_{53}, \tilde{Z}_{54}, \tilde{Z}_{63}$ and \tilde{Z}_{64} given in the previous equations and the other coefficient given by

$$\begin{aligned} \tilde{Z}_{26} &= Z_{26}; \tilde{Z}_{36} = Z_{36}; \tilde{Z}_{55} = Z_{55}; \tilde{Z}_{56} = Z_{56}; \tilde{Z}_{65} = Z_{65}; \tilde{Z}_{66} = Z_{66} \\ Z_{22} &= \tilde{H}_{3+}\tilde{H}_{1+}; Z_{32} = \tilde{H}_{1+}; \\ Z_{41} &= \tilde{S}_{r+}; Z_{42} = \tilde{C}_{r+}; Z_{51} = \tilde{H}_{1+}\tilde{S}_{r+}; Z_{52} = \tilde{H}_{1+}\tilde{C}_{r+}; Z_{61} = \tilde{H}_{1+}\tilde{r}_+\tilde{C}_{r+}; Z_{62} \\ &= -\tilde{H}_{1+}\tilde{r}_+\tilde{S}_{r+}; \\ Z_{12} &= Z_{14} = 1; Z_{16} = Z_{11} = Z_{13} = Z_{15} = Z_{21} = Z_{23} = Z_{25} = Z_{32} = Z_{34} = Z_{36} \\ &= Z_{45} = Z_{46} = 0 \end{aligned} \quad (2.158)$$

For a SCSF plate, the edges $\eta = 0$ and $\eta = 1$ are taken free and clamped, respectively. The coefficients of the matrix Z are

- For Ω smaller than both Ω_-^t and Ω_+^t

$$\begin{aligned} Z_{12} &= H_{3+}H_{1+}; Z_{14} = H_{3-}H_{1-}; Z_{16} = \chi\bar{\beta}(1-\nu)m\pi u_+; Z_{21} = H_{2+}r_+; Z_{23} \\ &= H_{2-r-}; Z_{25} = m\pi\bar{\beta}; \\ Z_{31} &= -2\chi m\pi H_{1+}r_+; Z_{33} = -2\chi m\pi H_{1-r-}; Z_{35} = \bar{\beta}[\chi^2 u_+^2 + (m\pi)^2]; Z_{41} \\ &= S_{r+}; Z_{42} = C_{r+}; \\ Z_{43} &= S_{r-}; Z_{44} = C_{r-}; Z_{51} = H_{1+}S_{r+}; Z_{52} = H_{1+}C_{r+}; Z_{53} = H_{1-}S_{r-}; Z_{54} = H_{1-}C_{r-}; \\ Z_{55} &= -\frac{\bar{\beta}\chi}{m\pi}u_+S_{u+}; Z_{56} = -\frac{\bar{\beta}\chi}{m\pi}u_+C_{u+}; Z_{61} = H_{1+}r_+C_{r+}; Z_{62} = H_{1+}r_+S_{r+}; \\ Z_{63} &= H_{1-r-}C_{r-}; Z_{64} = H_{1-r-}S_{r-}; Z_{65} = -\bar{\beta}\frac{m\pi}{\chi}C_{u+}; Z_{66} = -\bar{\beta}\frac{m\pi}{\chi}S_{u+} \\ Z_{11} &= Z_{13} = Z_{15} = Z_{22} = Z_{24} = Z_{26} = Z_{32} = Z_{34} = Z_{36} = Z_{45} = Z_{46} = 0 \end{aligned} \quad (2.159)$$

- For $\Omega_-^t < \Omega$ the coefficients $Z_{14}, Z_{23}, Z_{33}, Z_{43}, Z_{44}, Z_{53}, Z_{54}, Z_{63}$ and Z_{64} are replaced by

$$\begin{aligned} Z_{14} &= \tilde{H}_{3-}\tilde{H}_{1-}; Z_{23} = \tilde{H}_{2-}\tilde{r}_-; Z_{33} = -2m\pi\chi\tilde{H}_{1-}\tilde{r}_-; Z_{43} = \tilde{S}_{r-}; Z_{44} = \tilde{C}_{r-} \\ Z_{53} &= \tilde{H}_{1-}\tilde{S}_{r-}; Z_{54} = \tilde{H}_{1-}\tilde{C}_{r-}; Z_{63} = \tilde{H}_{1-}\tilde{r}_-\tilde{C}_{r-}; Z_{64} = -\tilde{H}_{1-}\tilde{r}_-\tilde{S}_{r-} \end{aligned} \quad (2.160)$$

- For Ω greater than both Ω_-^t and Ω_+^t , the matrix Z is given by the coefficients \tilde{Z}_{ij} with $\tilde{Z}_{24}, \tilde{Z}_{34}, \tilde{Z}_{43}, \tilde{Z}_{44}, \tilde{Z}_{53}, \tilde{Z}_{54}, \tilde{Z}_{63}$ and \tilde{Z}_{64} given in the previous equations and the other coefficient given by

$$\begin{aligned} \tilde{Z}_{16} &= Z_{16}; \tilde{Z}_{25} = Z_{25}; \tilde{Z}_{35} = Z_{35}; \tilde{Z}_{55} = Z_{55}; \tilde{Z}_{56} = Z_{56}; \tilde{Z}_{65} = Z_{65}; \tilde{Z}_{66} = Z_{66} \\ Z_{12} &= \tilde{H}_{3+}\tilde{H}_{1+}; Z_{21} = \tilde{H}_{2+}\tilde{r}_+; Z_{31} = -2m\pi\chi\tilde{H}_{1+}\tilde{r}_+; Z_{41} = \tilde{S}_{r+}; Z_{42} = \tilde{C}_{r+}; \\ Z_{51} &= \tilde{H}_{1+}\tilde{S}_{r+}; Z_{52} = \tilde{H}_{1+}\tilde{C}_{r+}; Z_{61} = \tilde{H}_{1+}\tilde{r}_+\tilde{C}_{r+}; Z_{62} = -\tilde{H}_{1+}\tilde{r}_+\tilde{S}_{r+} \\ Z_{11} &= Z_{13} = Z_{15} = Z_{22} = Z_{24} = Z_{26} = Z_{32} = Z_{34} = Z_{36} = Z_{45} = Z_{46} = 0 \end{aligned} \quad (2.161)$$

2.2.2.3. Discussion

The five first non-dimensional natural frequencies Ω for plates having two edges that are simply supported are calculated in Tables 9-11 for the six different sets of boundary conditions for a Poisson's ratio taken equal to 0.3. Two aspect ratios are considered, equal to unity and two, respectively. In order to study the effect of rotary inertia and shear effects that increase with the thickness ratio of the plate, the frequencies are obtained for three different thickness ratios are considered: $\bar{h} = 0.01$ (thin plate), $\bar{h} = 0.1$ and $\bar{h} = 0.2$. The results have been validated by comparing with those obtained found in the literature (Leissa [159] for the Kirchhoff-Love thin plate theory, Wang and Wang [229] and Hashemi and Arsanjani [162] for the original Uflyand-Mindlin thick plate model).

The shear correction factor has been taken equal to 0.8667 in order to perform the comparison. However, different values could be considered [108]: $\pi^2/12$ [103,104], 0.822, 0.88 [236,237]. In the present thesis, the shear coefficient has been determined as a function of the Poisson's ratio through an asymptotic analysis. The comparison of the natural frequencies for different coefficients shows that the results are extremely similar when it is selected among one of the previously cited values.

In this thesis, all the results are calculated from the closed-form solution for a plate with all edges simply supported and from an exact solution for a plate having two opposite edges that are simply supported. Thus, their accuracy is maximal.

First of all, it is seen in the different tables that whatever the boundary conditions, the thickness ratio or the aspect ratio, the non-dimensional fundamental frequency of a square plate is nearly the same between the different Uflyand-Mindlin plate models. Thus, Fig. 11 depicts the fundamental frequency for a square plate with a thickness ratio of 0.1 and Figs. 12 and 13 show the non-dimensional fundamental frequency for a SCSC plate and various couples (\bar{h}, χ) .

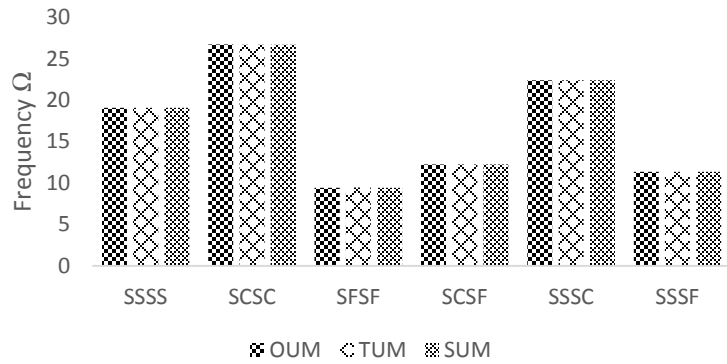


Fig. 11. Nondimensional fundamental frequency determined through the three Uflyand-Mindlin plate models (original, truncated and based on slope inertia) for different boundary conditions, with $\bar{h} = 0.1, \chi = 1$

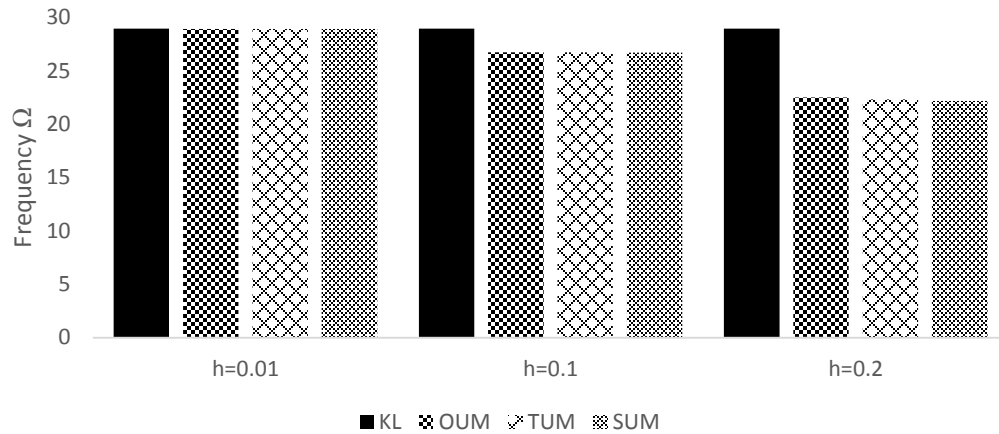


Fig. 12. Nondimensional fundamental frequency obtained through the KL model and the three Uflyand-Mindlin plate models (original, truncated and based on slope inertia) and considering different thickness ratios for a square SCSC plate

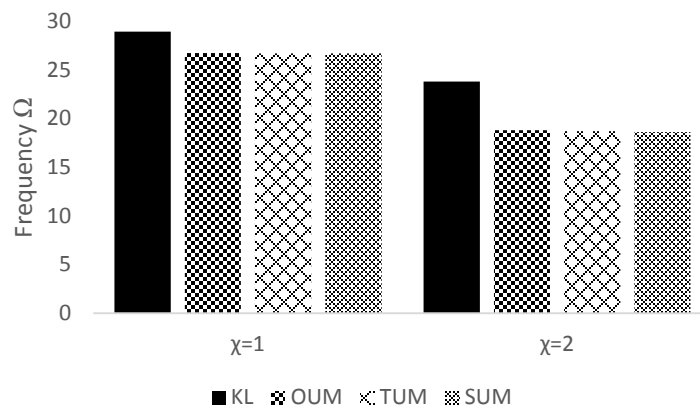


Fig. 13. Nondimensional fundamental frequency obtained through the KL model and the three Uflyand-Mindlin plate models (original, truncated and based on slope inertia) and considering different aspect ratios for a SCSC plate with a thickness ratio equal to 0.1

For higher order of natural frequencies, it is seen that the Uflyand-Mindlin plate model based on slope inertia leads to smaller natural frequencies compared to the ones determined through the truncated model. This has already been observed and explained a plate, simply supported at all edges, by comparing the closed form expression of the frequencies (see Eq. (2.122)).

Moreover, it appears interesting to compare the influence of the thickness ratio, associated to the rotary inertia and the shear effects, on the natural frequencies calculated in the different Uflyand-Mindlin plate models. In this purpose, for each boundary condition, the aspect ratio is taken constant and the non-dimensional natural frequencies are determined for a thickness ratio \bar{h} equal to 0.01, 0.1 and 0.2. For a thickness ratio equal to 0.01, the plate is thin, the rotary inertia and the shear effects are not important: the results of the Uflyand-Mindlin plate models are close to those of the Kirchhoff-Love plate model obtained by Leissa [158]. When the thickness ratio increases, the rotary inertia and the shear effect become important and cannot be ignored. A difference occurs between the Kirchhoff-Love plate model and the thick plate model. This difference increase with the order of the frequency and the thickness ratio.

Now, to compare the influence of the boundary conditions on the natural frequencies of the plate, the thickness and aspect ratios are arbitrarily taken equal to 0.2 and 1 (thick square plate). It is seen in Tables 9-11 that the difference between the different models, whatever the considered boundary conditions increases with the mode number and the natural frequency strongly depends on the boundary conditions. Thus, $\Omega_{SFSF} < \Omega_{SSSF} < \Omega_{SCSF} < \Omega_{SSSS} < \Omega_{SSSC} < \Omega_{SCSC}$, as shown in Fig. 11. Indeed, an edge that is clamped has more constraints than a simply supported edge, itself being having more constraints than a free edge. A decrease of the constraints results in a decrease of the rigidity of the plate. The natural frequency depends on the flexibility of the plate. Consequently, the choice of the boundary conditions is extremely important and has a huge impact on the mechanical behavior in vibration of the plate.

Furthermore, a comparison of the natural frequencies calculated for an aspect ratio equal to unity and two, for a constant thickness ratio, show that, whatever the boundary conditions, the frequencies decrease with the aspect ratio.

Thus, three different versions of the Uflyand-Mindlin plate models (original, truncated and based on slope inertia) have been derived. The well-known original model is derivable from the equilibrium equations and variationally. Scientists suggested that it overcorrects the shear effect and the truncated model has been developed. This truncated theory is derived through the use of equilibrium equations. It is shown that it is asymptotically consistent at the second order. The variational derivation of this truncated results in a Uflyand-Mindlin plate model based on slope inertia, only derived variationnally and is not asymptotically consistent, whatever the considered order.

For each of these models, the first five natural frequencies have been calculated for a plate having two opposite edges that are simply supported. For the fundamental natural frequencies, the three models match. However, for higher order of frequencies, a difference occurs. This difference increases with the aspect ratio, the ratio of frequency and strongly depends on the boundary conditions. Thus, when the flexural rigidity of the plate increases, the natural frequencies decrease whereas the difference between the models increases.

	χ	$\bar{h} = 0.01$			$\bar{h} = 0.1$			$\bar{h} = 0.2$		
		OUM	TUM	SUM	OUM	TUM	SUM	OUM	TUM	SUM
S S S	1	99.96	99.96	99.96	96.68	96.65	96.61	88.68	88.30	87.81
		99.91	99.91	99.91	92.37	92.19	91.97	77.78	76.54	74.62
		99.85	99.86	99.86	88.68	88.29	87.81	70.40	68.50	65.11
		99.82	99.82	99.82	84.47	85.96	85.26	66.59	64.37	60.08
		99.77	99.77	99.77	83.53	82.78	81.73	61.94	59.36	46.22
S S S	2	99.91	99.91	99.91	92.37	92.19	91.97	77.78	76.54	74.62
		99.85	99.86	99.86	88.68	88.30	87.81	70.40	68.50	65.10
		99.77	99.77	99.77	83.53	82.78	81.73	61.94	59.37	53.91
		99.70	99.70	99.70	80.08	79.04	77.49	57.10	54.21	47.49
		99.65	99.65	99.65	77.97	76.54	74.62	54.16	51.12	43.62
S C S C	1	99.93	99.93	99.93	92.36	92.28	92.17	77.73	77.14	76.59
		99.87	99.87	99.87	89.98	89.76	89.53	73.32	71.99	70.16
		99.83	99.83	99.83	85.79	85.52	85.20	65.00	63.42	61.77

		99.77	99.77	99.77	83.72	83.25	82.72	62.51	60.39	57.52
		99.80	99.80	99.80	85.32	84.77	84.06	64.93	62.67	58.54
	2	99.68	99.63	99.60	78.90	78.48	78.06	54.71	52.70	51.47
		99.62	99.62	99.62	77.75	77.16	76.61	54.37	52.05	49.77
		99.57	99.57	99.57	76.21	75.32	74.29	53.06	50.16	45.97
		99.50	99.50	99.46	73.32	71.99	70.16	46.92	42.88	38.94
		99.30	99.30	99.30	65.62	64.17	62.82	42.72	39.82	34.35

Table 9. First natural frequencies of a SSSS and a SCSC plate considering the KL, OUM, TUM and SUM theories for different aspect and thickness ratios ($\kappa = 0.86667$; $\nu = 0.3$)

	χ	$\bar{h} = 0.01$			$\bar{h} = 0.1$			$\bar{h} = 0.2$		
		OUM	TUM	SUM	OUM	TUM	SUM	OUM	TUM	SUM
S F	1	99.94	99.90	99.91	98.03	98.10	98.01	93.41	93.58	93.16
		99.76	99.69	99.68	95.39	95.89	95.35	87.56	88.98	87.00
		99.68	99.70	99.68	92.33	93.47	92.11	79.65	82.52	77.65
		99.89	99.89	99.89	93.53	93.57	93.26	80.72	80.21	78.40
		99.78	99.78	99.77	91.76	92.12	91.40	77.37	77.62	74.54
S F	2	99.54	99.54	99.54	97.77	97.90	97.81	93.36	93.73	93.23
		99.33	99.35	99.33	90.66	92.40	90.60	77.45	82.60	76.43
		99.84	99.85	99.85	93.43	93.58	93.17	80.71	80.47	78.44
		99.47	99.49	99.47	87.59	89.01	87.02	70.25	73.21	66.53
		99.78	99.78	99.78	87.32	87.26	86.31	68.31	67.01	62.57

S S S F	1	99.73	99.73	99.73	97.18	97.32	97.14	91.55	92.02	91.16
		99.79	99.80	99.79	94.35	94.79	94.22	83.70	84.73	82.31
		99.85	99.85	99.85	93.08	93.15	92.81	79.79	79.37	77.30
		99.78	99.79	99.78	90.38	90.56	89.84	74.25	73.85	72.98
		99.78	99.79	99.78	90.14	90.77	89.55	73.68	74.58	74.16
	2	99.70	98.98	98.98	95.41	95.51	95.02	87.56	88.82	86.99
		99.78	99.75	99.75	91.60	92.10	91.34	77.37	77.58	74.50
		99.68	99.68	99.65	88.13	89.71	87.35	70.12	73.70	65.31
		99.67	99.72	99.71	86.09	86.17	84.96	66.39	65.36	60.23
		99.50	99.54	99.51	83.74	84.76	82.35	63.02	64.90	55.34

Table 10. First natural frequencies of a SFSF and a SSSF plate considering the KL, OUM, TUM and SUM theories for different aspect and thickness ratios ($\kappa = 0.86667$; $\nu = 0.3$)

	χ	$\bar{h} = 0.01$			$\bar{h} = 0.1$			$\bar{h} = 0.2$		
		OUM	TUM	SUM	OUM	TUM	SUM	OUM	TUM	SUM
S S S C	1	99.97	99.97	99.97	94.81	94.76	94.71	83.70	83.24	82.71
		99.89	99.89	99.89	91.39	91.19	90.96	75.87	74.58	72.69
		99.86	99.86	99.86	89.22	88.98	88.71	71.24	69.82	66.31
		99.82	99.82	99.82	86.38	85.95	85.44	66.57	64.56	61.41
		99.81	99.82	99.82	85.99	85.45	84.74	65.87	63.61	59.39
	2	99.75	99.75	99.75	85.74	85.48	85.13	64.95	63.40	61.77
		99.78	99.78	99.78	83.70	83.24	82.71	62.52	60.40	57.57

		99.69	99.70	99.69	80.37	79.54	78.49	57.90	55.13	50.26
		99.59	99.60	99.59	73.14	71.98	70.37	48.27	44.82	40.03
		99.51	99.51	99.51	75.28	73.98	72.10	51.70	48.49	41.59
S C	1	99.87	99.87	99.88	96.45	96.64	96.41	89.64	90.18	89.23
		99.78	99.79	99.79	92.14	92.69	91.95	78.29	79.30	76.77
		99.86	99.87	99.87	92.82	92.91	92.51	79.26	78.85	76.77
		99.75	99.75	99.75	88.82	89.04	88.25	71.48	71.08	67.73
		99.75	99.75	99.75	86.95	87.55	86.26	67.53	68.03	63.56
S F	2	99.68	99.68	99.72	92.79	93.43	92.72	81.03	82.56	80.10
		99.70	99.70	99.78	89.75	90.24	89.38	73.97	74.29	71.14
		99.66	99.67	99.68	82.02	83.50	81.01	58.59	61.10	58.96
		99.61	99.61	99.64	84.25	84.37	83.09	64.44	63.38	65.27
		99.40	99.41	99.41	78.32	79.30	76.80	55.26	56.47	59.51

Table 11. First natural frequencies of a SSSC and SCSF plate considering the KL, OUM, TUM and SUM theories for different aspect and thickness ratios ($\kappa = 0.86667$; $\nu = 0.3$)

3. NONLOCAL PHENOMENOLOGICAL MODELS: ASYMPTOTIC AND ENGINEERING APPROACHES

As explained in the first chapter constituting a review of the different results existing in the literature, for nanomaterials such as carbon nanotubes or graphene nanoplates, different small scale effects (for instance the interatomic interactions) have to be taken into account. Thus, the classical local theories are not sufficient to describe the mechanical behavior of beams and plates and there is a real need to develop nonlocal theories that do not ignore those effects. In this chapter, two kinds of theories are presented.

The first approach is the asymptotic approach. The local asymptotic model for beams and plates has been derived at the lowest and second order in the previous chapter. It has been shown that the local Bernoulli-Euler beam model and the Kirchhoff-Love plate model and the truncated Bresse-Timoshenko and Uflyand-Mindlin models are asymptotically consistent at the zeroth and second order, respectively. Nevertheless, the asymptotic justification of these nonlocal beam models is still missing. Thus, one of the objective of the present chapter is to extend the asymptotic derivation of asymptotic beam and plate models by taking into account the nonlocal effect [238,239]. For both beams and plates models, three different nonlocal asymptotic approaches will be considered.

Furthermore, in the literature, the original and the truncated Bresse-Timoshenko and Uflyand-Mindlin theories have been derived by taking into account the nonlocal effect. These models are called fourth order phenomenological models. Indeed, they are derived from a postulated nonlocal constitutive laws following the gradient formulation of the stress-strain relationship given by Eringen and they lead to a governing differential equation containing only fourth order derivative terms in time or following x or y . Thus, in this chapter, the different Bresse-Timoshenko and Uflyand-Mindlin models (original, truncated and based on slope inertia) are derived. For thin beams and plates, it is also proposed an alternative sixth order phenomenological model.

The natural frequencies will be determined for simply supported carbon nanotubes and nanoplates, using the different values of parameters given in the literature and the different approaches will be compared.

3.1. Different beam models

3.1.1. Asymptotic derivation of nonlocal beam models

Three different nonlocal asymptotic models, different in the postulated stress-displacement partial differential equations are considered. Indeed, for a beam, the nonlocality in the relation can be along the horizontal, the vertical or both directions. These three cases have to be studied and none of them should be ignored.

3.1.1.1. Asymptotic model with a partial nonlocality along the horizontal direction

Consider the same beam as in the previous chapter, with a width b , thickness h and a length L . It is assumed that the nonlocal characteristic length η is such as $\eta \ll h \ll L$.

The nonlocal stress-displacement partial differential equations are:

$$\begin{aligned} \left(1 - \eta^2 \frac{\partial^2}{\partial x^2}\right) \sigma_x &= \frac{E}{(1 - \nu^2)} \left(\frac{\partial u}{\partial x} + \nu \frac{\partial v}{\partial y}\right); \\ \left(1 - \eta^2 \frac{\partial^2}{\partial x^2}\right) \sigma_y &= \frac{E}{(1 - \nu^2)} \left(\frac{\partial v}{\partial y} + \nu \frac{\partial u}{\partial x}\right); \\ \left(1 - \eta^2 \frac{\partial^2}{\partial x^2}\right) \tau_{xy} &= \frac{E}{2(1 + \nu)} \left(\frac{\partial u}{\partial y} + \frac{\partial v}{\partial x}\right) \end{aligned} \quad (3.1)$$

So, multiplying the local governing equations of motion in dynamics (see Eq. (2.17) by $(1 - \eta^2 \partial^2 / \partial x^2)$ and combining them with Eq. (3.1):

$$\frac{2}{(1-\nu)} c^2 \frac{\partial^2 u}{\partial x^2} + \frac{1+\nu}{1-\nu} c^2 \frac{\partial^2 v}{\partial x \partial y} + c^2 \frac{\partial^2 u}{\partial y^2} - \frac{\partial^2 u}{\partial t^2} + \eta^2 \frac{\partial^4 u}{\partial x^2 \partial t^2} = 0 \quad (3.2)$$

$$\frac{1+\nu}{1-\nu} c^2 \frac{\partial^2 u}{\partial x \partial y} + c^2 \frac{\partial^2 v}{\partial x^2} + \frac{2}{(1-\nu)} c^2 \frac{\partial^2 v}{\partial y^2} - \frac{\partial^2 v}{\partial t^2} + \eta^2 \frac{\partial^4 v}{\partial x^2 \partial t^2} = 0 \quad (3.3)$$

where $c^2 = \rho/G$.

Compared to the local equations Eq. (2.18) and (2.19), additional nonlocal terms appear.

Combining Eqs. (2.21), (3.2) and (3.3) for k , positive integer

$$\begin{aligned} \frac{2}{(1-\nu)} c^2 \frac{\partial^2 u_{2k-1}}{\partial x^2} + \frac{1+\nu}{1-\nu} c^2 \frac{\partial v_{2k}}{\partial x} + c^2 u_{2k+1} - \frac{\partial^2 u_{2k-1}}{\partial t^2} + \eta^2 \frac{\partial^4 u_{2k-1}}{\partial x^2 \partial t^2} \\ = 0 \end{aligned} \quad (3.4)$$

$$\frac{1+\nu}{1-\nu} c^2 \frac{\partial u_{2k+1}}{\partial x} + c^2 \frac{\partial^2 v_{2k}}{\partial x^2} + \frac{2}{(1-\nu)} c^2 v_{2k+2} - \frac{\partial^2 v_{2k}}{\partial t^2} + \eta^2 \frac{\partial^4 v_{2k}}{\partial x^2 \partial t^2} = 0 \quad (3.5)$$

In this case, it leads to, setting the dimensionless variable $\bar{\eta} = \eta/L$,

$$\bar{u}_{2k+1} = \mathcal{A}_{NL}^b \bar{u}_{2k-1} + \mathcal{B}_L^b \bar{v}_{2k} \quad (3.6)$$

$$\bar{v}_{2(k+1)} = \mathcal{C}_{NL}^b \bar{v}_{2k} + \mathcal{F}_L^b \bar{u}_{2k+1} \quad (3.7)$$

where the nonlocal operators \mathcal{A}_{NL}^b and \mathcal{C}_{NL}^b are defined as follows:

$$\mathcal{A}_{NL}^b = \left[\bar{h}^2 \frac{\partial^2}{\partial \bar{t}^2} - \bar{h}^2 \bar{\eta}^2 \frac{\partial^4}{\partial \bar{x}^2 \partial \bar{t}^2} - \frac{2}{(1-\nu)} \frac{\partial^2}{\partial \bar{x}^2} \right] \quad (3.8)$$

$$\mathcal{C}_{NL}^b = \frac{1-\nu}{2} \left(\bar{h}^2 \frac{\partial^2}{\partial \bar{t}^2} - \frac{\partial^2}{\partial \bar{x}^2} - \bar{h}^2 \bar{\eta}^2 \frac{\partial^4}{\partial \bar{x}^2 \partial \bar{t}^2} \right)$$

The local operators \mathcal{B}_L^b and \mathcal{F}_L^b are given in the previous chapter.

As for the local problem, the boundary conditions are given by Eq. (2.26). Thus, at the fourth order, it yields Eqs. (2.30) and (2.31). Substituting the different equations, a system of two equations is obtained, written under the matrix form such as in Eq. (2.35). For a sake of simplicity, in this chapter, the coefficients M_{11} , M_{12} , M_{21} and M_{22} are not given. Vanishing the determinant of the matrix it gives in displacement at the two first orders:

Zeroth order

$$\left(1 - \bar{\eta}^2 \frac{\partial^2}{\partial \bar{x}^2} \right) \frac{\partial^2 \bar{v}_0}{\partial \bar{t}^2} + \frac{2}{3} (1 + \nu) \frac{\partial^4 \bar{v}_0}{\partial \bar{x}^4} = 0 \quad (3.9)$$

Second order

$$\begin{aligned} - \left[\frac{2}{3} (\nu + 2) \left(1 - \bar{\eta}^2 \frac{\partial^2}{\partial \bar{x}^2} \right) \frac{\partial^4 \bar{v}_0}{\partial \bar{x}^2 \partial \bar{t}^2} + \frac{2}{15} (1 + \nu) \frac{\partial^6 \bar{v}_0}{\partial \bar{x}^6} \right] \bar{h}^2 \\ + \left(1 - \bar{\eta}^2 \frac{\partial^2}{\partial \bar{x}^2} \right) \frac{\partial^2 \bar{v}_0}{\partial \bar{t}^2} + \frac{2}{3} (1 + \nu) \frac{\partial^4 \bar{v}_0}{\partial \bar{x}^4} = 0 \end{aligned} \quad (3.10)$$

Using the dimensional operators, it leads to:

Zeroth order

$$EI \frac{\partial^4 v}{\partial x^4} + \rho A \left(1 - \eta^2 \frac{\partial^2}{\partial x^2} \right) \frac{\partial^2 v}{\partial t^2} = 0 \quad (3.11)$$

Second order

$$EI \frac{\partial^4 v}{\partial x^4} + \rho A \left(1 - \eta^2 \frac{\partial^2}{\partial x^2} \right) \frac{\partial^2 v}{\partial t^2} - \frac{EI^2}{A\kappa_0} \frac{\partial^6 v}{\partial x^6} - \rho I \left(1 + \frac{E}{\kappa G} \right) \left(1 - \eta^2 \frac{\partial^2}{\partial x^2} \right) \frac{\partial^4 v}{\partial x^2 \partial t^2} = 0 \quad (3.12)$$

When the nonlocal effect is not taken into account, η is equal to zero, Eqs. (3.11) and (3.12) are reduced to Eqs. (2.38) and (2.39). As it has been said in the previous chapter, it is found in this case that the Bernoulli-Euler model is asymptotically consistent.

As for the local approach, in order to delete the sixth order space derivative term, it is suggested to multiply Eq. (3.10) by $[1 + (\bar{h}^2/5)(\partial^2/\partial \bar{x}^2)]$ leading to, using the variables under the dimensional form:

$$EI \frac{\partial^4 v}{\partial x^4} + \rho A \left(1 - \eta^2 \frac{\partial^2}{\partial x^2} \right) \frac{\partial^2 v}{\partial t^2} - \left(1 - \eta^2 \frac{\partial^2}{\partial x^2} \right) \rho I \left(1 + \frac{E}{\kappa G} \right) \frac{\partial^4 v}{\partial x^2 \partial t^2} = 0 \quad (3.13)$$

3.1.1.2. Asymptotic model with a partial nonlocality along the vertical direction

In this model, the partial nonlocality is not along the x direction but the vertical direction of the beam. Thus, the stress-displacement relationships are:

$$\left(1 - \eta^2 \frac{\partial^2}{\partial y^2} \right) \sigma_x = \frac{E}{(1 - \nu^2)} \left(\frac{\partial u}{\partial x} + \nu \frac{\partial v}{\partial y} \right); \quad (3.14)$$

$$\left(1 - \eta^2 \frac{\partial^2}{\partial y^2}\right) \sigma_y = \frac{E}{(1 - \nu^2)} \left(\frac{\partial v}{\partial y} + \nu \frac{\partial u}{\partial x}\right);$$

$$\left(1 - \eta^2 \frac{\partial^2}{\partial y^2}\right) \tau_{xy} = \frac{E}{2(1 + \nu)} \left(\frac{\partial u}{\partial y} + \frac{\partial v}{\partial x}\right)$$

So, multiplying the local equilibrium equation Eq. (2.17) by $(1 - \eta^2 \partial^2 / \partial y^2)$ and combining them with Eq. (3.14):

$$\frac{2}{(1 - \nu)} c^2 \frac{\partial^2 u}{\partial x^2} + \frac{1 + \nu}{1 - \nu} c^2 \frac{\partial^2 v}{\partial x \partial y} + c^2 \frac{\partial^2 u}{\partial y^2} - \frac{\partial^2 u}{\partial t^2} + \eta^2 \frac{\partial^4 u}{\partial y^2 \partial t^2} = 0 \quad (3.15)$$

$$\frac{1 + \nu}{1 - \nu} c^2 \frac{\partial^2 u}{\partial x \partial y} + c^2 \frac{\partial^2 v}{\partial x^2} + \frac{2}{(1 - \nu)} c^2 \frac{\partial^2 v}{\partial y^2} - \frac{\partial^2 v}{\partial t^2} + \eta^2 \frac{\partial^2 v}{\partial y^2 \partial t^2} = 0 \quad (3.16)$$

Substituting the expressions of the displacements given by Eq. (2.23) into Eqs. (3.15) and (3.16), using the dimensionless variables defined in Eq. (2.29), Eqs. (3.15) and (3.16) yield

$$\mathcal{H}_1 \bar{u}_{2k+1} = \mathcal{A}_2 \bar{u}_{2k-1} + \mathcal{B}_2 \bar{v}_{2k} \quad (3.17)$$

$$\mathcal{H}_2 \bar{v}_{2(k+1)} = \mathcal{C}_2 \bar{v}_{2k} + \mathcal{F}_2 \bar{u}_{2k+1} \quad (3.18)$$

where the operators $\mathcal{H}_1, \mathcal{H}_2$, are defined as follows:

$$\mathcal{H}_1 = \left(1 + \bar{h}^2 \bar{\eta}^2 \frac{\partial^2}{\partial \bar{t}^2}\right); \mathcal{H}_2 = \left(1 + \frac{1 - \nu}{2} \bar{h}^2 \bar{\eta}^2 \frac{\partial^2}{\partial \bar{t}^2}\right) \quad (3.19)$$

Multiplying Eqs. (2.30) and (2.31) by $\mathcal{H}_1^2\mathcal{H}_2^3$ and $\mathcal{H}_1^2\mathcal{H}_2^2$, respectively

$$\begin{aligned} \mathcal{H}_1^2\mathcal{H}_2^2(\mathcal{H}_2\bar{v}_2) + \nu\mathcal{H}_1^2\mathcal{H}_2^3\frac{\partial\theta}{\partial\bar{x}} + \frac{\bar{h}^2}{6}\left[\mathcal{H}_1\mathcal{H}_2(\mathcal{H}_1\mathcal{H}_2^2\bar{v}_4) + \nu\mathcal{H}_1\mathcal{H}_2^2\frac{\partial\mathcal{H}_1\mathcal{H}_2\bar{u}_3}{\partial\bar{x}}\right] \\ + \frac{\bar{h}^4}{120}\left[\mathcal{H}_1^2\mathcal{H}_2^3\bar{v}_6 + \nu\mathcal{H}_2\frac{\partial\mathcal{H}_1^2\mathcal{H}_2^2\bar{u}_5}{\partial\bar{x}}\right] = 0 \end{aligned} \quad (3.20)$$

$$\begin{aligned} \mathcal{H}_1^2\mathcal{H}_2^2\theta + \mathcal{H}_1^2\mathcal{H}_2^2\frac{\partial\bar{v}_0}{\partial\bar{x}} + \frac{\bar{h}^2}{2}\left[\mathcal{H}_1\mathcal{H}_2(\mathcal{H}_1\mathcal{H}_2\bar{u}_3) + \mathcal{H}_2\mathcal{H}_1^2\frac{\partial\mathcal{H}_2\bar{v}_2}{\partial\bar{x}}\right] \\ + \frac{\bar{h}^4}{24}\left(\mathcal{H}_1^2\mathcal{H}_2^2\bar{u}_5 + \mathcal{H}_1\frac{\partial\mathcal{H}_1\mathcal{H}_2^2\bar{v}_4}{\partial\bar{x}}\right) = 0 \end{aligned} \quad (3.21)$$

Substituting Eqs. (3.17) and (3.18) into Eqs. (3.20) and (3.21), it yields the system put under the matrix form with new coefficients M_{11} , M_{12} , M_{21} and M_{22} . The determinant of the matrix is vanishing:

Zeroth order

$$\left(1 - \bar{\eta}^2\nu\frac{\partial^2}{\partial\bar{x}^2}\right)\frac{\partial^2}{\partial\bar{t}^2} + \frac{2}{3}(1 + \nu)\frac{\partial^4}{\partial\bar{x}^4} = 0 \quad (3.22)$$

Second order

$$\begin{aligned} -\left[\frac{(2 + \nu)}{3}\frac{\partial^4\bar{v}_0}{\partial\bar{x}^2\partial\bar{t}^2} - (3 - \nu)\left(1 - \bar{\eta}^2\nu\frac{\partial^2}{\partial\bar{x}^2}\right)\bar{\eta}^2\frac{\partial^4}{\partial\bar{t}^4} + \frac{1}{15}(1 + \nu)\frac{\partial^6}{\partial\bar{x}^6}\right. \\ \left. + \frac{(2\nu^2 - 4\nu - 5)}{3}\bar{\eta}^2\frac{\partial^6}{\partial\bar{x}^4\partial\bar{t}^2}\right]\bar{h}^2 + \frac{1}{2}\left(1 - \bar{\eta}^2\nu\frac{\partial^2}{\partial\bar{x}^2}\right)\frac{\partial^2}{\partial\bar{t}^2} + \frac{1}{3}(1 + \nu)\frac{\partial^4}{\partial\bar{x}^4} = 0 \end{aligned} \quad (3.23)$$

By using the dimensional differential operators,:

Zeroth order

$$\rho A \left(1 - \eta^2 \nu \frac{\partial^2}{\partial x^2} \right) \frac{\partial^2}{\partial t^2} + EI \frac{\partial^4}{\partial x^4} = 0 \quad (3.24)$$

Second order

$$EI \frac{\partial^4}{\partial x^4} + \rho A \left(1 - \nu \eta^2 \frac{\partial^2}{\partial x^2} \right) \frac{\partial^2}{\partial t^2} - \rho I \left(1 + \frac{E}{\tilde{\kappa} G} \right) \frac{\partial^4 \bar{v}_0}{\partial x^2 \partial t^2} + \eta^2 \frac{\rho^2 A}{\kappa_2 G} \left(1 - \eta^2 \nu \frac{\partial^2}{\partial x^2} \right) \frac{\partial^4}{\partial t^4} - \frac{EI^2}{A \kappa_0} \frac{\partial^6}{\partial x^6} + \eta^2 \frac{\rho EI}{\kappa_1 G} \frac{\partial^6}{\partial x^4 \partial t^2} = 0 \quad (3.25)$$

with:

$$\kappa_1 = \frac{1 + \nu}{5 - 2\nu^2 + 4\nu}; \kappa_2 = \frac{1}{2(3 - \nu)}$$

As before, it is suggested to multiply the non-dimensional governing differential equation by $[1 + (\bar{h}^2/5)(\partial^2/\partial \bar{x}^2)]$ and using the dimensional variables:

$$EI \frac{\partial^4 v}{\partial x^4} + \rho A \left(1 - \nu \eta^2 \frac{\partial^2}{\partial x^2} \right) \frac{\partial^2 v}{\partial t^2} - \rho I \left(1 + \frac{E}{\kappa G} \right) \frac{\partial^4 v}{\partial x^2 \partial t^2} + \eta^2 \frac{\rho EI}{\tilde{\kappa}_1 G} \frac{\partial^6 v}{\partial x^4 \partial t^2} + \left(1 - \nu \eta^2 \frac{\partial^2}{\partial x^2} \right) \eta^2 \frac{\rho^2 A}{\tilde{\kappa}_2 G} \frac{\partial^4 \bar{v}_0}{\partial t^4} = 0 \quad (3.26)$$

with

$$\tilde{\kappa}_1 = \frac{10(\nu + 1)}{(50 - 20\nu^2 + 37\nu)}; \tilde{\kappa}_2 = \frac{1}{2(3 - \nu)}$$

Thus, a new asymptotic model is developed.

3.1.1.3. Asymptotic model with a full nonlocality

The third approach includes both the contribution of the nonlocality in the direction of the beam and the one of the nonlocality in the vertical direction:

$$\begin{aligned}
 (1 - \eta^2 \nabla^2) \sigma_x &= \frac{E}{(1 - \nu^2)} \left(\frac{\partial u}{\partial x} + \nu \frac{\partial v}{\partial y} \right); \\
 (1 - \eta^2 \nabla^2) \sigma_y &= \frac{E}{(1 - \nu^2)} \left(\frac{\partial v}{\partial y} + \nu \frac{\partial u}{\partial x} \right); \\
 (1 - \eta^2 \nabla^2) \tau_{xy} &= \frac{E}{2(1 + \nu)} \left(\frac{\partial u}{\partial y} + \frac{\partial v}{\partial x} \right)
 \end{aligned} \tag{3.27}$$

So, multiplying Eqs. (2.17) by $(1 - \eta^2 \nabla^2)$ and combining them with Eq. (3.27):

$$\begin{aligned}
 \frac{2}{(1 - \nu)} c^2 \frac{\partial^2 u}{\partial x^2} + \frac{1 + \nu}{1 - \nu} c^2 \frac{\partial^2 v}{\partial x \partial y} + c^2 \frac{\partial^2 u}{\partial y^2} - \frac{\partial^2 u}{\partial t^2} + \eta^2 \frac{\partial^4 u}{\partial x^2 \partial t^2} \\
 + \eta^2 \frac{\partial^4 u}{\partial y^2 \partial t^2} = 0
 \end{aligned} \tag{3.28}$$

$$\begin{aligned}
 \frac{1 + \nu}{1 - \nu} c^2 \frac{\partial^2 u}{\partial x \partial y} + c^2 \frac{\partial^2 v}{\partial x^2} + \frac{2}{(1 - \nu)} c^2 \frac{\partial^2 v}{\partial y^2} - \frac{\partial^2 v}{\partial t^2} + \eta^2 \frac{\partial^4 v}{\partial x^2 \partial t^2} \\
 + \eta^2 \frac{\partial^4 v}{\partial y^2 \partial t^2} = 0
 \end{aligned} \tag{3.29}$$

Finally, it yields the non-dimensional equations at different orders

Zeroth order

$$\frac{2}{3}(\nu + 1) \frac{\partial^4 \bar{v}_0}{\partial \bar{x}^4} + \frac{\partial^2 \bar{v}_0}{\partial \bar{t}^2} - \bar{\eta}^2 (\nu + 1) \frac{\partial^4 \bar{v}_0}{\partial \bar{x}^2 \partial \bar{t}^2} = 0 \quad (3.30)$$

Second order

$$\begin{aligned} - \left[\frac{2}{3}(\nu + 2) \frac{\partial^4}{\partial \bar{x}^2 \partial \bar{t}^2} + 2(\nu + 2) \bar{\eta}^2 \frac{\partial^4}{\partial \bar{t}^4} + \frac{2(2\nu - 7)(1 + \nu)}{3} \bar{\eta}^2 \frac{\partial^6}{\partial \bar{x}^4 \partial \bar{t}^2} \right. \\ \left. + 2(3 - \nu)(1 + \nu) \bar{\eta}^4 \frac{\partial^6}{\partial \bar{x}^2 \partial \bar{t}^4} + \frac{2}{15}(1 + \nu) \frac{\partial^6}{\partial \bar{x}^6} \right] \bar{h}^2 + (1 + \nu) \bar{\eta}^2 \frac{\partial^4}{\partial \bar{x}^2 \partial \bar{t}^2} \\ + \frac{\partial^2}{\partial \bar{t}^2} + \frac{2}{3}(1 + \nu) \frac{\partial^4}{\partial \bar{x}^4} = 0 \end{aligned} \quad (3.31)$$

Or, under the dimensional form

Zeroth order

$$EI \frac{\partial^4 v}{\partial x^4} + \rho A \left(1 - \frac{\eta^2}{\kappa_3} \frac{\partial^2}{\partial x^2} \right) \frac{\partial^2 v}{\partial t^2} = 0 \quad (3.32)$$

Second order

$$\begin{aligned} EI \frac{\partial^4 v}{\partial x^4} + \rho A \left(1 - \frac{\eta^2}{\kappa_3} \frac{\partial^2}{\partial x^2} \right) \frac{\partial^2 v}{\partial t^2} - \frac{EI^2}{A\kappa_0} \frac{\partial^6 v}{\partial x^6} - \rho I \left(1 + \frac{E}{\kappa G} \right) \frac{\partial^4 v}{\partial x^2 \partial t^2} \\ + \eta^2 \frac{\rho EI}{\kappa_1 G} \frac{\partial^6 \bar{v}_0}{\partial x^4 \partial t^2} + \eta^2 \frac{\rho^2 A}{\kappa_2 G} \frac{\partial^4 \bar{v}_0}{\partial t^4} = 0 \end{aligned} \quad (3.33)$$

with:

$$\kappa_1 = \frac{1}{7 - 2\nu}; \kappa_2 = \frac{1}{2(3 - \nu)}; \kappa_3 = \frac{1}{(1 + \nu)}$$

By multiplying Eq. (3.31) by $[1 + (\bar{h}^2/5)(\partial^2/\partial\bar{x}^2)]$, it leads to, using the variables under the dimensional form:

$$EI \frac{\partial^4 v}{\partial x^4} + \rho A \left(1 - \frac{\eta^2}{\kappa_3} \frac{\partial^2}{\partial x^2}\right) \frac{\partial^2 v}{\partial t^2} - \rho I \left(1 + \frac{E}{\kappa G}\right) \frac{\partial^4 v}{\partial x^2 \partial t^2} + \eta^2 \frac{\rho EI}{\tilde{\kappa}_1 G} \frac{\partial^6 v}{\partial x^4 \partial t^2} + \eta^2 \frac{\rho^2 A}{\tilde{\kappa}_2 G} \frac{\partial^4 \bar{v}_0}{\partial t^4} = 0 \quad (3.34)$$

with

$$\tilde{\kappa}_1 = \frac{10}{67 - 5\nu};$$

Eq. (3.34) differs from Eq. (3.24) following the expression of the parameter $\tilde{\kappa}_1$.

The asymptotic models have been derived starting from the gradient form of the stress-strain relationship given by Eringen [123]. It would be also possible to perform an analogous derivation by starting from the integral formulation of the asymptotic model.

3.1.2. Nonlocal engineering beam approaches

3.1.2.1. Bernoulli-Euler model: the fourth order phenomenological approach

The first nonlocal Bernoulli-Euler model between the stress gradient theory of Eringen [123] has been proposed by Peddieson et al. [240] and Sudak [241]. This is a phenomenological model, based on a postulated moment curvature relation:

$$\left[1 - \eta^2 \frac{\partial^2}{\partial x^2}\right] M = EI \frac{\partial^2 w}{\partial x^2} \quad (3.35)$$

Moreover, the local equilibrium equation for thin beams is

$$\frac{\partial^2 M}{\partial x^2} + \rho A \frac{\partial^2 v}{\partial t^2} = 0 \quad (3.36)$$

Thus, it leads to the following governing differential equation, as given in the literature [242-248]

$$EI \frac{\partial^4 v}{\partial x^4} + \rho A \left(1 - \eta^2 \frac{\partial^2}{\partial x^2} \right) \frac{\partial^2 v}{\partial t^2} = 0 \quad (3.37)$$

This governing differential equation may be obtained variationally and from the principle of virtual work. Variationnally, the strain energy U and the kinetic energy T are:

$$U = \int_0^L \frac{1}{2} EI \left(\frac{\partial^2 v}{\partial x^2} \right)^2 dx \quad (3.38)$$

$$T = \int_0^L \frac{1}{2} m_0 \left[\left(\frac{\partial v}{\partial t} \right)^2 + \eta^2 \left(\frac{\partial^2 v}{\partial x \partial t} \right)^2 \right] dx \quad (3.39)$$

It leads to the following boundary conditions [135]

$$\left[\left\{ EI \frac{\partial^3 v}{\partial x^3} - m_0 \eta^2 \frac{\partial^3 v}{\partial t^2 \partial x} \right\} \delta v \right]_0^L = 0 \quad (3.40)$$

$$\left[EI \frac{\partial^2 v}{\partial x^2} \delta \left(\frac{\partial v}{\partial x} \right) \right]_0^L = 0 \quad (3.41)$$

whereas from the principle of virtual work, the boundary conditions are given by Eq. (3.40) and

$$\left[\left\{ EI \frac{\partial^2 v}{\partial x^2} - m_0 \eta^2 \frac{\partial^2 v}{\partial t^2} \right\} \delta \left(\frac{\partial v}{\partial x} \right) \right]_0^L = 0 \quad (3.42)$$

In dynamics, comparing Eqs. (3.41) and (3.42), the dynamic contribution of the second boundary condition differs between the two approaches (see also [249]). It means that the Eringen's model differs from the variationally-based nonlocal model.

Furthermore, when the nonlocal effect is not taken into account, i.e. $\eta = 0$, it has been shown that the Bernoulli-Euler model is asymptotically consistent at the lowest order. When η is different from zero, Eqs. (3.11) and (3.37) match. The fourth order nonlocal Bernoulli-Euler model developed in the literature is asymptotically obtained at the zeroth order following the gradient asymptotic model with a partial nonlocality along the horizontal direction. However, it is seen that the engineering model does not match with the two other asymptotic models, including a partial nonlocality along the vertical direction and a full nonlocality, respectively. Indeed, they differ in

the expression of the length scale. This length scale is η for the Bernoulli-Euler model and the asymptotic model with a nonlocality along the horizontal direction, $(1 + \nu)\eta$ and $\nu\eta$ for the second and third asymptotic models, respectively.

3.1.2.2. Sixth order phenomenological thin beam model

In the literature [135], another phenomenological model has been proposed with a postulated constitutive law as follows:

$$\left[1 - \eta^2 \frac{d^2}{dx^2}\right] M = EI \left[1 + \eta^2 \frac{d^2}{dx^2}\right] \frac{d^2}{dx^2} w \quad (3.43)$$

Multiplying Eq. (3.36) by $[1 - \eta^2(d^2/dx^2)]$ and substituting Eq. (3.43). We obtain the governing differential equation

$$EI \left[1 + \eta^2 \frac{d^2}{dx^2}\right] \frac{d^4 w}{dx^4} - m_0 \omega^2 \left[1 - \eta^2 \frac{d^2}{dx^2}\right] w = 0 \quad (3.44)$$

This equation containing a sixth order space derivative term, it is called “sixth order phenomenological model”, in contrast to the previously derived fourth order phenomenological Bernoulli-Euler model that contains only fourth order space derivative terms.

Eq. (3.44) is also variationally obtained. It has been shown [135] that the only difference between the two phenomenological models in the variational derivation is the nonlocal term in the bending strain energy.

In this approach, the strain energy U is:

$$U = \int_0^L \frac{1}{2} EI \left[\left(\frac{\partial^2 v}{\partial x^2} \right)^2 - \eta^2 \left(\frac{\partial^3 v}{\partial x^3} \right)^2 \right] dx \quad (3.45)$$

Thus, it leads to Eq. (3.44) with the natural and essential boundary conditions

$$\left[- \left\{ EI \eta^2 \frac{d^5 w}{dx^5} + EI \frac{d^3 w}{dx^3} + m_0 \omega^2 \eta^2 \frac{dw}{dx} \right\} \delta w \right]_0^L = 0 \quad (3.46)$$

$$\left[EI \left\{ \eta^2 \frac{d^4 w}{dx^4} + \frac{d^2 w}{dx^2} \right\} \delta \left(\frac{dw}{dx} \right) \right]_0^L = 0 \quad (3.47)$$

$$\left[EI \eta^2 \frac{d^3 w}{dx^3} \delta \left(\frac{d^2 w}{dx^2} \right) \right]_0^L = 0 \quad (3.48)$$

The sixth order space derivative phenomenological model introduces two additional boundary conditions, one at each end, necessary to solve the sixth order governing differential equation. This model will be ignored hereinafter. Indeed, in contrast to the fourth order phenomenological model, this higher-order gradient elasticity functional is no more definite positive.

3.1.2.3. Nonlocal original Bresse-Timoshenko model

First of all, the constitutive laws are postulated as follows:

$$\left(1 - R_s \eta^2 \frac{\partial^2}{\partial x^2} \right) V = \kappa GA \left(\frac{\partial v}{\partial x} - \psi \right); \left(1 - \eta^2 \frac{\partial^2}{\partial x^2} \right) M = EI \frac{\partial \psi}{\partial x} \quad (3.49)$$

where R_s is a control parameter. In the literature, opinions differ about its value, equal to zero or unity [79]. Whereas authors [70,71,243,244,246,250] consider that the nonlocal effect is included in the shearing part of the constitutive law and R_s equal to unity, some others [72,251-254] suggested that the scale effect does not affect the expression of the shear force and R_s equal to zero. Hereinafter, both cases will be considered.

Manipulating the local equilibrium equation Eq. (2.5) and the nonlocal constitutive laws Eqs. (3.49), it yields the following governing differential equation in displacement

$$\begin{aligned} EI \frac{\partial^4 v}{\partial x^4} + \left(1 - R_s \eta^2 \frac{\partial^2}{\partial x^2} \right) \left(\rho A \frac{\partial^2 v}{\partial t^2} - \frac{\rho EI}{\kappa G} \frac{\partial^4 v}{\partial x^2 \partial t^2} \right) + \eta^2 (R_s - 1) \rho A \frac{\partial^4 v}{\partial x^2 \partial t^2} \\ - \rho I \left(1 - \eta^2 \frac{\partial^2}{\partial x^2} \right) \frac{\partial^2}{\partial t^2} \left[\frac{\partial^2 v}{\partial x^2} - \frac{\rho}{\kappa G} \left(1 - R_s \eta^2 \frac{\partial^2}{\partial x^2} \right) \frac{\partial^2 v}{\partial t^2} \right] = 0 \end{aligned} \quad (3.50)$$

The boundary conditions in the gradient model are [182]:

$$M\delta\psi|_0^L = 0; \quad V\delta v|_0^L = 0 \quad (3.51)$$

or, substituting Eqs. (3.49) into Eq. (3.51)

$$\left[EI \frac{\partial \psi}{\partial x} + \rho \eta^2 \left(A \frac{\partial^2 v}{\partial t^2} + I \frac{\partial^3 \psi}{\partial x \partial t^2} \right) \right] \delta \psi \Big|_0^L = 0 \quad (3.52)$$

$$\left[\kappa GA \left(\frac{\partial v}{\partial x} - \psi \right) + R_s \eta^2 \rho A \frac{\partial^3 v}{\partial x \partial t^2} \right] \delta v \Big|_0^L = 0 \quad (3.53)$$

This model is also derived variationnally by considering the strain and kinetic energy given by Eqs (2.9)-(2.11), respectively, and a nonlocal energy:

$$T^{NL} = \frac{R_s \eta^2}{2} \int_0^L \rho A \left(\frac{\partial^2 v}{\partial x \partial t} \right)^2 dx + \frac{\eta^2}{2} \int_0^L \rho I \left(\frac{\partial^2 \psi_x}{\partial x \partial t} \right)^2 dx \quad (3.54)$$

This functional, has no physical meaning. Hereinafter, it will be called the ‘‘Eringen energy’’.

Thus, the application of the Hamilton’s principle leads to the differential equations of motions:

$$\rho A \frac{\partial^2 v}{\partial t^2} - \kappa GA \left(\frac{\partial^2 v}{\partial x^2} - \frac{\partial \psi}{\partial x} \right) - R_s \eta^2 \rho A \frac{\partial^4 v}{\partial x^2 \partial t^2} = 0 \quad (3.55)$$

$$EI \frac{\partial^2 \psi}{\partial x^2} + \kappa GA \left(\frac{\partial v}{\partial x} - \psi \right) - \rho I \left(1 - \eta^2 \frac{\partial^2}{\partial x^2} \right) \frac{\partial^2 \psi}{\partial t^2} = 0 \quad (3.56)$$

Combining these equations, it yields:

$$EI \frac{\partial^4 v}{\partial x^4} + \left(1 - R_s \eta^2 \frac{\partial^2}{\partial x^2}\right) \left(\rho A \frac{\partial^2 v}{\partial t^2} - \frac{\rho EI}{\kappa G} \frac{\partial^4 v}{\partial x^2 \partial t^2} \right) - \rho I \left(1 - \eta^2 \frac{\partial^2}{\partial x^2}\right) \frac{\partial^2}{\partial t^2} \left[\frac{\partial^2 v}{\partial x^2} - \frac{\rho}{\kappa G} \left(1 - R_s \eta^2 \frac{\partial^2}{\partial x^2}\right) \frac{\partial^2 v}{\partial t^2} \right] = 0 \quad (3.57)$$

It is seen that for $R_s = 0$, Eq. (3.50) contains one more term compared to Eq. (3.57) and the two approaches do not match. For $R_s = 1$, the variational approach and the approach based on equilibrium equations lead to the same governing differential equation.

Furthermore, from the variational principle, one obtains the boundary conditions:

$$\left[EI \frac{\partial \psi}{\partial x} + \eta^2 \rho I \frac{\partial^3 \psi}{\partial x \partial t^2} \right] \delta \psi \Big|_0^L = 0 \quad (3.58)$$

$$\left[\kappa GA \left(\frac{\partial v}{\partial x} - \psi \right) + R_s \eta^2 \rho A \frac{\partial^3 v}{\partial x \partial t^2} \right] \delta v \Big|_0^L = 0 \quad (3.59)$$

In dynamics, the boundary conditions between the two different approaches do not match, confirming the results of Challamel et al. [248] for nonlocal Euler-Bernoulli beam models.

3.1.2.4. Truncated Bresse-Timoshenko model

The truncated version of the nonlocal Bresse-Timoshenko model is derived by replacing Eq. (2.4) by Eq. (2.14). Thus, it leads to:

$$EI \frac{\partial^4 v}{\partial x^4} + \left(1 - R_s \eta^2 \frac{\partial^2}{\partial x^2}\right) \left[\rho A \frac{\partial^2 v}{\partial t^2} - \frac{\rho EI}{\kappa G} \frac{\partial^4 v}{\partial x^2 \partial t^2} \right] + \eta^2 (R_s - 1) \rho A \frac{\partial^4 v}{\partial x^2 \partial t^2} - \rho I \left(1 - \eta^2 \frac{\partial^2}{\partial x^2}\right) \frac{\partial^4 v}{\partial t^2 \partial x^2} = 0 \quad (3.60)$$

When the nonlocal effect is not taken into account, i.e. η equal to zero, the truncated Bresse-Timoshenko model is asymptotically consistent at the second order. When the local effect is not

ignored, for $R_s = 1$, Eq. (3.13), governing differential equation derived through the first asymptotic model, matches with Eq. (3.60). Thus, the nonlocal truncated Bresse-Timoshenko model for $R_s = 1$ is asymptotically consistent at the second order approximation following the nonlocal asymptotic model with a partial nonlocality along the horizontal direction. It is worth noticing that for η different from zero, the second and third asymptotic models and the nonlocal truncated Bresse-Timoshenko models do not coincide.

3.1.2.5. Bresse-Timoshenko based on slope inertia

As explained before, the nonlocal formulation of the original Bresse-Timoshenko model introduces an Eringen energy T^{NL} . For the model based on slope inertia, the local kinetic energy is corrected because the shear effect was already taken into account in the bending strain energy. Considering that there is no nonlocal equivalent to the bending strain energy, there is no need to correct T^{NL} . Consequently, in this section, the Eringen energy is expressed by Eq. (3.54).

By applying the Hamilton principle with the energies given by Eqs. (2.10), (2.11) and (2.42), respectively, it yields the differential equation of motion:

$$\rho A \frac{\partial^2 v}{\partial t^2} - \kappa G A \left(\frac{\partial^2 v}{\partial x^2} - \frac{\partial \psi}{\partial x} \right) - R_s \eta^2 \rho A \frac{\partial^4 v}{\partial x^2 \partial t^2} - \rho I \frac{\partial^4 v}{\partial x^2 \partial t^2} = 0 \quad (3.61)$$

$$EI \frac{\partial^2 \psi}{\partial x^2} + \kappa G A \left(\frac{\partial v}{\partial x} - \psi \right) + \eta^2 \rho I \frac{\partial^4 \psi}{\partial x^2 \partial t^2} = 0 \quad (3.62)$$

It yields the following governing differential equation in displacement, also valid for ψ

$$\begin{aligned} EI \frac{\partial^4 v}{\partial x^4} + \rho A \frac{\partial^2 v}{\partial t^2} - \rho I \left(1 + \frac{E}{\kappa G} + R_s \eta^2 \frac{A}{I} \right) \frac{\partial^4 v}{\partial x^2 \partial t^2} \\ + \rho I \left(\frac{EI}{\kappa G A} + R_s \eta^2 \frac{E}{\kappa G} + \eta^2 \right) \frac{\partial^6 v}{\partial x^4 \partial t^2} - \eta^2 \frac{\rho^2 I}{\kappa G} \frac{\partial^6 v}{\partial x^2 \partial t^4} \\ + \eta^2 \frac{\rho^2 I}{\kappa G} \left(\frac{I}{A} + R_s \eta^2 \right) \frac{\partial^8 v}{\partial x^4 \partial t^4} = 0 \end{aligned} \quad (3.63)$$

and the boundary conditions are obtained as follows:

$$\left[EI \frac{\partial \psi}{\partial x} + \eta^2 \rho I \frac{\partial^3 \psi}{\partial x \partial t^2} \right] \delta \psi \Big|_0^L = 0 \quad (3.64)$$

$$\left[\kappa GA \left(\frac{\partial v}{\partial x} - \psi \right) + \rho I \frac{\partial^3 v}{\partial t^2 \partial x} + R_s \eta^2 \rho A \frac{\partial^3 v}{\partial x \partial t^2} \right] \delta v \Big|_0^L = 0 \quad (3.65)$$

3.1.3. Solution and parametric analysis

In order to compare the different models, it is proposed to calculate the natural frequencies for simply supported carbon nanotubes.

First of all, the three versions of the nonlocal Bresse-Timoshenko model are written in the general form as follows:

$$\begin{aligned} EI \frac{\partial^4 v}{\partial x^4} + \left(1 - R_s \eta^2 \frac{\partial^2}{\partial x^2} \right) \left(\rho A - \frac{\rho EI}{\kappa G} \frac{\partial^2}{\partial x^2} \right) \frac{\partial^2 v}{\partial t^2} + \delta_g (R_s - 1) \eta^2 \rho A \frac{\partial^4 v}{\partial x^2 \partial t^2} \\ - \rho I \frac{\partial^2}{\partial t^2} \left[\left(1 - \eta^2 \frac{\partial^2}{\partial x^2} \right) \frac{\partial^2 v}{\partial x^2} - \frac{I}{\kappa GA} \left(E + \eta^2 \rho \frac{\partial^2 v}{\partial t^2} \right) \frac{\partial^4 v}{\partial x^4} \right. \\ \left. - \left(\gamma_1 - \eta^2 \frac{\partial^2}{\partial x^2} \right) (\gamma_1 + \gamma_2) \frac{\rho}{\kappa G} \left(1 - R_s \eta^2 \frac{\partial^2}{\partial x^2} \right) \frac{\partial^2 v}{\partial t^2} \right] = 0 \end{aligned} \quad (3.66)$$

where δ_g is a control parameter equal to unity when the equation are derived through the equilibrium equation, and equal to zero otherwise.

Consider the nondimensional variables $\vartheta_1 = E/\tilde{\kappa}_1 G$ and $\vartheta_2 = E/\tilde{\kappa}_2 G$. The tube being simply supported at both ends, the solution is investigated by using the Navier expression given by Eq. (2.48)

So, substituting Eqs. (2.48) and (2.49) into Eq. (3.66), it yields the characteristic equation

$$\Lambda_1 \Omega^4 - \Lambda_2 \Omega^2 + \Lambda_3 = 0 \quad (3.67)$$

where the coefficients Λ_1 , Λ_2 and Λ_3 are given by

$$\begin{aligned}
\Lambda_1 &= \vartheta r^4 [\gamma_1 (1 + \bar{\eta}^2 (m\pi)^2) (1 + R_s \bar{\eta}^2 (m\pi)^2) \\
&\quad + \gamma_2 \bar{\eta}^2 (m\pi)^2 [1 + R_s \bar{\eta}^2 (m\pi)^2 + r^2 (m\pi)^2]] \\
\Lambda_2 &= 1 + [r^2 \vartheta + (R_s - \delta_g R_s + \delta_g) \bar{\eta}^2 + r^2] (m\pi)^2 \\
&\quad + [R_s \bar{\eta}^2 \vartheta + \bar{\eta}^2 + \gamma_2 \vartheta r^2] r^2 (m\pi)^4 \\
\Lambda_3 &= (m\pi)^4
\end{aligned} \tag{3.68}$$

Moreover, for each asymptotic model, it is possible to express the coefficients Λ_1 , Λ_2 and Λ_3 . The first asymptotic model, with a partial nonlocality along the horizontal direction, has been derived in section 3.1.1.1. The second asymptotic model, with a partial nonlocality along the vertical direction, has been derived in section 3.1.1.2. The third and last asymptotic model, with a full nonlocality, has been derived in section 3.1.1.3. Thus, the first asymptotic model with a partial nonlocality along the horizontal direction, is obtained for the couple $(R_s, \gamma_1) = (1, 0)$, resulting in the following triplet $(\Lambda_1, \Lambda_2, \Lambda_3)$.

$$\Lambda_1 = 0; \Lambda_2 = 1 + \bar{\eta}^2 (m\pi)^2 + [\vartheta + 1] r^2 (m\pi)^2 [1 + \bar{\eta}^2 (m\pi)^2]; \Lambda_3 = (m\pi)^4 \tag{3.69}$$

For the second asymptotic model

$$\begin{aligned}
\Lambda_1 &= r^2 [1 + v \bar{\eta}^2 (m\pi)^2] \bar{\eta}^2 \vartheta_2; \Lambda_2 \\
&= 1 + (r^2 + r^2 \vartheta + v \bar{\eta}^2) (m\pi)^2 + r^2 \bar{\eta}^2 \vartheta_1 (m\pi)^4 \\
\Lambda_3 &= (m\pi)^4
\end{aligned} \tag{3.70}$$

For the third asymptotic model,

$$\Lambda_1 = r^2 \bar{\eta}^2 \vartheta_2; \Lambda_2 = 1 + (m\pi)^2 \left(r^2 + r^2 \vartheta + \frac{\bar{\eta}^2}{\kappa_3} \right) + (m\pi)^4 r^2 \bar{\eta}^2 \vartheta_1; \Lambda_3 = (m\pi)^4 \tag{3.71}$$

The solutions of the equations are given by Eq. (2.131) (the reader may refer to Chapter 2).

The nonlocal Bernoulli-Euler model, leads to the following nondimensional natural frequency:

$$\Omega = (m\pi)^2 \sqrt{\frac{1}{[1 + \bar{\eta}^2(m\pi)^2]}} \quad (3.72)$$

This expression of the natural frequency is also valid for the first asymptotic model.

For the zeroth order second and third asymptotic models, it leads to

$$\Omega = (m\pi)^2 \sqrt{\frac{1}{\left[1 + \frac{\bar{\eta}^2}{\kappa_3}(m\pi)^2\right]}} \quad (3.73)$$

Consider a carbon nanotube of length 3.52 nm, with an inner and an outer radii R_i and R_o , taken to equal 0.18 nm and 0.52 nm, respectively and a Poisson's ratio equal to 0.3 [70]. In this case, the thickness ratio is defined as the difference between the outer and the inner radii with the length of the tube. The first five natural frequencies following the engineering and asymptotic models are given in Tables 12 and 13, respectively.

	Bernoulli	Bresse-Timoshenko						
	- Euler	Original		Truncated		Slope		
$\eta = 0$	9.869	8.681		8.635		8.577		
	39.478	27.304		26.464		24.932		
	88.826	48.689		45.826		39.011		
	157.914	70.627		65.003		48.937		
	246.740	92.537		83.852		55.630		
		$R_s = 0$		$R_s = 1$	$R_s = 0$	$R_s = 1$	$R_s = 0$	$R_s = 1$
		$\delta_g = 1$	$\delta_g = 0$					
$\eta = 0.2$	8.357	7.532	8.597	7.350	7.501	7.312	8.498	7.288
	24.582	19.467	25.439	17.002	19.062	16.479	23.665	16.393
	41.629	29.533	40.211	22.818	28.426	21.476	35.469	21.565
	58.380	37.059	48.684	26.111	35.333	24.032	43.060	24.403
	74.839	42.353	52.362	28.068	40.311	25.433	47.708	26.064
$\eta = 0.5$	5.300	4.967	8.186	4.662	4.958	4.637	8.108	4.646
	11.974	10.221	18.432	8.282	10.151	8.027	18.065	8.209
	18.439	13.960	21.438	10.107	13.821	9.513	21.262	9.992
	24.820	16.475	22.159	11.101	16.299	10.217	22.084	10.959
	31.164	18.142	22.401	11.688	17.962	10.591	22.362	11.530

Table 12. First five nondimensional natural frequencies Ω determined by the Bernoulli-Euler model and the Bresse-Timoshenko models for different nonlocal parameters η of a carbon nanotube

	1 st model		2 nd model		3 rd model	
	0 th order	2 nd order	0 th order	2 nd order	0 th order	2 nd order
$\eta = 0$	9.869	8.635	9.869	8.635	9.869	8.635
	39.478	26.464	39.478	26.464	39.478	26.464
	88.826	45.826	88.826	45.826	88.826	45.826
	157.914	65.003	157.914	65.003	157.914	65.003
	246.740	83.852	246.740	83.852	246.740	83.852
$\eta = 0.2$	8.357	7.312	9.332	8.175	8.023	6.754
	24.582	16.479	32.519	14.917	22.595	11.424
	41.629	21.476	61.799	15.801	37.472	12.643
	58.380	24.032	92.811	16.095	52.030	13.110
	74.839	25.433	129.978	16.23	66.347	13.336
$\eta = 0.5$	5.300	4.637	7.482	Imaginary	4.811	3.635
	11.974	8.027	19.836	6.543	10.616	4.864
	18.439	9.513	32.090	6.569	16.253	5.195
	24.820	10.217	44.063	6.580	21.831	5.324
	31.164	10.591	55.868	6.585	27.383	5.387

Table 13. First five nondimensional natural frequencies Ω determined by the Bernoulli-Euler model and the original and truncated Bresse-Timoshenko models for different nonlocal parameters η of a carbon nanotube

First of all, it is seen that whatever the considered model, when the nonlocal parameter $\bar{\eta}$ increases, the natural frequencies decrease. This is due to the fact that the nonlocal effect increases the flexibility of the beam. For instance, the natural frequency calculated through first asymptotic model at the second order (coinciding with the nonlocal truncated Bresse-Timoshenko model for $R_s = 1$) is equal to 4.637 for $\bar{\eta}$ equal to 0.5, 8.635 in the local approach ($\bar{\eta} = 0$), namely a difference of 46%. This difference increases with the order of frequency. Considering the ratio between the non-dimensional frequency obtained in the local approach and the one when $\bar{\eta} = 0.5$, for the third asymptotic model, it is equal to 2.4 for the fundamental frequency, 15.6 for the fifth one. Thus, the effects of nonlocality are important and they have to be taken into account in the study of nanomaterials. The nonlocal parameter η is equal to the product of a characteristic length (for instance the interatomic interaction) with a small length scale coefficient. Hereinafter, it will be proposed a calibration of the coefficient through the use of lattice models.

About the asymptotic model, it may be shown [238] that at the zeroth order, the first and third asymptotic model, differing only in the expression of the nonlocal length provide similar results. Three different asymptotic models have been derived: following the horizontal, vertical and both directions. The last model is a combination of the two first and naturally, it leads to lower natural frequencies compared to the two other models. In any case, for any order of frequency or value of the nonlocal parameter, the first asymptotic model with a nonlocality following the horizontal direction, coinciding with the truncated Bresse-Timoshenko model, has a larger effect on the frequency than the second asymptotic model with a nonlocality following the vertical direction.

In the derivation of the engineering thick beam models, the parameter R_s , not present in the asymptotic models, has been introduced and there is a debate about its value, zero or unity. Different arguments trend to show that $R_s = 1$. First of all, in this case, considering the original Bresse-Timoshenko model, both the derivations through the use of equilibrium equations and the variational principle lead to the same governing differential equation. Moreover, as it has been explained before, the truncated Bresse-Timoshenko model is asymptotically consistent in the local approach. When the nonlocal effect is taken into account, it is asymptotically consistent (for the asymptotic model with a nonlocality following the horizontal direction) only for R_s equal to unity. Furthermore, the Bernoulli-Euler model ignore the rotary inertia and the shear effects. Consequently, it is supposed to provide an upper bound of the natural frequency. However, for

R_s equal to zero, it is seen in Table 12 that for large non-dimensional nonlocal parameter $\bar{\eta}$ (for example 0.5), the models derived through the variational principle (original and based on slope inertia) lead to bigger natural frequencies compared to those obtained for the Bernoulli-Euler model, hence a contradiction. Thus, the three first frequencies are 8.108, 18.065 and 21.262 for the Bresse-Timoshenko model based on slope inertia versus 5.300, 11.974 and 18.439 for the Bernoulli-Euler model. For the next, R_s will be taken, for beam, equal to 1.

Furthermore, let us denote Ω^* , the ratio of the nondimensional fundamental natural frequencies, the local Bernoulli-Euler model being the reference model. Figure 14. depicts Ω^* for different aspect ratios R_o/L and different values of the small length scale coefficient, considering the three versions of the Bresse-Timoshenko model (original, truncated, based on slope inertia). When the aspect ratio is small (for instance 0.1), the length of the beam is much bigger than the thickness. The rotary inertia and the shear effects are not important and the different models almost coincide with the local Bernoulli-Euler model, valid for thin beams. The frequency ratio Ω^* increases with R_o/L because of these effects, specific to thick beams, that cannot be ignored. Thus, when the ratio R_o/L is close to 1, the carbon nanotube is very short, the Bernoulli-Euler model overestimates the natural frequencies and all the curves converges towards zero.

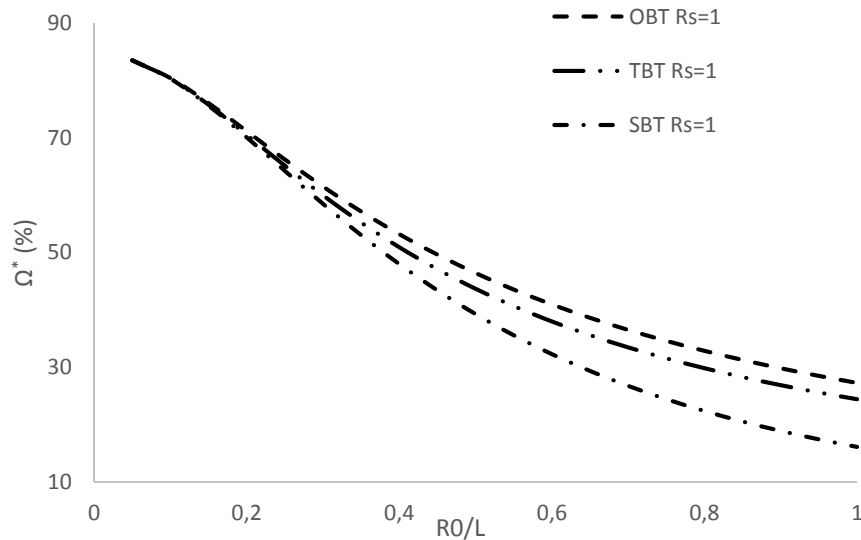


Fig. 14. Non dimensional natural frequency obtained through the original Bresse-Timoshenko model (OBT) and the Truncated Bresse-Timoshenko model (TBT) with the aspect ratio R_o/L

Analogically, Fig. 15. Depicts Ω^* with respect to R_o/L considering the different asymptotic models. As for the engineering models, when the ratio R_o/L is close to unity, the models coincide with the Bernoulli-Euler model and when this ratio increase, a difference occurs.

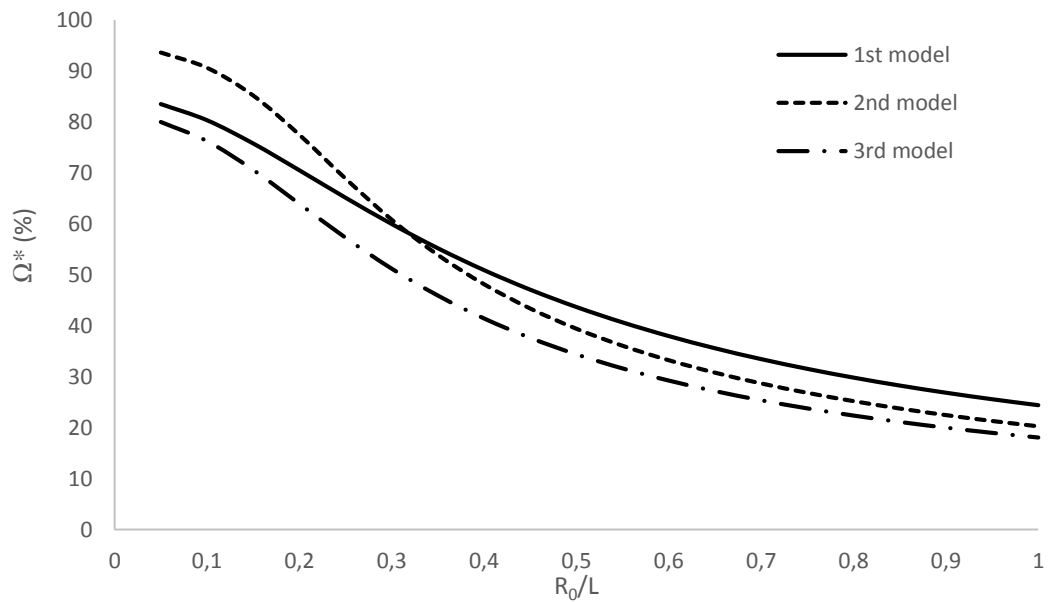


Fig. 15. Non dimensional natural frequency obtained through the three asymptotic models at the second order with (a) the aspect ratio R_o/L

It is now proposed to extend this study to the case of thick plates. It is expected to have analogical results.

3.2. Different plate models

3.2.1. Asymptotic derivation of nonlocal plate models

3.2.1.1. Asymptotic model with a partial nonlocality along the two directions of the plan

Consider a plate of length a , width b and thickness h (see Chapter 2). In this model, for a nonlocality along both the directions of the plate, the stress-displacement relationships are

$$[1 - \eta_*^2 \nabla^2] \boldsymbol{\sigma} = \lambda \left(\theta + \frac{\partial w}{\partial z} \right) \begin{pmatrix} 1 & 0 & 0 \\ 0 & 1 & 0 \\ 0 & 0 & 1 \end{pmatrix} + G \begin{pmatrix} 2 \frac{\partial u}{\partial x} & \frac{\partial u}{\partial y} + \frac{\partial v}{\partial x} & \frac{\partial u}{\partial z} + \frac{\partial w}{\partial x} \\ \frac{\partial u}{\partial y} + \frac{\partial v}{\partial x} & 2 \frac{\partial v}{\partial y} & \frac{\partial v}{\partial z} + \frac{\partial w}{\partial y} \\ \frac{\partial u}{\partial z} + \frac{\partial w}{\partial x} & \frac{\partial v}{\partial z} + \frac{\partial w}{\partial y} & 2 \frac{\partial w}{\partial z} \end{pmatrix} \quad (3.74)$$

where η_* is the microscopic nonlocal length and $\boldsymbol{\sigma}$ is the stress tensor.

Multiplying Eq. (2.73) by $[1 - \eta_*^2 \nabla^2]$ and substituting Eq. (3.74) both sides of the equations:

$$(\lambda + G) \begin{pmatrix} \frac{\partial}{\partial x} \\ \frac{\partial}{\partial y} \\ \frac{\partial}{\partial z} \end{pmatrix} \left(\theta + \frac{\partial w}{\partial z} \right) + G \left(\nabla^2 + \frac{\partial^2}{\partial z^2} \right) \begin{pmatrix} u \\ v \\ w \end{pmatrix} = \rho [1 - \eta_*^2 \nabla^2] \frac{\partial^2}{\partial t^2} \begin{pmatrix} u \\ v \\ w \end{pmatrix} \quad (3.75)$$

As for the case of thick local plates, it leads to a system of two equations:

$$\begin{aligned} (\lambda + G) \frac{\partial}{\partial z} \theta + (\lambda + 2G) \frac{\partial^2 w}{\partial z^2} + \left[G \nabla^2 w - \rho (1 - \eta_*^2 \nabla^2) \frac{\partial^2}{\partial t^2} \right] w &= 0 \\ \left[(\lambda + 2G) \nabla^2 \theta - \rho (1 - \eta_*^2 \nabla^2) \frac{\partial^2}{\partial t^2} \right] \theta + G \frac{\partial^2 \theta}{\partial z^2} + (\lambda + G) \nabla^2 \frac{\partial w}{\partial z} &= 0 \end{aligned} \quad (3.76)$$

Substituting Eq. (2.86) into Eq. (3.76) yields, considering the dimensionless variables $\bar{\eta}_* = \eta_*/a$:

$$\begin{aligned}\bar{\theta}_{N+3} &= \frac{1}{(N+3)(N+2)} \mathcal{A}_{NL}^p \bar{\theta}_{N+1} + \frac{1}{N+3} \mathcal{B}_L \bar{w}_{N+2}; \quad N = 0, 2, 4, \dots \\ \bar{w}_{N+2} &= \frac{1}{(N+1)(N+2)} \mathcal{C}_{NL}^p \bar{w}_N + \frac{1}{(N+2)} \mathcal{F}_L \bar{\theta}_{N+1}; \quad N = 0, 2, 4, \dots\end{aligned}\tag{3.77}$$

where the nonlocal operators \mathcal{A}_{NL} and \mathcal{C}_{NL} are defined as follows:

$$\begin{aligned}\mathcal{A}_{NL}^p &= - \left[\frac{(\lambda + 2G)}{G} \bar{\nabla}^2 - \bar{h}^2 (1 - \bar{\eta}_*^2 \bar{\nabla}^2) \frac{\partial^2}{\partial \bar{t}^2} \right] \\ \mathcal{C}_{NL}^p &= - \frac{G}{(\lambda + 2G)} \left[\bar{\nabla}^2 - \bar{h}^2 (1 - \bar{\eta}_*^2 \bar{\nabla}^2) \frac{\partial^2}{\partial \bar{t}^2} \right]\end{aligned}\tag{3.78}$$

\mathcal{B}_L^p and \mathcal{F}_L^p have been defined in the previous chapter devoted to the local derivation of thick plate models.

At the fourth order, Eq. (2.87) derived in local is still valid. Substituting Eq. (3.77) it yields Eq. (2.93) with:

$$\begin{aligned}M_{11} &= \left[(2G + 3\lambda) \bar{\nabla}^6 - 20(G - \lambda) (1 - \bar{\eta}_*^2 \bar{\nabla}^2) \bar{\nabla}^2 \frac{\partial^2}{\partial \bar{t}^2} \right] \bar{h}^4 \\ &\quad + \left[120(2G + \lambda) (1 - \bar{\eta}_*^2 \bar{\nabla}^2) \frac{\partial^2}{\partial \bar{t}^2} - 20\lambda \bar{\nabla}^4 \right] \bar{h}^2 - 120(2G + \lambda) \bar{\nabla}^2 \\ &\quad + O(\bar{h}^4, \bar{\eta}_*^4) \\ M_{12} &= 20(4G + 3\lambda) \bar{h}^2 \bar{\nabla}^2 - \left[(6G + 5\lambda) \bar{\nabla}^4 + 20(3G + 2\lambda) (1 - \bar{\eta}_*^2 \bar{\nabla}^2) \frac{\partial^2}{\partial \bar{t}^2} \right] \bar{h}^4 \\ &\quad - 120(2G + \lambda) + O(\bar{h}^4, \bar{\eta}_*^4) \\ M_{21} &= \bar{\nabla}^2 \left\{ \left[-12\lambda \bar{\eta}_*^2 \bar{\nabla}^2 \frac{\partial^2}{\partial \bar{t}^2} + (2G + 3\lambda) \bar{\nabla}^4 + 12\lambda \frac{\partial^2}{\partial \bar{t}^2} \right] \bar{h}^4 - 12\lambda \bar{h}^2 \bar{\nabla}^2 \right. \\ &\quad \left. - 24(2G + \lambda) \right\} + O(\bar{h}^4, \bar{\eta}_*^4)\end{aligned}\tag{3.79}$$

$$M_{22} = \left[-12(2G + \lambda)(1 - \bar{\eta}_*^2 \bar{\nabla}^2) \frac{\partial^2}{\partial \bar{t}^2} - (6G + 5\lambda) \bar{\nabla}^4 \right] \bar{h}^4 + 12(4G + 3\lambda) \bar{h}^2 \bar{\nabla}^2 - 24(2G + \lambda) + O(\bar{h}^4, \bar{\eta}_*^4)$$

When the nonlocal effect is not taken into account, the expressions of the different coefficients are reduced to the ones given by Eq (2.94).

The determinant of the matrix vanishing. It results in governing differential equations at different orders:

0th order

$$(G + \lambda) \bar{\nabla}^4 w + \frac{3}{4} (2G + \lambda) (1 - \bar{\eta}_*^2 \bar{\nabla}^2) \frac{\partial^2 w}{\partial \bar{t}^2} = 0 \quad (3.80)$$

2nd order

$$\begin{aligned} -10(3\lambda + 4G)(1 - \bar{\eta}_*^2 \bar{\nabla}^2) \bar{h}^2 \frac{\partial^2}{\partial \bar{t}^2} \bar{\nabla}^2 w - 4(\lambda + G) \bar{h}^2 \bar{\nabla}^6 w + 20(\lambda + G) \bar{\nabla}^4 w \\ + 15(\lambda + 2G)(1 - \bar{\eta}_*^2 \bar{\nabla}^2) \frac{\partial^2 w}{\partial \bar{t}^2} = 0 \end{aligned} \quad (3.81)$$

or, in the dimensional form:

0th order

$$D \nabla^4 w + \rho h (1 - \eta_*^2 \nabla^2) \frac{\partial^2 w}{\partial t^2} = 0 \quad (3.82)$$

2nd order

$$\begin{aligned} D \nabla^4 w + \rho h (1 - \eta_*^2 \nabla^2) \frac{\partial^2 w}{\partial t^2} - (1 - \eta_*^2 \nabla^2) \frac{2(2 - \nu) \rho h^3}{(1 - \nu)} \frac{\partial^2}{\partial t^2} \nabla^2 w - D \frac{h^2}{20} \nabla^6 w \\ = 0 \end{aligned} \quad (3.83)$$

Multiply Eq. (3.81) by $[1 + (\bar{h}^2/5)\bar{\nabla}^2]$, using the dimensional variables:

$$D\nabla^4 w + (1 - \eta_*^2 \nabla^2) \rho h \frac{\partial^2 w}{\partial t^2} - (1 - \eta_*^2 \nabla^2) \frac{\rho h^3}{12} \left[1 + \frac{12D}{h^3 G} \frac{6 - \nu}{5} \right] \frac{\partial^2}{\partial t^2} \nabla^2 w = 0 \quad (3.84)$$

The equation is reduced to the truncated version of Uflyand-Mindlin plate theory with a shear coefficient equal to $\kappa = 5/(6 - \nu)$. This value has been derived in the literature for local plate models [108,109,232,255] and more recently, for nonlocal plate models [239].

3.2.1.2. Asymptotic model with a partial nonlocality along the thickness of the plate

In this model, Eq. (3.74) is replaced by

$$\left[1 - \eta_*^2 \frac{\partial^2}{\partial z^2} \right] \boldsymbol{\sigma} = \lambda \left(\theta + \frac{\partial w}{\partial z} \right) \begin{pmatrix} 1 & 0 & 0 \\ 0 & 1 & 0 \\ 0 & 0 & 1 \end{pmatrix} + G \begin{pmatrix} 2 \frac{\partial u}{\partial x} & \frac{\partial u}{\partial y} + \frac{\partial v}{\partial x} & \frac{\partial u}{\partial z} + \frac{\partial w}{\partial x} \\ \frac{\partial u}{\partial y} + \frac{\partial v}{\partial x} & 2 \frac{\partial v}{\partial y} & \frac{\partial v}{\partial z} + \frac{\partial w}{\partial y} \\ \frac{\partial u}{\partial z} + \frac{\partial w}{\partial x} & \frac{\partial v}{\partial z} + \frac{\partial w}{\partial y} & 2 \frac{\partial w}{\partial z} \end{pmatrix} \quad (3.85)$$

Thus, in this case, it leads to

$$(\lambda + G) \begin{pmatrix} \frac{\partial}{\partial x} \\ \frac{\partial}{\partial y} \\ \frac{\partial}{\partial z} \end{pmatrix} \left(\theta + \frac{\partial w}{\partial z} \right) + G \left(\nabla^2 + \frac{\partial^2}{\partial z^2} \right) \begin{pmatrix} u \\ v \\ w \end{pmatrix} = \rho \left[1 - \eta_*^2 \frac{\partial^2}{\partial z^2} \right] \frac{\partial^2}{\partial t^2} \begin{pmatrix} u \\ v \\ w \end{pmatrix} \quad (3.86)$$

Differentiating the first and second equations with respect to x and y , respectively, and summing them, it leads to a system of two equations:

$$\begin{aligned} (\lambda + G) \frac{\partial}{\partial z} \theta + \left(\lambda + 2G + \rho \eta_*^2 \frac{\partial^2}{\partial t^2} \right) \frac{\partial^2 w}{\partial z^2} + \left[G \nabla^2 w - \rho \frac{\partial^2}{\partial t^2} \right] w &= 0 \\ \left[(\lambda + 2G) \nabla^2 \theta - \rho \frac{\partial^2}{\partial t^2} \right] \theta + \left(G + \rho \eta_*^2 \frac{\partial^2}{\partial t^2} \right) \frac{\partial^2 \theta}{\partial z^2} + (\lambda + G) \nabla^2 \frac{\partial w}{\partial z} &= 0 \end{aligned} \quad (3.87)$$

Substituting Eq. (2.86) into Eq. (3.87) yields

$$\begin{aligned}
& \left(G\nabla^2 - \rho \frac{\partial^2}{\partial t^2} \right) w_{2n} + \left(\lambda + 2G + \rho\eta_*^2 \frac{\partial^2}{\partial t^2} \right) (2n+1)(2n+2)w_{2n+2} \\
& \quad + (\lambda + G)(2n+1)\theta_{2n+1} = 0; \quad n \in \mathbb{N} \\
& (\lambda + G)2n\nabla^2 w_{2n} + \left((\lambda + 2G)\nabla^2 - \rho \frac{\partial^2}{\partial t^2} \right) \theta_{2n-1} \\
& \quad + \left(G + \rho\eta_*^2 \frac{\partial^2}{\partial t^2} \right) 2n(2n+1)\theta_{2n+1} = 0; \quad n \in \mathbb{N}^*
\end{aligned} \tag{3.88}$$

Using the dimensionless variables defined in Eq. (2.88), it becomes

$$\begin{aligned}
\mathcal{H}_1 \bar{\theta}_{N+3} &= \frac{1}{(N+3)(N+2)} \mathcal{A}_L^p \bar{\theta}_{N+1} + \frac{1}{N+3} \mathcal{B}_L^p \bar{w}_{N+2}; \quad N = 0, 2, 4, \dots \\
\mathcal{H}_2 \bar{w}_{N+2} &= \frac{1}{(N+1)(N+2)} \mathcal{C}_L^p \bar{w}_N + \frac{1}{(N+2)} \mathcal{F}_L^p \bar{\theta}_{N+1}; \quad N = 0, 2, 4, \dots
\end{aligned} \tag{3.89}$$

The differential operators \mathcal{H}_1 and \mathcal{H}_2 , \mathcal{B}_{NL}^p and \mathcal{B}_{NL}^p are given by:

$$\mathcal{H}_1 = \left(1 + \bar{h}^2 \bar{\eta}_*^2 \frac{\partial^2}{\partial \bar{t}^2} \right); \quad \mathcal{H}_2 = \left(1 + \frac{G}{(\lambda + 2G)} \bar{h}^2 \bar{\eta}_*^2 \frac{\partial^2}{\partial \bar{t}^2} \right) \tag{3.90}$$

The local operators \mathcal{A}_L^p , \mathcal{B}_L^p , \mathcal{C}_L^p and \mathcal{F}_L^p are given by Eq. (2.92).

Similarly to the previous section, the two equations are written in a matrix form (see section 2.1.2), leading to the governing differential equation at different orders:

0th order

$$\frac{4}{3} (\lambda + G) \bar{\nabla}^4 + (\lambda + 2G) \frac{\partial^2}{\partial \bar{t}^2} - \lambda \bar{\eta}_*^2 \bar{\nabla}^2 \frac{\partial^2}{\partial \bar{t}^2} = 0 \tag{3.91}$$

2nd order

$$\begin{aligned}
& \frac{4}{3}(\lambda + G)\bar{\nabla}^4 + (\lambda + 2G)\frac{\partial^2}{\partial \bar{t}^2} - \lambda\bar{\eta}_*^2\bar{\nabla}^2\frac{\partial^2}{\partial \bar{t}^2} \\
& - \left\{ 4\lambda\frac{(3G + \lambda)}{(\lambda + 2G)}\bar{\eta}_*^4\bar{\nabla}^2\frac{\partial^4}{\partial \bar{t}^4} - \frac{2(20G^2 + 28G\lambda + 7\lambda^2)}{3(\lambda + 2G)}\bar{\eta}_*^2\bar{\nabla}^4\frac{\partial^2}{\partial \bar{t}^2} \right. \\
& \left. + \frac{4}{15}(\lambda + G)\bar{\nabla}^6 - 4(\lambda + 3G)\bar{\eta}_*^2\frac{\partial^4}{\partial \bar{t}^4} + \frac{2}{3}(3\lambda + 4G)\bar{\nabla}^2\frac{\partial^2}{\partial \bar{t}^2} \right\} \bar{h}^2 \\
& = 0
\end{aligned} \tag{3.92}$$

Or, in the dimensional form:

0th order

$$D\nabla^4 + \rho h \left[1 - \frac{v\eta_*^2\nabla^2}{1-v} \right] \frac{\partial^2}{\partial t^2} = 0 \tag{3.93}$$

2nd order

$$\begin{aligned}
& D\nabla^4 + \rho h \left(1 - \frac{v}{1-v}\eta_*^2\nabla^2 \right) \frac{\partial^2}{\partial t^2} \\
& - \left\{ \frac{2v(3-4v)}{(1-v)^2}\eta_*^4\nabla^2\frac{\rho^2 h}{G}\frac{\partial^4}{\partial t^4} \right. \\
& - \frac{\rho h^3}{12}\frac{2(5-26v-v^2)}{(1-v)^2}\eta_*^2\nabla^4\frac{\partial^2}{\partial t^2} + \frac{1}{20}Dh^2\nabla^6 \\
& \left. - \frac{2(3-4v)}{(1-v)}\eta_*^2\frac{\rho^2 h}{G}\frac{\partial^4}{\partial t^4} + \frac{\rho h^3}{12}\frac{2(2-v)}{(1-v)}\nabla^2\frac{\partial^2}{\partial t^2} \right\} = 0
\end{aligned} \tag{3.94}$$

Multiplying Eq. (3.92) by $[5 + \bar{\nabla}^2\bar{h}^2]$ leads to, using the dimensional numbers

$$\begin{aligned}
& D\nabla^4 + (1 - \kappa_1\eta_*^2\nabla^2)\rho h \left(1 + \kappa_3\frac{\rho}{G}\eta_*^2\frac{\partial^2}{\partial t^2} \right) \frac{\partial^2}{\partial t^2} - \frac{\rho h^3}{12} \left[1 + \frac{12D}{\kappa h^3 G} \right] \frac{\partial^2\nabla^2}{\partial t^2} \\
& + \kappa_2\frac{\rho h^3}{12}\eta_*^2\nabla^4\frac{\partial^2}{\partial t^2} = 0
\end{aligned} \tag{3.95}$$

where

$$\kappa_1 = \frac{v}{1-v}; \kappa_2 = \frac{(100 - 63v - 7v^2)}{15(1-v)^2}; \kappa_3 = \frac{2(3-4v)}{(1-v)} \tag{3.96}$$

3.2.1.3. Asymptotic model with a full nonlocality

In this model, Eq. (3.74) is replaced by

$$\left[1 - \eta_*^2 \left(\nabla^2 + \frac{\partial^2}{\partial z^2} \right)\right] \sigma = \lambda \left(\theta + \frac{\partial w}{\partial z} \right) \begin{pmatrix} 1 & 0 & 0 \\ 0 & 1 & 0 \\ 0 & 0 & 1 \end{pmatrix} + G \begin{pmatrix} 2 \frac{\partial u}{\partial x} & \frac{\partial u}{\partial y} + \frac{\partial v}{\partial x} & \frac{\partial u}{\partial z} + \frac{\partial w}{\partial x} \\ \frac{\partial u}{\partial y} + \frac{\partial v}{\partial x} & 2 \frac{\partial v}{\partial y} & \frac{\partial v}{\partial z} + \frac{\partial w}{\partial y} \\ \frac{\partial u}{\partial z} + \frac{\partial w}{\partial x} & \frac{\partial v}{\partial z} + \frac{\partial w}{\partial y} & 2 \frac{\partial w}{\partial z} \end{pmatrix} \quad (3.97)$$

Thus, in this case, it yields:

$$(\lambda + G) \begin{pmatrix} \frac{\partial}{\partial x} \\ \frac{\partial}{\partial y} \\ \frac{\partial}{\partial z} \end{pmatrix} \left(\theta + \frac{\partial w}{\partial z} \right) + G \left(\nabla^2 + \frac{\partial^2}{\partial z^2} \right) \begin{pmatrix} u \\ v \\ w \end{pmatrix} = \rho \left[1 - \eta_*^2 \left(\nabla^2 + \frac{\partial^2}{\partial z^2} \right) \right] \frac{\partial^2}{\partial t^2} \begin{pmatrix} u \\ v \\ w \end{pmatrix} \quad (3.98)$$

Differentiating the first and second equations with respect to x and y , respectively, and summing them, it leads to a system of two equations:

$$(\lambda + G) \frac{\partial}{\partial z} \theta + \left(\lambda + 2G + \rho \eta_*^2 \frac{\partial^2}{\partial t^2} \right) \frac{\partial^2 w}{\partial z^2} + \left[G \nabla^2 w - \rho (1 - \eta_*^2 \nabla^2) \frac{\partial^2}{\partial t^2} \right] w = 0 \quad (3.99)$$

$$\left[(\lambda + 2G) \nabla^2 \theta - \rho (1 - \eta_*^2 \nabla^2) \frac{\partial^2}{\partial t^2} \right] \theta + \left(G + \rho \eta_*^2 \frac{\partial^2}{\partial t^2} \right) \frac{\partial^2 \theta}{\partial z^2} + (\lambda + G) \nabla^2 \frac{\partial w}{\partial z} = 0$$

Substituting Eq. (2.86) into Eq. (3.99) yields

$$\begin{aligned} & \left(G \nabla^2 - \rho (1 - \eta_*^2 \nabla^2) \frac{\partial^2}{\partial t^2} \right) w_{2n} \\ & + \left(\lambda + 2G + \rho \eta_*^2 \frac{\partial^2}{\partial t^2} \right) (2n + 1)(2n + 2) w_{2n+2} \\ & + (\lambda + G)(2n + 1) \theta_{2n+1} = 0; \quad n \in \mathbb{N} \end{aligned} \quad (3.100)$$

$$\begin{aligned}
& (\lambda + G)2n\nabla^2 w_{2n} + \left((\lambda + 2G)\nabla^2 - \rho(1 - \eta_*^2\nabla^2) \frac{\partial^2}{\partial t^2} \right) \theta_{2n-1} \\
& + \left(G + \rho\eta_*^2 \frac{\partial^2}{\partial t^2} \right) 2n(2n + 1)\theta_{2n+1} = 0; \quad n \in \mathbb{N}^*
\end{aligned}$$

Using the dimensionless variables defined in Eq. (2.88), it becomes:

$$\mathcal{H}_1 \bar{\theta}_{N+3} = \frac{1}{(N+3)(N+2)} \mathcal{A}_{NL}^p \bar{\theta}_{N+1} + \frac{1}{N+3} \mathcal{B}_L^p \bar{w}_{N+2}; \quad N = 0, 2, 4, \dots \quad (3.101)$$

$$\mathcal{H}_2 \bar{w}_{N+2} = \frac{1}{(N+1)(N+2)} \mathcal{C}_{NL}^p \bar{w}_N + \frac{1}{(N+2)} \mathcal{F}_L^p \bar{\theta}_{N+1}; \quad N = 0, 2, 4, \dots$$

In this case, the two equations are written in a matrix form, leading to the following equation at different orders:

0th order

$$\frac{4}{3}(\lambda + G)\bar{\nabla}^4 + \left[(\lambda + 2G) - \frac{1}{2}(\lambda + G)\bar{\eta}_*^2\bar{\nabla}^2 \right] \frac{\partial^2}{\partial \bar{t}^2} = 0 \quad (3.102)$$

2nd order

$$\begin{aligned}
& \left\{ -\frac{8(\lambda + 3G)(\lambda + G)}{(\lambda + 2G)} \bar{\eta}_*^4 \bar{\nabla}^2 \frac{\partial^4}{\partial \bar{t}^4} + \frac{4(5\lambda + 14G)(\lambda + G)}{(\lambda + 2G)} \bar{\eta}_*^2 \bar{\nabla}^4 \frac{\partial^2}{\partial \bar{t}^2} \right. \\
& \quad - \frac{4}{15}(\lambda + G)\bar{\nabla}^6 + 4(\lambda + 3G)\bar{\eta}_*^2 \frac{\partial^4}{\partial \bar{t}^4} \\
& \quad \left. - \frac{2}{3}(3\lambda + 4G)\bar{\nabla}^2 \frac{\partial^2}{\partial \bar{t}^2} \right\} \bar{h}^2 - \frac{1}{2}(\lambda + G)\bar{\eta}_*^2\bar{\nabla}^2 \frac{\partial^2}{\partial \bar{t}^2} \\
& \quad + \frac{4}{3}(\lambda + G)\bar{\nabla}^4 + (\lambda + 2G) \frac{\partial^2}{\partial \bar{t}^2} = 0 \quad (3.103)
\end{aligned}$$

Or, in the dimensional form:

0th order

$$D\nabla^4 + \left(1 - \frac{1}{4(1-\nu)} \eta_*^2 \nabla^2 \right) \rho h \frac{\partial^2}{\partial t^2} = 0 \quad (3.104)$$

2nd order

$$\begin{aligned}
& -\frac{2(3-4\nu)\rho^2 h}{(1-\nu)^2} \frac{\eta_*^4 \nabla^2}{G} \frac{\partial^4}{\partial t^4} + \frac{19-28\nu\rho h^3}{(1-\nu)^2} \frac{\eta_*^2 \nabla^4}{12} \frac{\partial^2}{\partial t^2} - \frac{h^2}{20} D \nabla^6 \\
& + \frac{2(3-4\nu)\rho^2 h}{(1-\nu)} \frac{\eta_*^2}{G} \frac{\partial^4}{\partial t^4} - \frac{2(2-\nu)\rho h^3}{1-\nu} \frac{\nabla^2}{12} \frac{\partial^2}{\partial t^2} + D \nabla^4 \\
& + \left(1 - \frac{1}{4(1-\nu)} \eta_*^2 \nabla^2\right) \rho h \frac{\partial^2}{\partial t^2} = 0
\end{aligned} \tag{3.105}$$

Multiplying Eq. (3.103) by $[5 + \bar{\nabla}^2 \bar{h}^2]$ leads to, under the dimensional form

$$\begin{aligned}
D \nabla^4 w + \rho h [1 - \kappa_1 \eta_*^2 \nabla^2] \frac{\partial^2 w}{\partial t^2} - \left[1 + \frac{12D}{\kappa h^3 G}\right] \frac{\rho h^3}{12} \nabla^2 \frac{\partial^2 w}{\partial t^2} \\
+ \eta_*^2 \frac{\rho^2 h}{G} \kappa_3 [1 - 4\kappa_1 \eta_*^2 \nabla^2] \frac{\partial^4 w}{\partial t^4} + \kappa_2 \frac{\rho h^3}{12} \eta_*^2 \nabla^4 \frac{\partial^2 w}{\partial t^2} = 0
\end{aligned} \tag{3.106}$$

where

$$\kappa_1 = \frac{1}{4(1-\nu)}; \kappa_2 = \frac{(277-357\nu)}{20(1-\nu)^2}; \kappa_3 = \frac{2(3-4\nu)}{(1-\nu)} \tag{3.107}$$

3.2.2. Nonlocal engineering plate approaches

3.2.2.1. The nonlocal fourth order phenomenological Kirchhoff-Love model

In the stress gradient Kirchhoff-Love plate model, the constitutive relations for a rectangular KL plate can be written as [134,135,256]:

$$(1 - \eta^2 \nabla^2) M_{xx} = D \left(\frac{\partial^2 w}{\partial x^2} + \nu \frac{\partial^2 w}{\partial y^2} \right) \tag{3.108}$$

$$(1 - \eta^2 \nabla^2) M_{yy} = D \left(\frac{\partial^2 w}{\partial y^2} + \nu \frac{\partial^2 w}{\partial x^2} \right) \tag{3.109}$$

$$(1 - \eta^2 \nabla^2) M_{xy} = D(1 - \nu) \frac{\partial^2 w}{\partial x \partial y} \tag{3.110}$$

where M_{xx} , M_{yy} are the bending moments is M_{xy} the twisting moment.

The nonlocal equilibrium equation of a rectangular plate is given by [80, 257,258], neglecting the rotary inertia

$$\frac{\partial^2 M_{xx}}{\partial x^2} + 2 \frac{\partial^2 M_{xy}}{\partial x \partial y} + \frac{\partial^2 M_{yy}}{\partial y^2} = -\rho h \frac{\partial^2 w}{\partial t^2} \quad (3.111)$$

Multiplication of Eq. (3.111) by $(1 - \eta^2 \nabla^2)$ and substitution of Eqs. (3.108)-(3.110) results in [134,135,239]

$$D \nabla^4 w + (1 - \eta^2 \nabla^2) \rho h \frac{\partial^2 w}{\partial t^2} = 0 \quad (3.112)$$

In the local approach $\eta = 0$ and at the zeroth-order, the three asymptotic models derived from three-dimensional considerations and governed by Eqs. (3.82), (3.93) and (3.104) are reduced to the local Kirchhoff-Love thin plate model as already shown in the literature [109] and in a previous chapter.

The nonlocal Kirchhoff-Love plate model, as derived before and in the literature, is asymptotically consistent following one specific asymptotic model, namely the one with a partial nonlocality following the directions of the neutral plane of the plate. Furthermore, the three different models lead to different values of the small length scale differs between the models. Thus, the macroscopic length scale, used in the engineering models, such as the Kirchhoff-Love plate model, is related to the microscopic length scale introduced in the asymptotic models through the following relationship:

$$\eta = \sqrt{\kappa_1} \eta_* \quad (3.113)$$

where κ_1 is equal to $\nu/(1 - \nu)$ and $1/4(1 - \nu)$ for the asymptotic model with a partial nonlocality following the thickness of the plate and a full nonlocality, respectively.

Eq. (3.112) may be obtained variationally using the following bending strain energy, kinetic energy [259]:

$$U(w) = \frac{1}{2} \iint_{\mathcal{D}} D \left[\left(\frac{\partial^2 w}{\partial x^2} \right)^2 + 2\nu \frac{\partial^2 w}{\partial x^2 \partial y^2} + \left(\frac{\partial^2 w}{\partial y^2} \right)^2 + 2(1 - \nu) \left(\frac{\partial^2 w}{\partial x \partial y} \right)^2 \right] dx dy \quad (3.114)$$

$$T(w) = \frac{1}{2} \iint_{\mathcal{D}} \frac{\partial^2}{\partial t^2} \left[w^2 + \eta^2 \left(\left(\frac{\partial w}{\partial x} \right)^2 + \left(\frac{\partial w}{\partial y} \right)^2 \right) \right] dx dy \quad (3.115)$$

It is worth noting that the nonlocal effect does not affect the bending strain energy.

Thus, by applying the Hamilton principle, Eq. (3.112) is obtained and, for boundary conditions, for edges parallel to the x axis,

$$D \left(\frac{\partial^2 w}{\partial x^2} + \nu \frac{\partial^2 w}{\partial y^2} \right) \quad \text{or} \quad \frac{\partial w}{\partial x} \quad \text{are specified}$$

$$D \frac{\partial}{\partial x} \nabla^2 w - \eta^2 \rho h \frac{\partial^3 w}{\partial t^2 \partial x} \quad \text{or} \quad w$$

3.2.2.2. 6th order phenomenological thin plate model

We start from the constitutive law postulated as:

$$[1 - \eta^2 \nabla^2] M_{xx} = D \left[\frac{\partial^2 w}{\partial x^2} + \nu \frac{\partial^2 w}{\partial y^2} - \eta^2 \left(\frac{\partial^4 w}{\partial x^2 \partial y^2} - \frac{\partial^4 w}{\partial x^4} \right) \right] \quad (3.116)$$

$$[1 - \eta^2 \nabla^2] M_{yy} = D \left[\frac{\partial^2 w}{\partial y^2} + \nu \frac{\partial^2 w}{\partial x^2} - \eta^2 \left(\frac{\partial^4 w}{\partial x^2 \partial y^2} - \frac{\partial^4 w}{\partial y^4} \right) \right] \quad (3.117)$$

$$[1 - \eta^2 \nabla^2] M_{xy} = D(1 - \nu) \frac{\partial^2 w}{\partial x \partial y} \quad (3.118)$$

This model is close to the previously studied nonlocal fourth order phenomenological Kirchhoff-Love plate model. It changes in the expression of the right hand side. In this model, it includes an additional term. It is worth nothing that Eq. (3.118) coincides with Eq. (3.110).

Multiplying Eq. (3.111) by $[1 - (e_0 a)^2 \nabla^2]$ and substituting Eqs. (3.116)-(3.118)

$$D \left[\nabla^4 w + \eta^2 \left(\frac{\partial^4}{\partial x^4} - 2 \frac{\partial^4}{\partial x^2 \partial y^2} + \frac{\partial^4}{\partial y^4} \right) \nabla^2 w \right] + [1 - \eta^2 \nabla^2] \rho h \frac{\partial^2 w}{\partial t^2} = 0 \quad (3.119)$$

This equation containing sixth derivative terms following a same contribution, namely x and y , it is called sixth order phenomenological model.

This equation may be also obtained from U, T and W given by:

$$\begin{aligned}
 U(w) = \frac{1}{2} \iint_{\mathfrak{D}} D \left[\left(\frac{\partial^2 w}{\partial x^2} \right)^2 + 2\nu \frac{\partial^4 w}{\partial x^2 \partial y^2} + \left(\frac{\partial^2 w}{\partial y^2} \right)^2 + 2(1-\nu) \left(\frac{\partial^2 w}{\partial x \partial y} \right)^2 \right. \\
 \left. - \eta^2 \left(\left(\frac{\partial^3 w}{\partial x^3} \right)^2 + \left(\frac{\partial^3 w}{\partial y^3} \right)^2 \right) \right. \\
 \left. + \eta^2 \left(\left(\frac{\partial^3 w}{\partial x^2 \partial y} \right)^2 + \left(\frac{\partial^3 w}{\partial x \partial y^2} \right)^2 \right) \right] dx dy
 \end{aligned} \tag{3.120}$$

$$T(w) = \frac{1}{2} \iint_{\mathfrak{D}} \frac{\partial^2}{\partial t^2} \left[w^2 + \eta^2 \left(\left(\frac{\partial w}{\partial x} \right)^2 + \left(\frac{\partial w}{\partial y} \right)^2 \right) \right] dx dy \tag{3.121}$$

For boundary conditions, for edges parallel to the x axis, it yields:

$$\begin{aligned}
 D \left\{ \frac{\partial^2 w}{\partial x^2} + \nu \frac{\partial^2 w}{\partial y^2} - \eta^2 \left(\frac{\partial^4 w}{\partial x^2 \partial y^2} - \frac{\partial^4 w}{\partial x^4} \right) \right\} \delta \left(\frac{\partial w}{\partial x} \right) = 0 \\
 \eta^2 D \left[\frac{\partial^3 w}{\partial x^2 \partial y} \frac{\partial^2 \delta w}{\partial x^2} - \frac{\partial^3 w}{\partial y^3} \frac{\partial^2 \delta w}{\partial y^2} \right] = 0 \\
 \left\{ D \left[\frac{\partial}{\partial x} \nabla^2 w + \eta^2 \left(\frac{\partial^5 w}{\partial x^5} - \frac{\partial^5 w}{\partial x^3 \partial y^2} \right) \right] + \eta^2 m_0 \omega^2 \frac{\partial w}{\partial x} \right\} \delta w = 0
 \end{aligned}$$

As for beam, this model will not be considered hereinafter.

3.2.2.3. Nonlocal original Uflyand-Mindlin model

In the nonlocal stress gradient Uflyand-Mindlin plate mode, the nonlocal equilibrium equations of a rectangular plate match those of the local equations given by Eq. (2.75) and the nonlocal constitutive laws are given by

$$\begin{aligned}
 (1 - \eta^2 \nabla^2) M_{xx} &= D \left(\frac{\partial \psi_x}{\partial x} + \nu \frac{\partial \psi_y}{\partial y} \right) \\
 (1 - \eta^2 \nabla^2) M_y &= D \left(\frac{\partial \psi_y}{\partial y} + \nu \frac{\partial \psi_x}{\partial x} \right)
 \end{aligned} \tag{3.122}$$

$$(1 - \eta^2 \nabla^2) M_{xy} = \frac{D}{2} (1 - \nu) \left(\frac{\partial \psi_x}{\partial y} + \frac{\partial \psi_y}{\partial x} \right)$$

$$(1 - R_s \eta^2 \nabla^2) Q_x = \kappa G h \left(\psi_x + \frac{\partial w}{\partial x} \right); (1 - R_s \eta^2 \nabla^2) Q_y = \kappa G h \left(\psi_y + \frac{\partial w}{\partial y} \right)$$

R_s is the control parameter defined before. In the literature, for plates and in contrast to beams, to our best knowledge, R_s is taken equal to unity. In this thesis, the case of R_s equal to zero will not be ignored.

Successive manipulations of these equations of motion lead to the governing differential equation

$$\begin{aligned} D \nabla^4 w + (1 - R_s \eta^2 \nabla^2) \left(h - \frac{D \nabla^2}{\kappa G} \right) \rho \frac{\partial^2 w}{\partial t^2} + \eta^2 (R_s - 1) \rho h \frac{\partial^2 \nabla^2 w}{\partial t^2} \\ - \frac{\rho h^3}{12} (1 - \eta^2 \nabla^2) \frac{\partial^2}{\partial t^2} \left[\nabla^2 w - (1 - R_s \eta^2 \nabla^2) \frac{\rho}{\kappa G} \frac{\partial^2 w}{\partial t^2} \right] = 0 \end{aligned} \quad (3.123)$$

Furthermore, the nonlocal OUM plate model is also derived variationally by setting an additional Eringen energy T^{NL} :

$$\begin{aligned} T^{NL} = \frac{\eta^2}{2} \iint_{\mathfrak{D}} R_s \rho h \left[\left(\frac{\partial^2 w}{\partial x \partial t} \right)^2 + \left(\frac{\partial^2 w}{\partial y \partial t} \right)^2 \right] \\ + \frac{\rho h^3}{12} \left[\left(\frac{\partial^2 \psi_x}{\partial x \partial t} \right)^2 + \left(\frac{\partial^2 \psi_x}{\partial y \partial t} \right)^2 + \left(\frac{\partial^2 \psi_y}{\partial x \partial t} \right)^2 + \left(\frac{\partial^2 \psi_y}{\partial y \partial t} \right)^2 \right] dx dy \end{aligned} \quad (3.124)$$

Hamilton's principle, considering the strain and kinetic energies given by Eqs. (2.9)-(2.11) and (3.124), leads to the equations of motion:

$$\begin{aligned} D \left(\frac{\partial^2 \psi_x}{\partial x^2} + \nu \frac{\partial^2 \psi_y}{\partial x \partial y} \right) + \frac{D(1 - \nu)}{2} \left(\frac{\partial^2 \psi_x}{\partial y^2} + \frac{\partial^2 \psi_y}{\partial x \partial y} \right) - \kappa G h \left(\psi_x + \frac{\partial w}{\partial x} \right) \\ = \frac{\rho h^3}{12} (1 - \eta^2 \nabla^2) \frac{\partial^2 \psi_x}{\partial t^2} \end{aligned} \quad (3.125)$$

$$\begin{aligned} D \left(\frac{\partial^2 \psi_y}{\partial y^2} + \nu \frac{\partial^2 \psi_x}{\partial x \partial y} \right) + \frac{D(1 - \nu)}{2} \left(\frac{\partial^2 \psi_y}{\partial x^2} + \frac{\partial^2 \psi_x}{\partial x \partial y} \right) - \kappa G h \left(\psi_y + \frac{\partial w}{\partial y} \right) \\ = \frac{\rho h^3}{12} (1 - \eta^2 \nabla^2) \frac{\partial^2 \psi_y}{\partial t^2} \end{aligned}$$

$$\kappa Gh \left(\frac{\partial \psi_x}{\partial x} + \frac{\partial^2 w}{\partial x^2} + \frac{\partial \psi_y}{\partial y} + \frac{\partial^2 w}{\partial y^2} \right) = \rho h (1 - R_s \eta^2 \nabla^2) \frac{\partial^2 w}{\partial t^2}$$

At the boundary of the plate:

$$D \left(\frac{\partial \psi_n}{\partial n} + \nu \frac{\partial \psi_s}{\partial s} \right) + \eta^2 \frac{\rho h^3}{12} \frac{\partial^3 \psi_n}{\partial t^2 \partial n} = 0 \text{ or } \psi_n$$

$$\frac{D(1-\nu)}{2} \left(\frac{\partial \psi_n}{\partial s} + \frac{\partial \psi_s}{\partial n} \right) + \eta^2 \frac{\rho h^3}{12} \frac{\partial^3 \psi_s}{\partial t^2 \partial n} = 0 \text{ or } \psi_s$$

$$\kappa Gh \left(\psi_n + \frac{\partial w}{\partial n} \right) + R_s \eta^2 \rho h \frac{\partial^3 w}{\partial t^2 \partial n} = 0 \text{ or } w$$

are specified.

The equations of motion lead to the governing differential equation:

$$D \nabla^4 w + (1 - R_s \eta^2 \nabla^2) \left(\rho h \frac{\partial^2 w}{\partial t^2} - \frac{\rho}{\kappa G} D \nabla^2 \frac{\partial^2 w}{\partial t^2} \right) - \frac{\rho h^3}{12} (1 - \eta^2 \nabla^2) \frac{\partial^2}{\partial t^2} \left(\nabla^2 w - (1 - R_s \eta^2 \nabla^2) \frac{\rho}{\kappa G} \frac{\partial^2 w}{\partial t^2} \right) = 0 \quad (3.126)$$

It is worth noticing that, for $R_s = 1$, the governing differential equations in displacement derived through the use of the equilibrium equations and the variational principles are identical. However, for $R_s = 0$, Eq. (3.126), derived through the variational principle, compared to Eq. (3.123) does not contain the term $\eta^2 \rho h \partial^2 \nabla^2 w / \partial t^2$.

3.2.2.4. Truncated Uflyand-Mindlin model

As for the local plate models, it is suggested to replace in the equations of motion of the original Uflyand-Mindlin plate model $\partial^2\psi_x/\partial t^2$ and $\partial^2\psi_y/\partial t^2$ by $\partial^3w/\partial x\partial t^2$ and $\partial^3w/\partial y\partial t^2$, respectively. Thus, for the model derived through equilibrium equations, it yields [70]

$$D\nabla^4w + (1 - R_s\eta^2\nabla^2)\left(h - \frac{D\nabla^2}{\kappa G}\right)\rho\frac{\partial^2w}{\partial t^2} + \eta^2(R_s - 1)\rho h\frac{\partial^2\nabla^2w}{\partial t^2} - \frac{\rho h^3}{12}(1 - \eta^2\nabla^2)\frac{\partial^2\nabla^2w}{\partial t^2} = 0 \quad (3.127)$$

3.2.2.5. Uflyand-Mindlin based on slope inertia

As for the nonlocal theory of beam, the expression of the kinetic energy given in Eq. (3.124) is retained.

Using Hamilton's principle in conjunction with Eq. (2.101) rather than Eq. (2.80) yields to the equations of motion,

$$D\left(\frac{\partial^2\psi_x}{\partial x^2} + \nu\frac{\partial^2\psi_y}{\partial x\partial y}\right) + \frac{D(1-\nu)}{2}\left(\frac{\partial^2\psi_x}{\partial y^2} + \frac{\partial^2\psi_y}{\partial x\partial y}\right) - \kappa Gh\left(\psi_x + \frac{\partial w}{\partial x}\right) = -\eta^2\nabla^2\frac{\rho h^3}{12}\frac{\partial^2\psi_x}{\partial t^2}$$

$$D\left(\frac{\partial^2\psi_y}{\partial y^2} + \nu\frac{\partial^2\psi_x}{\partial x\partial y}\right) + \frac{D(1-\nu)}{2}\left(\frac{\partial^2\psi_y}{\partial x^2} + \frac{\partial^2\psi_x}{\partial x\partial y}\right) - \kappa Gh\left(\psi_y + \frac{\partial w}{\partial y}\right) = -\eta^2\nabla^2\frac{\rho h^3}{12}\frac{\partial^2\psi_y}{\partial t^2} \quad (3.128)$$

$$\kappa Gh\left(\frac{\partial\psi_x}{\partial x} + \frac{\partial^2w}{\partial x^2} + \frac{\partial\psi_y}{\partial y} + \frac{\partial^2w}{\partial y^2}\right) + \frac{\rho h^3}{12}\frac{\partial^2}{\partial t^2}\nabla^2w = \rho h(1 - R_s\eta^2\nabla^2)\frac{\partial^2w}{\partial t^2}$$

It leads to the following governing differential equation,

$$-\frac{\rho}{\kappa G}(1 - R_s\eta^2\nabla^2)D\nabla^2\frac{\partial^2w}{\partial t^2} + \frac{\rho h^2}{12\kappa G}D\frac{\partial^2}{\partial t^2}\nabla^4w + D\nabla^4w + \rho h(1 - R_s\eta^2\nabla^2)\frac{\partial^2w}{\partial t^2} - \frac{\rho h^3}{12}\frac{\partial^2\nabla^2w}{\partial t^2} = \frac{\eta^2\rho h^3}{12}\frac{\partial^2\nabla^2}{\partial t^2}\left[\frac{\rho}{\kappa G}(1 - R_s\eta^2\nabla^2)\frac{\partial^2w}{\partial t^2} - \frac{\rho h^2}{12\kappa G}\frac{\partial^2}{\partial t^2}\nabla^2w - \nabla^2w\right] \quad (3.129)$$

And, at the boundary of the plate:

$$D \left(\frac{\partial \psi_n}{\partial n} + \nu \frac{\partial \psi_s}{\partial s} \right) + \eta^2 \frac{\rho h^3}{12} \frac{\partial^3 \psi_n}{\partial t^2 \partial n} = 0 \text{ or } \psi_n$$

$$\frac{D(1-\nu)}{2} \left(\frac{\partial \psi_n}{\partial s} + \frac{\partial \psi_s}{\partial n} \right) + \eta^2 \frac{\rho h^3}{12} \frac{\partial^3 \psi_s}{\partial t^2 \partial n} = 0 \text{ or } \psi_s$$

$$\kappa G h \left(\psi_n + \frac{\partial w}{\partial n} \right) + \frac{\rho h^3}{12} \frac{\partial^3 w}{\partial t^2 \partial n} + R_s \eta^2 \rho h \frac{\partial^3 w}{\partial t^2 \partial n} = 0 \text{ or } w$$

are specified

3.2.3. Solution

Now, it is proposed to conduct a numerical comparison of the natural frequencies obtained through the different nonlocal asymptotic and engineering (KL, OUM, TUM and SUM) models for a nanoplate simply supported at all edges.

The governing differential equation, for the nonlocal engineering thick plate models is written under the general form as follows:

$$D \nabla^4 w + (1 - R_s \eta^2 \nabla^2) \left(\rho h - \frac{\rho}{\kappa G} D \nabla^2 \right) \frac{\partial^2 w}{\partial t^2} + \delta_g \eta^2 (R_s - 1) \nabla^2 \rho h \frac{\partial^2 w}{\partial t^2}$$

$$- \frac{\rho h^3}{12} \frac{\partial^2}{\partial t^2} \left\{ (1 - \eta^2 \nabla^2) \nabla^2 w \right.$$

$$- (\gamma_1 - \eta^2 \nabla^2) (\gamma_1 + \gamma_2) \frac{\rho}{\kappa G} (1 - R_s \eta^2 \nabla^2) \frac{\partial^2 w}{\partial t^2}$$

$$\left. - \frac{\gamma_2}{\kappa G} \left(\frac{D}{h} + \frac{\eta^2 \rho h^2}{12} \frac{\partial^2}{\partial t^2} \right) \nabla^4 w \right\} = 0 \quad (3.130)$$

The following nondimensional numbers are introduced:

$$\beta = \frac{E}{G(1-\nu^2)} = \frac{2}{(1-\nu)}; y = \mu b = \frac{\mu}{\chi} a; \bar{h} = \frac{h}{a}; \xi = \frac{x}{a}; \chi = \frac{a}{b}; \bar{\eta} = \frac{\eta}{a} \quad (3.131)$$

As for local plate models, the solution is given by Navier (see Eq. (2.118)). Substituting Eq. (2.118) and (3.131) into Eq. (3.130), It yields:

$$\Lambda_1 \Omega^4 - \Lambda_2 \Omega^2 + \Lambda_3 = 0 \quad (3.132)$$

where, for the engineering models for thick plates (original and truncated Uflyand-Mindlin and Uflyand-Mindlin based on slope inertia):

$$\begin{aligned} \Lambda_1 &= \frac{\beta \bar{h}^4}{144\kappa} \chi^8 \left[\gamma_1 \Xi (1 + R_s \bar{\eta}^2 \bar{\nabla}_{mn}) + \gamma_2 \left[1 + R_s \bar{\eta}^2 \bar{\nabla}_{mn} + \frac{\bar{h}^2}{12} \right] \bar{\eta}^2 \bar{\nabla}_{mn} \right] \\ \Lambda_2 &= \left[(1 + R_s \bar{\eta}^2 \bar{\nabla}_{mn}) \left(1 + \frac{\bar{h}^2 \beta}{12 \kappa} \bar{\nabla}_{mn} \right) - \delta_g \bar{\eta}^2 (R_s - 1) \bar{\nabla}_{mn} + \Xi \frac{\bar{h}^2}{12} \bar{\nabla}_{mn} + \gamma_2 \frac{\bar{h}^4 \beta}{144 \kappa} \bar{\nabla}_{mn}^2 \right] \chi^4 \\ \Lambda_3 &= \bar{\nabla}_{mn}^2 \end{aligned} \quad (3.133)$$

with $\Xi = (1 + \bar{\eta}^2 \bar{\nabla}_{mn})$.

The coefficients for the first asymptotic model, coinciding with the truncated Bresse-Timoshenko model with $R_s = 1$ are given for a couple (γ_1, γ_2) equal to $(0,0)$:

$$\Lambda_1 = 0; \Lambda_2 = \left[(1 + \bar{\eta}^2 \bar{\nabla}_{mn}) \left(1 + \frac{\bar{h}^2 \beta}{12 \kappa} \bar{\nabla}_{mn} \right) + \Xi \frac{\bar{h}^2 \beta}{12 \kappa} \bar{\nabla}_{mn}^2 \right] \chi^4 \quad (3.134)$$

For the second asymptotic model with a partial nonlocality following the thickness of the plate, at the second order,

$$\begin{aligned} \Lambda_1 &= (1 + \kappa_1 \bar{\eta}_*^2 \bar{\nabla}_{mn}) \kappa_3 \chi^8 \frac{\bar{h}^2}{12} \beta \bar{\eta}_*^2 \\ \Lambda_2 &= \left\{ 1 + \kappa_1 \bar{\eta}_*^2 \bar{\nabla}_{mn} + \bar{\nabla}_{mn} \frac{\bar{h}^2}{12} \left[1 + \frac{\beta}{\kappa} \right] + \kappa_2 \frac{\bar{h}^2}{12} \bar{\eta}_*^2 \bar{\nabla}_{mn}^2 \right\} \chi^4 \end{aligned} \quad (3.135)$$

For the third asymptotic model with a full nonlocality, at the second order,

$$\begin{aligned} \Lambda_1 &= \bar{\eta}_*^2 \chi^8 \frac{\beta \bar{h}^2}{12} \kappa_3 [1 + 4\kappa_1 \bar{\eta}_*^2 \bar{\nabla}_{mn}] \\ \Lambda_2 &= \left\{ 1 + \kappa_1 \bar{\eta}_*^2 \bar{\nabla}_{mn} + \left[1 + \frac{\beta}{\kappa} \right] \frac{\bar{h}^2}{12} \bar{\nabla}_{mn} + \kappa_2 \frac{\bar{h}^2}{12} \bar{\eta}_*^2 \bar{\nabla}_{mn}^2 \right\} \chi^4 \end{aligned} \quad (3.136)$$

The expression of Λ_3 is the same for all the models (asymptotic and engineering).

For the original Uflyand-Mindlin plate model and the second nonlocal asymptotic model at the second order, the solution is given by Eq. (2.131)

For the truncated Uflyand-Mindlin plate model, $\gamma_1 = 0$ and

$$\Omega = \frac{\bar{\nabla}_{mn}}{\chi^2} \sqrt{\frac{1}{(1 + R_s \bar{\eta}^2 \bar{\nabla}_{mn}) \left(1 + \frac{\bar{h}^2 \beta}{12 \kappa} \bar{\nabla}_{mn}\right) - \delta_g \bar{\eta}^2 (R_s - 1) \bar{\nabla}_{mn} + \Xi \frac{\bar{h}^2}{12} \bar{\nabla}_{mn}}} \quad (3.137)$$

The solution is much simpler than the one derived for the original Uflyand-Mindlin plate model.

The solution derived for the KL plate model is derived in the literature [256,260-263]

$$\Omega = \bar{\nabla}_{mn} \sqrt{\frac{1}{\chi^4 (1 + \bar{\eta}^2 \bar{\nabla}_{mn})}} \quad (3.138)$$

The solution of the zeroth order asymptotic models is given by:

$$\Omega = \bar{\nabla}_{mn} \sqrt{\frac{1}{\chi^4 (1 + \kappa_1 \bar{\eta}_*^2 \bar{\nabla}_{mn})}} \quad (3.139)$$

κ_1 is equal to 1, $\nu/(1 - \nu)$ and $1/4(1 - \nu)$ for the first, second and third asymptotic model with a nonlocality following the directions of the plate, with a partial nonlocality following the thickness of the plate and with a full nonlocality, respectively.

The five first non-dimensional natural frequencies are calculated in Table 14 for a square plate, simply supported at all edges, with a thickness ratio \bar{h} equal to 0.1 in order to not ignore the rotary inertia and the shear effects, evaluated by the fourth order phenomenological Kirchhoff-Love plate model and the three versions of the nonlocal Uflyand-Mindlin plate model (original, truncated and based on slope inertia), the truncated model coinciding with the first asymptotic model at the second order. The Poisson's ratio, as for beams, is taken equal to 0.3. The shear parameters κ is calculated from its value determined in the local second order asymptotic model. Three values of the nonlocal parameter are chosen: $\bar{\eta} = 0$ (local approach), $\bar{\eta} = 0.15$ and $\bar{\eta} = 0.3$.

	KL	OUM		TUM	SUM			
Local $\bar{\eta} = 0$	19.739	19.089		19.082	19.075			
	49.348	45.615		45.524	45.417			
	78.957	70.091		69.786	69.404			
	98.696	85.464		84.939	84.255			
	128.305	107.327		106.362	105.026			
		$R_s = 0$		$R_s = 1$	$R_s = 0$	$R_s = 1$	$R_s = 0$	$R_s = 1$
		$\delta_g = 0$	$\delta_g = 1$					
$\bar{\eta} = 0.15$	16.426	19.028	16.007	15.885	16.003	15.879	19.013	18.832
	33.369	44.840	32.356	31.400	32.322	31.337	44.655	42.551
	47.385	67.497	44.409	42.064	44.322	41.881	66.896	60.506
	54.996	80.991	51.073	47.622	50.943	47.330	79.983	69.701
	65.079	99.061	59.697	54.439	59.495	53.949	97.289	80.208
$\bar{\eta} = 0.3$	11.846	18.846	11.642	11.456	11.639	11.452	15.877	11.453
	21.155	42.706	20.502	19.555	20.492	19.516	31.336	19.539
	27.732	60.923	26.555	24.618	26.535	24.511	41.913	24.587
	31.395	70.315	29.835	27.186	29.808	27.019	47.408	27.146
	36.221	81.095	34.043	30.299	34.004	30.027	54.127	30.245

Table 14. Natural frequencies Ω obtained for different values of the nonlocal parameter for the KL plate model, the OUM, TUM and SUM models for $\bar{\eta} = 0, \bar{\eta} = 0.15, \bar{\eta} = 0.3$ and $(\bar{h}, \chi) = (0.1, 1)$

First of all, similar observations to the beam cases can be done. The nonlocal effect tends to increase the flexibility of the beam and then an increase of the nonlocal parameter results in a decrease of the natural frequency. The nonlocal effect is more important for high order of frequencies. For instance, for the truncated Uflyand-Mindlin plate, for $\bar{\eta}$ and R_s equal to 0.3 and 0, respectively, the fourth frequency is 2.8 times smaller than for the equivalent local fourth frequency. For the fundamental frequency, the nonlocal frequency is only 1.6 times smaller than the equivalent local one.

Moreover, as for beams, the different engineering thick plate model introduce a parameter R_s , equal to unity when the nonlocal effect affects both the shear and the bending parts of the constitutive laws. Although in the literature, only the case $R_s = 1$ is considered, the case R_s equal to zero cannot be ignored a priori. The extension of the Bernoulli-Euler beam model for plates is the Kirchhoff-Love plate model and as for beams, this model is supposed to provide an upper bound of the natural frequencies. Yet, when $R_s = 0$, for $\bar{\eta}$ equal to 0.3, the the three first frequencies are 18.846, 42.706 and 60.923 for the nonlocal Uflyand-Mindlin plate model based on slope inertia versus 11.846, 21.155 and 27.732 for the nonlocal Kirchhoff-Love plate model, leading to a contradiction. Moreover, for the original Uflyand-Mindlin plate model, the governing differential equation should not depend on the derivation. For $R_s = 0$, when the nonlocal effect is taken into account, it is seen that the natural frequencies obtained for δ_g equal to unity (derivation through the use of the equilibrium equations) are different from the frequencies found for δ_g equal to zero (derivation by using the variational principle). The natural frequencies should not depend on the process of derivation of the equations. Thus, this short comparison justifies the use of R_s equal to unity. Hereinafter, for plates, this parameter will be only taken equal to unity.

Furthermore, Ω^* is defined as the frequency ratio, the Kirchhoff-Love plate model being the reference model: $\Omega^* = \Omega/\Omega(\text{KL})$. Ω^* is depicted in Figs. 16 and 18 for a square plate and the three versions of the Uflyand-Mindlin plate model (original, truncated and based on slope inertia) for various nonlocal parameters $\bar{\eta}$ and a fixed thickness ratio \bar{h} equal to 0.1 (Fig. 16) and for different thickness ratios \bar{h} and a fixed nonlocal parameter $\bar{\eta}$ equal to 0.15 (Fig. 17). It is seen that the three versions of the Uflyand-Mindlin plate model coincides for small values of $\bar{\eta}$ and \bar{h} . A very small difference occurs for very high thickness ratios. The general trend of the curves show that

the fundamental frequency decreases when the thickness ratio or the nonlocal parameter increases.

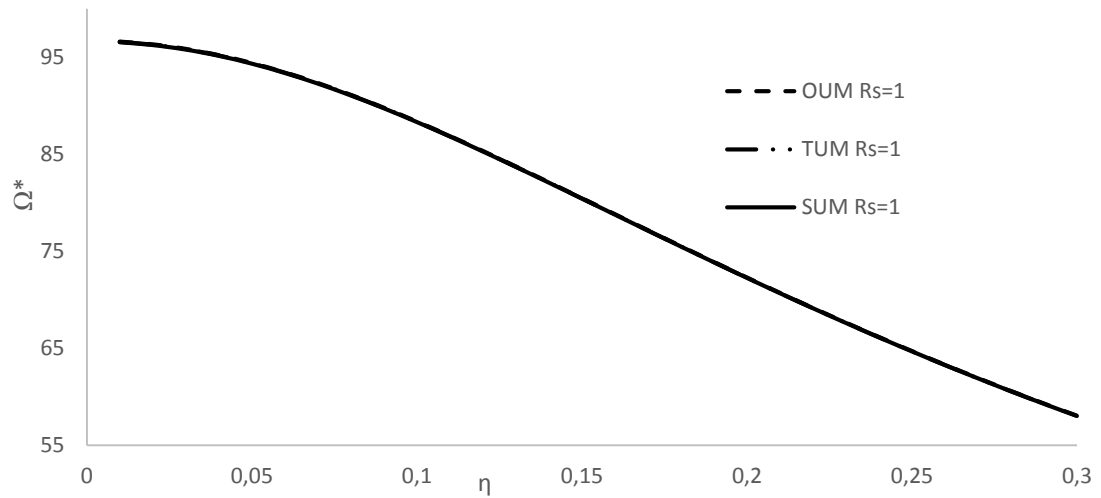


Fig. 16. Frequency ratio Ω^* considering the nonlocal Kirchhoff-Love plate (KL) plate model, the original Uflyand-Mindlin plate model (OUM) and the nonlocal truncated Uflyand-Mindlin plate model (TUM) for various values of the non-dimensional nonlocal parameter $\bar{\eta}$

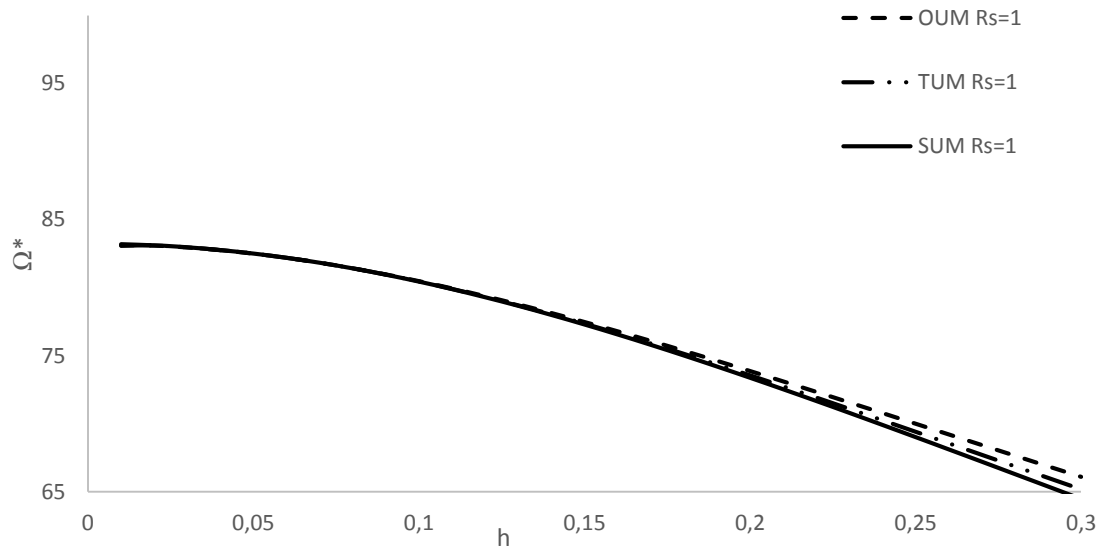


Fig. 17. Frequency ratio Ω^* considering the nonlocal Kirchhoff-Love plate (KL) plate model, the original Uflyand-Mindlin plate model (OUM) and the nonlocal truncated Uflyand-Mindlin plate model (TUM) for various values of thickness ratio \bar{h}

Moreover, in order to clearly show the influence of the vibration mode number on the natural frequency, Fig. 18 depicts the values of the ratio $\Omega/\Omega_{KL}(\bar{\eta} = 0)$ for the Kirchhoff-Love plate model and the original Uflyand-Mindlin plate model with R_s arbitrarily equal to unity versus $m^2 + n^2$, representative of the order of the frequency. Two values of the nonlocal parameters of the nonlocal parameter $\bar{\eta}$ are arbitrarily chosen: 0.15 and 0.25. For the original Uflyand-Mindlin plate model, the frequency depends on the thickness ratio. So, \bar{h} is taken equal to 0.1 and 0.2. One can see that for a fixed $\bar{\eta}$, whatever the thickness ratio, the Kirchhoff-love plate model provides an upper bound of the frequency. Interestingly, for a fixed value of \bar{h} , for instance equal to 0.1, the difference between the natural frequencies calculated for $\bar{\eta} = 0.15$ and $\bar{\eta} = 0.25$ does not significantly change with the order of the frequency. However, for a fixed value of the nonlocal parameter $\bar{\eta}$, for instance 0.15, the difference between the case $\bar{h} = 0.1$ and $\bar{h} = 0.2$ decreases with the order of the frequency.

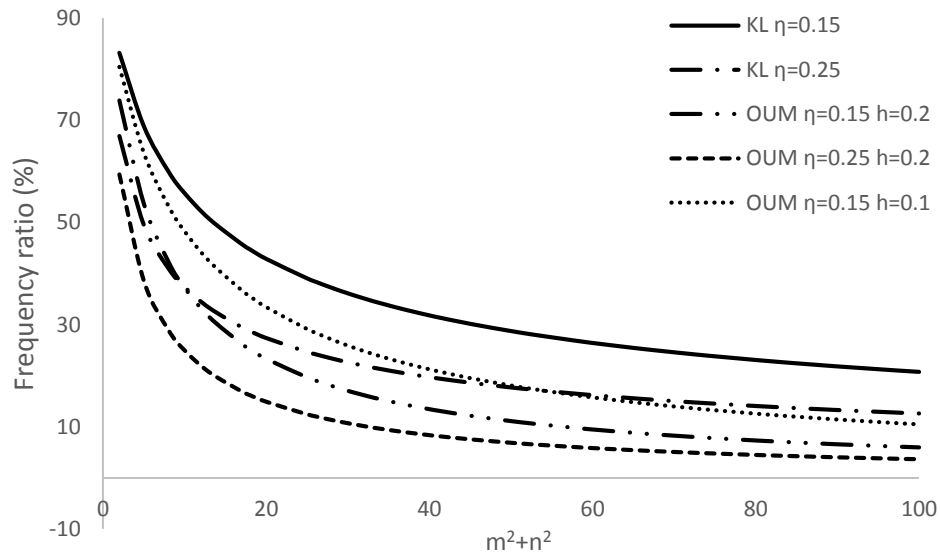


Fig. 18. Frequency ratio $\Omega/\Omega_{KL}(\bar{\eta} = 0)$ considering the nonlocal Kirchhoff-Love plate (KL) plate model and the original Uflyand-Mindlin plate model for $\bar{\eta}$ equal to 0.15 or 0.25 and \bar{h} equal to 0.1 or 0.2

In order to compare our results with those of the literature, the frequency ratio Ω^* is given in Fig. 19 for various length of the squared plate and the different nonlocal length η considering the nonlocal original Uflyand-Mindlin plate model with R_s equal to unity for a thickness equal to 0.34. The trends of the curves within the figure coincide with those in the literature. Whatever the length of the curve, the frequency strongly depends on the nonlocal length. For a small length of the plate, the rotary inertia and the shear effects are important. Consequently, the difference between the curves is important. When the length of the plate a increases, it decreases these effects and all the curves merge in one curve for very high values of the plate length. This curve is the one of the local model.

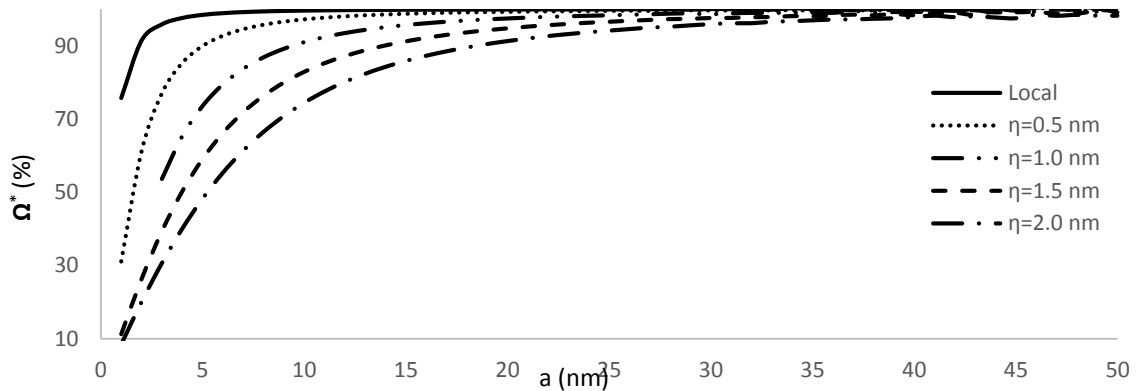


Fig. 19. Frequency ratio considering the original Uflyand-Mindlin squared plate model for various values of the length of the plate and the nonlocal parameter η

Now, consider the different asymptotic models. It has been established that the one with a partial nonlocality following the two directions of the plate coincides with the Kirchhoff-Love plate model and the truncated Uflyand-Mindlin plate model for R_s equal to unity at the zeroth and second order, respectively. At the lowest order, the three models differ in the expression of the macroscopic nonlocal length, as shown before. It results in a difference in the values of the natural frequencies, higher for first asymptotic model than for the two other ones. It is worth noticing in Table 14 that, for a specific quadruplet of parameters $(\bar{\eta}_*, \bar{h}, m, n)$ equal to $(0.15, 0.1, 3, 1)$, the second and third asymptotic models lead to complex values of the natural frequency. This issue does not occur for the first asymptotic model with a nonlocality following the directions of the plate, valid for any value of the chosen parameters. Thus, the second and third asymptotic models at the second order are less robust than the engineering nonlocal models.

Moreover, Figs. 20-22 depict the ratio Ω^* for various values of the nonlocal parameters for the three different asymptotical models at the zeroth and second order, respectively. At the second order, the natural frequency depends on the value of the thickness ratios and two cases are considered: a ratio equal to 0.1 (Fig. 21) and a ratio equal to 0.2 (Fig. 22) Because the coefficient κ_1 differs between the three asymptotic models, a difference occurs in the expression of the fundamental frequency and this difference increases with the nonlocal length.

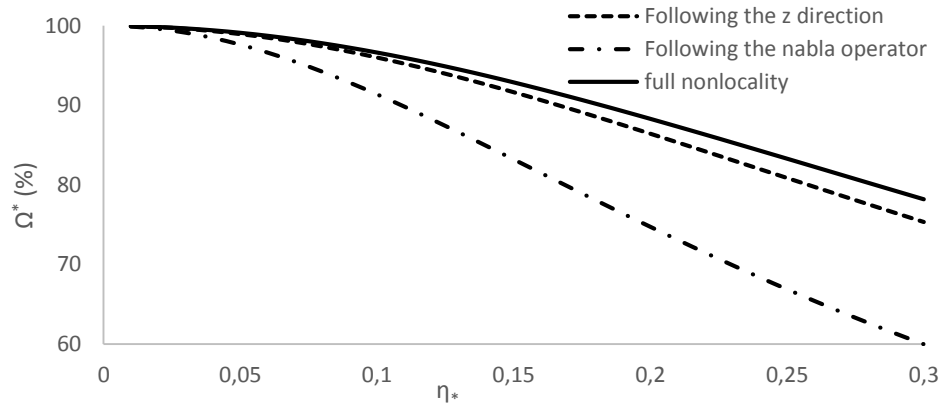


Fig. 20. Frequency ratio Ω^* considering the three asymptotic models at the zeroth order for $\bar{h} = 0.1$ and various values of the non-dimensional nonlocal parameter $\bar{\eta}_*$

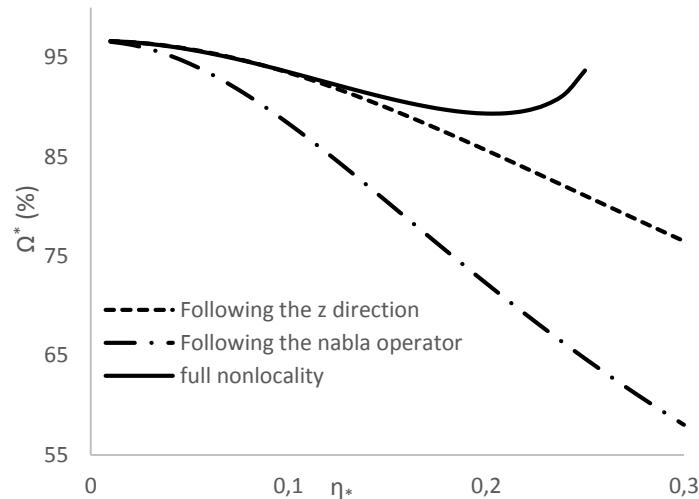


Fig. 21. Frequency ratio Ω^* considering the three asymptotic models at the second order for $\bar{h} = 0.1$ and various values of the non-dimensional nonlocal parameter $\bar{\eta}_*$

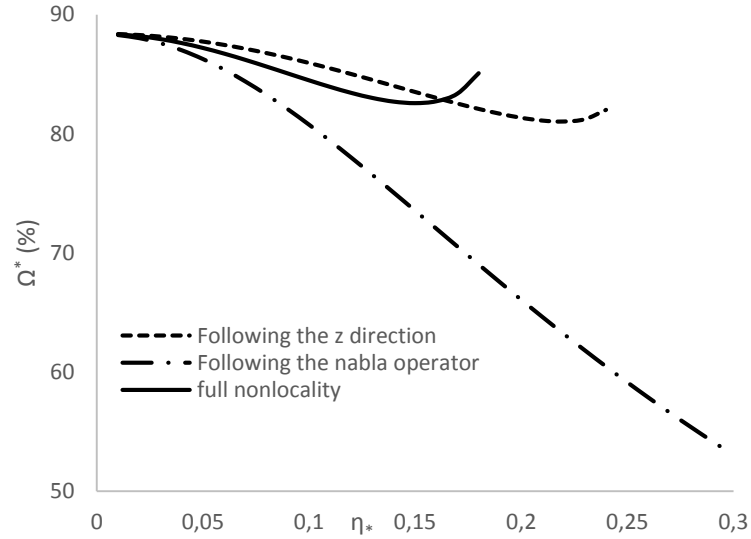


Fig. 22. Frequency ratio Ω^* considering the three asymptotic models at the second order for $\bar{h} = 0.2$ and various values of the non-dimensional nonlocal parameter $\bar{\eta}_*$

As for the Kirchhoff-Love model and the three versions of the Uflyand-Mindlin plate model, an increase of the non-dimensional nonlocal parameter results in a decrease of the natural frequency. Comparing Figs. 21 and 22, it is shown that the difference between the different models is more important for large thickness ratios (for instance equal to 0.2). Also, for large non-dimensional nonlocal parameters, Figs. 21 and 22 show that after a certain value of the nonlocal parameter, the natural frequencies calculated from the asymptotic model with a partial nonlocality following the thickness of the plate and the one with a full nonlocality increase and no value is plotted for big values of $\bar{\eta}_*$. Indeed, these models, as previously explained, do not always lead to real values of the frequencies. Thus, for a thickness ratio equal to 0.2, the asymptotic model with a full nonlocality cannot predict natural frequencies for a non dimensional nonlocal parameter $\bar{\eta}_*$ larger than 0.2 for the asymptotic model with a full nonlocality, larger than 0.25 for the asymptotic model with a partial nonlocality following the z direction. Moreover, in order to study the effect of the thickness ratio on the natural frequency, Fig. 23 depicts the frequency ratio Ω^* for a nonlocal parameter $\bar{\eta}_*$ equal to 0.15 and various values of \bar{h} calculated from the different asymptotic models at the second order. It is seen, similarly to Figs. 20-22 that an increase of the thickness ratio results in a decrease of the frequency ratio because of the rotary inertia and the shear effects that cannot be ignored. Hereinafter, it will be proposed a calibration of $\bar{\eta}_*$ with respect to lattice mechanics.

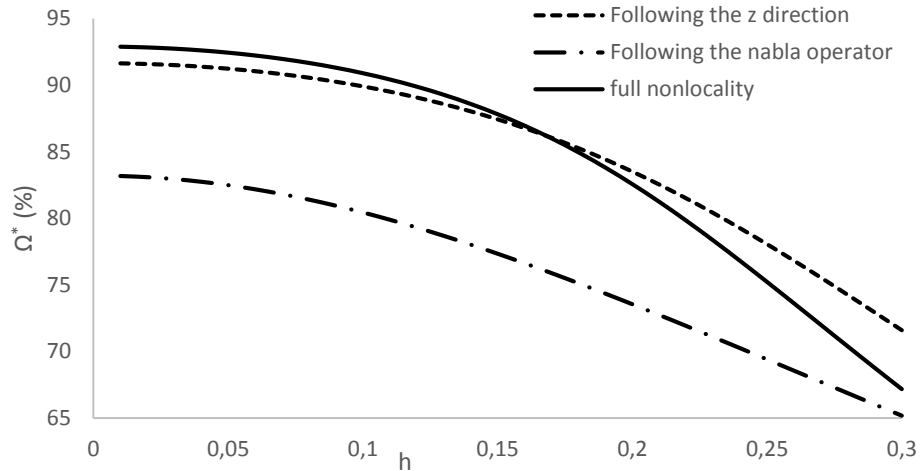


Fig. 23. Frequency ratio Ω^* considering the three asymptotic models at the second order for $\bar{\eta}_* = 0.15$ and various values of the thickness ratio \bar{h}

Thus, in this chapter, different nonlocal models have been derived. First of all, nonlocal beam and plate models have been derived from an asymptotic approach starting from three-dimensional stress gradient elasticity. Based on power series expansions in displacement, different asymptotic models have been considered, leading to different governing differential equations at the zeroth and second order. In addition to these models, the three versions of the Bresse-Timoshenko models and the Uflyand-Mindlin plate models, presented in a previous chapter have been extended to take into account the nonlocal effect. As expected from the previous chapter, the truncated versions of these models are asymptotically consistent following a partial nonlocality following the directions of the structure (beam or plate). There is a debate in the literature in order to know whether the nonlocal effect should affect or not the shear part of the constitutive law. This study shows that it should affect both the bending and the shear parts of the law.

In each of the models that have been derived in this chapter, a small length scale coefficient has been introduced. This coefficient is supposed constant and its value has to be determined. It is suggested to calibrate it from a physical reference model based on lattice mechanics.

4. MICROSTRUCTURED AND CONTINUALIZED MODELS, CALIBRATION OF THE SMALL LENGTH SCALE COEFFICIENT: THE RESOLUTION OF THE SMALL LENGTH SCALE COEFFICIENT PARADOX

In the previous chapter, different phenomenological models based on postulated constitutive laws have been proposed. These models introduce a small length scale coefficient. This coefficient is assumed constant. Its value may be calibrated by equating the buckling load in statics or the natural frequency in dynamics with those of the lattice model.

This chapter starts by presenting the discrete model for thin beams and plates. Then, the small length scale coefficient is calibrated, yielding to, as explained before, a paradoxical result. Thus, to solve this paradox, a new family of nonlocal structural models are proposed. These models are based on the continualization of the discrete models.

These results will be extended to the case of thick plates (for thick beams, the reader may refer to the paper of Duan et al. [127]).

4.1. Different nonlocal thin beam models

4.1.1. Microstructured model

The idea of the lattice, or microstructured, model is to represent the pattern by periodic cells in order to take into account the discrete nature of the matter at a finer scale. The atoms of the plates are represented by the points of the lattice and the interactions between the atoms, by frictionless joints. In this approach, the bending moments are lumped at places that rotations are localized [132]. This structural model may be called Hencky's model [131].

Thus, consider that the thin beam of the previous chapters, analytically described in the literature by the Bernoulli-Euler model, is an assembly of n beams of length a ($L = na$) and concentrated inertia mass m connected by elastic rotational springs of stiffness $C = EI/a$, (see Fig. 24). The beam is subjected to a compressive load N . We define m_0 such as $m_0 = m/a$. In the continuous representation, $m_0 = \rho A$. At the i th node, the deflection is w_i and the bending moment is M_i .

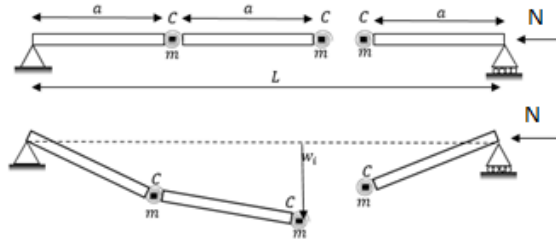


Fig. 24. Microstructured beam model

The discrete constitutive law and equilibrium equation are:

$$M_i = EI \left(\frac{v_{i+1} - 2v_i + v_{i-1}}{a^2} \right) \quad (4.1)$$

$$\frac{M_{i+1} - 2M_i + M_{i-1}}{a^2} = -N \frac{v_{i+1} - 2v_i + v_{i-1}}{a^2} + m_0 \omega^2 v_i \quad (4.2)$$

that are the Finite Difference formulation of the continuous equations

$$M = EI \frac{d^2 v}{dx^2} \quad (4.3)$$

$$N \frac{d^2 v}{dx^2} + \frac{d^2 M}{dx^2} - m_0 \omega^2 v = 0 \quad (4.4)$$

Combining Eqs. (4.3) and Eq. (4.4) leads to the discrete governing differential equation:

$$N \left(\frac{v_{i+1} - 2v_i + v_{i-1}}{a^2} \right) + EI \left(\frac{v_{i+2} - 4v_{i+1} + 6v_i - 4v_{i-1} + v_{i-2}}{a^4} \right) - m_0 \omega^2 v_i = 0 \quad (4.5)$$

The beam being simply supported at both ends, the solution of the governing fourth-order difference equation is assumed to be, analogously to the Navier's expression for continuous plates given in previous chapters

$$v_i = v_0 \sin \left(\frac{m\pi i}{n} \right) \quad (4.6)$$

We set the non-dimensional buckling:

$$\lambda = L^2 \frac{N}{\pi^2 EI} \quad (4.7)$$

For the next, the subscript (*micro*) denotes the lattice model.

The substitution of Eq. (4.6) into Eq. (4.5) furnishes the following exact buckling load [129,147,264-266]:

$$\lambda_{(micro)} = \min_m \left[\frac{2n}{\pi} \sin \left(\frac{m\pi}{2n} \right) \right]^2 \quad (4.8)$$

In free vibration, $N = 0$ and the non-dimensional natural frequency is, substituting Eq. (4.6) into Eq. (4.5), [71,267]:

$$\Omega_{(micro)}^2 = \left[\frac{2n}{\pi} \sin \left(\frac{m\pi}{2n} \right) \right]^4 \quad (4.9)$$

Thus, the discrete buckling load and natural frequency are determined. By the next, they will be used as references to calibrate the small length scale coefficient e_0 , introduced in the phenomenological models.

4.1.2. Phenomenological models: the small length scale paradox

4.1.2.1. Fourth order Eringen phenomenological model

The governing differential equation for thin beams of the fourth order phenomenological model, also called nonlocal Bernoulli-Euler model, as given in the previous chapter by including a compressive force is [135]

$$EI \frac{d^4 v}{dx^4} + N \left[1 - (e_0 a)^2 \frac{d^2}{dx^2} \right] \frac{d^2 v}{dx^2} - m_0 \omega^2 \left[1 - (e_0 a)^2 \frac{d^2}{dx^2} \right] v = 0 \quad (4.10)$$

In free vibration, this equation has been derived through the use of constitutive laws and the equilibrium equation. The objective of this section is to calibrate the coefficient e_0 by equating the solutions of the phenomenological model and the one of the microstructured mode, previously determined.

For a beam simply supported at both end, the solution is given through the Navier expression of the displacement. Substituting Eq. (2.48) into Eq. (4.10), it yields:

$$m^4 - (\lambda m^2 + \Omega^2) \left[1 + \left(\frac{e_0 a m \pi}{L} \right)^2 \right] = 0 \quad (4.11)$$

In statics ($\Omega = 0$), the nondimensional critical buckling load parameter is:

$$\lambda = \min_m m^2 \frac{1}{1 + \left(\frac{e_0 a m \pi}{L}\right)^2} = \frac{1}{1 + \left(\frac{e_0 a \pi}{L}\right)^2} \quad (4.12)$$

The small length scale coefficient is obtained by equating Eq. (4.8) and Eq. (4.12):

$$\frac{1}{1 + \left(\frac{e_0 a \pi}{L}\right)^2} = \left[\frac{2n}{\pi} \sin\left(\frac{\pi}{2n}\right)\right]^2 \quad (4.13)$$

By expanding asymptotically the two sides of the equations, it leads to a calibration of the length scale coefficient as follows

$$e_{0,b} = 1/2\sqrt{3} \approx 0.288 \quad (4.14)$$

where the subscript b denotes a parameter, herein the small length scale calibrated, investigated in statics. Analogously, the subscript v will be used in free vibration.

In free vibration, the nondimensional frequency parameter is

$$\Omega^2 = m^2 \frac{1}{1 + \left(\frac{e_0 a m \pi}{L}\right)^2} \quad (4.15)$$

As for the static case, in free vibration, the small length scale coefficient is calibrated by equating the continuous natural frequency given by Eq. (4.15) and the one of the discrete model (see Eq. (4.9))

$$m^2 \frac{1}{1 + \left(\frac{e_0 a m \pi}{L}\right)^2} = \left[\frac{2n}{\pi} \sin\left(\frac{\pi}{2n}\right)\right]^4 \quad (4.16)$$

By expanding asymptotically for both sides of Eq. (4.16) for $m = 1$, it leads to the calibrated small length scale coefficient:

$$e_{0,v} = 1/\sqrt{6} \approx 0.408 \quad (4.17)$$

It is worth noticing that $e_{0,v}$ is different from $e_{0,b}$. Thus, the small length scale coefficient is structural dependent.

4.1.2.2. Sixth order phenomenological model

A sixth order phenomenological model has been presented in the previous chapter in free vibration. In the literature [135], the extension of this model to include a compressive force leads to the following governing differential equation:

$$EI \left[1 + (e_0 a)^2 \frac{d^2}{dx^2} \right] \frac{d^4 v}{dx^4} + N \left[1 - (e_0 a)^2 \frac{d^2}{dx^2} \right] \frac{d^2 v}{dx^2} - m_0 \omega^2 \left[1 - (e_0 a)^2 \frac{d^2}{dx^2} \right] v = 0 \quad (4.18)$$

For a simply supported beam, using the non-dimensional parameters, the equations becomes:

$$\left[1 - \left(\frac{e_0 a m \pi}{L} \right)^2 \right] m^4 - \lambda \left[1 + \left(\frac{e_0 a m \pi}{L} \right)^2 \right] m^2 - \bar{\Omega}^2 \left[1 + \left(\frac{e_0 a m \pi}{L} \right)^2 \right] = 0 \quad (4.19)$$

In statics ($\omega = 0$), the nondimensional buckling load is given by:

$$\lambda = \min_m m^2 \left[1 - \left(\frac{e_0 a m \pi}{L} \right)^2 \right] / \left[1 + \left(\frac{e_0 a m \pi}{L} \right)^2 \right] \quad (4.20)$$

Moreover, e_0 is calibrated by equating Eq. (4.8) and Eq. (4.20):

$$m^2 \left[1 - \left(\frac{e_0 a m \pi}{L} \right)^2 \right] / \left[1 + \left(\frac{e_0 a m \pi}{L} \right)^2 \right] = \left[\frac{2n}{\pi} \sin \left(\frac{m\pi}{2n} \right) \right]^2 \quad (4.21)$$

It yields the calibrated small length scale coefficient of

$$e_{0,b} = 1/2\sqrt{6} \approx 0.204 \quad (4.22)$$

In the free vibration case ($P = 0$), the nondimensional frequency parameter is:

$$\Omega^2 = m^2 \left[1 - \left(\frac{e_{0,v} m \pi}{n} \right)^2 \right] / \left[1 + \left(\frac{e_{0,v} m \pi}{n} \right)^2 \right] \quad (4.23)$$

By equating Eqs. (4.9) and (4.23), the following calibrated small length scale coefficient is obtained:

$$e_{0,v} = 1/2\sqrt{3} \approx 0.288 \quad (4.24)$$

The small length scale coefficient differs in statics and in buckling. As for the fourth order phenomenological model, the nonlocal sixth order phenomenological model cannot be calibrated with a constant length scale parameter.

Thus, the phenomenological models as presented in the literature and in this thesis are not consistent because they are based on the use of a theoretical constant coefficient which cannot be calibrated with a fixed value. Thus, there is a need to develop new nonlocal models to better describe the mechanical behavior of nanomaterials. The nonlocal continualized models are recent and lead to extremely promising results.

4.1.3. Resolution of the paradox: the continualized model

4.1.3.1. Fourth order continualized model

The nonlocal continualized models are built from the reference lattice model. The continualization process is explained below. The discrete displacement of the i th node v_i for the discrete model is equal to the displacement of the equivalent continuous system v : $v_i = v(x_i) = v(x)$. Following a similar reasoning, the previous and next particles v_{i-1} and v_{i+1} are replaced by $v(x_i - a)$ and $v(x_i + a)$, respectively. By applying Taylor series to the difference operators that describe discrete particle interactions, it yields to:

$$v_{i\pm 1} = v(x_i \pm a) = \sum_{k=0}^{\infty} (\pm 1)^k \frac{a^k}{k!} \frac{d^k}{dx^k} v(x) = \left[e^{\pm a \frac{d}{dx}} \right] [v] \quad (4.25)$$

Thus, at the second order of the Taylor expansion, the second derivative of the discrete model is equivalent to a continuous higher-order differential operator:

$$\frac{v_{i+1} - 2v_i + v_{i-1}}{a^2} = \frac{d^2}{dx^2} \left[1 + \frac{a^2}{12} \frac{d^2}{dx^2} \right] v(x) + o(a^2) \quad (4.26)$$

The second term represents the effect due to discreteness, with a being the trace of the microscopic system. Using the Padé approximation, the discrete laplacian can be expanded as:

$$\frac{v_{i+1} - 2v_i + v_{i-1}}{a^2} = \frac{\frac{d^2}{dx^2}}{1 - \frac{a^2}{12} \frac{d^2}{dx^2}} v + o(a^2) \quad (4.27)$$

Similarly, at the fourth order,

$$\frac{v_{i+2} - 4v_{i+1} + 6v_i - 4v_{i-1} + v_{i-2}}{a^2} = \frac{d^4}{dx^4} \left(1 + \frac{a^2}{6} \frac{d^2}{dx^2} \right) v + o(a^2) \quad (4.28)$$

Or

$$\frac{v_{i+2} - 4v_{i+1} + 6v_i - 4v_{i-1} + v_{i-2}}{a^2} = \frac{\frac{d^4}{dx^4}}{\left(1 - \frac{a^2}{12} \frac{d^2}{dx^2} \right)^2} v + o(a^2) \quad (4.29)$$

Eqs. (4.28) and (4.29) show that at least two continualization processes are possible, through the use of the Padé approximants or just the Taylor expansion up to the second order term. Indeed, substituting Eq. (4.27) into the discrete moment curvature relation Eq. (4.1) may

$$M = EI \frac{\frac{d^2}{dx^2}}{1 - \frac{a^2}{12} \frac{d^2}{dx^2}} v + o(a^2) \quad (4.30)$$

Analogically, substituting Eq. (4.27) into the discrete equilibrium equation Eq. (4.2):

$$\frac{\frac{d^2}{dx^2}}{1 - \frac{a^2}{12} \frac{d^2}{dx^2}} (M + Nv) - m_0 \omega^2 v + o(a^2) = 0 \quad (4.31)$$

Multiplying Eqs. (4.30) and (4.31) by $[1 - (a^2/12)(d^2/dx^2)]$, it yields the continualized constitutive law and equilibrium equation:

$$M - \frac{a^2}{12} \frac{d^2 M}{dx^2} = EI \frac{d^2 v}{dx^2} + o(a^2) \quad (4.32)$$

$$\frac{d^2 M}{dx^2} = -N \frac{d^2 v}{dx^2} + m_0 \omega^2 \left(v - \frac{a^2}{12} \frac{d^2 v}{dx^2} \right) + o(a^2) \quad (4.33)$$

The nonlocal effect occurs in these equations through the length a . Thus, in contrast to the phenomenological models, the continualized models do not preserve the locality of the equilibrium equation.

Substituting Eq. (4.32) into Eq. (4.33), it provides a moment-displacement relationship:

$$M = EI \frac{d^2 v}{dx^2} - \frac{Na^2}{12} \frac{d^2 v}{dx^2} + m_0 \omega^2 \frac{a^2}{12} \left(v - \frac{a^2}{12} \frac{d^2 v}{dx^2} \right) + o(a^4) \quad (4.34)$$

e_0 is, constant and arbitrarily taken equal to $1/\sqrt{12}$. The substitution of Eq. (4.34) into Eq. (4.33), by neglecting the higher order term in a , it results in the following governing differential equation:

$$EI \frac{d^4 v}{dx^4} + P \left[1 - \frac{a^2}{12} \frac{d^2}{dx^2} \right] \frac{d^2 v}{dx^2} - m_0 \omega^2 \left[1 - \frac{a^2}{6} \frac{d^2}{dx^2} \right] v = 0 \quad (4.35)$$

Furthermore, this equation can be equivalently obtained directly by continualization of the discrete governing differential equation Eq. (4.5). As shown in the literature [135] the two processes would lead to the same governing differential equation.

Thus, substituting Eqs. (4.27) and (4.29) into Eq. (4.5) leads to

$$EI \frac{\frac{d^4}{dx^4}}{\left(1 - \frac{a^2}{12} \frac{d^2}{dx^2}\right)^2} v + N \frac{\frac{d^2}{dx^2}}{1 - \frac{a^2}{12} \frac{d^2}{dx^2}} v - m_0 \omega^2 v + o(a^2) = 0 \quad (4.36)$$

Multiplying Eq. (4.36) by $[1 - (a^2/12)(d^2/dx^2)]^2$, the governing differential equation of the fourth order continualized model is obtained, retaining only the second order terms in a [135]:

The boundary conditions of this continualized model are obtained from the variational approach [135]:

$$\left[\left\{ \left[EI - P \frac{a^2}{12} \right] \frac{d^3 v}{dx^3} + \left[N + m_0 \omega^2 \frac{a^2}{6} \right] \frac{dv}{dx} \right\} \delta v \right]_0^L = 0 \quad (4.37)$$

$$\left[\left\{ \left[EI - N \frac{a^2}{12} \right] \frac{d^2 v}{dx^2} \right\} \delta \left(\frac{dv}{dx} \right) \right]_0^L = 0 \quad (4.38)$$

The solution is provided for a simply supported beam. By substituting Eq. (2.48) into Eq. (4.35), we obtain

$$m^4 - \lambda \left[1 + \left(\frac{e_0 a m \pi}{L} \right)^2 \right] m^2 - \bar{\Omega}^2 \left[1 + 2 \left(\frac{e_0 a m \pi}{L} \right)^2 \right] = 0 \quad (4.39)$$

In statics ($\omega = 0$), the nondimensional buckling load parameter is:

$$\lambda = \min_m m^2 \frac{1}{1 + \left(\frac{e_0 a m \pi}{L} \right)^2} = \frac{1}{1 + \left(\frac{e_0 a \pi}{L} \right)^2} \quad (4.40)$$

In free vibration ($P = 0$), the nondimensional frequency parameter is:

$$\Omega^2 = m^2 \frac{1}{1 + 2 \left(\frac{e_0 a m \pi}{L} \right)^2} \quad (4.41)$$

4.1.3.2. Sixth order continualized model

It is suggested to use Eq. (4.26) instead of Eq. (4.27) in the continualization of the local constitutive law and the equilibrium equation, leading to

$$M = EI \left[\frac{d^2 v}{dx^2} + \frac{a^2}{12} \frac{d^4 v}{dx^4} + o(a^2) \right] \quad (4.42)$$

The nonlocal constitutive law Eq. (4.42) is different from Eq. (4.30). Thus, it will lead to a new continualized model. The nonlocal equilibrium equation Eq. (4.31) is retained. The substitution of Eq. (4.42) into Eq. (4.31) and multiplying by $[1 - (a^2/12)(d^2/dx^2)]$ yields, choosing $e_0 = 1/\sqrt{12}$ and by neglecting the term of higher order in a :

$$EI \left[1 + (e_0 a)^2 \frac{d^2}{dx^2} \right] \frac{d^4 v}{dx^4} + N \frac{d^2 v}{dx^2} - m_0 \omega^2 \left[1 - (e_0 a)^2 \frac{d^2}{dx^2} \right] v = 0 \quad (4.43)$$

It is worth noticing that Eq. (4.48) may be asymptotically obtained from Eq. (4.35), by multiplying it by $[1 + (a^2/12)(d^2/dx^2)]$ and neglecting the terms in a^4 .

Comparing the continualized nonlocal model with the sixth order phenomenological model, the term associated with the dynamic effect is different from the one associated with the static effect. Thus, in dynamics, in presence of a compressive load, the continualized and phenomenological models do not match.

This governing equation contains a sixth-order space derivative term, in contrast to the fourth order one that contains only second and fourth order space derivative terms. The only difference between these two models is the scheme of continualization used in the bending constitutive law. Thus, the order of the governing differential equation can be increased by using a different continualization process.

Because of the presence of a sixth order space derivative term in the governing differential equation, it requires two additional boundary conditions. These conditions are obtained from the derivation of the governing differential equation through the variational principle. Thus, the natural boundary conditions are [135]:

$$\begin{aligned} \left[\left\{ EI \left[\frac{a^2}{12} \frac{d^5 v}{dx^5} + \frac{d^3 v}{dx^3} \right] + \left[N + m_0 \omega^2 \frac{a^2}{12} \right] \frac{dv}{dx} \right\} \delta v \right]_0^L &= 0 \\ \left[EI \left\{ \frac{a^2}{12} \frac{d^4 v}{dx^4} + \frac{d^2 v}{dx^2} \right\} \delta \left(\frac{dv}{dx} \right) \right]_0^L &= 0 \\ \left[EI \frac{a^2}{12} \frac{d^3 v}{dx^3} \delta \left(\frac{d^2 v}{dx^2} \right) \right]_0^L &= 0 \end{aligned} \quad (4.44)$$

For a simply supported beam, by substituting Eq. (2.48) into Eq. (4.43),

$$\left[1 - \left(\frac{e_0 a m \pi}{L} \right)^2 \right] m^4 - \lambda m^2 - \Omega^2 \left[1 + \left(\frac{e_0 a m \pi}{L} \right)^2 \right] = 0 \quad (4.45)$$

In statics ($\omega = 0$), the nondimensional buckling load parameter is:

$$\lambda = \min_m \left[m^2 - \left(\frac{e_0 a m^2 \pi}{L} \right)^2 \right] = 1 - \left(\frac{e_0 a \pi}{L} \right)^2 \quad (4.46)$$

In free vibration ($P = 0$), the nondimensional frequency parameter is:

$$\Omega^2 = m^2 \left[1 - \left(\frac{e_0 a m \pi}{L} \right)^2 \right] / \left[1 + \left(\frac{e_0 a m \pi}{L} \right)^2 \right] \quad (4.47)$$

The expressions of the natural frequencies and buckling loads are not the same between the two continualized approaches. This difference is due to the continualization process, based on the use of Padé approximants for the fourth order phenomenological model and the Taylor approximants for the sixth order one.

4.2. Different nonlocal thin plate models

The previous derivation is now extended to plates.

4.2.1. Microstructured model

Following the idea presented in the previous section, a rectangular plate under compressive load is represented as an assembly of chain net systems of rigid straight elements connected at frictionless joints where rotations are localized as shown in Fig. 25. This model is an extension of the Hencky's approach valid for beams and plates. The lattice plate model has been developed by Wifi vet al. [136] and El Naschie [132].

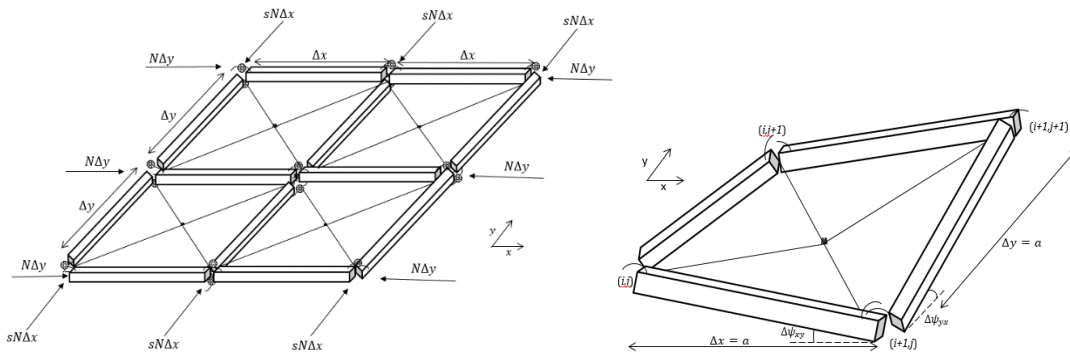


Fig. 25. Microstructured beam-grid model (a), torsional deformation of a unit cell (b)

w_{i-j} and w_{i+j} denote the transverse displacements of the right end of the i^{th} beam element and the left end of the $(i+1)^{\text{th}}$ beam element, respectively, and $w_{ij} = w_{i-j}$. Thus, $w_{i,j}$ is the transverse displacement of node (i, j) . In addition to the transverse displacement, two rotations $\psi_x^{i+1/2,j}$ and $\psi_y^{i+1/2,j}$ are defined in the middle of the elements and denote the rotations of the element between node (i, j) and node $(i + 1, j)$.

Δx and Δy are the lengths of beam elements in the x - and y -directions. For thin plates, the rotations are related to the displacements by:

$$\psi_{i+\frac{1}{2},j} = \frac{w_{i^+j} - w_{(i+1)^-j}}{\Delta x}; \psi_{i,j+\frac{1}{2}} = \frac{w_{ij^+} - w_{i(j+1)^-}}{\Delta y} \quad (4.48)$$

s is a parameter such as when $s = 0$, the load is uniaxial [148] and when $s = 1$, the load is the same along the two directions [133]. As for the beam case, the bending of the plate is made possible by rotational springs at individual nodes. In vibration, the masses are at the nodes of the lattice structure. The torsion deformation is modeled by a rectangular repetitive unit cell composed of four rigid beam elements with springs in the central domain [132].

In the discrete model, the centered difference forms of the moment-rotation relationships is formulated as:

$$M_x^{i,j} = D (\Delta_x[\psi_x^{i,j}] + \nu \Delta_y[\psi_y^{i,j}]); M_y^{i,j} = D (\Delta_y[\psi_y^{i,j}] + \nu \Delta_x[\psi_x^{i,j}]) \quad (4.49)$$

$$M_{xy}^{i,j} = M_{yx}^{i,j} = \frac{D(1-\nu)}{2} (\Delta_x[\psi_y^{i,j}] + \Delta_y[\psi_x^{i,j}]) \quad (4.50)$$

The centered difference operators are defined as follows:

$$\Delta_x[w_{i,j}] = \frac{w_{i+1/2,j} - w_{i-1/2,j}}{\Delta x}; \Delta_y[w_{i,j}] = \frac{w_{i,j+1/2} - w_{i,j-1/2}}{\Delta y}; \quad (4.51)$$

and $\Delta_{\alpha\beta}[w_{i,j}] = \Delta_\alpha(\Delta_\beta[w_{i,j}])$

The strain energy function caused by bending of the rotational springs is given by:

$$\begin{aligned} U_b &= \frac{1}{2} \sum_{i=1}^{n_x-1} \sum_{j=1}^{n_y-1} [M_x^{i,j} (\Delta_x[\psi_x^{i,j}] \Delta x) \Delta y + M_y^{i,j} (\Delta_y[\psi_y^{i,j}] \Delta y) \Delta x] \Delta x \Delta y \\ &= \frac{D}{2} \sum_{i=1}^{n_x-1} \sum_{j=1}^{n_y-1} \left[(\Delta_x[\psi_x^{i,j}])^2 + (\Delta_y[\psi_y^{i,j}])^2 \right. \\ &\quad \left. + 2\nu \Delta_y[\psi_x^{i,j}] \Delta_x[\psi_y^{i,j}] \right] \Delta x \Delta y \end{aligned} \quad (4.52)$$

where n_x and n_y are the numbers of discrete rigid elements in the x - and y -directions, respectively. They are also seen as the number of atoms in the length of the plate.

Substituting Eq. (4.51), it leads to

$$\begin{aligned}
U_b = \frac{D}{2} \sum_{i=1}^{n_x-1} \sum_{j=1}^{n_y-1} & \left[\left(\frac{w_{i+1,j} - 2w_{i,j} + w_{i-1,j}}{\Delta x} \right)^2 \frac{\Delta y}{\Delta x} \right. \\
& + \left(\frac{w_{i,j+1} - 2w_{i,j} + w_{i,j-1}}{\Delta y} \right)^2 \frac{\Delta x}{\Delta y} \\
& \left. + 2\nu \frac{(w_{i+1,j} - 2w_{i,j} + w_{i-1,j})(w_{i,j+1} - 2w_{i,j} + w_{i,j-1})}{\Delta x \Delta y} \right]
\end{aligned} \tag{4.53}$$

In addition to the bending strain energy, a torsional energy is present due to the torsion of four connected rigidity bars in an enclosed rectangular unit cell of the lattice model. Thus, the total torsional energy is given by [132]

$$\begin{aligned}
U_t = \frac{1}{2} \sum_{i=1}^{n_x-1} \sum_{j=1}^{n_y-1} & [(M_{xy}^{i,j} \Delta \psi_{xy}^{i,j}) \Delta x + (M_{yx}^{i,j} \Delta \psi_{yx}^{i,j}) \Delta y] \\
= \frac{D}{4} (1 - \nu) \sum_{i=1}^{n_x-1} \sum_{j=1}^{n_y-1} & [(\Delta_x [\psi_y^{i,j}])^2 + (\Delta_y [\psi_x^{i,j}])^2] \Delta x \Delta y
\end{aligned} \tag{4.54}$$

where the torsional angles are

$$\Delta \psi_{xy}^{i,j} = (\Delta_x [\psi_y^{i,j}] + \Delta_y [\psi_x^{i,j}]) \Delta y; \Delta \psi_{yx}^{i,j} = (\Delta_x [\psi_y^{i,j}] + \Delta_y [\psi_x^{i,j}]) \Delta x \tag{4.55}$$

Substituting Eq. (4.51) into Eq. (4.54), it yields to the torsional energy for thin plates:

$$\begin{aligned}
U_t = \frac{D}{4} (1 - \nu) \sum_{i=1}^{n_x-1} \sum_{j=1}^{n_y-1} & \left[\left(\frac{w_{i,j+1} - w_{i+1,j+1} - w_{i,j} + w_{i+1,j}}{\Delta x} \right)^2 \right. \\
& \left. + \left(\frac{w_{i,j+1} - w_{i,j} - w_{i+1,j+1} + w_{i+1,j}}{\Delta y} \right)^2 \right]
\end{aligned} \tag{4.56}$$

For a discrete thin plate, the kinetic energy is express as

$$T = \frac{1}{2} m_0 \Delta x^2 \omega^2 \sum_{i=0}^{n_x} \sum_{j=0}^{n_y} w_{i,j}^2 \tag{4.57}$$

where m_0 is the mass per unit cell area. In the continuous model, $m_0 = \rho h$.

Under the action of compressive load, the work is given by:

$$W = \frac{1}{2} N \Delta x \Delta y \left[\sum_{i \in \mathbb{O}} \sum_{j \in \mathbb{O}} (\Delta_x [w_{i,j}])^2 + \sum_{i \in \mathbb{O}} \sum_{j \in \mathbb{O}} s (\Delta_y [w_{i,j}])^2 \right] \tag{4.58}$$

where \mathbb{O} denotes the group of halves of odd numbers $\mathbb{O} = \{(2k + 1)/2 \mid k \in \mathbb{N}\}$

For an isotropic material, $\Delta x = \Delta y = a = \chi L/n_y = L/n_x$.

The governing differential equation is obtained by minimizing the total energy:

$$\frac{\partial \delta(U_t + U_b - W - T)}{\partial w_{i,j}} = 0 \quad (4.59)$$

whence the discrete governing difference equation in displacement of the microstructured model:

$$n_y^4 L[w_{i,j}] + n_y^2 \lambda_{(micro)} (H_x + sH_y)[w_{i,j}] - \Omega_{(micro)}^2 w_{i,j} = 0 \quad (4.60)$$

where the discrete operators L , H_x and H_y are

$$L[w_{i,j}] = 20w_{i,j} + (w_{i,j-2} + w_{i,j+2} + w_{i-2,j} + w_{i+2,j}) - 8(w_{i,j-1} + w_{i,j+1} + w_{i-1,j} + w_{i+1,j}) + 2(w_{i+1,j-1} + w_{i+1,j+1} + w_{i-1,j-1} + w_{i-1,j+1}) \quad (4.61)$$

$$H_y[w_{i,j}] = w_{i,j-1} - 2w_{i,j} + w_{i,j+1}; H_x[w_{i,j}] = w_{i-1,j} - 2w_{i,j} + w_{i+1,j} \quad (4.62)$$

$$\Omega_{(micro)}^2 = \frac{m_0 \omega^2 (\chi L)^4}{D}; \lambda_{(micro)} = \frac{N(\chi L)^2}{D}$$

where $\Omega_{(micro)}$ is the dimensionless vibration frequency of the microstructured beam-grid model and λ the nondimensional buckling stress.

The discrete equation Eq. (4.60) can be seen as the finite difference formulation of the continuous Kirchhoff-Love plate equation [134].

Equation (4.60) is also obtainable by considering the finite difference formulation of both the constitutive law and the equilibrium equations. The finite difference scheme applied to the constitutive law is expressed as:

$$M_x^{i,j} = D \left(\frac{w_{i+1,j} - 2w_{i,j} + w_{i-1,j}}{\Delta x^2} + \nu \frac{w_{i,j+1} - 2w_{i,j} + w_{i,j-1}}{\Delta y^2} \right) \quad (4.63)$$

$$M_y^{i,j} = D \left(\frac{w_{i,j+1} - 2w_{i,j} + w_{i,j-1}}{\Delta y^2} + \nu \frac{w_{i+1,j} - 2w_{i,j} + w_{i-1,j}}{\Delta x^2} \right) \quad (4.64)$$

$$M_{xy}^{i,j} = M_{yx}^{i,j} = D(1 - \nu) \frac{-w_{i,j+1} + w_{i+1,j+1} + w_{i,j} - w_{i+1,j}}{\Delta x \Delta y} \quad (4.65)$$

For the equilibrium equation, it is expressed as:

$$\frac{M_{xx}^{i+1,j} - 2M_{xx}^{i,j} + M_{xx}^{i-1,j}}{\Delta x^2} + 2 \frac{M_{xy}^{i,j} - M_{xy}^{i-1,j} - M_{xy}^{i,j-1} + M_{xy}^{i-1,j-1}}{\Delta x \Delta y} + \frac{M_{yy}^{i,j+1} - 2M_{yy}^{i,j} + M_{yy}^{i,j-1}}{\Delta y^2} + N \left(\frac{w_{i+1,j} - 2w_{i,j} + w_{i-1,j}}{\Delta x^2} + s \frac{w_{i,j+1} - 2w_{i,j} + w_{i,j-1}}{\Delta y^2} \right) - m_0 \omega^2 w_{i,j} = 0 \quad (4.66)$$

Substituting Eqs. (4.63)-(4.65) into Eq. (4.66), it leads to Eq. (4.60).

For a discrete plate that is simply supported at all edges, analogically to the continuous approach, the Navier expression of the displacement is expressed as:

$$w_{i,j} = w_0 \sin \frac{m\pi i}{n_x} \sin \frac{n\pi j}{n_y} = w_0 \sin \frac{\alpha m\pi i}{n_y} \sin \frac{n\pi j}{n_y} \quad (4.67)$$

By substituting Eq. (4.67) into Eq. (4.60), one obtains the following equation:

$$\begin{aligned} \Omega_{(micro)}^2 - 4n_y^4 \left(2 - \cos \frac{m\pi}{n_x} + \cos \frac{n\pi}{n_y} \right)^2 \\ + 2\lambda_{(micro)} n_y^2 \left(1 + s - \cos \frac{m\pi}{n_x} - s \cos \frac{n\pi}{n_y} \right) = 0 \end{aligned} \quad (4.68)$$

In statics, $\Omega_{(micro)} = 0$ and the critical buckling load equals

$$\lambda_{(micro)} = \min_{(m,n)} \left(- \frac{2n_y^2 \left(\cos \frac{m\pi}{n_x} + \cos \frac{n\pi}{n_y} - 2 \right)^2}{\cos \frac{m\pi}{n_x} + s \cos \frac{n\pi}{n_y} - 1 - s} \right) \quad (4.69)$$

Zhang et al. [148] derived this equation for a uniaxial load ($s = 0$)

In free vibration, $N = 0$ and the non-dimensional natural frequency is

$$\Omega_{(micro)}^2 = 4n_y^4 \left(2 - \cos \frac{m\pi}{n_x} + \cos \frac{n\pi}{n_y} \right)^2 \quad (4.70)$$

This lattice model is used to calibrate the small length scale coefficient of the continuous models and to build continualized models in order to have a constant coefficient.

4.2.2. Phenomenological thin plate model

4.2.2.1. Fourth order phenomenological model

The governing differential equation of the fourth order phenomenological plate model, also called nonlocal Kirchhoff-Love plate model, has been given in a previous chapter in free vibration. It is now extended to take into account the compressive forces:

$$D\nabla^4 w - [1 - (e_0 a)^2 \nabla^2] m_0 \omega^2 w + [1 - (e_0 a)^2 \nabla^2] N \left(\frac{\partial^2 w}{\partial x^2} + s \frac{\partial^2 w}{\partial y^2} \right) = 0 \quad (4.71)$$

In a similar manner to the investigation of nonlocal beam models, the small length scale coefficient has to be calibrated. First of all, the solution is determined for a plate, simply supported

at all edges. It is assumed a half sine wave in the y direction ($n = 1$). In view of the simply supported boundary conditions, the substitution of the Navier expression of the displacement into Eq. leads to the following non-dimensional critical buckling load, in statics ($\omega = 0$):

$$\lambda = \min_m \frac{\left(\frac{\chi L}{a}\right)^2 [(\chi m)^2 + 1]^2 \pi^2}{e_0^2 \pi^2 [(\chi m)^4 + (\chi m)^2(1 + s) + s] + \left(\frac{\chi L}{a}\right)^2 [(\chi m)^2 + s]} \quad (4.72)$$

and, in free vibration ($N = 0$), the non-dimensional natural frequency

$$\Omega^2 = \frac{\left(\frac{\chi L}{a}\right)^2 [(\chi m)^2 + 1]^2 \pi^4}{\left(\frac{\chi L}{a}\right)^2 + e_0^2 \pi^2 [(\chi m)^2 + n^2]} \quad (4.73)$$

By equating these solutions with those of the discrete models, it leads to the calibrated small length scale coefficient in buckling and vibration, respectively, when the number of elements n_y goes to infinite:

$$e_{0,b} = \frac{1}{\sqrt{12}} \sqrt{\frac{\chi^6 m^6 + 2\chi^4 m^4 s - \chi^4 m^4 - \chi^2 m^2 s + 2\chi^2 m^2 + s}{\chi^6 m^6 + \chi^4 m^4 s + 2\chi^4 m^4 + \chi^2 m^2 + 2\chi^2 m^2 s + s}} \quad (4.74)$$

$$e_{0,v} = \frac{1}{\sqrt{6}} \sqrt{\frac{(m^2 \chi^2 + 1)^2}{1 + m^4 \chi^4}} \quad (4.75)$$

The calibrated small length scale coefficient lies between $1/\sqrt{24}$ and $1/\sqrt{6}$. It depends on the initial load, the buckling or vibration mode and the geometry (aspect ratio χ) [134,135]. For instance, Fig. 26 depicts the calibrated small length scale coefficient with the aspect ratio in statics for a uniaxial load ($s = 0$) and the first buckling and vibration mode.

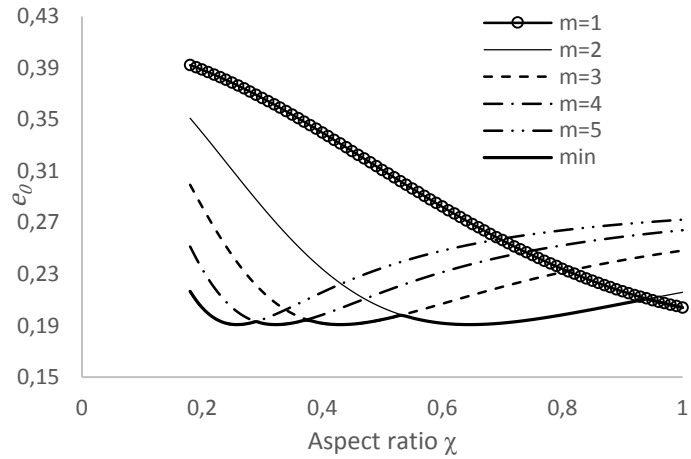


Fig. 26. Small length coefficient with respect to different aspect ratio in all round simply supported rectangular plate in statics following the fourth order phenomenological Eringen's model with $s = 0$

The expression of the coefficient is not the same in statics and in free vibration, as shown in Fig. 27.

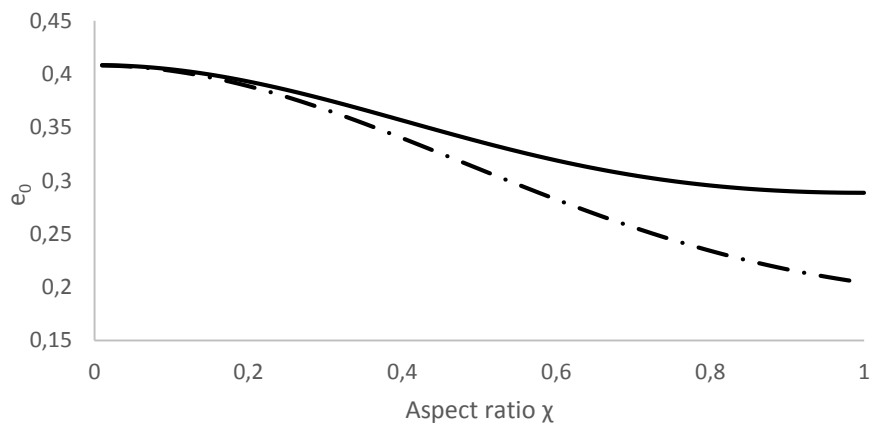


Fig. 27. Calibrated small length scale coefficient calculated in static case (dashed line) and free vibration case (continuous line) with respect to aspect ratio for $m = 1$, considering the fourth order phenomenological model

It is seen that the gap between the value in statics in dynamics and statics increases with respect to the aspect ratio χ . As it will be explained, the reference value of the small length scale coefficient, given through the continualized approaches (see hereinafter), is $1/\sqrt{12}$. Setting Δe_0 the relative error between the value calculated in the phenomenological model and the reference coefficient, Δe_0 is given in the following figures for different values of the aspect ratio and $m = 1$.

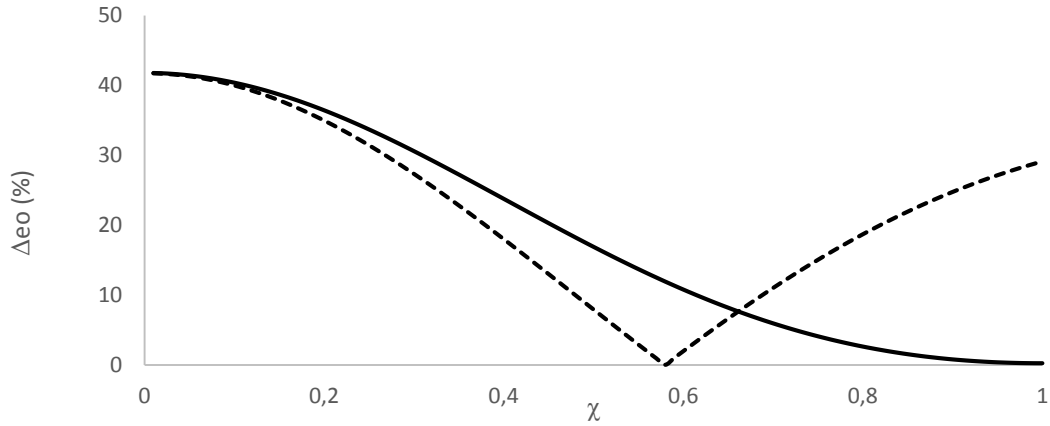


Fig. 28. Relative error of the small length scale coefficient obtained in the fourth order phenomenological model compared to the reference coefficient in the static case (dashed line) and dynamic case in free vibration (continuous line) and the calibrated coefficient calibrated

Consequently, because of the strong dependence of the small length scale coefficients on the different parameters, the fourth order phenomenological is not reliable (or at least, it gives apparent structural-dependent length scale calibration with respect to the plate lattice).

4.2.2.2. Sixth order phenomenological model

The governing partial differential equation of the sixth order phenomenological model is given in the previous chapter in free vibration and is now extended to take into account compressive loads:

$$\begin{aligned}
 D \left[\nabla^4 w + (e_0 a)^2 \left(\frac{\partial^4}{\partial x^4} - 2 \frac{\partial^4}{\partial x^2 \partial y^2} + \frac{\partial^4}{\partial y^4} \right) \nabla^2 w \right] \\
 + [1 - (e_0 a)^2 \nabla^2] \left[N \left(\frac{\partial^2}{\partial x^2} + s \frac{\partial^2}{\partial y^2} \right) w - m_0 \omega^2 w \right] = 0
 \end{aligned} \tag{4.76}$$

As for the fourth order phenomenological model, the small length scale coefficient introduced in this model has to be calibrated. For a plate that is simply supported at all edges, taking $n = 1$, using the Navier solution of the displacement, it results in the non-dimensional critical buckling load, expressed as follows, in statics ($\omega = 0$):

$$\lambda = \min_m \frac{\left(\frac{\chi L}{a}\right)^2 [(\chi m)^2 + 1]^2 \pi^2 - e_0^2 \pi^4 [(\chi m)^2 - 1]^2 [(\chi m)^2 + 1]}{e_0^2 \pi^2 (\chi m)^2 (1 + s) + e_0^2 \pi^2 [(\chi m)^4 + s] + \left(\frac{\chi L}{a}\right)^2 [(\chi m)^2 + s]} \quad (4.77)$$

The non-dimensional natural frequency is given, in free vibration, by:

$$\Omega^2 = \frac{\left(\frac{\chi L}{a}\right)^2 [(\chi m)^2 + 1]^2 \pi^4 - e_0^2 \pi^6 [(\chi m)^2 + 1][(\chi m)^2 - 1]^2}{\left(\frac{\chi L}{a}\right)^2 + e_0^2 \pi^2 [(\chi m)^2 + n^2]} \quad (4.78)$$

Using the discrete model as the reference model and assuming that the discrete equation matches with the one of the continuous model, the calibrated small length scale coefficient in buckling and vibration, respectively, when the number of elements n_y goes to infinite, is:

$$e_{0,b} = \frac{1}{\sqrt{24}} \sqrt{\frac{\chi^6 m^6 + 2\chi^4 m^4 s - \chi^4 m^4 - \chi^2 m^2 s + 2\chi^2 m^2 + s}{\chi^6 m^6 + \chi^4 m^4 s + \chi^2 m^2 + s}} \quad (4.79)$$

$$e_{0,v} = \frac{1}{\sqrt{12}} \quad (4.80)$$

The expression differs in statics and in free vibration (see Fig. 29). Remarkably, it is seen that in free vibration, the small length scale coefficient is constant and is equal to $1/\sqrt{12}$. This value coincides with the one that will be found for continualized models. In statics, the coefficient is between $1/\sqrt{24}$ and $1/\sqrt{12}$ and it depends on the load parameter s , the buckling mode m and the aspect ratio χ [134,135]. Thus, the magnitude of the fluctuation is less important than for the fourth order phenomenological model. Fig. 30 depicts $e_{0,b}$ with the aspect ratio for a uniaxial load ($s = 0$) and the first buckling modes.

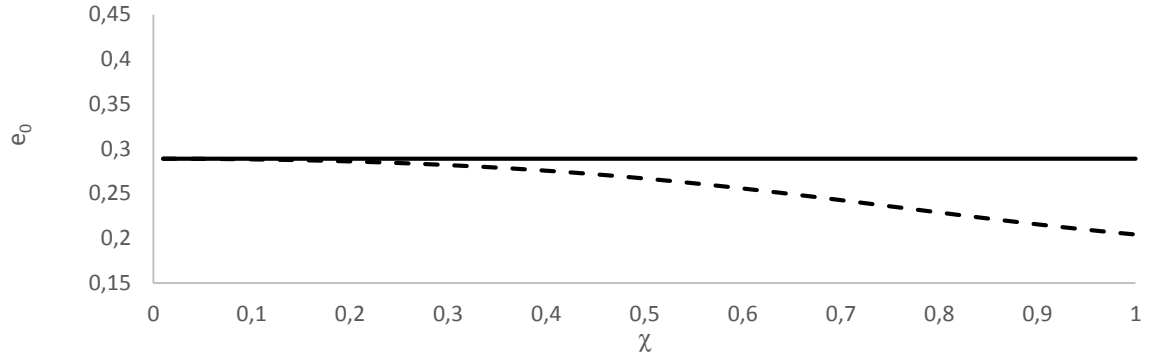


Fig. 29. Variation of calibrated small length scale coefficient calculated in static case (dashed line) and free vibration case (continuous line) with respect to aspect ratio, considering the sixth order phenomenological model.

Again, the difference between the small length scale coefficient calibrated in statics and the one in dynamics increases the aspect ratio χ .

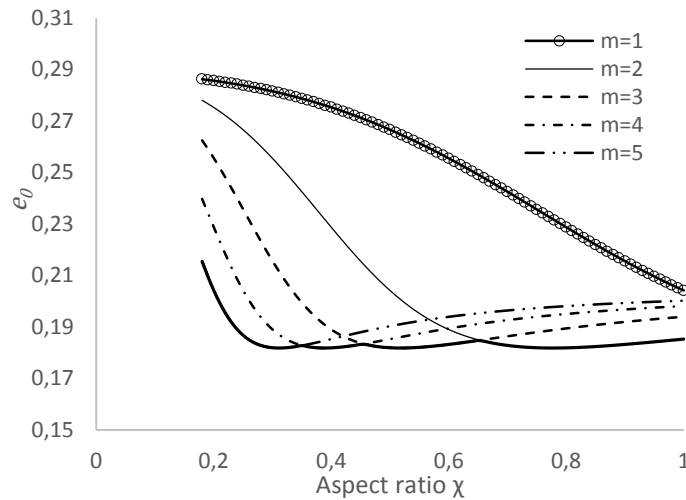


Fig. 30. Small length coefficient with respect to different aspect ratio in all round simply supported rectangular plate (buckled with half wave in y direction) following the sixth order phenomenological model with a uniaxial load.

Furthermore, the gap Δe_0 is given for various values of the aspect ratio in Fig. 31. This is constant, equal to zero, in free vibration because in this case, the value of the calibrated small length scale coefficient is the same as the value of the coefficient given in the continualized models (see hereinafter). In statics, the gap increases with the aspect ratio.

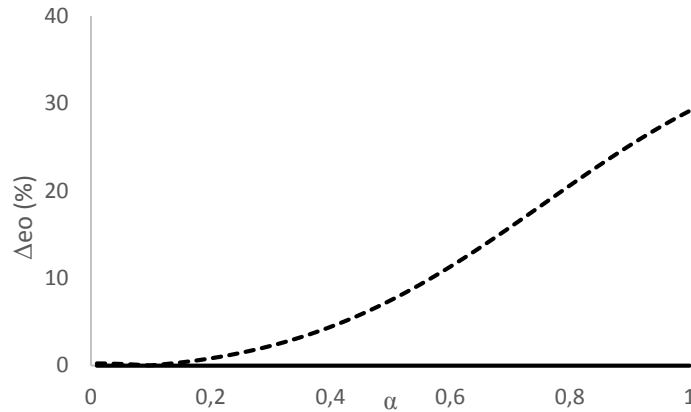


Fig. 31. Gap between the small length scale coefficient obtained in the continualized model in the static (dashed line) and dynamic case in free vibration (continuous line) and the calibrated coefficient calibrated in the sixth order phenomenological model)

It is worth noticing that the sixth order phenomenological model requires two additional boundary conditions than the fourth order phenomenological model. One may wonder whether it is not overcomplicated. However, by increasing the order of the model, the calibrated coefficient is constant in free vibration and consequently, the model provides better results than for the fourth order phenomenological model.

Thus, two phenomenological models with different orders have been derived. Both introduce a small length scale coefficient. This coefficient is supposed constant and yet, when it is calibrated from the discrete model, it is shown that it depends on different parameters such as the load or the aspect ratio. Assuming that the small length scale coefficient is $1/\sqrt{12} \approx 0.288$, defined in the derivation of the continualized models, presented hereinafter, the fourth and sixth order phenomenological models underestimate or overestimate this value. This gap cannot be ignored and it appears that the phenomenological models, traditionally used in the literature, are not consistent at least strictly as compared to lattice plate models. Consequently, there is a need to develop models that are more consistent than the traditional phenomenological ones (stress gradient nonlocal models of Eringen's type). The continualized models, as it has been established for beams, can be viewed as alternative nonlocal models to the phenomenological models.

4.2.3. Continualized models

4.2.3.1. Fourth order continualized model

The derivation of two continualized models, at different orders, is now proposed. These models are built based on the microstructured plate analysis and is anticipated to provide better results than phenomenological models

As in the beam problem, a dense lattice is assumed. The principle of the continualized approach for plates is the same as for the one-dimensional continualized beam models. As for beams, the discrete displacement is asymptotically equivalent to the continuous one $w_{i,j} = w(x_i, y_i) = w(x)$. In the discrete model, the displacements $w_{i\pm 1,j}$ and $w_{i,j\pm 1}$ are replaced by $w(x_i \pm a, y_i)$ and $w(x_i, y_i \pm a)$, respectively. By applying Taylor series to the difference equations, it yields, for plates [134,135,147]

$$\begin{aligned} w_{i+1,j} = w(x_i + a, y_i) &= \sum_{k=0}^{\infty} \frac{a^k}{k!} \frac{\partial^k}{\partial x^k} w(x, y) \\ w_{i-1,j} = w(x_i - a, y_i) &= \sum_{k=0}^{\infty} (-1)^k \frac{a^k}{k!} \frac{\partial^k}{\partial x^k} w(x, y) \end{aligned} \quad (4.81)$$

Thus, at the second order:

$$\frac{w_{i+1,j} - 2w_{i,j} + w_{i-1,j}}{a^2} = \frac{\partial^2}{\partial x^2} \left[1 + \frac{a^2}{12} \frac{\partial^2}{\partial x^2} \right] w(x, y) + o(a^2) \quad (4.82)$$

It is also possible to use the Padé approximants, it leads to

$$\frac{w_{i+1,j} - 2w_{i,j} + w_{i-1,j}}{a^2} = L_{a,x}[w]; \quad \frac{w_{i,j+1} - 2w_{i,j} + w_{i,j-1}}{a^2} = L_{a,y}[w] \quad (4.83)$$

Where the differentials operators $L_{a,x}$ and $L_{a,y}$ are defined as follows:

$$L_{a,x} = \frac{\frac{\partial^2}{\partial x^2}}{1 - \frac{a^2}{12} \frac{\partial^2}{\partial x^2}}; \quad L_{a,y} = \frac{\frac{\partial^2}{\partial y^2}}{1 - \frac{a^2}{12} \frac{\partial^2}{\partial y^2}} \quad (4.84)$$

Following the study of Rosenau [144]

$$L_{a,x}^{\frac{1}{2}} = \frac{\frac{\partial}{\partial x}}{1 - \frac{a^2}{24} \frac{\partial^2}{\partial x^2}}; \quad L_{a,y}^{\frac{1}{2}} = \frac{\frac{\partial}{\partial y}}{1 - \frac{a^2}{24} \frac{\partial^2}{\partial y^2}} \quad (4.85)$$

Considering the discrete constitutive law and equilibrium equation:

$$M_x = D(L_{a,x} + \nu L_{a,y})[w] \quad (4.86)$$

$$M_y = D(L_{a,y} + \nu L_{a,x})[w] \quad (4.87)$$

$$M_{xy} = D(L_{a,x}L_{a,y})^{1/2}[w] \quad (4.88)$$

$$L_{a,x}[M_{xx}] + 2(L_{a,x}L_{a,y})^{1/2}[M_{xy}] + L_{a,y}[M_{yy}] + PL_{a,x}[w] + sPL_{a,y}w - m_0\omega^2w = 0 \quad (4.89)$$

As for beams, for plates, the continualized models do not preserve the locality of the balance equation.

Substituting Eq. (4.85) into Eqs.(4.86)-(4.89), one obtains:

$$M_{xx} = D \left(\frac{\frac{\partial^2 w}{\partial x^2}}{1 - \frac{a^2}{12} \frac{\partial^2}{\partial x^2}} + \nu \frac{\frac{\partial^2 w}{\partial y^2}}{1 - \frac{a^2}{12} \frac{\partial^2}{\partial y^2}} \right) + o(a^2) \quad (4.90)$$

$$M_{yy} = D \left(\frac{\frac{\partial^2 w}{\partial y^2}}{1 - \frac{a^2}{12} \frac{\partial^2}{\partial y^2}} + \nu \frac{\frac{\partial^2 w}{\partial x^2}}{1 - \frac{a^2}{12} \frac{\partial^2}{\partial x^2}} \right) + o(a^2) \quad (4.91)$$

$$M_{xy} = \frac{D(1-\nu) \frac{\partial^2 w}{\partial x \partial y}}{\left(1 - \frac{a^2}{24} \frac{\partial^2}{\partial x^2}\right) \left(1 - \frac{a^2}{24} \frac{\partial^2}{\partial y^2}\right)} + o(a^2) \quad (4.92)$$

$$\begin{aligned} & \frac{\frac{\partial^2 M_{xx}}{\partial x^2}}{1 - \frac{a^2}{12} \frac{\partial^2}{\partial x^2}} + \frac{2 \frac{\partial^2 M_{xy}}{\partial x \partial y}}{\left[1 - \frac{a^2}{24} \frac{\partial^2}{\partial x^2}\right] \left[1 - \frac{a^2}{24} \frac{\partial^2}{\partial y^2}\right]} + \frac{\frac{\partial^2 M_{yy}}{\partial y^2}}{1 - \frac{a^2}{12} \frac{\partial^2}{\partial y^2}} + \frac{N \frac{\partial^2 w}{\partial x^2}}{1 - \frac{a^2}{12} \frac{\partial^2}{\partial x^2}} + \frac{sN \frac{\partial^2 w}{\partial y^2}}{1 - \frac{a^2}{12} \frac{\partial^2}{\partial y^2}} \\ & - m_0\omega^2w + o(a^2) = 0 \end{aligned} \quad (4.93)$$

By using the Taylor expansion, Eqs. (4.90)-(4.92) leads to:

$$M_{xx} = D \left(\frac{\partial^2}{\partial x^2} \left(1 + \frac{a^2}{12} \frac{\partial^2}{\partial x^2}\right) w + \nu \frac{\partial^2}{\partial y^2} \left(1 + \frac{a^2}{12} \frac{\partial^2}{\partial y^2}\right) w \right) + o(a^2) \quad (4.94)$$

$$M_{yy} = D \left(\frac{\partial^2}{\partial y^2} \left(1 + \frac{a^2}{12} \frac{\partial^2}{\partial y^2}\right) w + \nu \frac{\partial^2}{\partial x^2} \left(1 + \frac{a^2}{12} \frac{\partial^2}{\partial x^2}\right) w \right) + o(a^2) \quad (4.95)$$

$$M_{xy} = D(1-\nu) \left(1 + \frac{a^2}{24} \frac{\partial^2}{\partial x^2}\right) \left(1 + \frac{a^2}{24} \frac{\partial^2}{\partial y^2}\right) \frac{\partial^2}{\partial x \partial y} w + o(a^2) \quad (4.96)$$

Multiplying Eq. (4.93) by $[1 - (a^2/12)\nabla^2]^2$ and substituting Eqs. (4.94)-(4.96) results in the governing differential equation

$$D \left[\nabla^4 w - \frac{a^2}{3} \frac{\partial^4 \nabla^2 w}{\partial x^2 \partial y^2} \right] - m_0 \omega^2 \left[1 - \frac{a^2}{6} \nabla^2 w \right] + N \left[\frac{\partial^2 w}{\partial x^2} + s \frac{\partial^2 w}{\partial y^2} - \frac{a^2}{12} \left(2(s+1) \frac{\partial^4 w}{\partial x^2 \partial y^2} + \frac{\partial^4 w}{\partial x^4} + s \frac{\partial^4 w}{\partial y^4} \right) \right] + o(a^2) = 0 \quad (4.97)$$

In contrast to the phenomenological models, the small length scale coefficient does not appear explicitly in the equation and has to be introduced. e_0 is chosen arbitrarily equal to $1/\sqrt{12}$. By definition, it does not depend on the load, the geometry or any other parameter. Thus, the governing differential equation is rewritten as:

$$D \left[\nabla^4 w - 4(e_0 a)^2 \frac{\partial^4 \nabla^2 w}{\partial x^2 \partial y^2} \right] - m_0 \omega^2 [1 - 2(e_0 a)^2 \nabla^2 w] + N \left[\frac{\partial^2 w}{\partial x^2} + s \frac{\partial^2 w}{\partial y^2} - (e_0 a)^2 \left(2(s+1) \frac{\partial^4 w}{\partial x^2 \partial y^2} + \frac{\partial^4 w}{\partial x^4} + s \frac{\partial^4 w}{\partial y^4} \right) \right] = 0 \quad (4.98)$$

This equation is also derivable from the continualization of the discrete governing differential equation Eq. (4.60):

$$D \left[\frac{\frac{\partial^4 w}{\partial x^4}}{\left(1 - \frac{a^2}{12} \frac{\partial^2}{\partial x^2}\right)^2} + 2 \frac{\frac{\partial^4 w}{\partial x^2 \partial y^2}}{\left(1 - \frac{a^2}{12} \frac{\partial^2}{\partial x^2}\right) \left(1 - \frac{a^2}{12} \frac{\partial^2}{\partial y^2}\right)} + \frac{\frac{\partial^4 w}{\partial y^4}}{\left(1 - \frac{a^2}{12} \frac{\partial^2}{\partial y^2}\right)^2} \right] - m_0 \omega^2 w + \frac{N \frac{\partial^2 w}{\partial x^2}}{1 - \frac{a^2}{12} \frac{\partial^2}{\partial x^2}} + \frac{sN \frac{\partial^2 w}{\partial y^2}}{1 - \frac{a^2}{12} \frac{\partial^2}{\partial y^2}} + o(a^2) = 0 \quad (4.99)$$

Multiplying by $[1 - (a/12)^2 \nabla^2]^2$ and neglecting the higher order term in a results in Eq. (4.98).

Eq. (4.98) requires six boundary conditions which may be obtained from the variational principle. For edges parallel to the x axis, the boundary conditions are:

$$D \left(\frac{\partial^2 w}{\partial x^2} + \nu \frac{\partial^2 w}{\partial y^2} \right) - D \frac{a^2}{3} \frac{\partial^4 w}{\partial x^2 \partial y^2} - \frac{a^2}{12} N \left[\nabla^2 w + s \frac{\partial^2 w}{\partial y^2} \right] = 0 \text{ or } \frac{\partial w}{\partial x}$$

$$\frac{a^2}{3} D \frac{\partial^3 w}{\partial y^2 \partial x} = 0 \text{ or } \frac{\partial^2 w}{\partial y^2}$$

$$D \left[\frac{\partial}{\partial x} \nabla^2 w - \frac{a^2}{3} \frac{\partial^5 w}{\partial x^3 \partial y^2} \right] + N \frac{\partial w}{\partial x} - \frac{a^2}{12} N \left[\frac{\partial}{\partial x} \nabla^2 w + s \frac{\partial^3 w}{\partial x \partial y^2} \right] + \frac{a^2}{6} m_0 \omega^2 \frac{\partial w}{\partial y} = 0 \text{ or } w$$

are specified.

The calibration of the small length scale coefficient, in contrast to the phenomenological models, is unnecessary since, by definition, it is equal to $1/\sqrt{12}$. Thus, the fourth order continualized model (as the sixth order continualized model that will be presented hereinafter) are much better than the phenomenological models based on postulated nonlocal constitutive laws, at least with respect to the calibration with lattice mechanics.

4.2.3.2. Sixth order continualized model

Another continualized model is derived by using another continualization scheme. Instead of using the Taylor expansion on Eqs. (4.90) and (4.91), these equations are multiplied by $[1 - (a^2/12)\nabla^2]$ and Eq. (4.92) by $[1 - (a^2/24)\nabla^2]$

$$\left(1 - \frac{a^2}{12} \nabla^2\right) M_{xx} = D \left[\frac{\partial^2 w}{\partial x^2} + \nu \frac{\partial^2 w}{\partial y^2} - \frac{a^2}{12} (1 + \nu) \frac{\partial^4 w}{\partial x^2 \partial y^2} \right] + o(a^2) \quad (4.100)$$

$$\left(1 - \frac{a^2}{12} \nabla^2\right) M_{yy} = D \left[\frac{\partial^2 w}{\partial y^2} + \nu \frac{\partial^2 w}{\partial x^2} - \frac{a^2}{12} (1 + \nu) \frac{\partial^4 w}{\partial x^2 \partial y^2} \right] + o(a^2) \quad (4.101)$$

$$\left(1 - \frac{a^2}{24} \nabla^2\right) M_{xy} = D(1 - \nu) \frac{\partial^2}{\partial x \partial y} w + o(a^2) \quad (4.102)$$

Substituting Eqs. (4.100)-(4.102) into Eq. (4.93), multiplying by $[1 - (e_0 a)^2 \partial^2 / \partial x^2][1 - (e_0 a)^2 \partial^2 / \partial y^2]$ one obtains

$$\begin{aligned}
D \left[\nabla^4 w + \frac{a^2}{12} \left(\frac{\partial^6 w}{\partial x^6} - \frac{\partial^4 \nabla^2 w}{\partial x^2 \partial y^2} + \frac{\partial^6 w}{\partial y^6} \right) \right] - m_0 \omega^2 \left[1 - \frac{a^2}{12} \nabla^2 \right] w \\
- \frac{a^2}{12} N(1+s) \frac{\partial^4 w}{\partial x^2 \partial y^2} + N \left(\frac{\partial^2 w}{\partial x^2} + s \frac{\partial^2 w}{\partial y^2} \right) = 0
\end{aligned} \tag{4.103}$$

e_0 is chosen equal to $1/\sqrt{12}$. It results in the following governing differential equation

$$\begin{aligned}
D \left[\nabla^4 w + (e_0 a)^2 \left(\frac{\partial^6 w}{\partial x^6} - \frac{\partial^4 \nabla^2 w}{\partial x^2 \partial y^2} + \frac{\partial^6 w}{\partial y^6} \right) \right] - m_0 \omega^2 [1 - (e_0 a)^2 \nabla^2] w \\
- (e_0 a)^2 N(1+s) \frac{\partial^4 w}{\partial x^2 \partial y^2} + N \left(\frac{\partial^2 w}{\partial x^2} + s \frac{\partial^2 w}{\partial y^2} \right) = 0
\end{aligned} \tag{4.104}$$

It is also obtainable via variational formulation [134]. Thus, for boundary conditions, for edges parallel to the x axis:

$$\begin{aligned}
\left\{ D \left(\frac{\partial^2 w}{\partial x^2} + \nu \frac{\partial^2 w}{\partial y^2} \right) - D \frac{a^2}{12} \left(\frac{\partial^4 w}{\partial x^2 \partial y^2} - \frac{\partial^4 w}{\partial x^4} \right) - \frac{a^2}{24} N(1+s) \frac{\partial^2 w}{\partial y^2} \right\} \delta \left(\frac{\partial w}{\partial x} \right) = 0 \\
\frac{a^2}{12} D \left[\frac{\partial^3 w}{\partial x \partial y^2} \frac{\partial^2 \delta w}{\partial y^2} - \frac{\partial^3 w}{\partial x^3} \frac{\partial^2 \delta w}{\partial x^2} \right] = 0
\end{aligned}$$

$$\left\{ D \left[\frac{\partial}{\partial x} \nabla^2 w + \frac{a^2}{12} \left(\frac{\partial^5 w}{\partial x^5} - \frac{\partial^5 w}{\partial x^3 \partial y^2} \right) \right] - N \left(\frac{\partial w}{\partial x} - \frac{a^2}{24} (1+s) \frac{\partial^3 w}{\partial x \partial y^2} \right) + \frac{a^2}{12} m_0 \omega^2 \frac{\partial w}{\partial x} \right\} \delta w = 0$$

It has been shown in the literature that other sixth order continualized models could be derived. All these models are equivalents at the second order in a [134].

The different phenomenological and continualized models at the fourth and sixth order are now extended to describe the mechanical behavior of thick plates. The first investigations about the nonlocal thick plate models are recent [226,257,258,268,269]. However, the calibration of the small length scale coefficient of nonlocal Uflyand-Mindlin plate models, from lattice theory, has not been carried out.

4.3. Nonlocal thick plate models

As for the thin beam and plate models, the lattice model has to be derived first in order to calibrate the small length scale coefficient introduced in the thick plate models.

4.3.1. Microstructured beam-grid model

Compared to the discrete lattice plate model, in the microstructured beam-grid model, in addition to rotational springs, two successive rigid beams are connected via a shear spring as shown in Fig. 32.

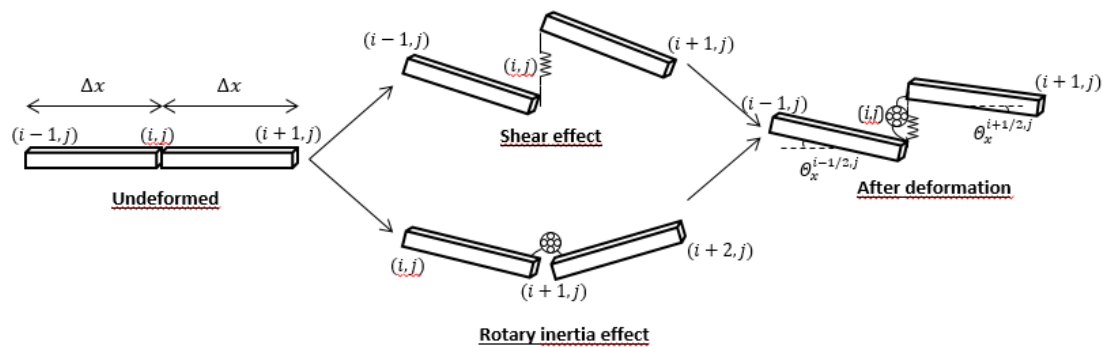


Fig. 32. Deformation of two successive elements following the x direction considering the rotary inertia and the shear effects.

Because of the discontinuity of the displacement when the rotary inertia and the shear effects are taken into account, w_{i-j} is different from w_{i+j} and the rotation-displacement relationship given by Eq. (4.48) for thin plates is no longer valid. Some alternative shear lattice plates could be considered in order to preserve continuity of the displacement, as presented for shear beams in [139]. This model is an extension to the thin plate model that has been presented before and the discrete thick beam model given by Duan et al. [127] and Zhang et al. [128].

In the discrete thick plate models, Eq. (4.53) for the bending strain energy and Eq. (4.58) for the work are retained but because of the discontinuity of the displacement, Eqs. (4.56) and (4.57) are not valid.

In contrast to the discrete model for thin plates [129,134,135,270] for which a beam is connected by another via a rotational spring, there is another degree of freedom at each individual node modeled by a shear spring of constants S_x and S_y for two adjacent beams in the x and y direction, respectively. These springs introduce shear effects between the nodes via a discontinuity of the displacement between two successive nodes. In the first microstructured models [132,136], presented before, the shear springs were not present and the shear contribution was ignored. Following the papers of Duan et al. [127] and Zhang et al. [128] that describe the behavior of discrete thick beams, the strain energy function due to deformed shear spring is given by:

$$U_s = \frac{1}{2} \sum_{i \in \mathbb{O}} \sum_{j \in \mathbb{O}}^{i \leq n_x, j \leq n_y} \left[S_x (\Delta_x [w_{i,j}] + \psi_x^{i,j})^2 \Delta x^2 + S_y (\Delta_y [w_{i,j}] + \psi_y^{i,j})^2 \Delta y^2 \right] \quad (4.105)$$

where the constants of the springs are given by $S_x = \kappa Gh \Delta y / \Delta x$ and $S_y = \kappa Gh \Delta x / \Delta y$.

In the discrete kinetic energy, there is an additional term compared to Eq. (4.57) for thin plates:

$$T = \frac{1}{2} \Delta x \Delta y \left\{ \omega^2 \sum_{i=0}^{n_x} \sum_{j=0}^{n_y} m_0 w_{i,j}^2 + \sum_{i \in \mathbb{O}} \sum_{j \in \mathbb{O}}^{i \leq n_x, j \leq n_y} m_2 \left\{ (\theta_x^{i,j})^2 + (\theta_y^{i,j})^2 \right\} \right\} \quad (4.106)$$

where m_2 is the mass per unit cell area. In the continuous model, $m_2 = \rho h^3 / 12$.

For an isotropic plate $S_x = S_y$ and the Euler-Lagrange equation can be obtained from Eq. (4.59) and :

$$\frac{\partial U_t + U_b + U_s - T}{\partial \psi_x^{i,j}} = \frac{\partial U_t + U_b + U_s - T}{\partial \psi_y^{i,j}} = 0 \quad (i, j) \in \mathbb{O} \quad (4.107)$$

It results in the equations of motion, with (i, j) a couple of half-integers

$$\begin{aligned} & \frac{D(1+\nu)}{2} \{ \Delta_{xx} [\psi_x^{i,j}] + \Delta_{xy} [\psi_y^{i,j}] \} + \frac{D(1-\nu)}{2} \{ \Delta_{xx} + \Delta_{yy} \} [\psi_x^{i,j}] \\ & \quad - \kappa Gh (\Delta_x [w_{i,j}] + \psi_x^{i,j}) = -m_2 \omega^2 \psi_x^{i,j} \\ & \frac{D(1+\nu)}{2} \{ \Delta_{xy} [\psi_x^{i,j}] + \Delta_{yy} [\psi_y^{i,j}] \} + \frac{D(1-\nu)}{2} \{ \Delta_{xx} + \Delta_{yy} \} [\psi_y^{i,j}] \\ & \quad - \kappa Gh (\Delta_y [w_{i,j}] + \psi_y^{i,j}) = -m_2 \omega^2 \psi_y^{i,j} \\ & \kappa Gh (\Delta_{xx} [w_{i,j}] + \Delta_{yy} [w_{i,j}] + \Delta_y [\psi_y^{i,j}] + \Delta_x [\psi_x^{i,j}]) - N (\Delta_{xx} [w_{i,j}] + s \Delta_{yy} [w_{i,j}]) \\ & \quad = -m_0 \omega^2 w_{i,j} \end{aligned} \quad (4.108)$$

When $\psi_y^{i,j} = \Delta_y [\psi_y^{i,j}] = \Delta_y [\psi_x^{i,j}] = \Delta_y [w_{i,j}] = 0$, the equations are reduced to those for thin plates (see before).

Eqs. (4.108) are the discrete equivalent of the equations of motions given by Eq. (2.77) from the local Uflyand-Mindlin plate model [103].

Applying Δ_x and Δ_y to the first and second equation of motion, respectively, after some manipulations, it leads to the following governing differential equation

$$\begin{aligned} D(\Delta_{xxxx} + 2\Delta_{xxyy} + \Delta_{yyyy})[w_{i,j}] - m_0\omega^2 w_{i,j} \\ + \left\{ \frac{m_0}{\kappa Gh} D + m_2 \right\} \omega^2 (\Delta_{xx} + \Delta_{yy})[w_{i,j}] + m_2 \omega^4 \frac{m_0}{\kappa Gh} w_{i,j} \\ + \left[N - \frac{ND}{\kappa Gh} (\Delta_{xx} + \Delta_{yy}) \right] (\Delta_{xx}[w_{i,j}] + s\Delta_{yy}[w_{i,j}]) = 0 \end{aligned} \quad (4.109)$$

Eq. (4.109) is the central finite difference scheme of the local and continuous Mindlin plate equation studied in chapter 2 and extended to take into account the compressive loads.

Thus, the discrete governing differential equations is rewritten as:

$$\begin{aligned} n_y^4 \alpha^2 L[w_{i,j}] - \chi^2 \Omega_{(micro)}^2 w_{i,j} + \Omega_{(micro)}^2 n_y^2 \{ \tilde{D}_h + \tilde{m} \} (H_x + H_y) w_{i,j} \\ + \frac{\tilde{m} \tilde{D}_h}{\chi^2} \Omega_{(micro)}^4 w_{i,j} + n_y^2 \chi^2 \lambda_{(micro)} (H_x + sH_y) [w_{i,j}] \\ - \tilde{D}_h n_y^4 \lambda_{(micro)} (M_1 + sM_2) [w_{i,j}] = 0 \end{aligned} \quad (4.110)$$

where the following non-dimensional parameters are defined

$$\tilde{m} = \frac{m_2}{m_0 L^2}; \tilde{D}_h = \frac{D}{\kappa Gh L^2} = \frac{\bar{h}^2}{6\kappa(1-\nu)} = \mu_s \tilde{m}; \mu_s = \frac{2}{\kappa(1-\nu)} \quad (4.111)$$

Moreover, in addition to the operators L , H_x and H_y , given by Eqs. (4.61), the following discrete operators are defined

$$\begin{aligned} M_1[w_{i,j}] &= w_{i+2,j} + w_{i-2,j} + w_{i+1,j+1} + w_{i-1,j+1} + w_{i+1,j-1} + w_{i-1,j-1} \\ &\quad - 6w_{i+1,j} - 6w_{i-1,j} - 2w_{i,j+1} - 2w_{i,j-1} + 10w_{i,j} \\ M_2[w_{i,j}] &= w_{i,j+2} + w_{i,j-2} + w_{i+1,j+1} + w_{i-1,j+1} + w_{i+1,j-1} + w_{i-1,j-1} \\ &\quad - 6w_{i,j+1} - 6w_{i,j-1} - 2w_{i+1,j} - 2w_{i-1,j} + 10w_{i,j} \end{aligned} \quad (4.112)$$

For a plate that is simply supported at all edges, the solution is obtained by substituting Eq. (4.67) into Eq. (4.110).

$$\begin{aligned}
\delta^2 + \frac{\mu_s}{n_y^4} \frac{1}{\zeta^4} \Omega_{(micro)}^4 - \left[\frac{1}{n_y^4} + \frac{(\mu_s + 1)}{\zeta^2 n_y^2} \delta \right] \Omega_{(micro)}^2 \\
+ \frac{2\lambda_{(micro)}}{n_y^2} (\cos \sqrt{\alpha_1} + s \cos \sqrt{\alpha_2} - 1 - s) \\
- \frac{4\mu_s \lambda_{(micro)}}{\zeta^2} \left[2(1 + s) + \cos^2 \sqrt{\alpha_1} + s \cos^2 \sqrt{\alpha_2} - (3 + s) \cos \sqrt{\alpha_1} \right. \\
\left. - (3s + 1) \cos \frac{n\pi}{n_y} + (1 + s) \cos \sqrt{\alpha_1} \cos \sqrt{\alpha_2} \right] = 0
\end{aligned} \tag{4.113}$$

where different non-dimensional parameters are defined as follows:

$$\begin{aligned}
\zeta = \frac{\chi}{\sqrt{\tilde{m}}}; \alpha_1 = \left(\frac{\chi m \pi}{n_y} \right)^2; \alpha_2 = \left(\frac{n\pi}{n_y} \right)^2 \\
\tilde{\alpha} = \alpha_1 + \alpha_2; \delta = 2(2 - \cos \sqrt{\alpha_1} - \cos \sqrt{\alpha_2})
\end{aligned} \tag{4.114}$$

In statics, $\omega = 0$ and the critical buckling load is

$$\begin{aligned}
\lambda_{(micro)} = \frac{1}{2} \delta^2 \left\{ \frac{2\mu_s}{\zeta^2} [2(1 + s) + \cos^2 \sqrt{\alpha_1} + s \cos^2 \sqrt{\alpha_2} - (3 + s) \cos \sqrt{\alpha_1} \right. \\
\left. - (3s + 1) \cos \sqrt{\alpha_2} + (1 + s) \cos \sqrt{\alpha_1} \cos \sqrt{\alpha_2}] \right. \\
\left. - \frac{1}{n_y^2} (\cos \sqrt{\alpha_1} + s \cos \sqrt{\alpha_2} - 1 - s) \right\}^{-1}
\end{aligned} \tag{4.115}$$

For a thin plate, ζ goes to infinite and the results are reduced to those obtained before [134,135].

In free vibration, $\lambda_{(micro)} = 0$ and the equation is rewritten as:

$$\mu_s \beta^2 \tilde{\Omega}_{(micro)}^4 - [1 + (1 + \mu_s) \beta \tilde{\delta}] \tilde{\Omega}_{(micro)}^2 + \tilde{\delta}^2 = 0 \tag{4.116}$$

where β and Ω are defined as follows:

$$\beta = \frac{[(\chi m \pi)^2 + (n\pi)^2]}{\zeta^2}; \tilde{\Omega} = \frac{\Omega}{(\chi m \pi)^2 + (n\pi)^2} \tag{1}$$

For thin plates, $\tilde{m} = 0$, it is worth noticing that the result matches the one given a previous section and in the literature (see for instance [126,133-135]). Taking $n = 0$, the plate problem is reduced to the beam one and the equation coincides with the one given by Duan et al. [127].

Thus, the closed-form expression of the discrete squared nondimensional natural frequency is [127]

$$\tilde{\Omega}_{(micro)}^2 = \frac{\tilde{\delta}}{2\beta} \left(\frac{1}{\mu_s} + 1 \right) + \frac{1}{2\mu_s \beta^2} \left[1 \pm \sqrt{(\mu_s - 1)^2 \beta^2 \tilde{\delta}^2 + 2(1 + \mu_s) \beta \tilde{\delta} + 1} \right] \tag{4.117}$$

For thin plates, $\beta = 0$ and $\tilde{\Omega}_{(micro)}^2 = \tilde{\delta}^2$, coinciding with Eq. (4.70), determined in a previous section.

To study the non-dimensional natural frequencies of the thick plates model and to calibrate the small length scale coefficient, in a sake of simplicity, it is suggested to expand Eq. (4.117) through the use of the Maclaurin series expansion such as the degree of each term is smaller than unity. Thus, the higher root is expanded as

$$\tilde{\Omega}^2 = -1 + \frac{1}{6} \frac{(\alpha_1^2 + \alpha_2^2)}{(\alpha_1 + \alpha_2)} + (1 + \mu_s)\beta + \frac{(1 + \mu_s)\beta + 1}{\mu_s\beta^2} + O(\alpha_1^2, \alpha_2^2, \beta^2) \quad (4.118)$$

when β goes to zero, although the case is reduced to the one of a thin plate, a singularity appears in the expression of the natural frequency. Thus, for the next, the higher roots will be ignored.

The other root, the lowest one, is given by:

$$\begin{aligned} \tilde{\Omega}^2 = & \frac{(13 - 27\beta - 270\mu_s\beta)}{720} \frac{\alpha_1\alpha_2(\alpha_1^3 + \alpha_2^3)}{(\alpha_1 + \alpha_2)^3} + \frac{(3\beta + 3\mu_s\beta - 1)}{1080} \frac{\alpha_1^3\alpha_2^3}{(\alpha_1 + \alpha_2)^3} \\ & + \frac{-18(\mu_s - 1)\beta + 7}{360} \frac{\alpha_1^2\alpha_2^2}{(\alpha_1 + \alpha_2)^2} \\ & + (1 + \mu_s^2 \\ & + 3\mu_s)\beta^2 \left[\frac{19(\alpha_1^4 + \alpha_2^4) + 4(\alpha_1^3\alpha_2 + \alpha_2^3\alpha_1) + 30\alpha_1^2\alpha_2^2}{360(\alpha_1 + \alpha_2)^2} \right. \\ & \left. - \frac{(\alpha_1^2 + \alpha_2^2)}{3(\alpha_1 + \alpha_2)} + 1 \right] + \frac{1}{10} \left[\frac{1}{8} - \frac{7}{24}(1 + \mu_s)\beta \right] \frac{(\alpha_1^5 + \alpha_2^5)}{(\alpha_1 + \alpha_2)^3} \\ & + \left[\frac{1}{4}(1 + \mu_s)\beta - \frac{1}{6} \right] \frac{(\alpha_1^2 + \alpha_2^2)^2 + 2\alpha_1\alpha_2(\alpha_1^2 + \alpha_2^2)}{(\alpha_1 + \alpha_2)^3} + 1 \\ & - (1 + \mu_s)\beta \end{aligned} \quad (4.119)$$

4.3.2. Nonlocal Uflyand-Mindlin plate model

The derivation of the nonlocal original Uflyand-Mindlin plate model or fourth order phenomenological thick plate model or fourth order Eringen model, has been derived in a previous chapter in free vibration. It can be shown that the general form of the governing differential equation of the nonlocal original Uflyand-Mindlin plate model extended to take into account compressive forces [271,272] is:

$$\begin{aligned}
& \frac{[1 - R_s(e_0 a)^2 \nabla^2]}{\kappa G h} \{D \nabla^2 + m_2 \omega^2 [1 - (e_0 a)^2 \nabla^2]\} \left\{ N \left(\frac{\partial^2}{\partial x^2} + s \frac{\partial^2}{\partial y^2} \right) - m_0 \omega^2 \right\} w \\
& + [1 - (e_0 a)^2 \nabla^2] \left[(m_0 - m_2 \nabla^2) \omega^2 - N \left(\frac{\partial^2}{\partial x^2} + s \frac{\partial^2}{\partial y^2} \right) \right] w \\
& = D \nabla^4 w
\end{aligned} \tag{4.120}$$

The value of the parameter R_s has been widely debated in the previous chapter. It was concluded that R_s is equal to unity. This value will be kept for the next, although it would be possible to also consider the case of R_s equal to zero [271].

The value of the small length scale coefficient e_0 , supposed constant, is unknown. As for the phenomenological thin plate models, it has to be calibrated from the reference discrete model. Two cases have to be considered and distinguished: in statics ($\omega = 0, N \neq 0$) and in free vibration ($\omega \neq 0, N = 0$). Indeed, the small length scale coefficient is calibrated by equating the buckling load in statics and the free vibration in free vibration of the phenomenological model with the one of the discrete model.

4.3.2.1. Solution in statics

First of all, the buckling load has to be determined in statics for the phenomenological model. Considering a plate with all edges simply supported, for $n = 1$, substituting Eq. (2.118) into Eq. (4.120) and using the nondimensional numbers, the critical buckling load is:

$$\lambda = \min_m \frac{\pi^2 \frac{[(\chi m)^2 + 1]^2}{[(\chi m)^2 + s]}}{1 + \left[\frac{\mu_s}{\zeta^2} + \left(\frac{e_0 a}{\chi L} \right)^2 \right] \pi^2 [(\chi m)^2 + 1] + \frac{\mu_s}{\zeta^2} \left(\frac{e_0 a}{\chi L} \right)^2 \pi^4 [(\chi m)^2 + 1]^2} \tag{4.121}$$

When ζ goes to infinite, the shear effect is neglected and the nondimensional buckling load of the thick plate is reduced to the one found in a previous section for thin plate given by Eq. (4.72).

In order to observe the dependence of the buckling load on the small length scale coefficient, it is given in Figs. 33 and 34 for a square plate ($\chi = 1$), a thickness ratio \bar{h} equal to 0.1 and various values of the number of elements n_y for the first buckling mode m . Two cases are considered: a load in all directions $s = 1$ (Fig. 33) and a uniaxial load $s = 0$ (Fig. 34). Different values of e_0 are considered: 0, $1/\sqrt{24}$, $1/\sqrt{12}$ and $1/\sqrt{6}$. As expected, it is seen that the value of the small length scale coefficient has a big influence on the value of the buckling load. Thus a correct calibration of the small length scale coefficient is crucial in order to predict the behavior of the plate in buckling.

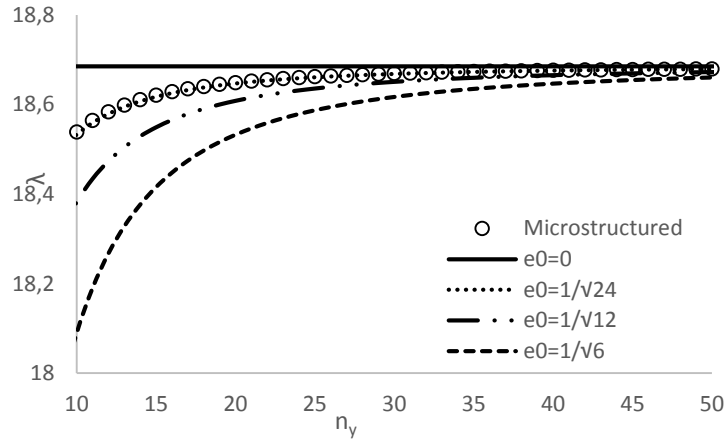


Fig. 33. Buckling load of all round simply supported nonlocal plate with respect to the length scale coefficient and n_y for a set of parameters $(\chi, m, n, s) = (1, 1, 1, 1)$ and different values of $e_0 (0, 1/\sqrt{6}, 1/\sqrt{12}, 1/\sqrt{24})$ considering the fourth order phenomenological model

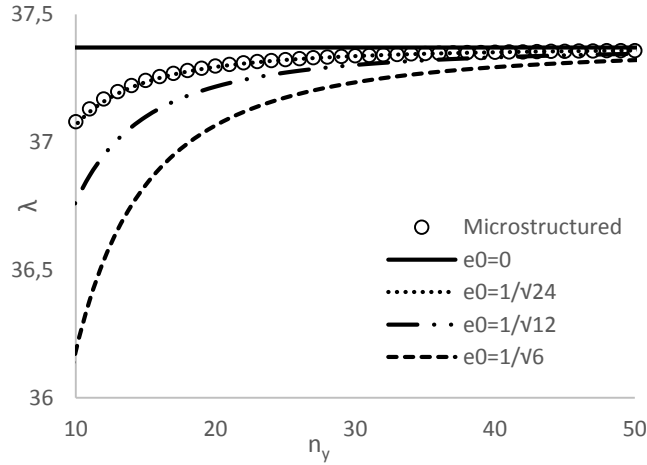


Fig. 34 Buckling load of all round simply supported nonlocal plate with respect to the length scale coefficient and n_y for a set of parameters $(\chi, m, n, s) = (1, 1, 1, 0)$ and different values of $e_0 (0, 1/\sqrt{6}, 1/\sqrt{12}, 1/\sqrt{24})$ considering the fourth order phenomenological model

For a load uniform in all directions ($s = 1$), by equating the buckling load from Eqs. (4.115) and (4.121), when the number of elements n_y goes to infinite,

$$e_{0,b} = \frac{1}{\sqrt{12}} \sqrt{\frac{\chi^4 m^4 + 1}{\frac{\mu_s}{\zeta^2} \pi^2 [(\chi m)^6 + 3(\chi m)^4 + 3(\chi m)^2 + 1] + [(\chi m)^2 + 1]^2}} \quad (4.122)$$

When ζ goes to infinite, it is reduced to Eq. (4.74).

For a uniaxial load ($s = 0$), by equating the buckling stress from Eqs. (4.115) and (4.121), the calibrated e_0 is expressed as, when the number of elements goes to infinite:

$$e_{0,b} = \frac{1}{\sqrt{12}} \sqrt{\frac{\frac{\mu_s}{\zeta^2} \pi^2 [1 - (\chi m)^4] + (\chi m)^4 - (\chi m)^2 + 2}{\frac{\mu_s}{\zeta^2} \pi^2 [(\chi m)^6 + 3(\chi m)^4 + 3(\chi m)^2 + 1] + (\chi m)^4 + 2(\chi m)^2 + 1}} \quad (4.123)$$

It is seen that e_0 is not constant and depends on the aspect ratio χ , the buckling mode m , the nondimensional shear parameter ζ and the load through the parameter s .

The calibrated small length scale coefficient for a thick plate is different from the one for thin plate. Thus, the shear effect, through the parameter ζ significantly changes the behavior of the plate in buckling. When the buckling mode m goes to infinite, the small length scale coefficient goes to zero for thick plates whereas for thin plate, it has been shown in a previous section that it goes to a constant value, the same as the one defined in the continualized model, namely $1/\sqrt{12}$. Thus, the nonlocal effect decreases with the buckling mode and it leads to a paradoxical result.

In order to study the influence of the different parameters such as the aspect ratio or the shear parameter ζ on the value of the calibrated small length scale coefficient, it is proposed to calculate it by using the values of the shear parameter and the Poisson's ratio found in the literature, namely 5/6 and 0.3, respectively [226]. It is assumed a one-half wave in the y -direction ($n = 1$). Figures 35 and 36 depict the calibrated small length scale coefficient for different values of the aspect ratio χ and buckling mode m for a couple $(\bar{h}; \tilde{D}_h)$ equal to (0.1; 0.0028571) for an uniform load along all the directions ($s = 1$, Fig. 35) and a uniaxial load ($s = 0$, Fig. 36).

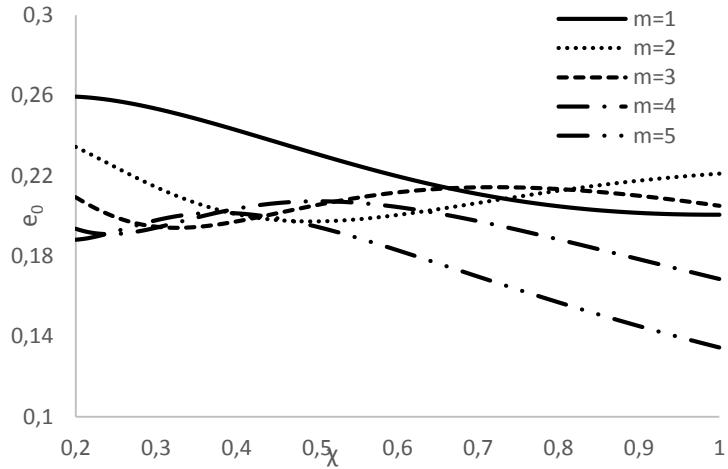


Fig. 35. Calibrated small length coefficient e_0 with respect to the aspect ratio χ following the Eringen's nonlocal Uflyand-Mindlin plate model for various values of the buckling load and a couple $(\bar{h}; \bar{D}_h)$ equal to $(0.1; 0.0028571)$ with a load uniform in all directions ($s = 1$)

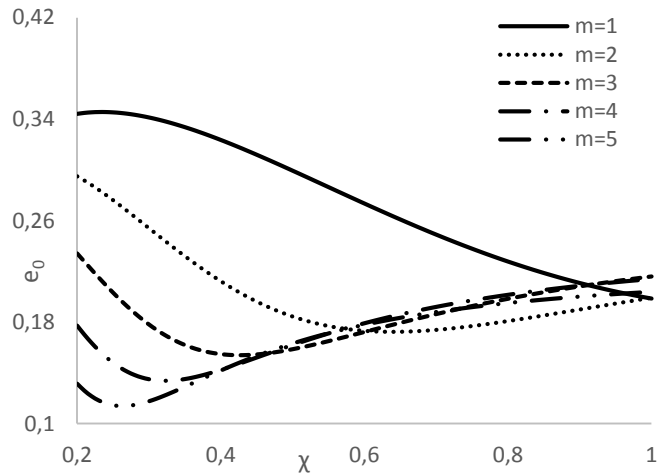


Fig. 36. Calibrated small length coefficient e_0 with respect to the aspect ratio χ following the Eringen's nonlocal Uflyand-Mindlin plate model for various values of the buckling load and a couple $(\bar{h}; \bar{D}_h)$ equal to $(0.1; 0.0028571)$ with a uniaxial load ($s = 0$)

It is seen that the small length scale coefficient, calibrated from the discrete model, is strongly dependent on the aspect ratio and the buckling mode. Likewise, Figs. 37 and 38 show e_0 versus the aspect ratio for different values of the aspect ratio χ and the parameter s for the first buckling mode ($m = 1$) and confirm that it is also dependent on the shear parameter \tilde{D}_h .

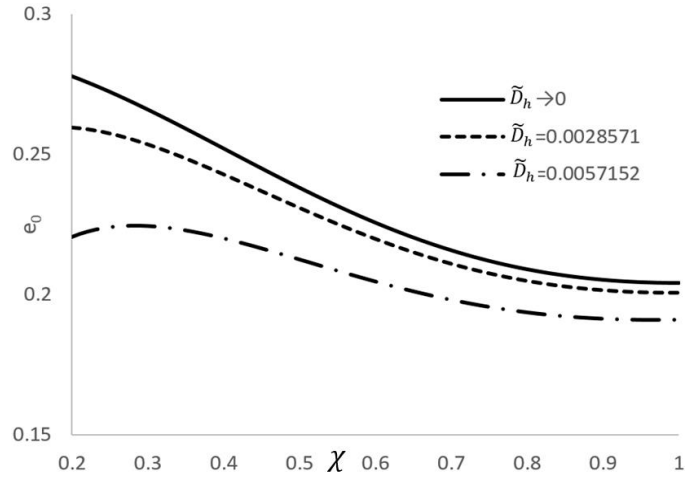


Fig. 37. Calibrated Small length coefficient e_0 versus the aspect ratio χ following the fourth order phenomenological Uflyand-Mindlin thick plate model, for different values of \tilde{D}_h and a couple (m, s) equal to $(1, 1)$

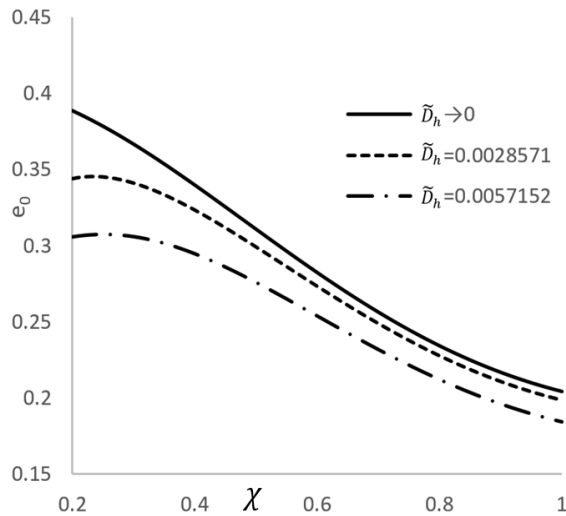


Fig. 38. Calibrated Small length coefficient e_0 versus the aspect ratio χ following the fourth order phenomenological Uflyand-Mindlin thick plate model, for different values of \tilde{D}_h and a couple (m, s) equal to $(1, 0)$

Thus, considering a set of parameters (χ, m, n, s) equal to $(1,1,1,1)$, the buckling load λ is depicted in Fig. 39 for various values of the number of elements n_y . For these parameters, the calibrated small length scale coefficient is taken equal to $1/\sqrt{24}$.

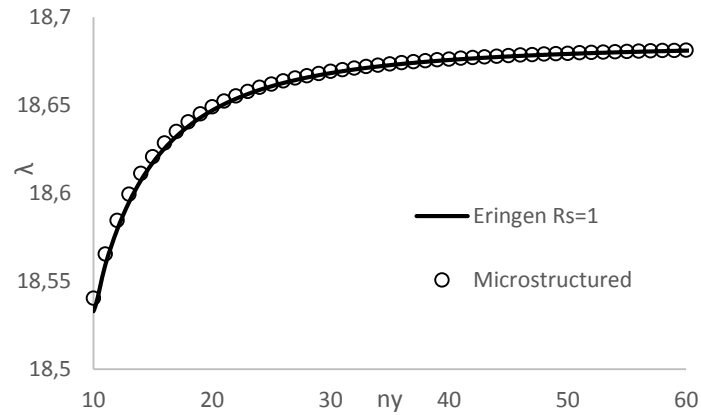


Fig. 39. Buckling loads of a simply supported nonlocal plate and lattice model for different n_y , following the fourth order phenomenological thick plate model ($e_0 = 1/\sqrt{24}$) for a set of parameters (χ, m, n, s) equal to $(1,1,1,1)$

It is seen that the buckling load perfectly fits the one of the lattice model. Thus, $e_0 = 1/\sqrt{24}$ is an excellent value of the small length scale coefficient for this particular set of parameters (χ, m, n, s) . However, as explained before, for different parameters, the calibrated small length scale coefficient will change. For instance, Fig. 40 shows the buckling load of the discrete model and the one of the fourth order phenomenological thick plate model considering a set of parameters (χ, m, n, s) equal to $(2,2,1,1)$ for a small length scale coefficient equal to $1/\sqrt{24} \approx 0.204$ and 0.257 , value calibrated from this new set of parameters.

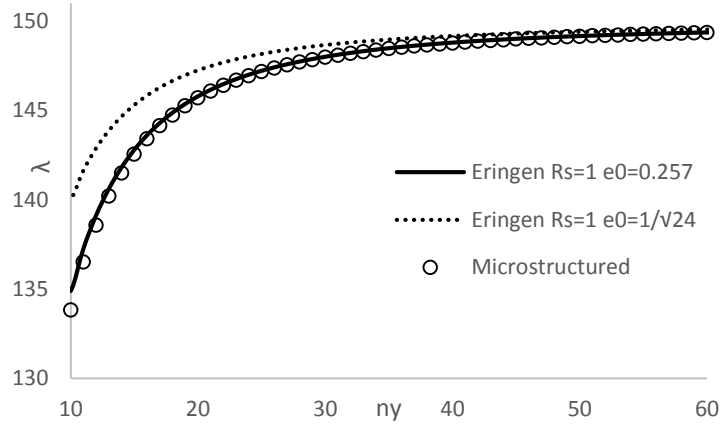


Fig. 40. Buckling loads of a simply supported nonlocal plate and lattice model for different n_y , following the fourth order Eringen model for a set of parameters (χ, m, n, s) equal to $(2, 2, 1, 1)$ and e_0 equal to $1/\sqrt{24}$ and 0.257

Thus, it is seen that $e_0 = 1/\sqrt{24}$ led to an excellent approximation of the non dimensionnal buckling load for the triplet $(\chi = 1, m = 1, n = 1)$ but it cannot be used for another set of parameters.

4.3.2.2. Solution for free vibration

Likewise, in the case of free vibration, $\lambda = 0$ and the natural frequency has to be determined in order to calibrate the small length scale coefficient.

The non-dimensional natural frequency of the fourth order phenomenological thick plate model or fourth order Eringen's model is expressed as follows:

$$\tilde{\Omega}^2 = \frac{1}{2[1 + e_0^2 \tilde{\alpha}]^2 \mu_s \beta^2} \left\{ 1 + (\mu_s + 1)\beta + (1 + \beta\mu_s + \beta)e_0^2 \tilde{\alpha} \pm \left\{ [1 + (\mu_s + 1)\beta + (1 + \beta\mu_s + \beta)e_0^2 \tilde{\alpha}]^2 - 4[1 + e_0^2 \tilde{\alpha}]^2 \mu_s \beta^2 \right\}^{\frac{1}{2}} \right\} \quad (4.124)$$

As explained in a previous chapter and before, in the phenomenological nonlocal Uflyand-Mindlin plate model, there are two branches of natural frequencies. The transition frequency depends on the parameters of the problems such as the vibration mode or the aspect ratio. In a sake of

simplicity, as for the discrete model, only the lowest value of the small length scale coefficient will be retained.

As in statics, it is proposed to determine the non-dimensional natural frequency considering the reference lattice model and the fourth order phenomenological thick plate model versus the number of elements n_y for a set of parameters (χ, m, n, β) equal to $(1, 1, 1, 0.5)$ and various values of the small length scale coefficient: $0, 1/\sqrt{24}, 1/\sqrt{12}$ and $1/\sqrt{6}$ (see Fig. 41).

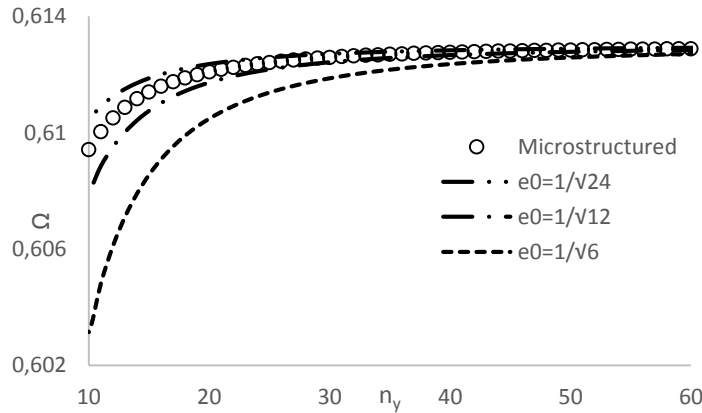


Fig. 41. Nondimensional frequency of all round simply supported nonlocal plate with respect to the length scale coefficient and n_y for a set of parameters $(\chi, m, n) = (1, 1, 1)$ and different values of e_0 ($0, 1/\sqrt{6}, 1/\sqrt{12}, 1/\sqrt{24}$) considering the fourth order phenomenological model

As expected and seen in statics, the value of the small length scale coefficient has a strong influence on the value of the buckling mode. Thus a correct calibration of the small length scale coefficient is crucial in order to predict the behavior of the plate in buckling.

The calibrated small length scale coefficient is obtained by equating Eqs. (4.117) and (4.124). It yields:

$$e_0^2 = \frac{1 + \beta(\mu_s + 1) - 2\mu_s\beta^2\tilde{\Omega}_{micro}^2 \pm \{[1 - \beta(\mu_s - 1)]^2 + 4\beta\mu_s\}^{\frac{1}{2}}}{2\mu_s\beta^2\tilde{\Omega}_{micro}^2\tilde{\alpha}} \quad (4.125)$$

It is worth noticing that for $\alpha_2 = 0$, the case is reduced to the one of a thick beam, already investigated in the literature [126] for beams. For β equal to zero, the shear effect is neglected, the thickness of the plate goes to zero and the small length scale coefficient coincides with the one found in a previous section.

Furthermore, substituting Eq. (4.119) into Eq. (4.125), the Maclaurin series expansion with respect to α_1, α_2 and β , keeping only the term for which the degree of the rational function in α_1 and α_2 is smaller than 2, yields

$$\begin{aligned}
e_0^2 = \frac{1}{720\tilde{\alpha}^8} & \left([11C_1 + 3C_2 + 30\mu_s\beta^2 + 8C_3](\alpha_1^9 + \alpha_2^9) \right. \\
& + [51C_1 + 13C_2 + 38C_3 + 140\mu_s\beta^2](\alpha_1^8\alpha_2 + \alpha_1\alpha_2^8) \\
& + \frac{1}{24\tilde{\alpha}^8} [4C_1 + C_2 + 11\mu_s\beta^2 + 3C_3] (\alpha_1^7\alpha_2^2 + \alpha_1^2\alpha_2^7) \\
& + \frac{1}{360\tilde{\alpha}^8} [108C_1 + 29C_2 + 295\mu_s\beta^2 + 79C_3](\alpha_1^6\alpha_2^3 + \alpha_1^3\alpha_2^6) \quad (4.126) \\
& + \frac{1}{360\tilde{\alpha}^8} [153C_1 + 44C_2 + 415\mu_s\beta^2 + 109C_3]\alpha_1^4\alpha_2^4\tilde{\alpha} \\
& + \frac{1}{12\tilde{\alpha}^8} [2C_1 + C_2 + C_3 + 5\mu_s\beta^2][6(\alpha_1^7\alpha_2 + \alpha_1\alpha_2^7) + 30\alpha_1^4\alpha_2^4 \\
& \left. + 16(\alpha_1^6\alpha_2^2 + \alpha_1^2\alpha_2^6) + (\alpha_1^8 + \alpha_2^8) + 26(\alpha_1^5\alpha_2^3 + \alpha_1^3\alpha_2^5)] \right)
\end{aligned}$$

where

$$C_1 = \mu_s^2\beta^2 - \mu_s\beta + 1; C_2 = \mu_s\beta(1 - \mu_s\beta - \beta); C_3 = \beta^2 - \beta$$

Thus, the calibrated small length scale coefficient, in dynamics, depends on α_1, α_2 and β . It is proposed to study the influence of each of these parameters. Figs. 42 and 43 depict the calibrated small length scale coefficient versus α_1 for various values of α_2 , with β constant, equal to 0.1 (Fig. 42) and 0.5 (Fig. 43).

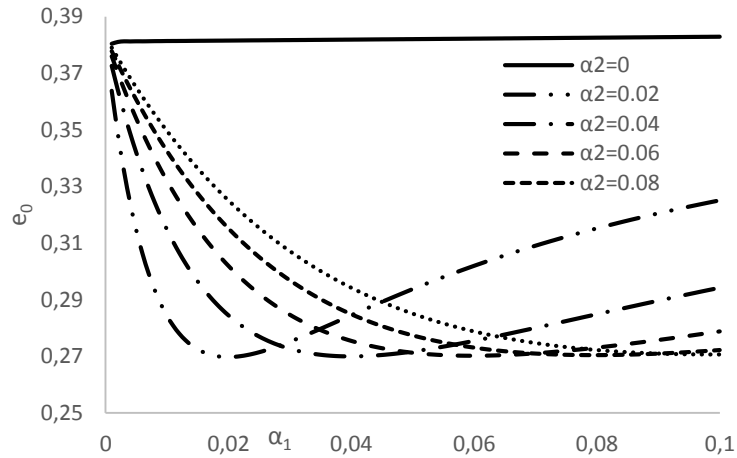


Fig. 42. Calibrated small length scale coefficient in free vibration versus α_1 for $\beta = 0.1$ and different values of α_2

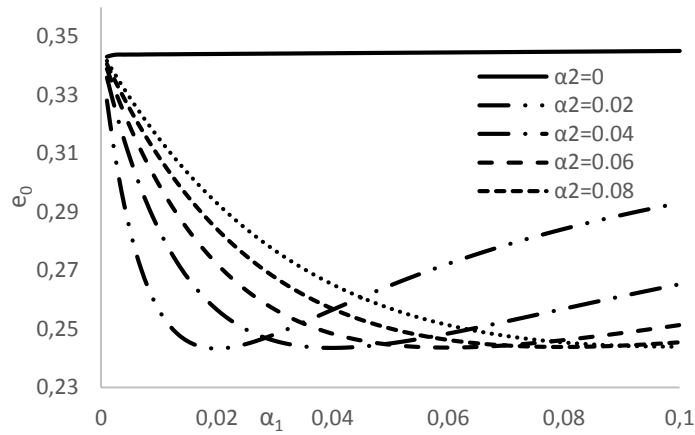


Fig. 43. Calibrated small length scale coefficient in free vibration versus α_1 for $\beta = 0.1$ and different values of α_2

α_2 is the thick beam case. It is worth noticing that in this case, the calibrated small length scale coefficient is nearly constant with respect to α_1 , as it has been shown in the literature [127]. For α_1 and α_2 both not equal to zero, it is seen that the calibrated small length scale coefficient is not constant and strongly depends on the value of α_1 .

Likewise, the small length scale coefficient is calibrated in Fig. 44 versus β for different values of α_2 with α_1 constant, equal to 0.05.

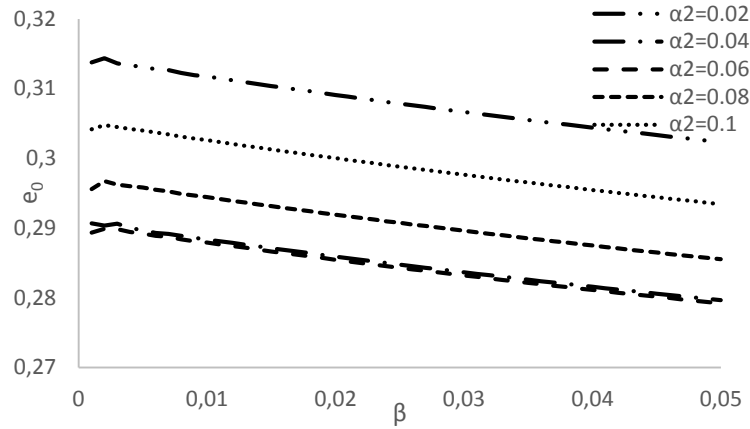


Fig. 44. Calibrated small length scale coefficient in free vibration versus β for $\alpha_1 = 0.05$ and different values of β

Again, the small length scale coefficient is not constant. It depends on α_2 and β . Thus, e_0 decreases when β increases.

For a particular set of parameter (χ, m, n, β) equal to $(1, 1, 1, 0.5)$, it is seen that the calibrated small length scale coefficient is equal to 0.243. Taking this value, as shown in Fig. 45, the curve of the non-dimensional natural frequency perfectly fits the one of the reference lattice model:

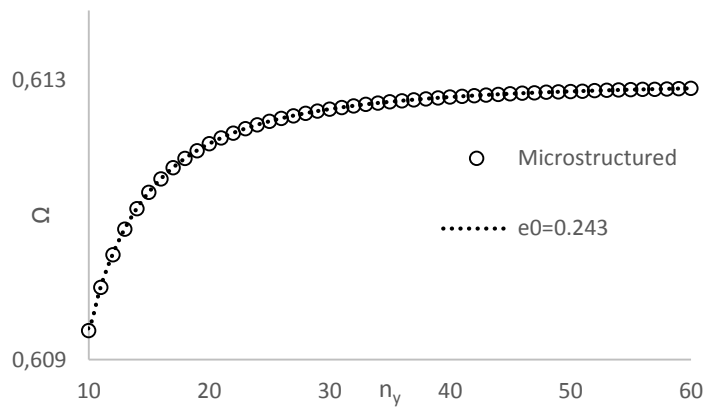


Fig. 45. Nondimensional frequency of all round simply supported nonlocal plate with respect to the length scale coefficient and n_y for a set of parameters $(\chi, m, n, \beta) = (1, 1, 1, 0.5)$ and $e_0 = 0.243$ considering the fourth order phenomenological model

This value of the small length scale coefficient is valid for this particular set of parameters. Thus, Fig. 46 depicts the non-dimensional natural frequency for a set of parameters (χ, m, n, β) equal to $(2,2,1,0.5)$ versus the number of elements n_y for $e_0 = 0.243$ and $e_0 = 0.329$, calibrated coefficient for this new set of parameters.

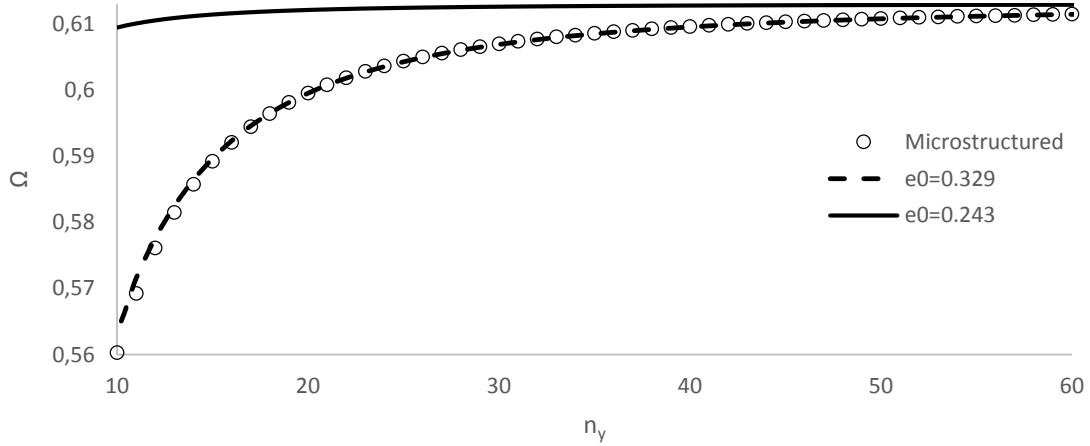


Fig. 46. Nondimensional frequency of all round simply supported nonlocal plate with respect to the length scale coefficient and n_y for a set of parameters $(\chi, m, n, \beta) = (2,2,1,0.5)$ and e_0 equal to 0.243 and 0.329 considering the fourth order phenomenological model

Thus, the first calibrated small length scale coefficient is no longer valid for another set of parameters.

4.3.3. Fourth order continualized model

Applying the Padé approximants defined before on the discrete governing difference equation:

$$\begin{aligned}
 & [L_{a,x}^2 + 2L_{a,x}L_{a,y} + L_{a,y}^2][w] - \frac{N}{\kappa Gh} [L_{a,x}^2 + (s+1)L_{a,x}L_{a,y} + sL_{a,y}^2][w] \\
 & + \frac{N}{D} (L_{a,x} + sL_{a,y})[w] - \frac{m_0\omega^2}{D} w + \frac{1}{D} \left(\frac{m_0}{\kappa Gh} D + m_2 \right) (L_{a,x} + L_{a,y})\omega^2[w] \quad (4.127) \\
 & + \frac{m_0m_2\omega^4}{\kappa GhD} w = 0
 \end{aligned}$$

or,

$$\begin{aligned}
& \left[\frac{\frac{\partial^4}{\partial x^4}}{\left(1 - \frac{a^2}{12} \frac{\partial^2}{\partial x^2}\right)^2} + 2 \frac{\frac{\partial^4}{\partial x^2 \partial y^2}}{\left(1 - \frac{a^2}{12} \frac{\partial^2}{\partial x^2}\right) \left(1 - \frac{a^2}{12} \frac{\partial^2}{\partial y^2}\right)} + \frac{\frac{\partial^4}{\partial y^4}}{\left(1 - \frac{a^2}{12} \frac{\partial^2}{\partial y^2}\right)^2} \right] w \\
& - \frac{N}{\kappa Gh} \left[\frac{\frac{\partial^4}{\partial x^4}}{\left(1 - \frac{a^2}{12} \frac{\partial^2}{\partial x^2}\right)^2} + \frac{(s+1) \frac{\partial^4}{\partial x^2 \partial y^2}}{\left(1 - \frac{a^2}{12} \frac{\partial^2}{\partial x^2}\right) \left(1 - \frac{a^2}{12} \frac{\partial^2}{\partial y^2}\right)} \right. \\
& \left. + s \frac{\frac{\partial^4}{\partial y^4}}{\left(1 - \frac{a^2}{12} \frac{\partial^2}{\partial y^2}\right)^2} \right] w + \frac{N}{D} \left(\frac{\frac{\partial^2}{\partial x^2}}{1 - \frac{a^2}{12} \frac{\partial^2}{\partial x^2}} + s \frac{\frac{\partial^2}{\partial y^2}}{1 - \frac{a^2}{12} \frac{\partial^2}{\partial y^2}} \right) w \\
& - \frac{m_0 \omega^2}{D} w + \frac{1}{D} \left(\frac{m_0}{\kappa Gh} D + m_2 \right) \left(\frac{\frac{\partial^2}{\partial x^2}}{1 - \frac{a^2}{12} \frac{\partial^2}{\partial x^2}} + \frac{\frac{\partial^2}{\partial y^2}}{1 - \frac{a^2}{12} \frac{\partial^2}{\partial y^2}} \right) \omega^2 w \\
& + \frac{m_0 m_2 \omega^4}{\kappa Gh D} w = 0
\end{aligned} \tag{4.128}$$

As for the fourth and sixth order continualized thin plate problem, the small length scale coefficient is arbitrarily chosen equal to $1/\sqrt{12}$. This value is retained in this model.

Multiplying by $[1 - (e_0 a)^2 \nabla^2]^2$

$$\begin{aligned}
& \left[\nabla^2 - 4(e_0 a)^2 \frac{\partial^4}{\partial x^2 \partial y^2} \right] \nabla^2 w \\
& + \frac{\lambda}{(\chi L)^2} \left\{ [1 - (e_0 a)^2 \nabla^2] \left(\frac{\partial^2}{\partial x^2} + s \frac{\partial^2}{\partial y^2} \right) \right. \\
& \left. - (s+1)(e_0 a)^2 \frac{\partial^4}{\partial x^2 \partial y^2} \right\} w \\
& - \frac{\mu_s}{\zeta^2} \lambda \left\{ \frac{\partial^4}{\partial x^4} + s \frac{\partial^4}{\partial y^4} - 2(e_0 a)^2 \frac{\partial^4}{\partial x^2 \partial y^2} \left(\frac{\partial^2}{\partial x^2} + s \frac{\partial^2}{\partial y^2} \right) \right. \\
& \left. + (s+1)[1 - (e_0 a)^2 \nabla^2] \frac{\partial^4}{\partial x^2 \partial y^2} \right\} w \\
& - \frac{1}{(\chi L)^4} (1 - 2(e_0 a)^2 \nabla^2) \left[1 - \frac{\mu_s}{\zeta^4} \Omega^2 \right] \Omega^2 w \\
& + \frac{\Omega^2 (\mu_s + 1)}{(\chi L \zeta)^2} \left(\nabla^2 - (e_0 a)^2 \nabla^4 - 2(e_0 a)^2 \frac{\partial^4}{\partial x^2 \partial y^2} \right) w = 0
\end{aligned} \tag{4.129}$$

For a plate that is simply supported at all edges, the solution is obtained by substituting Eq.

(2.118) into Eq. (4.129):

$$\begin{aligned}
& \left[(\chi m)^2 + n^2 - 4 \left(\frac{e_0 a \pi m n}{L} \right)^2 \right] \pi^4 [(\chi m)^2 + n^2] \\
& - \pi^2 \lambda \left\{ (\chi m)^2 + s n^2 + \left(\frac{e_0 a \pi}{\chi L} \right)^2 [(\chi m)^4 + 2(s+1)(\chi m n)^2 + s n^4] \right\} \\
& - \pi^4 \frac{\mu_s}{\zeta^2} \lambda \left\{ (\chi m)^4 + (s+1)(\chi m n)^2 + s n^4 \right. \\
& \left. + (e_0 a)^2 \left(\frac{\pi}{\chi L} \right)^2 [(s+3)(\chi m)^4 n^2 + (3s+1)(\chi m)^2 n^4] \right\} \\
& - \left(1 + 2(e_0 a)^2 \left(\frac{\pi}{\chi L} \right)^2 [(\chi m)^2 + n^2] \right) \left[1 - \frac{\mu_s}{\zeta^4} \Omega^2 \right] \Omega^2 \\
& - \frac{\pi^2}{\zeta^2} \Omega^2 (\mu_s + 1) \left((\chi m)^2 + n^2 + \left(\frac{e_0 a \pi}{\chi L} \right)^2 [(\chi m)^2 + 4(\chi m n)^2 + n^2] \right) = 0
\end{aligned} \tag{4.130}$$

Assuming $n = 1$, in statics, $\Omega = 0$ and the buckling load is expressed as follows

$$\begin{aligned}
\lambda = \min_m \left\{ [(\chi m)^2 + s] \left[(m\pi)^2 \tilde{D}_h + \frac{\pi^2 \mu_s}{\zeta^2} + 1 \right] \right. \\
+ \left(\frac{e_0 a \pi}{\chi L} \right)^2 \{ (\chi m)^4 + 2(s+1)(\chi m)^2 + s \\
+ [(s+3)(\chi m)^2 + (3s+1)](m\pi)^2 \tilde{D}_h \} \Bigg\}^{-1} \left[(\chi m)^2 + 1 \right. \\
\left. + 4 \left(\frac{e_0 a \pi m}{L} \right)^2 \right] \pi^2 [(\chi m)^2 + 1]
\end{aligned} \tag{4.131}$$

It is seen that when ζ decreases, the shear effect becomes more important and, as for natural frequencies in dynamics, the nondimensional buckling load decreases. When ζ goes to infinite, the shear effect is negligible and the nondimensional buckling load is reduced to the one obtained in the case of thin plates.

In free vibration, $\lambda = 0$ and Eq. (4.130) becomes

$$[\tilde{\alpha} + 4e_0^2 \alpha_1 \alpha_2] - (1 + 2e_0^2 \tilde{\alpha}) \tilde{\alpha} [1 - \mu_s \beta^2 \tilde{\Omega}^2] \tilde{\Omega}^2 - \beta \tilde{\Omega}^2 (\mu_s + 1) (\tilde{\alpha} + e_0^2 \tilde{\alpha}^2 + 2e_0^2 \alpha_1 \alpha_2) = 0 \tag{4.132}$$

yielding to the following non dimensional natural frequency:

$$\begin{aligned}
\tilde{\Omega}^2 = \frac{1}{2\mu_s \beta^2 (1 + 2e_0^2 \tilde{\alpha}) \tilde{\alpha}} \left\{ (1 + 2e_0^2 \tilde{\alpha}) \tilde{\alpha} + \beta (\mu_s + 1) (\tilde{\alpha} + e_0^2 \tilde{\alpha}^2 + 2e_0^2 \alpha_1 \alpha_2) \right. \\
\left. \pm \{ [(1 + 2e_0^2 \tilde{\alpha}) \tilde{\alpha} + \beta (\mu_s + 1) (\tilde{\alpha} + e_0^2 \tilde{\alpha}^2 + 2e_0^2 \alpha_1 \alpha_2)]^2 \right. \\
\left. - 4\mu_s \beta^2 (1 + 2e_0^2 \tilde{\alpha}) \tilde{\alpha} (\tilde{\alpha} + 4e_0^2 \alpha_1 \alpha_2) \}^{\frac{1}{2}} \right\}
\end{aligned} \tag{4.133}$$

4.3.4. Sixth order continualized model

The sixth order continualized model is based on the continualization of the equations of motion Eq. (4.108):

$$\begin{aligned}
 D \left[L_{a,x}[\psi_x] + \frac{(1-\nu)}{2} L_{a,y}[\psi_x] + \frac{(1+\nu)}{2} L_{a,x}^{\frac{1}{2}} L_{a,y}^{\frac{1}{2}}[\psi_y] \right] - \kappa^2 Gh \left(\psi_x + L_{a,x}^{\frac{1}{2}}[w] \right) &= -m_2 \omega^2 \theta_x \\
 D \left[\frac{(1-\nu)}{2} L_{a,x}[\psi_y] + \frac{(1+\nu)}{2} L_{a,x}^{\frac{1}{2}} L_{a,y}^{\frac{1}{2}}[\psi_x] + L_{a,y}[\psi_y] \right] - \kappa^2 Gh \left(\psi_y + L_{a,y}^{\frac{1}{2}}[w] \right) &= -m_2 \omega^2 \theta_y \\
 L_{a,x}(\kappa^2 Gh - N)[w] + L_{a,y}(\kappa^2 Gh - sN)[w] + \kappa^2 Gh L_{a,x}^{\frac{1}{2}}[\psi_x] + \kappa^2 Gh L_{a,y}^{\frac{1}{2}}[\psi_y] &= -m_0 \omega^2 w
 \end{aligned} \tag{4.134}$$

or, using the Taylor expansion at the second order in a ,

$$\begin{aligned}
 D \left[\left(1 + \frac{a^2}{12} \frac{\partial^2}{\partial x^2} \right) \frac{\partial^2 \psi_x}{\partial x^2} + \frac{(1-\nu)}{2} \left(1 + \frac{a^2}{12} \frac{\partial^2}{\partial y^2} \right) \frac{\partial^2 \psi_x}{\partial y^2} + \frac{(1+\nu)}{2} \left(1 + \frac{a^2}{24} \nabla^2 \right) \frac{\partial^2 \psi_y}{\partial x \partial y} \right] \\
 - \kappa^2 Gh \left[\psi_x + \left(1 + \frac{a^2}{24} \frac{\partial^2}{\partial x^2} \right) \frac{\partial w}{\partial x} \right] &= -m_2 \omega^2 \theta_x \\
 D \left[\frac{(1-\nu)}{2} \left(1 + \frac{a^2}{12} \frac{\partial^2}{\partial x^2} \right) \frac{\partial^2 \psi_y}{\partial x^2} + \frac{(1+\nu)}{2} \left(1 + \frac{a^2}{24} \frac{\partial^2}{\partial x^2} + \frac{a^2}{24} \frac{\partial^2}{\partial y^2} \right) \frac{\partial^2 \psi_x}{\partial x \partial y} + \left(1 + \frac{a^2}{12} \frac{\partial^2}{\partial y^2} \right) \frac{\partial^2 \psi_y}{\partial y^2} \right] \\
 - \kappa^2 Gh \left[\psi_y + \left(1 + \frac{a^2}{24} \frac{\partial^2}{\partial y^2} \right) \frac{\partial w}{\partial y} \right] &= -m_2 \omega^2 \theta_y \\
 \kappa^2 Gh \left[\left(1 + \frac{a^2}{12} \frac{\partial^2}{\partial x^2} \right) \frac{\partial^2 w}{\partial x^2} + \left(1 + \frac{a^2}{12} \frac{\partial^2}{\partial y^2} \right) \frac{\partial^2 w}{\partial y^2} + \left(1 + \frac{a^2}{24} \frac{\partial^2}{\partial x^2} \right) \frac{\partial \psi_x}{\partial x} + \left(1 + \frac{a^2}{24} \frac{\partial^2}{\partial y^2} \right) \frac{\partial \psi_y}{\partial y} \right] \\
 - N \left\{ \left(1 + \frac{a^2}{12} \frac{\partial^2}{\partial x^2} \right) \frac{\partial^2 w}{\partial x^2} + s \left(1 + \frac{a^2}{12} \frac{\partial^2}{\partial y^2} \right) \frac{\partial^2 w}{\partial y^2} \right\} &= -m_0 \omega^2 w
 \end{aligned} \tag{4.135}$$

Manipulating these three equations of motion leads to the governing differential equation in displacement, arbitrarily choosing e_0 equal to $1/\sqrt{12}$

$$\begin{aligned}
& \left[\nabla^4 + 2(e_0 a)^2 \left(\frac{\partial^4}{\partial x^4} + \frac{\partial^4}{\partial y^4} \right) \nabla^2 \right] w \\
& - \frac{N}{\kappa^2 G h} \left[\frac{\partial^4}{\partial x^4} + 2(e_0 a)^2 \frac{\partial^6}{\partial x^6} + (s+1)(1 + (e_0 a)^2 \nabla^2) \frac{\partial^4}{\partial x^2 \partial y^2} \right. \\
& \left. + s \frac{\partial^4}{\partial y^4} + 2(e_0 a)^2 s \frac{\partial^6}{\partial y^6} \right] w \\
& + \frac{N}{D} \left\{ \left(1 + (e_0 a)^2 \frac{\partial^2}{\partial x^2} \right) \frac{\partial^2}{\partial x^2} w + s \left(1 + (e_0 a)^2 \frac{\partial^2}{\partial y^2} \right) \frac{\partial^2}{\partial y^2} w \right\} \\
& - \frac{m_0 \omega^2}{D} w + \left(\frac{m_0}{\kappa G h} + \frac{m_2}{D} \right) \left[\nabla^2 + (e_0 a)^2 \left(\frac{\partial^4}{\partial x^4} + \frac{\partial^4}{\partial y^4} \right) \right] \omega^2 w \\
& + \frac{m_0 m_2 \omega^4}{\kappa G h D} w = 0
\end{aligned} \tag{4.136}$$

Considering an all edges simply supported plate, substituting Eq. (2.118) into Eq. (4.136), it leads

$$\begin{aligned}
& \pi^4 \left[(\chi m)^2 + n^2 - 2[(\chi m)^4 + n^4] \left(\frac{e_0 a \pi}{\chi L} \right)^2 \right] [(\chi m)^2 + n^2] \\
& - \pi^4 \frac{\lambda \mu_s}{\zeta^2} \left[(\chi m)^4 + (s+1)(\chi m n)^2 + s n^4 \right. \\
& \left. - \left(\frac{e_0 a \pi}{\chi L} \right)^2 [2(\chi m)^6 + (s+1)(\chi m)^4 n^2 + (s+1)(\chi m)^2 n^4 + 2s n^6] \right] \\
& - \pi^2 \lambda \left\{ (\chi m)^2 + s n^2 - \left(\frac{e_0 a \pi}{\chi L} \right)^2 [(\chi m)^4 + s n^4] \right\} - \Omega^2 \\
& - \Omega^2 (\mu_s + 1) \left(\frac{\pi}{\zeta} \right)^2 \left[(\chi m)^2 + n^2 - \left(\frac{e_0 a \pi}{\chi L} \right)^2 [(\chi m)^4 + n^4] \right] + \frac{\mu_s}{\zeta^4} \Omega^4 = 0
\end{aligned} \tag{4.137}$$

In statics, the non-dimensional critical buckling load is expressed as

$$\begin{aligned}
\lambda = \min_{(m,n)} & \left\{ \mu_s \frac{\pi^2}{\zeta^2} [(\chi m)^2 + n^2][(\chi m)^2 + sn^2] \right. \\
& - \mu_s \frac{\pi^2}{\zeta^2} \left(\frac{e_0 a \pi}{\chi L} \right)^2 [2(\chi m)^6 + 2sn^6 + (s+1)(\chi m)^4 n^2 \\
& + (s+1)(\chi m)^2 n^4] + (\chi m)^2 + sn^2 \\
& \left. - \left(\frac{e_0 a \pi}{\chi L} \right)^2 [(\chi m)^4 + sn^4] \right\}^{-1} \left\{ (\chi m)^2 + n^2 \right. \\
& \left. - 2 \left(\frac{e_0 a \pi}{\chi L} \right)^2 [(\chi m)^4 + n^4] \right\} \pi^2 [(\chi m)^2 + n^2]
\end{aligned} \tag{4.138}$$

Thus, the buckling load has been determined for both continualized models. In this expression, the small length scale coefficient is assumed constant, equal to $1/\sqrt{12}$. Figure 47 depicts the non-dimensional buckling load calculated from the reference lattice model and the two continualized models (fourth and sixth order) versus the number of elements n_y for a set of parameter (χ, m, n, s) arbitrarily chosen equal to $(1,1,1,0)$. It is seen that the curves coincide and both continualized models lead to an excellent approximation of the buckling load. This result is valid for any other set of parameters (χ, m, n, s) .

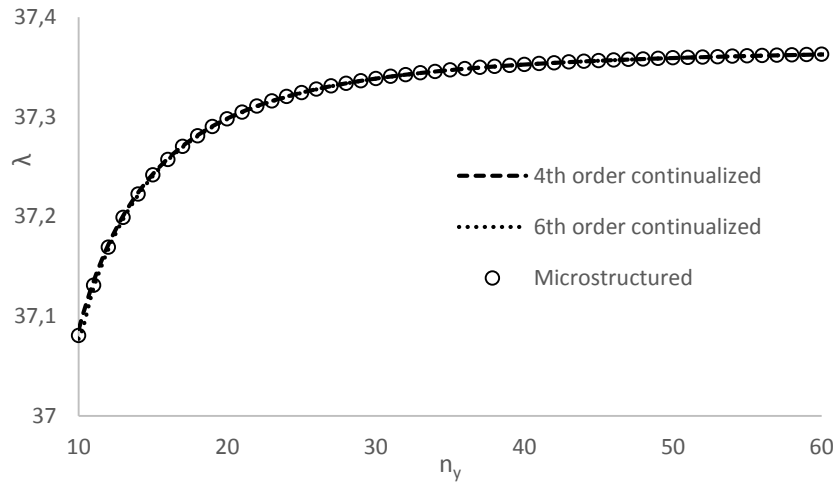


Fig. 47. Buckling loads of a simply supported nonlocal plate and lattice model for different n_y , following the fourth and sixth order continualized models for a set of parameters (χ, m, n, s) equal to $(1,1,1,0)$

Likewise, as for the phenomenological model, the small length scale coefficient has to be determined in free vibration.

In this case, for the sixth order continualized model, Eq. (4.137) becomes

$$\begin{aligned} \tilde{\alpha} - 2[\alpha_1^2 + \alpha_2^2]e_0^2 - \tilde{\alpha}\tilde{\Omega}^2 - \tilde{\alpha}\beta(\mu_s + 1)\tilde{\Omega}^2 + [\alpha_1^2 + \alpha_2^2]e_0^2\beta(\mu_s + 1)\tilde{\Omega}^2 \\ + \tilde{\alpha}\mu_s\beta^2\tilde{\Omega}^4 = 0 \end{aligned} \quad (4.139)$$

The non-dimensional natural frequency is obtained:

$$\begin{aligned} \tilde{\Omega}^2 = \frac{1}{2\tilde{\alpha}\mu_s\beta^2} \left\{ [\tilde{\alpha} + \tilde{\alpha}\beta(\mu_s + 1) - (\alpha_1^2 + \alpha_2^2)e_0^2\beta(\mu_s + 1)] \right. \\ \pm \{ [\tilde{\alpha} + \tilde{\alpha}\beta(\mu_s + 1) - (\alpha_1^2 + \alpha_2^2)e_0^2\beta(\mu_s + 1)]^2 \\ \left. - 4\tilde{\alpha}\mu_s\beta^2[\tilde{\alpha} - 2(\alpha_1^2 + \alpha_2^2)e_0^2] \}^{\frac{1}{2}} \right\} \end{aligned} \quad (4.140)$$

Thus, the non-dimensional natural frequencies have been derived for both continualized models. Figure 48 depicts $\tilde{\Omega}$ considering the reference lattice model and both continualized models (fourth and sixth order) versus the number of elements n_y for a set of parameters (χ, m, n, β) equal to $(1,1,1,0.5)$.

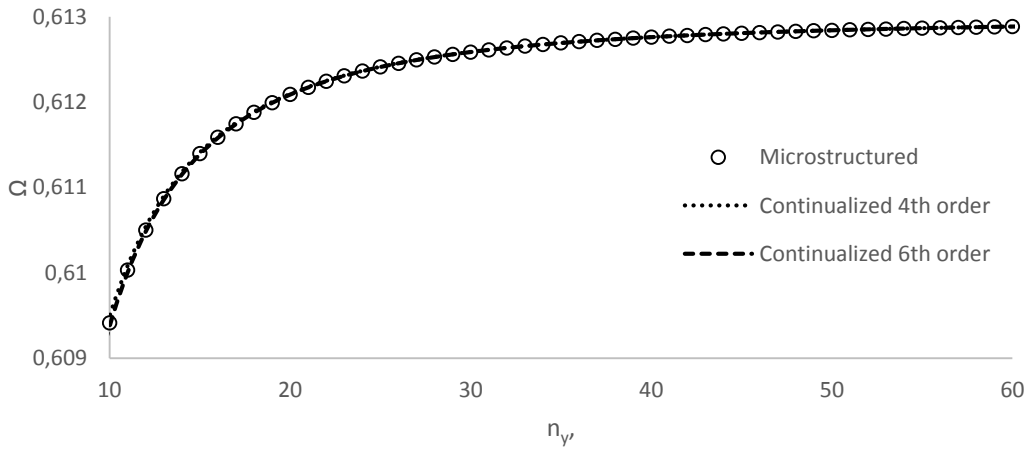


Fig. 48. Non-dimensional frequency $\tilde{\Omega}$ versus the number of elements n_y considering the microstructured model and the continualized models (fourth and sixth order), the phenomenological plate model $(\chi, m, n, \beta) = (1,1,1,0.5)$

The curves of the continualized model perfectly fit well the one of the reference model. Any other set of parameter (χ, m, n, β) would lead to the same result.

4.4. Discussion: superiority of the continualized models over the traditional phenomenological models

The different phenomenological models at the fourth and sixth order are derived before by postulating nonlocal constitutive laws and a local equilibrium equation. These models introduce a small length scale coefficient, assumed constant. When this coefficient is calibrated from the reference discrete model, it turns out to be structural, varying with the aspect and thickness ratio (through the shear parameter), the buckling and vibration mode and the type of analysis (buckling or vibration). Because of this dependence and this paradoxical result, the engineering phenomenological models provide unsatisfactory results and are not consistent; it is necessary to develop new micromechanically-based nonlocal models.

The continualized models are based on the derivation of continuous equations from the reference discrete model. Although they do not preserve the locality of the equilibrium equation, they consider, by construction of the model, a constant small length scale coefficient equal to $1/\sqrt{12}$ and lead to an excellent approximation of the buckling load. This value is independent on the type of analysis or the different previously given parameters.

When the non-dimensional buckling load or natural frequencies are calculated with respect to the number of elements n_y within the beam or plates, the phenomenological models constitute only an excellent approximation for one particular small length scale coefficient given for the particular set of parameters whereas for e_0 equal to $1/\sqrt{12}$, the continualized models lead to excellent results, whatever the parameters.

Thus, it clearly establishes the superiority of the continualized that provide much better results compared to the traditional phenomenological (stress gradient) models, at least with respect to lattice mechanics.

5. CONCLUSION AND RECOMMENDATIONS

This thesis derives several different beam and plate models and it is proposed in this section to briefly summarize them. First of all, at a macroscale, in addition to the well-known Bernoulli-Euler model valid for thin beam, three versions of the Bresse-Timoshenko thick beam model have been presented to take into account the rotary inertia and shear effects. The traditional original Bresse-Timoshenko model, widely used in the literature, derived through the use of equilibrium equations and the variational principle, may overcorrect the shear effect and it leads to two branches of natural frequencies. The second one does not appear in the asymptotic models at the second order. The second version is the truncated model. It is derived through the use of equilibrium equations and is asymptotically consistent at the second order. The last model is based on slope inertia and has been developed during this PhD. It is derived through the variational principle. The governing differential equation for these three models in free vibration is:

$$EI \frac{\partial^4 v}{\partial x^4} + \rho A \frac{\partial^2 v}{\partial t^2} - \rho I \left(1 + \frac{E}{\kappa G} \right) \frac{\partial^4 v}{\partial t^2 \partial x^2} + \gamma_1 \frac{\rho^2 I \partial^4 v}{\kappa G \partial t^4} + \gamma_2 \frac{\rho EI^2}{\kappa GA} \frac{\partial^6 v}{\partial x^4 \partial t^2} = 0 \quad (5.1)$$

where (γ_1, γ_2) is equal to $(1,0)$, $(0,0)$ and $(0,1)$ for the original Bresse-Timoshenko model, the truncated Bresse-Timoshenko theory and the Bresse-Timoshenko model based on slope inertia, respectively.

These models have been used to study some particular cases such as a beam with a tip mass (basic representation in robotics), a cracked beam, a beam in presence of a compressive force or a beam subjected to random transverse distributed loads.

The extension of the Bernoulli-Euler and Bresse-Timoshenko beam models to plates are the Kirchhoff-Love and Uflyand-Mindlin plate models. These models are governed by the following equation:

$$D \left(1 + \gamma_2 \frac{\rho h^2}{12 \kappa G} \frac{\partial^2}{\partial t^2} \right) \nabla^4 w + \rho h \frac{\partial^2 w}{\partial t^2} - \rho \frac{h^3}{12} \left(1 + \frac{12 D}{h^3 \kappa G} \right) \frac{\partial^2}{\partial t^2} \nabla^2 w + \gamma_1 \frac{\rho^2 h^3}{12 \kappa G} \frac{\partial^4 w}{\partial t^4} = 0 \quad (5.2)$$

with (γ_1, γ_2) equal to (1,0), (0,0) and (0,1) for the original Uflyand-Mindlin model, the truncated Uflyand-Mindlin model and the Uflyand-Mindlin model, respectively.

At a nanoscale, the interatomic interactions cannot be neglected and consequently, the nonlocal effect has to be introduced in the models. For thin beams and plates, different asymptotic models are possible following the direction of the nonlocality and differing at the zeroth order in the expression of the small length scale.

The engineering models, Bernoulli-Euler and Bresse-Timoshenko for beams, Kirchhoff-Love and Uflyand-Mindlin for plates, have been derived to take into account this additional effect. An alternative to the fourth order phenomenological Bernoulli-Euler thin beam model and fourth order phenomenological Kirchhoff-Love plate model has been suggested, namely the sixth order phenomenological model. For the thick beam and plate models, there is a debate in the literature to know whether the nonlocal effect should be included or not in the shear part of the constitutive law. The investigations carried out during this PhD show that the nonlocal effect affects both the bending and the shear part of the law. In this case, the nonlocal engineering model are governed by the following equation for beams

$$\begin{aligned} EI \frac{\partial^4 v}{\partial x^4} + \left(1 - \eta^2 \frac{\partial^2}{\partial x^2} \right) \left(\rho A - \frac{\rho EI}{\kappa G} \frac{\partial^2}{\partial x^2} \right) \frac{\partial^2 v}{\partial t^2} \\ - \rho I \frac{\partial^2}{\partial t^2} \left[\left(1 - \eta^2 \frac{\partial^2}{\partial x^2} \right) \frac{\partial^2 v}{\partial x^2} - \frac{I}{\kappa GA} \left(E + \eta^2 \rho \frac{\partial^2}{\partial t^2} \right) \frac{\partial^4 v}{\partial x^4} \right. \\ \left. - \left(\gamma_1 - \eta^2 \frac{\partial^2}{\partial x^2} \right) (\gamma_1 + \gamma_2) \frac{\rho}{\kappa G} \left(1 - \eta^2 \frac{\partial^2}{\partial x^2} \right) \frac{\partial^2 v}{\partial t^2} \right] = 0 \end{aligned} \quad (5.3)$$

with (γ_1, γ_2) equal to (1,0), (0,0) and (0,1) for the original Bresse-Timoshenko model, the truncated Bresse-Timoshenko model and the Bresse-Timoshenko model, respectively.

For plates:

$$\begin{aligned}
 D\nabla^4 w + (1 - \eta^2 \nabla^2) \left(\rho h - \frac{\rho}{\kappa G} D \nabla^2 \right) \frac{\partial^2 w}{\partial t^2} \\
 - \frac{\rho h^3}{12} \frac{\partial^2}{\partial t^2} \left\{ (1 - \eta^2 \nabla^2) \nabla^2 w - (\gamma_1 - \eta^2 \nabla^2) (\gamma_1 + \gamma_2) \frac{\rho}{\kappa G} (1 - \eta^2 \nabla^2) \frac{\partial^2 w}{\partial t^2} \right. \\
 \left. - \frac{\gamma_2}{\kappa G} \left(\frac{D}{h} + \frac{\eta^2 \rho h^2}{12} \frac{\partial^2}{\partial t^2} \right) \nabla^4 w \right\} = 0 \quad (5.4)
 \end{aligned}$$

with (γ_1, γ_2) equal to (1,0), (0,0) and (0,1) for the original Uflyand-Mindlin model, the truncated Uflyand-Mindlin model and the Uflyand-Mindlin model, respectively.

Furthermore, the small length scale coefficient introduced in the models had to be calibrated with respect to one microstructured physical model. In this purpose, the discrete thin beam and plate model and thick plate model have been derived. The latter is new and not given in the literature. By equating the buckling load in statics and the natural frequency in free vibration of the engineering models and the discrete models, the small length scale coefficient is found. This coefficient is paradoxically not constant, depending on different parameters such as the load or the geometry (aspect and thickness ratios) and the type of analysis, either buckling or vibration. Consequently, the stress gradient nonlocal models widely derived and used in the literature are not consistent because they are based on an assumption (a constant coefficient) that is not valid with respect to lattice mechanics.

Thus, to overcome this paradox, a new family of models has been investigated: the continualized models. These models are based on the derivation of continuous equations from the ones of the reference discrete models.

For thin beams, the governing differential equations are:

$$EI \left[1 + \gamma_1 (e_0 a)^2 \frac{d^2}{dx^2} \right] \frac{d^4 v}{dx^4} + N \left[1 - \gamma_2 (e_0 a)^2 \frac{d^2}{dx^2} \right] \frac{d^2 v}{dx^2} - m_0 \omega^2 \left[1 - \gamma_3 (e_0 a)^2 \frac{d^2}{dx^2} \right] v = 0 \quad (5.5)$$

where the triplet of parameters $(\gamma_1, \gamma_2, \gamma_3)$ is equal to $(0,1,2)$, $(1,0,1)$, $(0,1,1)$ and $(1,1,1)$ for the fourth and sixth order continualized model, the fourth and sixth order phenomenological models, respectively, the fourth order model coinciding with the Bernoulli-Euler model. In this case, the calibrated small length scale coefficients are:

$$e_{0,b} = \frac{1}{\sqrt{\gamma_1 + \gamma_2}} \frac{1}{2\sqrt{3}}; e_{0,v} = \frac{1}{\sqrt{\gamma_1 + \gamma_3}} \frac{1}{\sqrt{6}} \quad (5.6)$$

For thin plates:

$$\begin{aligned} D \left[\nabla^4 w + \gamma_1 (e_0 a)^2 \left(\frac{\partial^6 w}{\partial x^6} + \frac{\partial^6 w}{\partial y^6} \right) - (\gamma_1 + 4\gamma_3) (e_0 a)^2 \frac{\partial^4 \nabla^2 w}{\partial x^2 \partial y^2} \right] - m_0 \omega^2 w \\ + (1 + \gamma_3) (e_0 a)^2 \left[m_0 \omega^2 \nabla^2 w - P(1 + s) \frac{\partial^4 w}{\partial x^2 \partial y^2} \right] \\ + P \left(\frac{\partial^2 w}{\partial x^2} + s \frac{\partial^2 w}{\partial y^2} \right) - (\gamma_2 + \gamma_3) (e_0 a)^2 P \left(\frac{\partial^4 w}{\partial x^4} + s \frac{\partial^4 w}{\partial y^4} \right) = 0 \end{aligned} \quad (5.7)$$

with the triplet $(\gamma_1, \gamma_2, \gamma_3)$ is equal to $(0,0,1)$, $(1,0,0)$, $(0,1,0)$ and $(1,1,0)$ for the fourth order continualized model, the sixth order order continualized model, the fourth order phenomenological model and the sixth order phenomenological model, respectively. The calibrated small length scale coefficient is:

$$\begin{aligned} \frac{1}{e_{0,b}} = \sqrt{12} \left\{ \frac{\alpha^2 m^2 (\alpha^2 m^2 + 1) (s + 1)}{\alpha^6 m^6 + 2\alpha^4 m^4 s - \alpha^4 m^4 - \alpha^2 m^2 s + 2\alpha^2 m^2 + s} \right. \\ + (\gamma_1 + \gamma_3) \frac{\alpha^6 m^6 + \alpha^4 m^4 s - 2\alpha^4 m^4 - 2\alpha^2 m^2 s + \alpha^2 m^2 + s}{\alpha^6 m^6 + 2\alpha^4 m^4 s - \alpha^4 m^4 - \alpha^2 m^2 s + 2\alpha^2 m^2 + s} \\ \left. + \gamma_2 \frac{\alpha^6 m^6 + \alpha^4 m^4 + \alpha^2 m^2 s + s}{\alpha^6 m^6 + 2\alpha^4 m^4 s - \alpha^4 m^4 - \alpha^2 m^2 s + 2\alpha^2 m^2 + s} \right\}^{\frac{1}{2}} \quad (5.8) \\ \frac{1}{e_{0,v}} = \sqrt{6} \sqrt{\frac{(m^2 \alpha^2 + 1)^2 + (\gamma_1 + \gamma_3) (m^2 \alpha^2 - 1)^2}{1 + m^4 \alpha^4}} \end{aligned}$$

For thick plates:

$$\begin{aligned}
& \left\{ \nabla^4 + 2 \left[\gamma_3 \left(\frac{\partial^4}{\partial x^4} + \frac{\partial^4}{\partial y^4} \right) - 2\gamma_2 \frac{\partial^4}{\partial x^2 \partial y^2} \right] (e_0 a)^2 \nabla^2 \right\} w \\
& - \frac{N}{\kappa G h} \left[\frac{\partial^4}{\partial x^4} + (s+1)(1 + (e_0 a)^2 \nabla^2) \frac{\partial^4}{\partial x^2 \partial y^2} + s \frac{\partial^4}{\partial y^4} \right] w \\
& - \frac{N(e_0 a)^2}{\kappa G h} \left[(2\gamma_3 - \gamma_1) \left(\frac{\partial^6}{\partial x^6} + s \frac{\partial^6}{\partial y^6} \right) \right. \\
& - ((\gamma_1 + \gamma_2)(2s+4) + \gamma_1 s) \frac{\partial^6}{\partial x^4 \partial y^2} \\
& \left. - ((\gamma_1 + \gamma_2)(4s+2) + \gamma_1) \frac{\partial^6}{\partial x^2 \partial y^4} \right] w \\
& + \frac{N}{D} \left\{ \left(1 + (e_0 a)^2 \frac{\partial^2}{\partial x^2} \right) \frac{\partial^2}{\partial x^2} + s \left(1 + (e_0 a)^2 \frac{\partial^2}{\partial y^2} \right) \frac{\partial^2}{\partial y^2} \right. \\
& - 2(\gamma_1 + \gamma_2)(e_0 a)^2 \nabla^2 \left(\frac{\partial^2}{\partial x^2} + s \frac{\partial^2}{\partial y^2} \right) - \gamma_1 (s+1)(e_0 a)^2 \frac{\partial^4}{\partial x^2 \partial y^2} \left. \right\} w \\
& - \frac{m_0}{D} \omega^2 [1 - (\gamma_1 + 2\gamma_2)(e_0 a)^2 \nabla^2] w + \left(\frac{m_0}{\kappa G h} + \frac{m_2}{D} \right) \nabla^2 \omega^2 w \\
& + \left(\frac{m_0}{\kappa G h} + \frac{m_2}{D} \right) (e_0 a)^2 \left[\frac{\partial^4}{\partial x^4} + \frac{\partial^4}{\partial y^4} + 2\gamma_1 \frac{\partial^4}{\partial x^2 \partial y^2} \right. \\
& \left. - 2(\gamma_1 + \gamma_2) \nabla^4 \right] \omega^2 w + \frac{m_0 m_2 \omega^4}{\kappa G h D} (1 - 2(e_0 a)^2 \nabla^2) w \\
& - \gamma_1 \frac{N}{\kappa G h} \frac{m_2}{D} \omega^2 [1 - 2(\gamma_1 + \gamma_2)(e_0 a)^2 \nabla^2] \left(\frac{\partial^2}{\partial x^2} + s \frac{\partial^2}{\partial y^2} \right) w = 0
\end{aligned} \tag{5.9}$$

with $(\gamma_1, \gamma_2, \gamma_3)$ equal to $(1,0,0)$, $(0,1,0)$ and $(0,0,1)$ for the fourth order phenomenological model, the fourth order continualized model and the sixth order continualized model, respectively.

In the futures, different investigations could be carried out.

First of all, all the results in this thesis are established for isotropic structures. All of them would deserve to be extended to the case of orthotropic and anisotropic beams and plates.

This thesis started by presenting different versions of the Bresse-Timoshenko beam model and the Uflyand-Mindlin plate model. The models based on slope inertia, developed during this PhD, are extremely recent. There is no experimental or numerical result in the literature that would provide more argument to establish the superiority of a model over the others. Indeed, many

papers have been devoted to the study of the original Bresse-Timoshenko and Uflyand-Mindlin models. More investigations about the truncated models and the models based on slope inertia would show the differences and the similarities between those models and would help to better understand the influence of the rotary inertia and the shear effect on the mechanical behavior of the structure in vibration.

Moreover, at a nanoscale, the nonlocal effect is taken into account by introducing one small length scale coefficient, assumed constant, in the models, following the approach of Eringen. It would be interesting to develop other models, for example by introducing not one but several nonlocal coefficients. Although it has been shown that the nonlocal effect affects both the bending and the shear parts of the constitutive law, other studies (analytical but also numerical and experimental) are necessary to confirm this result.

Furthermore, the last chapter is based on the calibration of the small length scale coefficient and the development of continualized models from a lattice model with rectangular cells. This study was crucial to understand the principle of continualized approaches. However, most of nanomaterials cannot be represented by rectangular lattice. For instance, in graphene, as explained in introduction, the atoms are arranged through a honeycomb lattice. Although some works have been initiated in the literature to model this particular lattice [273-275], to our best knowledge, the explicit discrete governing differential equation in displacement has not been derived. Indeed, the difficulty is that each node of the lattice is connected to three direct neighbors and is also influenced by nine other nodes. One of the biggest challenges in a very near future will be to derive the equations in displacements and then, to propose continualized models and to compare the natural frequencies derived in the models with those available in the literature by using the molecular dynamic simulations.

Also, the solutions for the nonlocal models have been determined for simply supported beams and plates. To study the influence of the boundary conditions on the small length scale coefficient would represent an ambitious project.

Thus, this thesis is a first step of very and fascinating long stairs and huge progress have still to be made to have a full understanding of the mechanical behavior of nanomaterials in vibration and buckling.

REFERENCES

- [1] M. Sathyamoorthy, *Nonlinear Analysis of Structures*, CRC Press, Boca Raton, 1998.
- [2] S.P. Timoshenko, *History of strength of materials: with a brief account of the history of theory of elasticity and theory of structures*, Courier Corporation, New-York, 1953.
- [3] H. Yang, *Vibration Control for a Cantilever Beam with an Eccentric Tip Mass Using a Piezoelectric Actuator and Sensor*, IJAV. 22 (2017) 84-92.
- [4] J.C. Bruch, T.P. Mitchell, *Vibration of a mass-loaded clamped-free Timoshenko beam*, J. Sound Vib. 114 (1987) 341-345.
- [5] M. Gürgöze, *On the eigenfrequencies of a cantilever beam with attached tip mass and a spring-mass system*, J. Sound Vib. 190 (1996), 149-162.
- [6] M. Yaman, *Adomian decomposition method for solving a cantilever beam of varying orientation with tip mass*, J. Comput. Nonlinear Dynam. 2 (2007), 52-57.
- [7] C.W.S. To, *Vibration of a cantilever beam with a base excitation and tip mass*, J. Sound Vib. 83 (1982) 445-460.
- [8] R. Bhat, M.A. Kulkarni, *Natural frequencies of a cantilever with slender tip mass*, AIAA Journal 14 (1976), 536-537.
- [9] N.G.R. Iyengar, *Effects of transverse shear and rotary inertia on the natural frequency of a cantilever beam with a tip mass*, in: *Proceedings of the Shock and Vibration Conference*, Monash University, Melbourne, 1974.
- [10] C.F.T. Matt, *On the application of generalized integral transform technique to wind-induced vibrations on overhead conductors*, Int. J. Num. Meth. Eng. 78 (2009), 901-930.

- [11] S. Chinchalkar, Detection of the crack location in beams using natural frequencies, *J. Sound Vib.* 247 (2001) 417-429.
- [12] G.M. Owolabi, A.S.J. Swamidas, R. Seshadri, Crack detection in beams using changes in frequencies and amplitudes of frequency response functions, *J. Sound Vib.* 265 (2003) 1-22.
- [13] S. Teidj, A. Khamlichi, A. Driouach, Identification of beam cracks by solution of an inverse problem, *Procedia Technology*, 22 (2016) 86-93.
- [14] W. Xie, *Dynamic Stability of Structures*. Cambridge University Press, Cambridge, 2016.
- [15] I. Elishakoff, *Probabilistic Theory of Structures*, Wiley 1983; Dover 1999; World Scientific, 2017.
- [16] L.D. Lutes, S. Sarkani, *Random vibrations: analysis of structural and mechanical systems*, Butterworth-Heinemann, New-York, 2004.
- [17] N.C. Nigam, S. Narayanan, *Applications of random vibrations*, Springer-Verlag, 1994.
- [18] P.H. Wirsching, T.L. Paez, K.. *Random vibrations: theory and practice*, Courier Corporation, New-York, 2006.
- [19] S.H. Crandall, W.D. Mark, *Random vibration in mechanical systems*, Academic Press, New-York, 1963.
- [20] K.M. Liew, C.M. Wang, Y. Xiang, S. Kitipornchai, *Vibration of Mindlin Plates : Programming the p-Version Ritz Method*, Elsevier, Oxford, 1998.
- [21] E.T. Thostenson, Z. Ren, T.W. Chou, Advances in the science and technology of carbon nanotubes and their composites: a review. *Compos. Sci. Technol.* 61 (2001), 1899-1912.
- [22] S.B. Sinnott, R. Andrews, Carbon nanotubes: synthesis, properties, and applications, *Crit. Rev. Solid State Mater. Sci.* 26 (2001), 145-249
- [23] R.H. Baughman, A.A. Zakhidov, W.A. De Heer, Carbon nanotubes--the route toward applications, *Science*, 297 (2002), 787-792.
- [24] V.N. Popov, Carbon nanotubes: properties and application, *Mater. Sci. Eng., R* 43 (2004), 61-102.
- [25] H. Dai, Carbon nanotubes: opportunities and challenges, *Surface Science*, 500 (2002), 218-241.
- [26] K.M. Liew, Y. Zhang, L.W. Zhang, Nonlocal elasticity theory for graphene modeling and simulation : prospects and challenges, *Journal of Modeling in Mechanics and Materials* 1 (2017).
- [27] S. Iijima, Helical microtubules of graphitic carbon, *Nature*, 354 (1991), 56.

- [28] S. Iijima, High resolution electron microscopy of crystal lattice of titanium-niobium oxide, *J. Appl. Phys.*, 42 (1971) 5891-5893.
- [29] S. Iijima, High resolution electron microscopy of phase objects: Observation of small holes and steps on graphite crystals, *Optik*, 47 (1977) 437-452.
- [30] S. Iijima, Direct observation of the tetrahedral bonding in graphitized carbon black by high resolution electron microscopy, *J. Crystal Growth*, 50 (1980) 675-683.
- [31] J. Wood, The top ten advances in material science, *Mater Today*, 11 (2008), 40-45.
- [32] M.F. De Volder, S.H. Tawfick, R.H. Baughman, A.J. Hart, Carbon nanotubes: present and future commercial applications, *Science*, 339 (2013), 535-539.
- [33] M.M.J Treacy, T.W. Ebbesen, T.M. Gibson, Exceptionally High young's modulus observed for individual carbon nanotubes, *Nature* 381 (1996) 680–687.
- [34] N. Yao, V. Lordi, Young's modulus of single-walled carbon nanotubes. *J. Appl. Phys.* 84 (1998) 1939-1943.
- [35] B.I. Yakobson, M.P. Campbell, C.J. Brabec, J. Bernholc, High strain rate fracture and C-chain unraveling in carbon nanotubes, *Comput. Mater. Sci.* 8 (1997) 341–8.
- [36] A. Bianco, K. Kostarelos, M. Prato, Applications of carbon nanotubes in drug delivery, *Curr. Opin. Chem. Biol.* 9 (2005) 674-679.
- [37] N. Sinha, J.W. Yeow, Carbon nanotubes for biomedical applications. *IEEE Trans. Nanobioscience* 4 (2005) 180-195.
- [38] M.S. Digge, R.S. Moon, S.G. Gattani, Applications of carbon nanotubes in drug delivery: a review. *Int. J. Pharmtech Res.* 4 (2012), 839-847.
- [39] S.R. Ji, C. Liu, B. Zhang, F. Yang, J. Xu, J. Long, X.J. Yu, Carbon nanotubes in cancer diagnosis and therapy, *Biochim. Biophys. Acta*, 1806 (2010) 29-35.
- [40] Z. Liu, J.T. Robinson, S.M. Tabakman, K. Yang, H. Dai, Carbon materials for drug delivery & cancer therapy, *Materials today*, 14 (2011), 316-323.
- [41] S. Vardharajula, S.Z. Ali, P.M. Tiwari, E. Eroğlu, K. Vig, V.A. Dennis, S.R. Singh, Functionalized carbon nanotubes: biomedical applications. *Int. J. Nanomed.* 7 (2012) 5361.
- [42] A. Elhissi, W. Ahmed, I.U. Hassan, V.R. Dhanak, K. Subramani, Carbon nanotubes in cancer therapy and drug delivery, *Emerging Nanotechnologies in Dentistry* (2012) 347-363.
- [43] M. Trojanowicz, Analytical applications of carbon nanotubes: a review, *TrAC*, 25 (2006), 480-489.

- [44] W. Yang, P. Thordarson, J.J. Gooding, S.P. Ringer, F. Braet, Carbon nanotubes for biological and biomedical applications. *Nanotechnology*, 18 (2007), 412001.
- [45] C.M. Tîlmaciu, M.C. Morris, Carbon nanotube biosensors, *Front. Chem.* 3 (2015) 59.
- [46] S. Saito, Y. Usui, K. Aoki, N. Narita, M. Shimizu, K. Hara, S. Taruta, Carbon nanotubes: biomaterial applications. *Chem. Soc. Rev.* 38 (2009) 1897-1903.
- [47] R. Hirlekar, M. Yamagar, H. Garse, M. Vij, V. Kadam, Carbon nanotubes and its applications: a review. *Asian J. Pharm. Clin. Res.* 2 (2009), 17-27.
- [48] E. Pop, D. Mann, Q. Wang, K. Goodson, H. Dai, Thermal conductance of an individual single-wall carbon nanotube above room temperature, *Nano letters* 6 (2006) 96-100.
- [49] P.G. Collins, P. Avouris, Nanotubes for electronics. *Scientific American* 283 (2000) 62–9.
- [50] K.S. Novoselov, A.K. Geim, S.V. Morozov, D. Jiang, Y. Zhang, S.V. Dubonos, A.A. Firsov, Electric field effect in atomically thin carbon films. *Science* 306 (2004) 666-669.
- [51] E. Gerstner, Nobel Prize 2010: Andre Geim & Konstantin Novoselov, *Nature Physics* 6 (2010) 836.
- [52] A.K. Geim, Nobel Lecture: Random walk to graphene. *Rev. Mod. Phys.* 83 (2011) 851.
- [53] K.S. Novoselov, Nobel lecture: Graphene: Materials in the flatland. *Rev. Mod. Phys.* 83 (2011) 837.
- [54] A.K. Geim, K.S. Novoselov, The rise of graphene. *Nature materials*, 6 (2007) 183-191.
- [55] H. Rafei-Tabar, E. Ghavanloo, S.A. Fazelzadeh, Nonlocal continuum-based modeling of mechanical characteristics of nanoscopic structures, *Physics Reports* 638 (2016) 1-97.
- [56] K.S. Novoselov, V.I. Fal, L. Colombo, P.R. Gellert, M.G. Schwab, K. Kim, A roadmap for grapheme, *Nature*, 490 (2012) 192-200.
- [57] N. Savage, Materials science: Super carbon, *Nature*, 483 (2012) 30-31.
- [58] K.A. Jenkins, Graphene in High-Frequency Electronics, *American Scientist*, 100 (2012), 388.
- [59] E.S. Reich, Graphene knock-offs probe ultrafast electronics, *Nature*, 497 (2013) 422-423.
- [60] K. Bourzac, Electronics: back to analogue. *Nature*, 483 (2012) 34-36.
- [61] S.V. Morozov, K.S. Novoselov, M.I. Katsnelson, F. Schedin, D.C. Elias, J.A. Jaszczak, A.K. Geim, Giant intrinsic carrier mobilities in graphene and its bilayer, *Phys. Rev. Lett.* 100 (2008) 016602.
- [62] A.S. Brown, Nanotechnology for the brain, *Mechanical Engineering*, 136 (2014) 30.
- [63] Y. Alapan, I. Sayin, U.A. Gurkan, Making the smallest medical devices, *Mechanical Engineering* 136 (2014) 36.

- [64] J.M. Hamm, O. Hess, Two two-dimensional materials are better than one. *Science* 340 (2013) 1298-1299.
- [65] E. Ghavanloo, S.A. Fazelzadeh, Vibration characteristics of single-walled carbon nanotubes based on an anisotropic elastic shell model including chirality effect, *Appl. Math. Modelling* 36 (2012) 4988-5000.
- [66] L.F. Wang, Q.S. Zheng, J.Z. Liu, Q. Jiang, Size dependence of the thin-wall models for carbon nanotubes, *Phys. Rev. Lett.* 95 (2005) 105501.
- [67] J.C. Hsu, R.P. Chang, W.J. Chang, Resonance frequency of chiral single-walled carbon nanotubes using Timoshenko beam theory, *Phys. Lett. A* 372 (2008) 2757-2759.
- [68] A. Benzair, A. Tounsi, A. Besseghier, H. Heireche, N. Moulay, L. Boumia, The thermal effect on vibration of single-walled carbon nanotubes using nonlocal Timoshenko beam theory. *J. Phys. D* 41 (2008) 225404.
- [69] M.A. Shah, T. Ahmad, *Principles of nanoscience and nanotechnology*. Alpha Science International, 2010.
- [70] I. Elishakoff, C. Soret, A consistent set of nonlocal Bresse–Timoshenko equations for nanobeams with surface effects, *J. Appl. Mech.* 80 (2013) 061001.
- [71] X.W. Lei, T. Natsuki, J.X. Shi, Q.Q. Ni, Surface effects on the vibrational frequency of double-walled carbon nanotubes using the nonlocal Timoshenko beam model, *Composites Part B* 43 (2012) 64–69.
- [72] H.L. Lee, W.J. Chang, Surface Effects on Frequency Analysis of Nanotubes Using Nonlocal Timoshenko Beam Theory. *J. Appl. Phys.* 108 (2010) 093503.
- [73] N. Challamel, I. Elishakoff, Surface stress effects may induce softening: Euler–Bernoulli and Timoshenko buckling solutions, *Physica E* 44 (2012) 1862–7.
- [74] Wang GF and Feng XQ. Timoshenko beam model for buckling and vibration of nanowires with surface effects. *J Phys D Appl Phys* 2009; 42:155411.
- [75] T. Belin, F. Epron, Characterization methods of carbon nanotubes: a review. *Mat. Sci. Eng.* 119 (2005) 105-118.
- [76] D.R. Cooper, B. D’Anjou, N. Ghattamaneni, B. Harack, M. Hilke, A. Horth, N. Majlis, M. Massicotte, L. Vandsburger, E. Whiteway, V. Yu, Experimental review of graphene. *ISRN Condensed Matter Physics* (2012).
- [77] M. Paradise, T. Goswami, Carbon nanotubes–production and industrial applications, *Materials & Design* 28 (2007) 1477-1489.

- [78] A. Chuvilin, U. Kaiser, E. Bichoutskaia, N.A. Besley, A.N. Khlobystov Direct transformation of graphene to fullerene, *Nature chemistry* 2 (2010) 450-453.
- [79] B. Arash, Q. Wang, A review on the application of nonlocal elastic models in modeling of carbon nanotubes and graphenes. *Comput. Mater. Sci.* 51 (2012) 303-313.
- [80] B. Arash, Q. Wang, K.M. Liew, Wave propagation in graphene sheets with nonlocal elastic theory via finite element formulation. *Comput. Methods Appl. Mech. Eng.* 223 (2012) 1-9.
- [81] E. Cadelano, P.L. Palla, S. Giordano, L. Colombo, Nonlinear elasticity of monolayer graphene, *Phys. Rev. Lett.* 102 (2009) 55021-55024.
- [82] H. Zhao, K. Min, N.R. Aluru, Size and chirality dependent elastic properties of graphene nanoribbons under uniaxial tension, *Nano. Lett.* 9 (2009) 3012–3015.
- [83] R. Chowdhury, S. Adhikari, F. Scarpa, M.I. Friswell, Transverse vibration of single-layer graphene sheets, *J. Phys. D* 44 (2011), 205401
- [84] B. Arash, Q. Wang, Vibration of single-and double-layered graphene sheets, *J. Nanotechnol. Eng. Med.* 2 (2011) 011012.
- [85] D. Bernoulli, De vibrationibus et sono laminarum lasticarum. *Commentarii Academiae Scientiarum Imperialis Petropolitanae*, 13 (1751) 105-120.
- [86] L. Euler, Methodus inveniendi lineas curvas maximi minimive proprietate gaudentes, Additamentum I, De curvis elasticis. Lausanne, Genf: Bousquet & Socios, 1744.
- [87] J. Bresse, Cours de Mécanique Appliquée. Mallet-Bachelier, Paris, 1859.
- [88] J.W.S. Rayleigh, The Theory of Sound, Macmillan, London, 1877.
- [89] S.P. Timoshenko, On the correction for shear of the differential equation for transverse vibrations of prismatic bars, *Philos. Mag.* 41 (1921) 744-746.
- [90] I. Elishakoff, J. Kaplunov, E. Nolde, Celebrating the centenary of Timoshenko’s study of effects of shear deformation and rotary inertia. *App. Mech. Rev.* 67 (2015) 060802.
- [91] F. Hache, I. Elishakoff, N. Challamel, Some closed-form solutions in random vibration of beams using different models. *Probabilistic Engineering Mechanics*, in submission, 2017.
- [92] I. Elishakoff, F. Hache, N. Challamel, Critical comparison of three versions of Bresse-Timoshenko beam theory for parametric instability, *AIAA journal.* 56 (2017) 438-442.
- [93] I. Elishakoff, F. Hache, N. Challamel, Parametric Instability of Bresse-Timoshenko Columns Revisited under a pulsating load, Submitted to *Journal of Sound and Vibration*, 2017.
- [94] I. Elishakoff, F. Hache, N. Challamel, Critical Contrasting of Three Versions of Vibrating Bresse-Timoshenko Beam with a Crack. *Int. J. Solids Struct.* 109 (2017) 143-151.

- [95] I. Elishakoff, F. Hache, N. Challamel, Variational Derivation of Governing Differential Equations for Truncated Version of Bresse-Timoshenko Beams, In submission, 2018.
- [96] Y.M. Ghugal, R.P. Shimpi, A review of refined shear deformation theories for isotropic and anisotropic laminated beams, *J. Reinf. Plast. Compos.* 20 (2001) 255-272.
- [97] M. Hajianmaleki, M.S. Qatu, Vibrations of straight and curved composite beams: A review, *Compos. Struct.* 100 (2013) 218-232.
- [98] S. Germain, Remarques sur la nature, les bornes et l'étendue de la question des surfaces élastiques et équation générale de ces surfaces, Paris, 1826 (in French).
- [99] J.L. Lagrange, Recherches sur la nature et la propagation du son, *Miscellanea Philosophico-Mathematica Societatis Privatae Taurinensis I*, 2nd Pagination, i- 112 (see also *Œuvres*, Tome 1, 39-148), 1759 (in French).
- [100] G. Kirchhoff, Über das Gleichgewicht und die Bewegung einer elastischen Scheibe, *J Angew Math* 40 (1850) 51-88. (in German)
- [101] K.H. Lee, G.T. Lim, C.M. Wang, Thick Lévy plates re-visited. *Int. J. Solids Struct.* 39 (2002) 127-144.
- [102] Y.S. Uflyand, The propagation of waves in the transverse vibrations of bars and plates, *Akad. Nauk SSSR Prikl. Math. Mech.* 12 (1948) 287-461.
- [103] Mindlin RD. Influence of rotatory inertia and shear on flexural motions of isotropic, elastic plates. *Trans. ASME Journal of Applied Mechanics* 1951;18:31-38.
- [104] R.D. Mindlin, A. Schacknow, H. Deresiewicz, Flexural vibrations of rectangular plates. *Trans. ASME J. Appl. Mech.* 23 (1956) 430-436.
- [105] I. Elishakoff, Generalization of the Bolotin's dynamic edge-effect method for vibration analysis of Mindlin plates. In: Cuschieri JM, Glegg SAL, Yeager DM, editors. *NOISE-CON 94. Proceedings of the 1994 National Conference on Noise Control Engineering ; 1994 May 01-04 ; Fort Lauderdale.*
- [106] G. Falsone, D. Settineri, I. Elishakoff, A new locking-free finite element method based on more consistent version of Mindlin plate equation, *Arch. Appl. Mech.* 84 (2014) 967-983.
- [107] G. Falsone, D. Settineri, I. Elishakoff, A new class of interdependent shape polynomials for the FE dynamic analysis of Mindlin plate Timoshenko beam, *Arch. Appl. Mech.* 50 (2015) 767-780.
- [108] F. Hache, I. Elishakoff, N. Challamel, Free vibration analysis of plates taking into account rotary inertia and shear deformation via three alternative theories: a Lévy-type solution, *Acta Mech.* 228 (2017), 3633-3655.

- [109] I. Elishakoff, F. Hache, N. Challamel, Vibrations of asymptotically and variationally based Uflyand-Mindlin plate models, *Int. J. Eng. Sc.* 116 (2017) 58-73.
- [110] H. Irschik, Membrane-Type Eigenmotions of Mindlin Plates, *Acta Mech.* 55 (1985) 1-20.
- [111] H. Irschik, R. Heuer, F. Ziegler, Statics and dynamics of simply supported polygonal Reissner-Mindlin plates by analogy, *Arch. Appl. Mech.* 70 (2000) 231-244.
- [112] E.J. Brunelle, S.R. Roberts, Initially stressed Mindlin plates, *AIAA Journal* 12 (1974) 1036-1045.
- [113] E.J. Brunelle, Buckling of transversely isotropic Mindlin plates. *AIAA Journal* 9 (1971) 1018-1022.
- [114] A. Sharma, H.B. Sharda, Y. Nath, Stability and Vibration of Mindlin sector plates: an analytical approach, *AIAA Journal* 4 (2005) 1109-1116.
- [115] J.A. Krumhansl, Generalized Continuum Field Representation for Lattice Vibrations. In: Wallis RK, editor. *Lattice Dynamics*. London: Pergamon; 1965. 627-634.
- [116] J.A. Krumhansl, *Mechanics of Generalized Continua*. Springer-Verlag, New-York, 1968.
- [117] D. Rogula, Influence of spatial acoustic dispersion on dynamical properties of dislocations, *Bull Acad Pol Sc Ser Sc Tech*, 13 (1965) 337-385.
- [118] A.C. Eringen, Linear theory of micropolar elasticity, *J. Math. Mech.* 15 (1966) 909-923.
- [119] A.C. Eringen, D.G.B. Edelen, On nonlocal elasticity. *Int. J. Eng. Sci.* 10 (1972) 233-248.
- [120] A.C. Eringen, *Nonlocal Continuum Field Theories*, Springer-Verlag, New-York, 2002.
- [121] E. Kröner, B.K. Datta, Nichtlokale elastostatik: Ableitung aus der gittertheorie, *Z Phys* 196 (1966) 203-211. (in German)
- [122] I.A. Kunin, Model of elastic medium with simple structure and space dispersion, *Prykl. Mat. Mekh.* 30 (1966) 542-550.
- [123] A.C. Eringen, On differential equations of nonlocal elasticity and solutions of screw dislocation and surface waves, *J. Appl. Phys.* 54 (1983) 4703-4710.
- [124] Q. Wang, V.K. Varadan, Vibration of carbon nanotubes studied using nonlocal continuum mechanics, *Smart. Mater. Struct.* 15 (2006) 659-666.
- [125] A.C. Eringen, B.S. Kim, Relation between nonlocal elasticity and lattice dynamics, *Cryst Latt Def Amorp* 7 (1977) 51-57.
- [126] Z. Zhang, C.M. Wang, N. Challamel, Eringen's length scale coefficient for vibration and buckling of nonlocal rectangular plates with simply supported edges. *J. Eng. Mech.* 141 (2015) 04014117.

- [127] W.H. Duan, N. Challamel, C.M. Wang, Z. Ding, Development of analytical vibration solutions for microstructured beam model to calibrate length scale coefficient in nonlocal Timoshenko beams, *J. Appl. Phys.* 114 (2013) 104312.
- [128] Z. Zhang, N. Challamel, C.M. Wang, Eringen's small length scale coefficient for buckling of nonlocal Timoshenko beam based on microstructured beam model, *J. Appl. Phys.* 114 (2013) 114902.
- [129] N. Challamel, C.M. Wang, I. Elishakoff, Discrete systems behave as nonlocal structural elements: Bending, buckling and vibration analysis. *Eur. J. Mech. A Solids* 44 (2014) 125-135
- [130] M. Ostoja-Starzewski, Lattice models in micromechanics, *Appl. Mech. Rev.* 55 (2002) 35-60.
- [131] H. Hencky, Über die angenäherte Lösung von Stabilitätsproblemen im Raummittels der elastischen Gelenkkette, *Der Eisenbau* 11 (1920) 437-452 (in German).
- [132] M.S. El Naschie, *Stress, stability and chaos in structural engineering: An energy approach*, McGraw Hill, London, 1991.
- [133] Z. Zhang, C.M. Wang, N. Challamel, Eringen's length scale coefficient for buckling of nonlocal rectangular plates from microstructured beam-grid model, *Int. J. Solids Struct.* 51 (2014) 4307-4315.
- [134] N. Challamel, F. Hache, I. Elishakoff, C.M. Wang, Buckling and vibrations of microstructured rectangular plates considering phenomenological and lattice-based nonlocal continuum model, *Compos. Struct.* 149 (2016) 145-156.
- [135] F. Hache, N. Challamel, I. Elishakoff, C.M. Wang, Comparison of nonlocal continualization schemes for lattice beams and plates, *Arch. Appl. Mech.* Doi: 10.1007/s00419-017-1235-z., 2017.
- [136] A.S. Wifi, C.W. Wu, K.A. Obeid, A simple discrete element mechanical model for the stability analysis of elastic structures. In: Kabil YH, Said ME, editors. *Current Advances in Mechanical Design and Production*. Pergamon Press (1989) 149-156.
- [137] H. Zhang, Y.P. Zhang, C.M. Wang, Hencky bar-net model for vibration of rectangular plates with mixed boundary conditions and point supports, *Int. J. Str. Stab. Dyn.* In Press (2017).
- [138] C.M. Wang, Y.P. Zhang, D.M. Pedroso, Hencky bar-net model for plate buckling, *Eng. Struct.* (2017) 947-954.
- [139] A. Kocsis, N. Challamel, G. Károlyi, Discrete and nonlocal models of Engesser and Haringx elastic. *Int. J. Mech. Sc.*, In Press (2017).
- [140] P.G. Kevrekidis, I.G. Kevrekidis, A.R. Bishop, E.S. Titi, Continuum approach to discreteness, *Phys. Rev. E* (2002).

- [141] N.J. Zabusky, M.D. Kruskal, Interaction of Solitons in a Collisionless Plasma and the Recurrence of Initial States, *Phys. Rev. Lett.* 15 (1985) 240–243.
- [142] I.V. Andrianov, J. Awrejcewicz, D. Weichert D. Improved continuous models for discrete media. *Math. Probl. Eng.* (2010) 986242.
- [143] P. Rosenau, Dynamics of nonlinear mass-spring chains near the continuum limit. *Phys. Lett. A* 118 (1986) 222-227.
- [144] P. Rosenau, Dynamics of dense lattices, *Phys. Rev. B* 36 (1987) 5868.
- [145] T.B. Benjamin, J.L. Bona, J.J. Mahony, Model equations for long waves in nonlinear dispersive systems, *Philos. Trans. R. Soc. Lond. Ser. A Math. Phys. Sci.* 272 (1972) 47–78.
- [146] M.A. Collins, A quasicontinuum approximation for solitons in an atomic chain, *Chem. Phys. Lett.* 77 (1981) 342–347.
- [147] N. Challamel, J. Lerbet, C.M. Wang, Z. Zhang, Analytical length scale calibration of nonlocal continuum from a microstructured buckling model, *Z. Angew Math. Mech.* 94 (2014) 402-413.
- [148] Y.Y. Zhang, C.M. Wang, N. Challamel, Bending, buckling and vibration of hybrid nonlocal beams, *J Eng Mech* 136 (2010) 562-574.
- [149] V.L. Berdichevskii, S.S. Kvashina, On equations describing the transverse vibrations of elastic bars, *J. Appl. Math. Mech.* 40 (1974) 104-119.
- [150] A.L. Goldenveizer, J.D. Kaplunov, E.V. Nolde, Asymptotic analysis and refinement of Timoshenko-Reisner-type theories of plates and shells, *Trans. Acad. Sci. USSR. Mekhanika Tverd. Tela* (1990).
- [151] V.L. Berdichevskii, Dynamic theory of thin elastic plates, *Izv. AN SSSR Mekhanika Tverdogo Tela*, 8 (1973) 99-109.
- [152] R. Chebakov, J. Kaplunov, G.A. Rogerson, A non-local asymptotic theory for thin elastic plates, *Proc R Soc A* (2017) 20170249.
- [153] J.D. Kaplunov, L.Y. Kossovitch, E.V. Nolde, Dynamics of thin walled elastic bodies. Academic Press, 1998.
- [154] P. Ciarlet, L. Trabucho, J.M. Viano, Asymptotic methods for elastic structures. Walter de Gruyter, Berlin, 1995.
- [155] D.H. Hodges, Nonlinear composite beam theory. DC: AIAA, Washington, 2006.
- [156] T.S. Vashakmadze, The theory of Anisotropic Elastic Plates, Kluwer Academic Publishers, Dordrecht, 1999.

- [157] O.E. Widera, An asymptotic theory for the motion of elastic plates, *Acta Mech.* 9 (1970) 54-66.
- [158] A.W. Leissa, *Vibration of Plates*. U.S Government Printing Office, NASA SP-160, reprinted by the Acoustical Society of America; 1969.
- [159] A.W. Leissa, The free vibration of rectangular plates. *J Sound Vib* 31 (1973) 257-293.
- [160] D.J. Gorman, *Free Vibration Analysis of Rectangular Plates*. New York, Elsevier-North Holland Publishing Co, 1982.
- [161] E. Ventsel, T. Krauthammer, *Thin plates and shells: theory: analysis, and applications*. CRC press, 2001.
- [162] S.H. Hashemi, M. Arsanjani, Exact characteristic equations for some of classical boundary conditions of vibrating moderately thick plates. *Int. J. Solids Struct.* 45 (2005) 819-853.
- [163] W. Ritz, Über eine neue Methode zur Lösung gewisser Variationprobleme der mathematischen, Physik. *J. Angew. Math.* 135 (1909) 1-61. (in German).
- [164] S.A. Eftekhari, A.A. Jafari, A simple and accurate Ritz formulation for free vibration of thick rectangular and skew plates with general boundary conditions, *Acta Mech.* 224 (2013) 193-209.
- [165] K. Naumenko, J. Altenbach, H. Altenbach, V.K. Naumenko, Closed and approximate analytical solutions for rectangular Mindlin plates. *Acta Mech.* 147 (2001) 153-172.
- [166] K.M. Liew, K.Y. Lam, Application of two-dimensional orthogonal plate function to flexural vibration of skew plates, *J Sound Vib.* 139 (1990) 241-252.
- [167] M. Levinson, D.W. Cooke, On the frequency spectra of Timoshenko beams. *J. Sound Vib.* 84 (1982) 319-326.
- [168] R.B. Bhat, Flexural vibration of polygonal plates using characteristic orthogonal polynomials in two-variables, *J. Sound Vib.* 114 (1987) 65-71.
- [169] R.B. Bhat, Natural frequencies of rectangular plates using characteristic orthogonal polynomials in the Rayleigh-Ritz method, *J. Sound Vib.* 102 (1985) 493-499.
- [170] D.J. Gorman, Free vibration analysis of cantilever plates by the method of superposition, *J. Sound and Vib.* 49 (1976) 453-467.
- [171] D.J. Gorman, Free vibration analysis of the completely free rectangular plate by the method of superposition, *J. Sound Vib.* 57 (1978) 437-447.
- [172] D.J. Gorman, *Vibration analysis of plates by the superposition method (Vol. 3)*, World Scientific, New-York, 2002.

- [173] D.J. Gorman, W. Ding, Accurate free vibration analysis of point supported Mindlin plates by the superposition method, *J. Sound Vib.* 219 (1999) 265–277.
- [174] A.A. Pisano, A. Sofi, P. Fuschi, Finite element solutions for nonhomogeneous nonlocal elastic problems, *Mechanics Research Communications* 36 (2009) 755-761.
- [175] M.K. Ravari, S. Talebi, A.R. Shahidi, Analysis of the buckling of rectangular nanoplates by use of finite-difference method, *Meccanica* 49 (2014) 1443-1455.
- [176] W. Weaver, S.P. Timoshenko, D.H. Young, *Vibration Problems in Engineering*, Fifth edition, John Wiley & Sons; New York, 1990.
- [177] R.R. Craig, A.J. Kurdila, *Fundamentals of Structural Dynamics*. John Wiley & Sons, New York, 2011.
- [178] C. Dym, I. Shames, *Solid Mechanics: a Variational Approach*. McGraw-Hill, New York, 1973.
- [179] S.S. Rao, *Vibration of Continuous Systems*. Wiley, New York, 2007.
- [180] I. Elishakoff, E. Lubliner, 1985, "Random vibration of a structure via classical and nonclassical theories," *Probabilistic Methods in the Mechanics of Solids and Structures*. S. Eggwertz and N.C. Lind, Springer, Berlin, pp. 455-468.
- [181] I. Elishakoff, D. Livshits, Some closed-form solutions in random vibration of Bresse-Timoshenko beams, *Probabilist. Eng. Mech.* 4 (1989) 49-54.
- [182] I. Elishakoff, D. Pentaras, K. Dujat, C. Versaci, G. Muscolino, J. Storch, S. Bucas, N. Challamel, T. Natsuki, Y.Y. Zhang, C.M. Wang, G. Ghyselinck, *Carbon Nanotubes and Nanosensors: Vibrations, Buckling and Ballistic Impact*. ISTE – Wiley, London, 2012.
- [183] I. Elishakoff, An equation both more consistent and simpler than the Bresse-Timoshenko equation, in: Gilat, R. and L. Sills-Banks, L. (Eds.), *Advances in Mathematical Modeling and Experimental Methods for Materials and Structures*. Springer Verlag, Berlin, 249-254, 2009.
- [184] I. Karnovsky, O.I. Lebed, *Non-Classical Vibrations of Arches and Beams: Eigenvalues and Eigenfunctions*, McGraw-Hill, New York, 2004.
- [185] N.G. Stephen, The second spectrum of Timoshenko beam theory – Further assessment, *J. Sound Vib.* 292 (2006) 372-389.
- [186] A. Love, *A treatise of the mathematical theory of elasticity*. IY edit. Cambridge University Press, 1959.
- [187] N.G. Stephen, M. Levinson, A second order beam theory. *J. Sound Vib.* 67 (1979) 293-305.
- [188] S.P. Timoshenko, On the transverse vibration of bars with uniform cross-section, *Philos. Mag.* 43 (1922) 125–131.

- [189] N.G. Stephen, Considerations on second order beam theories. *Int. J. Solids Structures*. 17 (1981) 325-333.
- [190] T. Kaneko, On Timoshenko's correction for shear in vibrating beams, *J. Physics D : Applied Physics*. 8 (1975) 1927-1939.
- [191] A. Moallemi-Oreh, M. Karkon, Finite element formulation for stability and free vibration analysis of Timoshenko beams, *Adv. Acoust. Vib.* (2013) 841215.
- [192] A.J.M. Ferreira, *MATLAB Codes for Finite Element Analysis*, Springer, Berlin, 2008.
- [193] J. Lee, W.W. Schultz, Eigenvalue analysis of Timoshenko beams and axisymmetric Mindlin plates by the pseudospectral method, *J. Sound Vib.* 269 (2004) 609–621.
- [194] A. Diaz-de-Anda, J. Flores, L. Gutiérrez, R.A. Méndez-Sánchez, G. Monsivais, A. Morales, Experimental study of the Timoshenko beam theory predictions, *J. Sound Vib.* 331 (2012) 5732–5744
- [195] A. Cazzani, F. Stochino, E. Turco, An analytical assessment of finite element and isogeometric analyses of the whole spectrum of Timoshenko beams, *Z. Angew. Math. Mech.* 96 (2016) 1220–1244.
- [196] A. Cazzani, F. Stochino, E. Turco, On the whole spectrum of Timoshenko beams. Part I: a theoretical revisitation, *Z. Angew. Math. Phys. (ZAMP)* 67 (2016). (article24).
- [197] A. Cazzani, F. Stochino, E. E. Turco, On the whole spectrum of Timoshenko beams. Part II: further applications, *Z. Angew. Math. Phys. (ZAMP)* 67 (2016). (article25).
- [198] G.R. Bhashyam, G. Prathap, The second frequency spectrum of Timoshenko beams, *J. Sound Vib.* 76 (1981) 407–420.
- [199] R.W. Traill-Nash, A.R. Collar, The effect of shear flexibility and rotary inertia on the bending vibrations of beams, *Q. J. Mech. Appl. Math. QJMAM* 6 (1953) 186–222
- [200] N.G. Stephen, The second frequency spectrum of Timoshenko beams, *J. Sound Vib.* 80 (1982) 578–582.
- [201] N. Khaji, M. Shafiei, M. Jalalpour, Closed-form solutions for crack detection problem of Timoshenko beams with various boundary conditions, *IJMS*. 51 (2009) 667–681.
- [202] A. Labuschagne, N.F.J. van Rensburg, A.J. van der Merwe, Comparison of linear beam theories, *Math. Comput. Model.* 49 (2009) 20–30

- [203] I. Elishakoff, N. Challamel, C. Soret, Y. Bekel, T. Gomez, Virus sensor based on single-walled carbon nanotube: improved theory incorporating surface effects, *Philos. Trans. R. Soc. A* 371 (2013) 20120424.
- [204] A. Erturk, D.J. Inman, Modal analysis of a uniform cantilever with a tip mass, in: *Piezoelectric Energy Harvesting*, John Wiley & Sons, 2001
- [205] R.E. Rossi, P.A.A. Laura, R.H. Gutierrez, A note of transverse vibrations of a Timoshenko beam of a non-uniform thickness clamped at one end and carrying a concentrated mass at the other, *J. Sound Vib.* 143 (1990) 491–502.
- [206] P. Gudmundson, Eigenfrequency changes of structures due to cracks, notches or other geometrical changes, *J. Mech. Phys. Solids.* 30 (1982) 339–353.
- [207] R.Y. Liang, F.K. Choy, J. Hu, Detection of cracks in beam structures using measurements of natural frequencies, *J. Franklin Inst.* 328 (1995) 131-149.
- [208] S.P. Lele, S.K. Maiti, Modeling of transverse vibration of short beams for crack detection and measurement of crack extension, *J. Sound Vib.* 257 (2002) 559–583.
- [209] J.A. Loya, L. Rubio, J. Fernandez-Saez, Natural frequencies for bending vibrations of Timoshenko cracked beams. *J. Sound Vib.* 290 (2006) 640-653.
- [210] V.V. Bolotin, *The Dynamic Stability of Elastic Systems*. Holden-Day, San Francisco, 1964.
- [211] M.C. Cartmell, *Introduction to Linear, Parametric and Non-linear Vibration*. Springer, 1990.
- [212] R.M. Evan-Iwanowski, On the Parametric Response of Structures, *Appl. Mech. Rev.* 18 (1965) 699-702.
- [213] A.V. Perelmuter, V. Slivker, *Handbook of Mechanical Stability in Engineering (Volume 3)*, World Scientific, Singapore, 2013.
- [214] G. Schimdt, *Parametererregerte Scwingungen*, Veb Deutscher Verlag der Wissenschaften. Berlin, 1975 (in German).
- [215] P. Hagedorn, L.R. Koval, On the parametric stability of a Timoshenko beam subjected to a periodic axial load, *Ingenieur-Archiv*, 40 (1971) 211-220.
- [216] S.H. Crandall, A. Yildiz, Random vibration of beams, *J. Appl. Mech.* 29 (1962) 267-275.
- [217] A.C. Eringen, Response of beams and plates to random loads, *J. Appl. Mech.* 24 (1957) 46-52.
- [218] A. Houdijk, Le Mouvement Brownien d'un Fil, *Archives Nerlandaises des Sciences exactes et Naturelles, Series III A* 11 (1928) 212-277

- [219] J.C. Samuels, A.C Eringen, On stochastic linear systems, *Studies in Applied Mechanics* 38 (1959) 83-103.
- [220] M.P. Singh, Random response of symmetric cross-ply composite beams with arbitrary boundary conditions, *AIAA Journal* 30 (1992) 1081-1088.
- [221] I. Elishakoff, D. Livshits, Some closed-form solutions in random vibration of Euler-Bernoulli beams, *Probabilist. Eng. Mech.* 4 (1984) 49-54.
- [222] S.H. Hashemi, K. Khorshidi, M. Amabili, Exact solution for linear buckling of rectangular Mindlin plates, *J Sound Vib.* 315 (2008) 318-342.
- [223] K.M. Liew, Y. Xiang, S. Kitipornchai, Research on thick plate vibration: a literature survey, *J. Sound Vib.*, 180 (1995) 163–176.
- [224] C.M. Wang, J.N. Reddy, K.H. Lee, *Shear deformable beams and plates: relationships with classical solutions*, Oxford, Elsevier, 2000.
- [225] Selezov, *Doslidzenia, Prykladna Mekhanika* (1960) 319-327.
- [226] E. Jomehzadeh, A.R. Saidi, A Lévy type solution for free vibration analysis of a nano-plate considering the small scale effect, *Recent Advances in Vibration Analysis* (2011) 47-58.
- [227] C.L.M.H. Navier, *Extrait des recherches sur la flexion des plans élastiques*, *Bull. Sci. Soc. Philomarhiques de Paris* 5 (1823) 95-102.
- [228] C.M. Wang, Natural frequencies formula for simply supported Mindlin plates, *Journal of Vibration and Acoustics* 116 (1994) 536-540.
- [229] C.Y. Wang, C.M. Wang, *Structural Vibration: Exact Solutions for Strings, Membranes, Beams, and Plates*, CRC Press, Boca Raton, 2014.
- [230] I. Shufrin, M. Eisenberger, Stability and vibration of shear deformable plates – first order and higher order analysis, *Int. J. Solids Struct.*, 42 (2005) 1225–1251.
- [231] K.M. Liew, Y. Xiang, S. Kitipornchai, Transverse vibration of thick rectangular plates – I. Comprehensive sets of boundary conditions, *Comput. Struct.* 49 (1993) 1–29.
- [232] N.G. Stephen, Mindlin plate theory: best shear coefficient and higher spectra validity, *J. Sound Vib.* 202 (1997) 539-553.
- [233] W.H. Wittrick, 1987, Analytical, three-dimensional elasticity solutions to some plate problems, and some observations on Mindlin’s plate theory, *Int. J. Solids Structures*, 23 (1987) 441-464.
- [234] W.C. Chen, W.H. Liu, Deflections and free vibration of laminated plates – Lévy-type solutions, *Int. J. Mech. Sci.* 32 (1990) 779-793.

- [235] R. Szilard, Theory and Analysis of Plates, Prentice-Hall, Englewood Cliffs, New Jersey, 1974.
- [236] D.J. Dawe, Finite strip models for vibration of Mindlin plates, J. Sound Vib. 59 (1978) 441-452.
- [237] S.R. Srinivas, C.V. Joga Rao, A.K. Rao, An exact analysis for vibration of simply supported homogeneous and laminated thick rectangular plates, J Sound Vib. 12 (1970) 187-199.
- [238] F. Hache, N. Challamel, I. Elishakoff, Asymptotic derivation of nonlocal beam models from two-dimensional nonlocal elasticity, Mathematics and Mechanics of Solids, in submission.
- [239] F. Hache, N. Challamel, I. Elishakoff, Asymptotic derivation of nonlocal plate models from three-dimensional nonlocal elasticity, in submission.
- [240] J. Peddieson, G.R. Buchanan, R.P. McNitt, Application of nonlocal continuum models to nanotechnology, Int. J. Eng. Sci. 41 (2003) 305-312.
- [241] L.J. Sudak, Column buckling of multiwalled carbon nanotubes using nonlocal continuum mechanics, J. Appl. Phys. 94 (2003) 7281-7285.
- [242] Ö. Civalek, Ç. Demir, Bending analysis of microtubules using nonlocal Euler–Bernoulli beam theory, Appl. Math. Model. 35 (2011) 2053-2067.
- [243] P. Lu, H.P. Lee, C. Lu, P.Q. Zhang, Application of nonlocal beam models for carbon nanotubes, Int. J. Solids Struct. 44 (2007) 5289–5300.
- [244] P. Lu, H.P. Lee, C. Lu, P.Q. Zhang, Dynamic properties of flexural beams using a nonlocal elasticity model, J. Appl. Phys. 99 (2006) 073510.
- [245] S. Narendar, S.S. Gupta, S. Gopalakrishnan, Wave propagation in single-walled carbon nanotube under longitudinal magnetic field using nonlocal Euler–Bernoulli beam theory, Appl. Math. Model. 36 (2012) 4529-4538.
- [246] J.N. Reddy, Nonlocal theories for bending, buckling and vibration of beams, Int. J. Eng. Sci. 45 (2007) 288-307.
- [247] M. Xu, Free transverse vibrations of nano-to-micron scale beams. Proc Math Phys Eng Sci. 462 (2006) 2977-2995.
- [248] Y.Q. Zhang, G.R. Liu, X.Y. Xie, Free transverse vibrations of double-walled carbon nanotubes using a theory of nonlocal elasticity, Phys Rev B 71 (2005) 195404.
- [249] N. Challamel, Z. Zhang, C.M. Wang, J.N. Reddy, Q. Wang, T. Michelitsch, B. Collet, On non-conservativeness of Eringen’s nonlocal elasticity in beam mechanics: correction from a discrete-based approach, Arch. Appl. Mech. 84 (2014) 1275-1292.

- [250] H.T. Thai, A nonlocal beam theory for bending, buckling and vibration of nanobeams, *Int J Eng Sci* 52 (2012) 56-64.
- [251] F. Ebrahimi, P. Nasirzadeh, A nonlocal Timoshenko beam theory for vibration analysis of thick nanobeams using differential transform method, *J Theor Appl Mech* 53 (2015) 1041-1052.
- [252] Y.G. Hu, K.M. Liew, Q. Wang, Modeling of vibrations of carbon nanotubes, *Procedia Eng* 31 (2012) 343-347.
- [253] C.M. Wang, Y.Y. Zhang, X.Q. He, Vibration of nonlocal Timoshenko beams, *Nanotechnology* 18 (2007) 105401.
- [254] C.M. Wang, Y.Y. Zhang, S.S. Ramesh, Buckling analysis of micro- and nano-rods/tubes based on nonlocal Timoshenko beam theory, *J Phys D Appl Phys* 39 (2006) 3904–3909.
- [255] J.R. Hutchinson, Vibrations of thick free circular plates, exact versus approximate solutions, *J. Appl. Mech.* 51 (1984) 581–585.
- [256] P. Lu, P.Q. Zhang, H.P. Lee, C.M. Wang, J.N. Reddy, Non-local elastic plate theories, *Proc R Soc A* 463 (2007) 3225-3240.
- [257] T. Murmu, S.C. Pradhan, Vibration analysis of nanoplates under uniaxial prestressed conditions via nonlocal elasticity, *J Appl Phys* 106 (2009) 104301.
- [258] T. Murmu, S.C. Pradhan, Small scale effect on the buckling of single-layered graphene sheets under biaxial compression via nonlocal continuum mechanics. *Comput. Mat. Sci.* 47 (2009) 268-274.
- [259] S. Chakraverty, L. Behera, Free vibration of rectangular nanoplates using Rayleigh-Ritz method, *Physica E Low Dimens. Syst. Nanostruct.* 56 (2014) 357-363.
- [260] S.C. Pradhan, J.K. Phadikar, Nonlocal elasticity theory for vibration of nanoplates, *J. Sound Vib.* 325 (2009) 206-223.
- [261] T. Aksencer, M. Aydogdu, Levy type solution method for vibration and buckling of nanoplates using nonlocal elasticity theory, *Physica E Low Dimens. Syst. Nanostruct.* 43 (2011) 954-959.
- [262] R. Ansari, B. Arash, H. Rouhi, Vibration characteristics of embedded multi-layered graphene sheets with different boundary conditions via nonlocal elasticity, *Compos. Struct.* 93 (2011) 2419-2429.
- [263] R. Ansari, B. Arash, H. Rouhi, Nanoscale vibration analysis of embedded multi-layered graphene sheets under various boundary conditions, *Comput. Mater. Sci.* 50 (2011) 3091-3100.

- [264] P. Seide, Accuracy of some numerical methods for column buckling, *J. Eng. Mech.* 101 (1975) 549-560.
- [265] C.T. Wang, Discussion on the paper of “Salvadori M.G., Numerical computation of buckling loads by finite differences”. *Trans. ASCE* 116 (1951) 629-631.
- [266] C.T. Wang, *Applied Elasticity*. McGraw-Hill, New-York, 1953.
- [267] R. Santoro, I. Elishakoff, Accuracy of the finite difference method in stochastic settings, *J. Sound. Vib.* 291 (2006) 275-284.
- [268] S. Hosseini-Hashemi, A.T. Samaei, Buckling analysis of micro/nanoscale plates via nonlocal elasticity theory, *Physica E.* 43 (2011) 1400-1404.
- [269] A.T. Samaei, S. Abbasion, M.M. Mirsayar, Buckling analysis of a single-layer graphene sheet embedded in an elastic medium based on nonlocal Mindlin plate theory, *Mechanics Research Communication* 38 (2011) 481-485.
- [270] N. Challamel, V. Picandet, B. Collet, T. Michelitsch, I. Elishakoff, C.M. Wang, Revisiting finite difference and finite element methods applied to structural mechanics within enriched continua, *Eur. J. Mech. A/Solids.* 53 (2015) 107-120.
- [271] F. Hache, N. Challamel, I. Elishakoff, Lattice and continualized models for the buckling study of nonlocal rectangular thick plates, *IJMS*, in submission.
- [272] F. Hache, N. Challamel, I. Elishakoff, Lattice and continualized models for the vibration study of nonlocal rectangular thick plates, *IJSSD*, in submission.
- [273] I.A. Butt, J.A.D. Wattis, Discrete breathers in a hexagonal two-dimensional Fermi-Pasta-Ulam lattice, *J Phys A: Math Theor.* 40 (2007) 1239.
- [274] J.A. Wattis, L.M. James, Discrete breathers in honeycomb Fermi–Pasta–Ulam lattices, *Journal of Physics A: Mathematical and Theoretical*, 47 (2014), 345101.
- [275] D. Caillerie, A. Mourad, A. Raoult, Discrete homogenization in graphene sheet modeling, *Journal of Elasticity*, 84 (2006) 33-68.

N° ordre 487